Cranfield
UNIVERSITY

School of Industrial and Manufacturing Science

Ph D Thesis

Academic Year 1995-96

C THIAGARAJAN

SMART CHARACTERISATION OF DAMAGE IN CARBON FIBRE REINFORCED COMPOSITES UNDER STATIC AND FATIGUE LOADING CONDITIONS BY MEANS OF ELECTRICAL RESISTIVITY MEASUREMENTS

Supervisor: P E Irving

February 1996

ABSTRACT

This thesis investigates the smart damage sensing capabilities of the electrical resistivity measurement technique in carbon fibre reinforced composite materials.

The static and fatigue damage mechanisms of unidirectional and cross-ply laminates are reviewed. The electrical resistivity measurement investigations of carbon fibre, epoxy resin and carbon fibre reinforced composites are described. Theoretical models related to damage and electrical conduction modelling are reviewed. The material properties, laminate fabrication, specimen design, tab design and electrode design details are presented. The experimental test set-up and test programme details are presented.

The details of the formulation and algorithms of a proposed new random resistor network model and the three-dimensional unit cell assemblage model are described. The results related to the applicability and the validation of these models are presented.

The influence of electrode effects on the electrical resistance are investigated. The relevant results are presented. The electrical properties of carbon fibre reinforced composites independent of specimen geometry and electrode configuration are established. The dependence of electrical resistance on the specimen geometry was investigated and the relevant results are presented.

The smart damage sensing capabilities are demonstrated using computational simulation studies using the proposed new three-dimensional model. The strain sensing and damage sensing capabilities of electrical resistivity measurement technique under static and fatigue loading conditions are presented. The dependence of electrical resistance to the applied stress and fatigue life of the samples subjected to fatigue loading is presented. The smart sensing capabilities are highlighted based on the experimental and theoretical results.

The static and fatigue behaviour of epoxy 914 and epoxy 920 based CFRP laminates is investigated. The failure mechanisms are established using the electrical resistance and other non-destructive test methods.

To my parents

AWARDS AND PUBLICATIONS

AWARDS

One of the paper (1) published out of this thesis work was awarded the SAFETY AWARD IN MECHANICAL ENGINEERING for the best paper published in the year 1994 for contribution towards safety in mechanical engineering by the Institute of Mechanical Engineers.

PUBLICATIONS

(1) Thiagarajan, C., and Irving, P. E. 1994. In service damage monitoring techniques in polymer composites. In: Aerotech Conference Proceedings, Seminar 37, Paper No. C470/37/159. 7 pages.

(2) Thiagarajan, C., Sturland, I., Tunnicliffe, D., and Irving, P. E. 1994. Electrical potential techniques for damage sensing in composite structures. In: Second European Conference on Smart structures and Materials, Glasgow, 12-14 October 1994. 128-131.

ACKNOWLEDGEMENTS

I would like to express my deep sense of gratitude to Prof. P. E. Irving for his guidance and for arranging materials and equipment's. I am grateful to the progress monitoring committee members, Dr. J. Spurrier and Prof. J. H. Robinson for their interest and encouragement. I am indebted to Dr. M. Lock for the provision of C-scan facilities, general advice and help.

I wish to thank the technical staff, Messrs. B. Walker, M. C. Crook, A. Baldwin and Mrs. C. Kimpton, without their help this thesis would not have materialised. I am thankful to Dr. I. Sturland and Dr. D. Tunnicliffe, BAe, Sowerby Research Centre, for their help in the preparation of the electrodes. A special appreciation is due to Ms. D. M. Rose for her secretarial help. Many thanks to all the computer centre staff for their help, especially to Miss Helen. Clinch for Her Help in Hspice. I take this opportunity to thank the Helpline for giving me an opportunity to solve others problem than my own.

I am thankful to Dr. Pai and Drs. Uma for their suggestions and help. I am thankful to all my friends here at Cranfield and abroad for a good laugh and nice time.

The help given by Mr. S. Mukherji, Student Welfare Officer, Indian High Commission, London is also gratefully acknowledged.

-C Thiagarajan,
February 1996.

CONTENTS

PART III
RESULTS AND DISCUSSION

APPENDICES

LIST OF TABLES

LIST OF FIGURES

NOMENCLATURE

A	Cross sectional area
A_c	Cross sectional area of the composite
A_f	Cross sectional area of the fibre
A_m	Cross sectional area of the matrix
D	Diffusion constant, Damage parameter, Diameter
D_f	Diameter of the fibre
dR	Change in resistance
E	Young's modulus
E_c	Activation energy
E_F	Fermi level
E_g	Energy gap
I	Current
k	Boltzmanns constant
n	Number of charge carriers
N	Number of cycles, Total number of fibres
n_n	Number of positive charge carriers
n_p	Number of negative charge carriers
q	Charge in Coulomb
R	Resistance
R_c	Resistance of the composite

R_e	Electrode resistance
R_f	Resistance of the fibre
R_l	Resistance of the electrical leads
R_m	Resistance of the matrix
T	Temperature
T_{RT}	Room temperature
V	Voltage
V_c	Critical volume fraction
V_f	Volume fraction of the fibres
V_m	Volume fraction of the matrix
ε	strain
ε_c	Static failure strain
ε_m	Matrix failure strain
σ	Stress, Conductivity
σ_r	Radial stress
σ_x	Axial stress
σ_{APP}	Applied stress
σ_{INT}	Initial stress
ρ_c	Composite resistivity
ρ_f	Fibre resistivity
ρ_L	Longitudinal resistivity
ρ_m	Matrix resistivity
ρ_T	Transverse resistivity
ρ_{RT}	Room temperature resistivity
ρ_o	Temperature independent constant
ρ_x	Resistivity along the x-axis
ρ_y	Resistivity along the y-axis
ρ_z	Resistivity along the z-axis
α	Coefficient of resistivity
μ	Poisson's ratio, mobility of charge carriers
μ_n	Mobility of the negative charge carriers
μ_p	Mobility of the positive charge carriers
τ	Shear stress
AR	Anisotropic Ratio

ASTM	American Society for Testing and Materials
CDM	Continuum Damage Mechanics
CDS	Characteristic Damage State
CED	Cambridge Electronic Design
CFRP	Carbon Fibre Reinforced Plastics
CLT	Classical Lamination Theory
CP	Cross-ply
CS	Copper Sputtered (electrodes)
DL	Dependence of Length test samples
DMM	Digital Multi-Meter
ERM	Electrical Resistivity Measurement
GFRP	Glass Fibre Reinforced Plastics
HM	High Modulus
HS	High Strength
HTT	Heat Treatment Temperature
ILSS	InterLaminar Shear Strength
IM	Intermediate Modulus
LR	Longitudinal Resistivity
MP	Mechanical Polished (electrodes)
MT	Mechanical Test samples
PAN	Polyacrylonitrile
PE	Plasma Etched (electrodes)
RoM	Rule of Mixtures
RT	Room Temperature
RVE	Representative Volume Element
SD	Standard Deviation
SE	Silver Epoxy
SM	Standard Modulus
SP	Silver Paint
TR	Transverse Resistivity
UD	Unidirectional
UHM	Ultra High Modulus
UP	UnPolished
UTM	Universal Testing Machine
UTS	Ultimate Tensile Stress

1

INTRODUCTION

The future is here. Future smart structures will monitor their own cure, sense strain or stress, monitor damage and finally will do the necessary corrective measures to optimise the performance. This concept of smart structures or intelligent structures is of current research interest. The concept of smart or the degree of smartness is not well defined, and It depends on the field of application. To monitor the health of a composite structure, embedded external sensors such as optical fibre or piezo-electric transducers are under development. The embedded sensors are aimed to serve the structure from 'cradle to grave'. Is there anything more fascinating than to use the same material as a sensor to achieve the smart goal. The electrical resistivity measurement technique is one of the prime techniques that can use the material itself as a sensor.

Electrical resistivity is one of the fundamental properties of materials and is related to the atomic level. Electrical resistivity is influenced by structural and environmental changes in the material. The resistance change in electrical resistivity measurements is of direct consequence of changes in the material. This can be due to strain, temperature, moisture and or damage. Therefore, any change in electrical resistance is due to a change in the internal state of the

material. The correlation or relationship between change in resistance and the internal structural change can be an important tool. This will lead to the development of a smart structure, just by monitoring and processing the resistance changes in the structure.

Use of external sensors has its own problems. Fibre optic techniques have been here for the past twenty years. Though they were introduced in the 1970s, they still remain as a laboratory tool. Fibre optics have exceptional advantages in communication and data transmission technology. However, use of fibre optics to sense damage in composite materials is questionable. Before employing fibre optics to monitor damage in CFRP structure, lots of technical problems have to be solved. There are many unanswered questions. It is anticipated that the use of embedded sensors can affect the integrity of the structure.

Composite materials are considered to have significantly greater resistance to fatigue loading than any other materials. Although this is true for advanced composites subjected to tensile stress in the fibre direction; for other stress and fibre orientations, fatigue of composites is more complex. Moreover, the current maximum design strain of composite materials is about 0.2 to 0.3 percent, which is well below the static strength capability, i.e., 1 to 1.2 percent. Currently the strength potential of composite materials are not fully exploited.

It is clear from the previous work that the fatigue loading can damage carbon fibre reinforced laminates. The damage accumulates with cycling and failure occurs when a critical level of damage is reached. The physical nature of the damage and the way it depends on loading conditions is not clear. There is not a good understanding of what constitutes terminal or fatal damage. The fatigue damage mechanisms of unidirectional composites are not well understood, although they are the basic building block of composite structures.

An important objective of fatigue research is to predict the fatigue life of composite materials. To achieve this, it is a necessity to understand the fatigue process and establish a quantitative representation that includes the controlling factors and mechanisms.

In order to understand the fatigue damage mechanisms, damage detection and characterisation methods are essential. Non-destructive and destructive tests such as X-ray, acoustic emission, ultrasonics, electromagnetic waves, microscopy, etc., have been used to detect and characterise damage. Among these, acoustic emission has been popularly employed to detect defects. This technique can provide qualitative information about the determination and location of defects. However, quantitative characterisation of damage from acoustic emission parameters is not straight forward. Microscopy and replication techniques provide valuable

information about the accumulation of damage on an exposed surface of a laminate. However these techniques fail to provide complete information about the global extent and distribution of damage throughout the laminate. X-ray techniques fail to detect fibre breaks, although they can detect matrix cracks in penetrant enhanced radiography. Ultrasonic techniques require specialised methods to characterise fibre breaks. Fibre breaks are one of the most important damage mechanisms and are the most difficult to detect non-destructively. The limitations with existing non-destructive test methods also emphasise the need for newer techniques.

It is known that the catastrophic failure of composite structure is due to failure of the main load carrying fibres. The fatigue life of the structure depends on the failure of these fibres. It is also known that carbon fibres are fatigue insensitive. Therefore, if we know (1) at what stage a fibre break occurs in life and (2) what causes the fibres to break, then in theory, it is possible to create a fatigue insensitive structure. In this thesis more importance is given to characterisation of fibre breaks.

The main aim of this work is to investigate the possibilities of quantitative and qualitative smart damage sensing capabilities of the electrical resistance measurement technique. This thesis is laid out to achieve the above goal by investigating static and fatigue damage mechanisms of unidirectional carbon fibre reinforced composite materials by means of electrical resistance measurements. To exploit the potential of the electrical resistivity measurement technique, the conduction mechanism should be understood first. Therefore, another objective of this thesis is to investigate the electrical conduction mechanism of CFRP laminates and to develop electrical conduction models.

This thesis is presented in three parts, the literature survey, experimental and theoretical work, and the results and discussion. Chapter two reviews damage mechanisms of composite materials. Chapter three, presents a literature review on electrical resistivity measurements. This chapter is first of its kind and hence detailed reviews of electrical properties and electrical resistivity measurements of carbon fibre, epoxy resin and carbon fibre reinforced composites are presented. Theoretical models to predict the electrical properties of CFRP laminates are reviewed. The physics of electrical conduction of material is also described with special reference to carbon fibres and epoxy resin.

Chapter four deals with materials, test methods and the test programme. The theoretical and computational model formulation and development details are described in chapter five. This chapter presents details of a proposed new random resistor network model and a three-dimensional unit cell assemblage model.

Chapters six to ten present the results and discussion. The factors that influence the measured resistance, details of electrode formation methods and the relevant results are presented in chapter six. Chapter seven is concerned with electrical properties. In this chapter, the electrical properties of CFRP are investigated. The temperature dependent resistivity results are also presented. Chapter eight is concerned with the experimental and computational simulation of damage. The results related to simulation of fibre breaks, longitudinal splits and delamination are presented. A comparison of experimental and computational model results is also presented. This chapter also examines the applicability of the parallel resistance model and the validation of the 3D model.

Chapter nine presents the results pertaining to tensile failure mechanisms. The tensile properties and the results related to electrical resistivity measurements are presented. Results relating to strain and damage sensing of 0°, 90° unidirectional and cross-ply laminates are also presented. Chapter ten presents the results relevant to fatigue damage mechanisms. The fatigue behaviour and the electrical resistivity measurements relating to fatigue damage sensing are also presented. The electrical resistivity measurement results are compared with the elastic modulus, acoustic emission and C-scan and X-ray results. Results relating to the dependence of applied stress and life are also presented. Chapter 11 presents the major conclusions and future work.

This thesis also includes three appendices. Appendix-A deals with the review of damage models and the proposed fatigue life prediction damage model. Appendix-B presents the finite element analysis results related to the specimen design. The statistical summary of the electrical and mechanical properties is presented in appendix-C.

PART I

LITERATURE SURVEY

2

DAMAGE MECHANISMS

This chapter presents the literature review on the damage mechanisms of unidirectional carbon fibre reinforced polymer composites subjected to static and fatigue tensile loading. Cross-ply laminates are also considered.

This chapter is organised as follows: Section 2.1 presents the damage modes observed in laminated composites such as fibre breaks, matrix cracks, longitudinal splitting and delamination, highlighting the significance, initiation, mechanistic aspects and the influence on the stiffness. The failure mechanisms and failure process of 0° and 90° unidirectional and cross-ply laminates under static loading condition are presented in section 2.2. The fatigue damage mechanisms of unidirectional and cross-ply laminates are described section 2.3.1 and 2.3.2, respectively. Section 2.3.3 presents the factors that influence the fatigue behaviour of composites. A brief introduction about the damage models that are based on damage mechanics and micromechanics approach is given in section 2.4

2.1 DAMAGE MODES

Damage in laminated composites can be classified into three types; fibre damage, matrix damage and interfacial damage. This section presents the general damage modes observed in laminated composites subjected to mechanical loading. Fibre breaks, matrix cracking, longitudinal splitting and delamination are the major damage modes generally observed in carbon fibre reinforced polymer composites (Talreja 1987, Curtis 1991). Figure 2.1 shows a schematic illustration of the major damage modes of a unidirectional laminate. This section outlines the above damage modes with the emphasis on the

significance,

initiation,

theoretical aspects and,

the influence on stiffness properties.

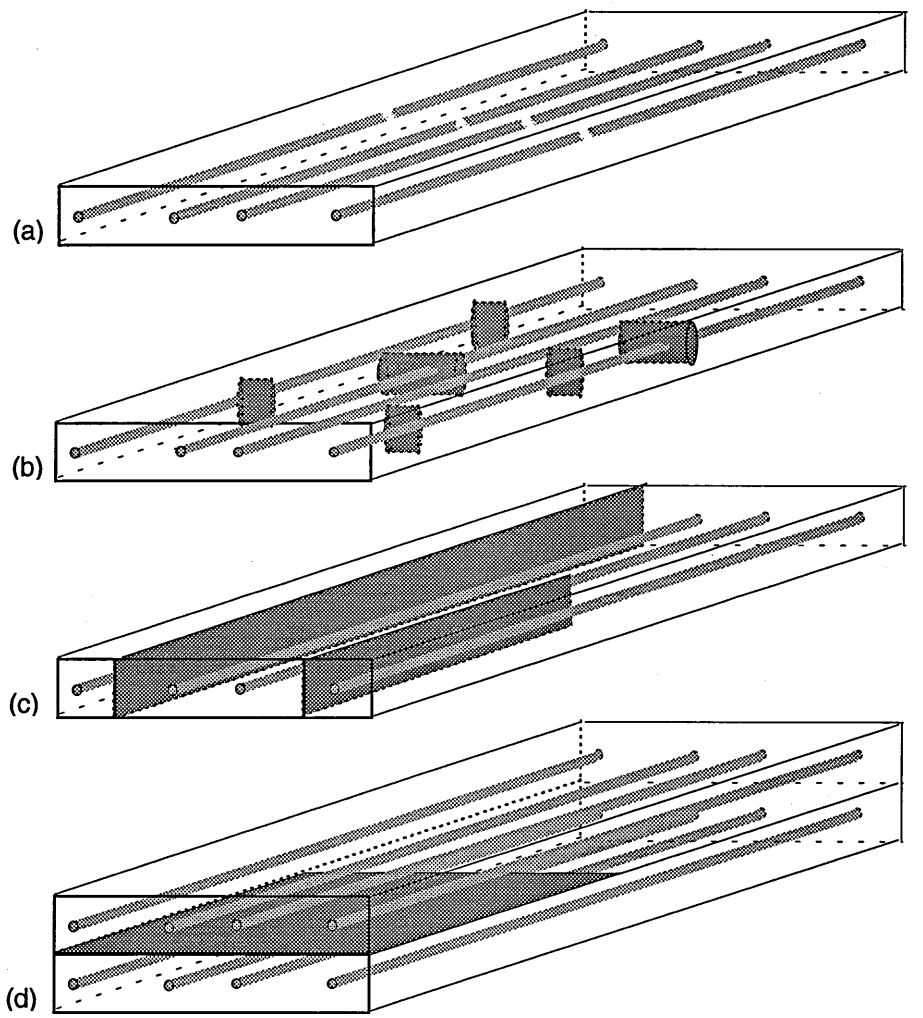

Figure 2.1. Schematic illustration of damage modes in a unidirectional composite: (a) fibre breaks, (b) matrix cracks, (c) longitudinal splits and (d) delamination.

2.1.1 Fibre breaks

A schematic illustration of fibre breaks is shown in Figure 2.1 (a). Fibres are the major load carrying members in a laminated composite. The final catastrophic failure of composite structure is due to failure of these fibres. Moreover, fibre breaks are the major damage mechanism controlling the life of the laminates subjected to mechanical loading. However, it is the least studied and therefore least understood of all the damage modes. The mechanisms of fibre fracture have not been described as extensively as other damage mechanisms (Reifsnider 1991).

Fibre damage is a non-progressive (i.e., catastrophic) type of damage (Konur and Matthews 1989). Fibre breaks in a laminated composite may initiate from a fibre at the weakest point along its length or at a point of local stress concentration (such as the tip of a matrix crack). It has been observed that fibre fracture occurs throughout the life of a cross-ply laminate subjected to fatigue loading (Batdorf 1982). The fibre fracture patterns are quite different for unidirectional and cross-ply laminates. The fibre fracture pattern was measured using the deply technique by Jamison (1985) in unidirectional laminates under static loading. He observed random fibre fracture pattern scattered throughout the sample in singlets and doublets and quite seldom in triplets. An example for a triplet is shown in Figure 2.2. However, in cross-ply laminates the fibre fracture in 0° plies was found to show a representative pattern as shown in Figure 2.3 at the locations of transverse cracks in the adjacent 90° ply.

Single isolated fibre breaks will occur in the composite according to the statistical distribution of the fibre strength. The statistical strength distribution of a typical carbon fibre (PAN based) is shown in Figure 2.4. Fibre fractures can cause significant disturbances in the stress field. However, breakdown of a single fibre alone may not necessarily lead to immediate failure of the entire structure, that is, material failure is not dictated by weakest link characteristics. The strength theories of fibre bundles based on statistics of fibre fracture have been considered in the literature for a long time. The tensile strength distribution of fibres has been studied since 1926 using statistical models (e.g., Peirce 1926; Weibull 1939). The statistical tensile strength theory of the so called classical fibre bundles (the strength is independent of the rate of loading) that obey the Weibull distribution was first developed by Daniels (1948) and extended to infinite bundles by Coleman (1958). Recently, Xia et al. (1994) proposed a statistical model to determine the rate dependent strength of fibres and fibre bundles. They have shown that these models explain the rate dependent behaviour of E-glass fibres. Their experimental investigation is mainly on glass fibres, however, it is mentioned here because the same model can be extended to carbon fibre bundles also. Moreover, to the author's knowledge, there is no rate

dependent fibre bundle failure theory that deals specifically with carbon fibres. Application of fibre bundle strength theories to unidirectional composites is described in section 2.2.1.

Fibre fracture is a source of initiation of other damage modes such as matrix cracks and longitudinal splits (Talreja 1987). Theoretical investigations of the after effects of fibre breaks are available in the literature. After a fibre break, two possible modes of failure can occur: a circular crack can propagate outward into the matrix, or a cylindrical crack can propagate along the fibre-matrix interface. Recently, Gent and Wang (1993) investigated the above problem using finite element analysis and obtained a general criterion to predict the mode of failure. They suggest that for sample with a perfect interface, pull-out of the fibre is expected when the fibre radius is less than about one-fifth of the sample radius. Also, they suggest that for fibres of larger radius, either pull-out or resin cracking can take place depending on the relative levels of interfacial fracture energy and resin fracture energy.

The influence of fibre fracture on laminate stiffness has been investigated theoretically by many investigators. Fibre fracture alone has been shown to have negligible influence on the stiffness of the laminate (Reifsnider and Highsmith 1982, Gottesman et al. 1980). However, Steif (1984) has shown that measurable reduction in stiffness occurs, if the fibre fracture is coupled with debonding.

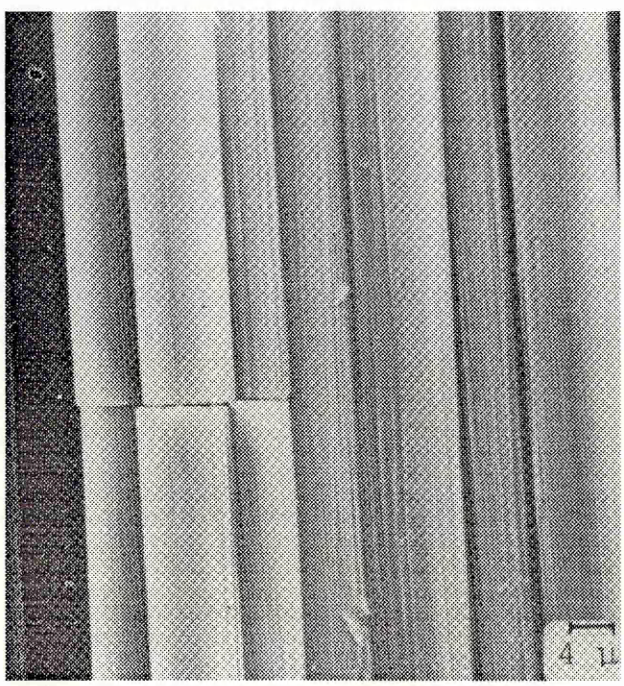

Figure 2.2. SEM-micrograph of fibre fracture in a unidirectional laminate, example of a triplet (Jamison 1985).

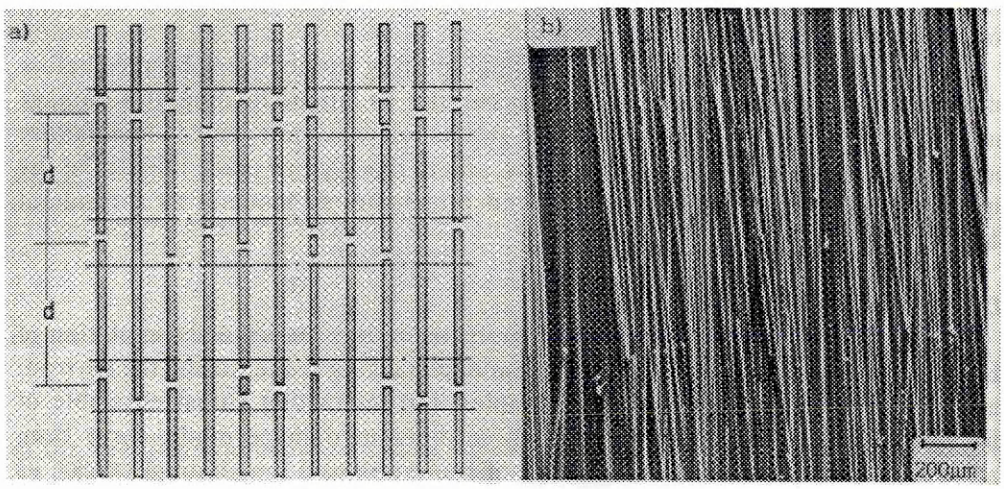

d -adjacent ply crack spacing

Figure 2.3. Fibre fracture pattern in 0° plies of a cross-ply laminate: (a) schematic and (b) SEM-micrograph (Schulte and Stinchcomb 1989).

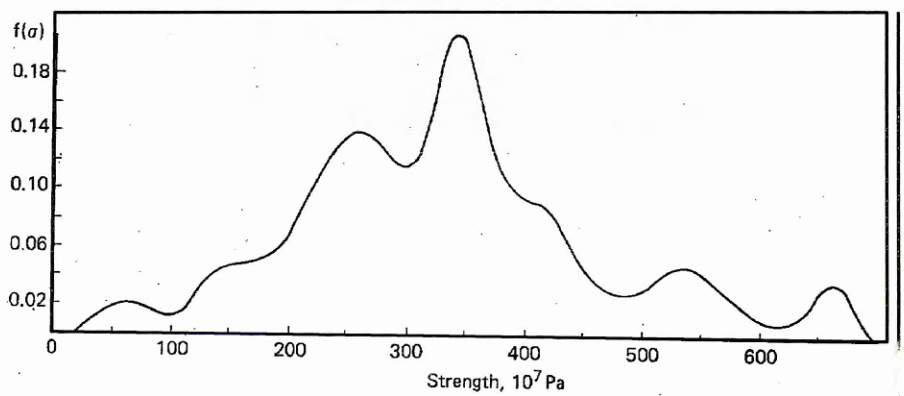

Figure 2.4. Strength distribution of carbon fibres (Konkin 1985)

2.1.2 Matrix cracks

Matrix cracking is a form of matrix damage (refer Figure 2.1 (b)). Matrix cracks are the initial damage mode in a multi-ply laminated composites. Matrix cracks can introduce corrosive pathways through which corrosive agents can penetrate into to the sample. Matrix cracks can act as a source of initiation of other damage modes such as delamination, fibre breaks and longitudinal splitting (Bailey et.al 1979, Stinchcomb and Bakis 1991). The presence of matrix crack can cause structural failure at conditions where leakage through matrix cracks is not allowed, such as in pressure vessel (Nairn and Hu 1994).

Yen and Buesking (1993) modelled the effects of matrix cracks to predict the stress-strain response of unidirectional composites using combined micromechanical and statistical approach. They have used the chain-of-bundles approach, originally proposed by Rosen (1964),

to model the effect of matrix cracks. They have related the density of transverse matrix cracks to the applied composite stress.

The effects of matrix cracks on cross-plied laminate is an extensively studied subject. Recently, Nairn and Hu (1994) have reviewed, experimental observations, stress analysis methods used to approximate the stresses in the presence of matrix cracks, and the various criteria used to predict the development of matrix cracks. In cross-ply composites, matrix cracks were found to initiate from voids in the matrix, regions of high volume fraction, fibre debonds and sometimes from resin rich areas. Figure 2.5 shows the development of transverse cracks in three types of cross-ply laminates under tensile loading. This figure shows the effects of tough matrix resins (APC-2/AS4) in delaying the development of matrix cracks.

Matrix cracks are shown to influence the stiffness of both unidirectional and cross-ply laminates (Yen and Buesking 1993, Nairn and Hu (1994). The stiffness reduction due to matrix cracks in cross-ply laminates has been investigated by several authors (Reifsnider 1977, Highsmith and Reifsnider 1982, Laws et al. 1985, Talreja 1985a, Hashin 1986, Chatterjee et.al. 1993). Lately, Renard et al. (1993) have modelled the stiffness reduction due to matrix cracks using a damage mechanics based model. They have introduced a damage variable to formulate a damage onset criterion and damage development law. They simulated the development of cracks, also. They have shown that the loss of stiffness depends on the number of cracks in the damaged ply and the thickness of the ply.

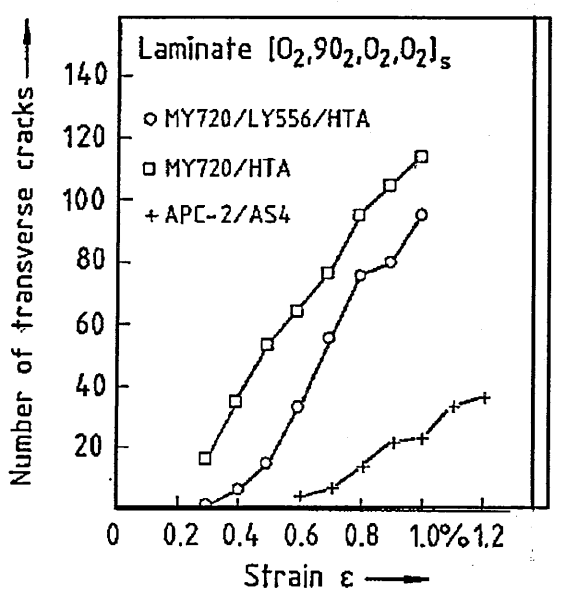

Figure 2.5. Development of transverse cracks in cross-ply laminates (Schulte and Stinchcomb 1989).

2.1.3 Longitudinal splits

Longitudinal splits are a form of interfacial damage (refer Figure 2.1 (c)). Longitudinal splits are longitudinal matrix cracks in the 0° plies oriented along the fibre direction. They are mainly due to interfacial debonding. The depth of longitudinal cracks may be equal to the thickness of the ply or the laminate.

Longitudinal splits can initiate from fibre breaks or matrix cracks (Talreja 1987). Longitudinal split initiation and growth depends on the fibre matrix interface. The newer toughened resin matrix composites are more susceptible to longitudinal splitting than the standard brittle resin matrix composites under fatigue loading (Curtis 1991).

Wolla and Goree (1987) experimentally evaluated longitudinal split initiation and growth patterns in unidirectional composites. After the initiation of longitudinal splits, they observed two modes of crack growth, a region of slow and steady split growth followed by a rapid growth region. They suggested that the normal transverse stresses are responsible for the initiation and the slow growth region of the split. The rapid growth region was suggested to be due to shear failure. Lately, Tohgo et al. (1993) proposed a criterion for longitudinal split initiation at a crack tip in unidirectional carbon/epoxy composites. Based on their experimental and theoretical investigations, they suggested that the tensile stress intensity factor along the fibre direction is responsible for the split crack initiation. In cross-ply laminates, the driving force for longitudinal split growth is provided by the transverse stresses generated by the Poisson's mismatch between adjacent plies (Bailey et al. 1979).

To the author's knowledge, there is no investigations that estimate the stiffness reduction due to longitudinal splits. Longitudinal splits are similar to delamination, in the sense that under longitudinal loading in unidirectional laminates the longitudinal strain and constraint states are similar. Therefore, it is suggested that the influence of longitudinal splits can be estimated using the same principle used for estimating the stiffness reduction due to delamination (refer next section).

2.1.4 Delamination

Delaminations are a form of matrix cracking that occurs generally between the plies (refer Figure 2.1 (d)). Delamination is produced by interfacial plane decohesion. This represents one of the prevalent life limiting failure modes in laminated composites. Delamination after impact is another critical damage mode. Moreover, delamination crack growth can lead to final catastrophic failure (Bathias 1989a).

Figure 2.6 (Wilkins et al. 1982) shows the common structural elements that generate interlaminar stress concentrations that may initiate delaminations under static and fatigue loading conditions. Imperfections such as air entrapment or regions of insufficient resin may also cause initial delamination in the composite during the fabrication process. In cross-ply laminates, internal delaminations can initiate at the point of intersection of 0° and 90° plies (Bailey et.al. 1979). The delamination initiation and growth basically depend upon the transverse tensile strength of the resin between the layers of fibres (Kam and Walker 1987).

Delamination growth can cause severe reductions in stiffness and strength. The stiffness reduction due to delamination can be estimated by modelling the delaminated laminate as a set of sub-laminates under the same axial strain but with no lateral constraint (O'Brien 1982).

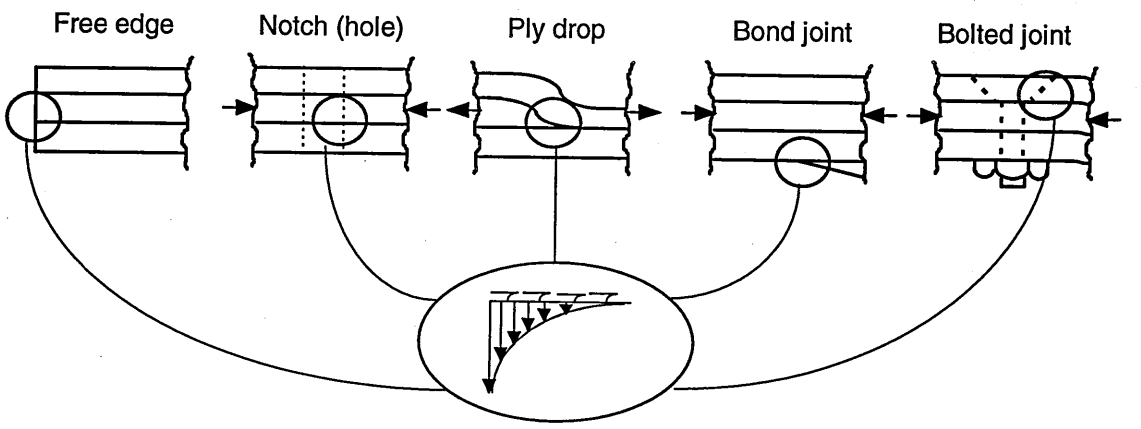

Figure 2.6. Common structural elements that generate interlaminar stress concentrations (after Wilkins et.al. 1982).

2.2 STATIC TENSILE FAILURE MECHANISMS

This section details the failure mechanisms and failure pattern of 0° and 90° unidirectional and cross-ply laminates subjected to static tensile loading. The current understanding of the overall behaviour is described followed by details of the investigations that highlight current understanding. Currently, there is much interest in the new breed of toughened resin matrix systems which delay first ply failure in laminated composites. Hence, the influence of matrix material on the properties of the laminates is also discussed.

2.2.1 0° unidirectional

In 0° unidirectional laminates, under monotonically increasing tensile loads, the failure initiates from the failure of the weakest fibre. Under increasing load, the fibre breaks can initiate matrix

cracks, interfacial debonding (as described in section 2.1.1) or more fibre breaks. Fibre breaks are most common in graphite epoxy composites. Tamuzs (1981) and Jamison (1985) have characterised fibre fracture rates for unidirectional carbon fibre composites subjected to tensile loading. Jamison (1985) measured the fibre fracture density of unidirectional samples subjected to various levels of tensile stress using scanning electron microscope. His results, the fibre fracture density Vs tensile stress are shown in Figure 2.7. Jamison (1985) also observed no sign of matrix damage in graphite/epoxy based UD laminates subjected even up to 105% of the UTS. The fibre breaks occur at different locations of the laminate. The final failure occurs when there are enough fibre breaks at one cross-section unable to support the applied load. This is the generalised failure process observed in unidirectional polymer composites.

The failure of a single fibre is governed by the statistical distribution of fibre strength as described in section 2.1.1. The tensile failure of composites is modelled using statistical models to predict tensile behaviour and strength. Application of fibre bundle statistical failure model to unidirectional composites was pioneered by Rosen (1964). Rosen modelled the tensile failure of unidirectional composites by assuming that the stress carried by the broken fibre is equally distributed to all its neighbours; the so called equal load sharing rule. However, this rule was found inappropriate for composites and it was thought then that in general, neighbours carry

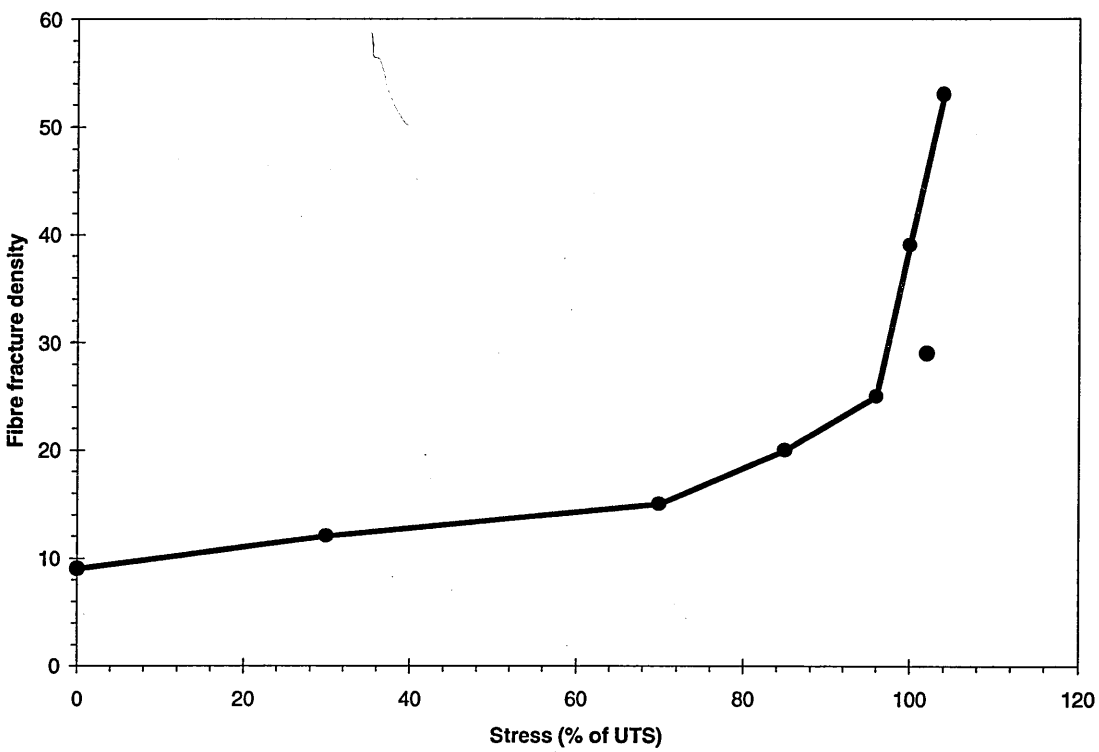

Figure 2.7. Fibre fracture density Vs tensile stress of unidirectional CFRP samples (Jamison 1985).

more of the redistributed stress than fibres that are further away from the broken site (Zweben 1968; Zweben and Rosen 1970). Later, more refined load sharing theories were proposed based on parameters such as the stress concentration and ineffective length (the length over which the broken fibre carries a reduced load), and are reviewed by Smith et al. (1983). These parameters have been investigated by many researchers (Cox 1952, Ochiai et al. 1991, Miwa and Endo 1994). However, the recent investigation by Nedele and Wisnom (1994) suggests that the stress concentration at fibre breaks plays a much smaller role in tensile failure than was previously thought. They suggest that a model based on the effect of the interaction of the fibre breaks at different positions along the length of the fibres can provide a realistic tensile strength prediction.

The commonly observed failure modes in a unidirectional laminate are shown in Figure 2.8 (Agarwal and Broutman 1990), and are as follows,

Brittle failure,

Brittle failure with fibre pullout and

Brittle failure with debonding and or matrix failure.

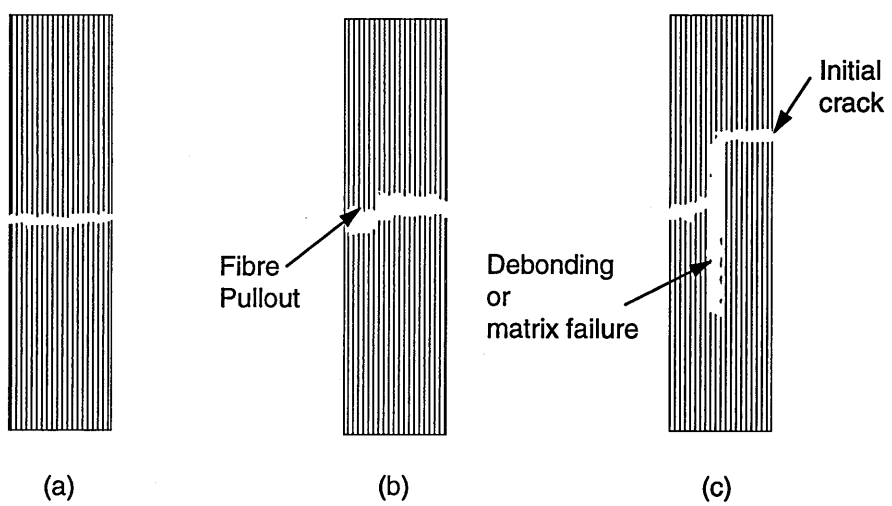

Figure 2.8. Failure modes of unidirectional composites subjected to tensile loading: (a) brittle failure, (b) brittle failure with fibre pullout and, (c) brittle failure with debonding and or matrix failure (redrawn after Agarwal and Broutman 1990).

2.2.2 90° unidirectional

In 90° laminates, the tensile behaviour is determined by the state of stress. This is the major condition that causes initiation of failure. The failure initiates at the fibre-matrix interface or in the matrix. The tensile strength of a 90° laminate is less than the matrix. This is due to the stress concentration effects of the fibre. The fibres act as stress raisers and are responsible for

the failure initiating at the interface or the matrix. The radial stress distribution around a fibre inclusion in a matrix is shown in Figure 2.9 (Schulte and Stinchcomb 1989). The general failure modes are matrix failure, interface failure or combination of both. If the fibres are weak in the transverse direction then the failure may be due to the failure of the fibres in the transverse direction.

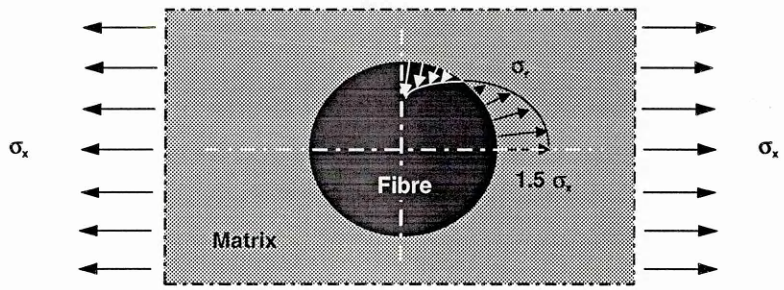

Figure 2.9. Radial stress distribution in the matrix around a cylindrical inclusion subjected to transverse tension (after Goodier 1933, redrawn from Schulte and Stinchcomb 1989).

Recently, O'Brien and Salpekar (1993) investigated the influence of material volume, i.e., specimen dimensions on the transverse tensile strength of graphite/epoxy composites. They have observed a decrease in transverse tensile strength with increase in material volume. They suggested that the static tensile strength results can be used to predict the matrix dominated failures in laminates with nonuniform tensile stress distributions.

2.2.3 Cross-ply

The failure mechanisms of cross-ply laminates under static tensile loading have been reviewed by Schulte and Stinchcomb (1989). In multidirectional laminates, the failure was found to initiate from the specimen free edge. Delaminations and transverse cracks are found to initiate at the free edge and then to develop into the interior. Fibre fractures initiated at the free edge are not propagated into the interior.

Ply failures initiate at the weakest ply, the so called 'first ply failure'. Matrix cracks develop in the 90° plies due to tensile loading because of the lower failure strain of these plies than the 0° plies (Reifsnider 1991). Matrix cracks developed in the 0° plies have been measured using the edge replication technique. The number of transverse cracks measured for three types of cross-ply laminate is shown in Figure 2.5.

Longitudinal cracks in cross-ply laminates are found to occur when the transverse tensile strain in the 0° plies exceeds the tensile fracture failure strain of a 90° unidirectional laminate. These

cracks have not been observed for carbon fibre composites before the final failure (Bailey et al. 1979). The final failure is due to failure of 0° plies. Fibre fractures initiate at the tip of the matrix crack of 90° layers. The fibre fractures are shown to follow a representative failure pattern as shown previously (Figure 2.3).

2.3 FATIGUE

A number of reviews have presented the state-of-the-art understanding of the fatigue damage mechanisms in composite materials (Harris 1977; Goetchius 1987; Reifsnider et al. 1983; Konur and Matthews 1989). Moreover, two recent books edited by Reifsnider (1991) and Talreja (1994) summarise the current understanding of fatigue and damage mechanics of composite materials, respectively. Recently, Konur and Matthews (1989) reviewed the effects of constituent materials on fatigue of unidirectional and cross-ply laminated composites.

Much of the earlier fatigue work is on glass fibre reinforced composites (Wierzbicki and Jones 1989). Research on the fatigue of so called advanced composites was started at the late 1960's after their introduction (Hwang and Han 1989).

2.3.1 Fatigue damage mechanisms (Unidirectional)

Research related to fatigue damage mechanisms of unidirectional composites has served as a basis for understanding complex fatigue behaviour. However, the literature on fatigue of unidirectional composites is less. Figure 2.10 shows the fatigue damage mechanisms of a typical unidirectional laminate subjected to longitudinal fatigue loading (Talreja 1981). The fatigue damage mechanisms of unidirectional laminate consist of fibre, matrix and interfacial damage (Talreja 1987).

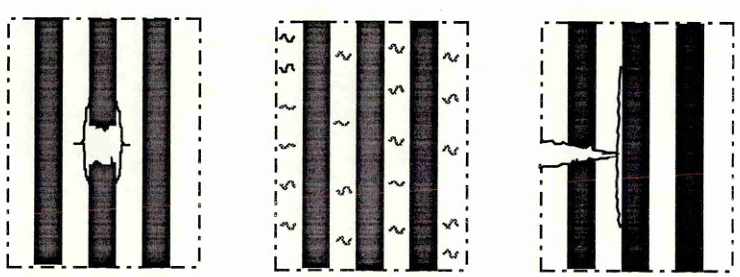

Figure 2.10. Fatigue damage mechanisms in unidirectional composites under longitudinal loading: (a) fibre breakage, interfacial debonding; (b) matrix cracking; (c) interfacial shear failure (redrawn after Talreja 1981).

Three different failure processes are possible depending on the type of damage initiation. It is suggested that fibre breakage in unidirectional composites occurs catastrophically where a local stress exceeds the strength of the weakest fibre (Sturgeon 1978, Talreja 1987, Wang et al. 1991). If the failure process initiates from fibre breakage, then an isolated fibre break can cause matrix cracking and or interfacial debonding due to shear-stress concentrations at the fibre-matrix interface near the broken fibre tip (Sturgeon 1978). The matrix crack can propagate perpendicular to the tensile loading and can initiate another fibre failure provided that the fibre-matrix interface is good. If the interface is poor, then debonding can occur along the fibre direction. The debond length depends on the shear strength of the interface. The initiation of fibre breakage in 0^0 laminates is considered as the major damage mechanism at strain levels close to the static failure strain (Bathias 1989b).

Crack initiation in a matrix is similar to metallic materials, i.e., matrix cracks initiate when the applied cyclic strain exceeds the fatigue failure strain of the matrix. The matrix undergoes a fatigue process of crack initiation and propagation and generates cracks normal to the longitudinal tensile stress. These cracks are randomly distributed and initially restricted by fibres. If the cyclic strain in the matrix is sufficiently low, the cracks would remain arrested by the fibres. When the local strain is higher than a certain threshold, the cracks break the fibres and propagate. In this progressive crack-growth mechanism, longitudinal splitting can occur if the interface is poor. Final failure occurs when the progressive crack growth mechanisms have generated a sufficiently large crack.

However, if the fibres are misaligned then other forms of damage initiation such as interface or matrix cracking parallel to the fibres is also possible (Wang et al. 1991b). This type of damage initiation in glass fibre reinforced composites has been shown to lead different types of failure process as shown below: (a) propagation of the crack in both longitudinal and thickness directions, forming longitudinal splitting along the fibre direction, (b) fracture of big bundles of fibres from splitting due to interaction between the interface crack and the fracture of misaligned fibres, (c) Initiation and rapid propagation of another crack starting from the fibre fracture, forming another split.

In a laminate all the above damage modes can operate simultaneously. In order to understand the interaction and sequence of the above damage modes with fatigue life, Talreja (1985b) proposed conceptual fatigue-life diagrams. These diagrams are basically strain-life diagrams as suggested originally by Boller (1969). A fatigue life diagram for a unidirectional laminate is shown in Figure 2.11 as proposed by Talreja. He has mapped the strain-life diagram into three regions. A horizontal scatter band region representing catastrophic failure centred about the

composite static failure strain, ε_c. Fibre breakage and the resulting interfacial debonding are the dominant damage mechanisms in this band. The next region is a sloping band representing progressive damage below the static failure strain. This region corresponds to matrix cracking and interfacial shear failure. The third region is below the sloping band and represents the fatigue strain limit of the matrix, ε_m.

One of the earliest investigations of the fatigue behaviour of unidirectional CFRP was carried out by Awerbuch and Hahn (1977). They suggested that the fatigue failure initiates mainly in the form of longitudinal splitting. Razvan and Reifsnider (1989) suggested that longitudinal splitting is the most important damage mode in unidirectional samples and upon initiation of longitudinal splitting, other factors such as fibre fracture and delamination become negligible and the final fracture is dictated by progression of the longitudinal splits. Recently, Curtis (1991a, 1991b) studied the tensile fatigue behaviour of five types of unidirectional laminates made of carbon and glass reinforced brittle and tough resin composites. He confirmed that tougher resin matrix composites are more fatigue sensitive. Based on his damage studies, he has suggested that longitudinal splitting is the primary damage growth mechanism in toughed resin composites. He also investigated the longitudinal split growth rate of samples with holes under tensile fatigue loading. His results confirmed that the tougher resin composites exhibit faster split growth rate than standard epoxy resin composites.

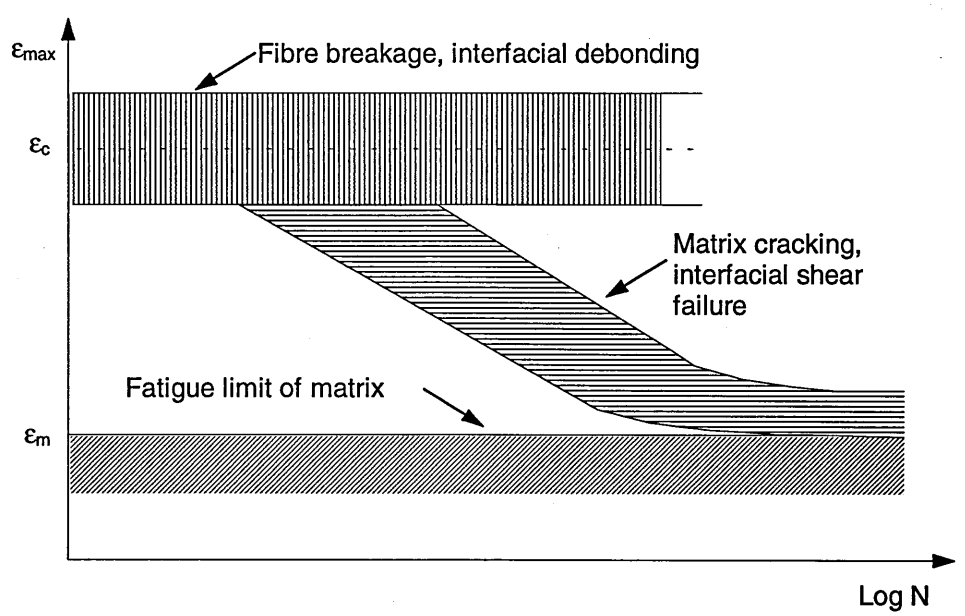

Figure 2.11. Schematic fatigue-life diagram for unidirectional composites under longitudinal loading (Talreja 1985).

2.3.2 Fatigue damage mechanisms (Cross-ply)

Fatigue damage mechanisms of cross-ply laminates are relatively well understood and documented. Fatigue damage mechanisms observed during tensile fatigue loading of CFRP cross-ply laminates have been summarised by Stinchcomb and Bakis (1991). The basic damage mechanisms are described as transverse ply cracks, edge and internal delamination, longitudinal cracks, interfacial debonding and fibre fracture (Reifsnider 1991, Talreja 1987, Poursartip and Ashby 1983).

Figure 2.12 shows a schematic of damage development in a cross-ply laminate under fatigue loading. Damage development involves three stages of specific damage mechanisms. The first stage consists of primary matrix cracking along the fibre direction in 90° plies. The density of matrix cracks increases until it attains a saturation level. This generic pattern of cracks was named as the Characteristic Damage State (CDS) first by Reifsnider (1977). Meanwhile matrix cracks parallel to the loading direction (longitudinal splitting) appear in the 0° plies (Stinchcomb and Bakis 1991). The occurrence of splitting constitutes the second damage accumulation mechanisms. The pattern of 0° and 90° plies initiates the formation of internal delamination at their intersection points. Internal delaminations are the third damage mechanism. The later

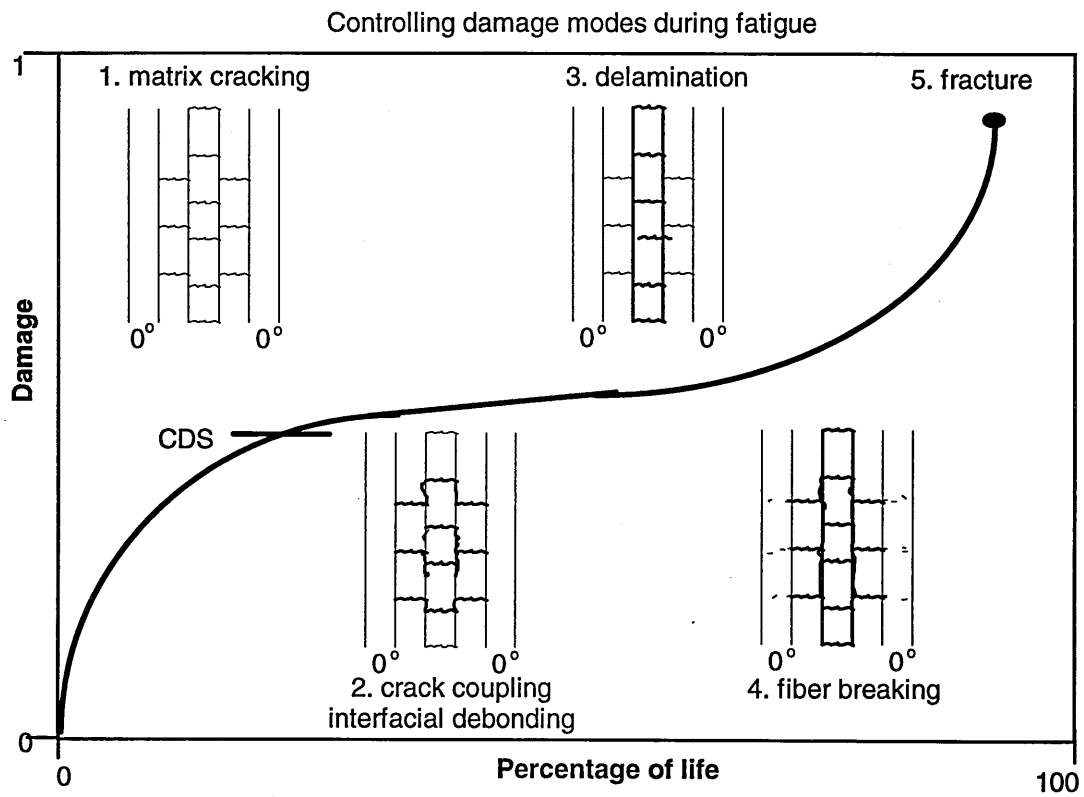

Figure 2.12. Development of damage in cross-ply composite laminates under fatigue loading (Redrawn after Reifsnider et.al. 1983).

stage of damage development is typified by rapidly increasing rate of all damage modes and this leads to final failure of the laminate (Talreja 1987). The terminal event usually consists of large scale fibre failure in the major load carrying plies (Jamison 1985).

Talreja (1987) has developed fatigue life diagrams for the cross-ply laminates, also. Recently Petitpas et al. (1989) have studied fatigue damage mechanisms with particular attention to decrease in modulus and the interaction between different types of damage. They observed that delamination was initiated from fibre break points and at the extremities of transverse cracks. They analysed the stress variation at this interface using the finite element method. They concluded that the damage will propagate in the transverse fracture extremity along the fibres by delamination and across the 0° layer by rupture of fibres. In another paper by Petitpas et al. (1990) a similar study was carried out on T300 and T400 fibre reinforced epoxy. They studied the stiffness reduction due to transverse ply cracking both experimentally and theoretically. They concluded that the reduction in stiffness is not only due to transverse ply cracks but also may be because of fibre breaks.

2.3.3 Factors influencing the fatigue behaviour

Results of fatigue testing are usually presented as a plot of applied stress Vs number of cycles, the so called S-N curve. For composite materials the S-N curve is influenced by various material and testing variables such as matrix material type, fibre type and properties, ply orientation, volume fraction, interface properties, type of loading, mean stress, frequency, environment and so on.

The factors influencing the fatigue life of composite materials have been studied and reviewed by many authors (e.g., Yang et al. 1981; Yang et al. 1983; Simonds et al. 1989; Konur and Matthews 1989). In the early 1970's investigations were carried out by several researchers into the effects of fibre properties on the fatigue performance (e.g., Owen 1974). More recently Curtis et al. (1986) studied the fatigue performance of different type of carbon fibres such as high strength, intermediate failure strain, high failure strain and intermediate modulus in a standard epoxy matrix. He concluded that fibre type has little effect on fatigue behaviour. However, he observed some slight shift of the S-N curve on the ordinate.

Razvan et al. (1992) investigated the effects of load train alignment on the fatigue failure characteristics of unidirectional graphite/epoxy composites. They showed that the fatigue life of misaligned samples was reduced drastically in comparison with the aligned samples. They also observed that the influence of load train misalignment is not as pronounced at higher stress levels than it is at lower stress levels.

The early work on the effect of matrix properties on fatigue behaviour of composites was carried out by Boller (1969). Curtis (1991a; 1991b) studied matrix effects on fatigue behaviour of different carbon fibres in different matrices (standard epoxy, toughened epoxy and thermoplastics). Curtis observed that toughened matrix carbon fibre composites had poorer fatigue performance than brittle matrices. Konur and Matthews (1989) in their reviews concluded that the influence of matrix properties such as toughness was not yet fully understood.

There is only limited information available on the effect of the interface on fatigue performance of composites. Owen (1970) studied the effect of surface treatment of carbon fibres on epoxy matrix composites. Curtis and Moore (1987), and Hahn (1979) studied the effects of the interface and concluded that a strong interface coupled with a strong matrix would lead to reduced fatigue performance.

Harris et al. (1990) studied the comparative behaviour of conventional carbon/epoxy (XAS/914) with intermediate modulus fibre reinforced tough resin (T800/6376) composites. They observed that the tensile fatigue behaviour conforms to single pattern. They studied the effect of R ratio and concluded that the T800/6376 laminate is superior in compression loading to XAS/914 laminates.

Henaff-Garding and Lafarie-Frenot (1991) have studied the influence on transverse ply cracking of the 90° layer thickness and loading amplitude. They observed that edge crack density increases with 90° layer thickness. Owen and Morris (1970) have indicated that CFRP does not show any significant temperature rise even at the high test frequency of 116 Hz.

2.4 DAMAGE MODELS

The objective of damage models is to represent and characterise damage mechanisms in composite materials. Damage models are then to be used in structural analysis procedures to provide a predictive tool for life prediction of structures under complex loading conditions. Different types of fatigue damage models are available in the literature based on various principles. The models based on first principles will be ideal. The available models are heavily based on empirical relations, experience and experimental data, and are aided by subdisciplines such as fracture mechanics and micromechanical formulation (Reifsnider 1991).

A detailed review of damage models for life prediction is given by Sendeckyi (1991). However he did not give much importance to damage models based on damage mechanics approaches.

Moreover, this approach provides an opportunity to model the damage as an internal variable and that can be measured non-destructively. This approach is relevant in the context of the present thesis, i.e., the electrical resistance may be incorporated as a damage parameter in these fatigue damage models. Therefore, fatigue damage models that are based on a damage mechanics approach are reviewed in the appendix A. This appendix also presents the details of a proposed fibre fracture based damage model.

2.5 SUMMARY

It is clear from the previous work that the major damage mechanisms of unidirectional laminates are fibre breakage and longitudinal splitting. However, it is not clear how the damage initiates and propagates. It appears that there is no detailed study on the effects of interfacial stress and the interface on splitting. In addition little is mentioned about final catastrophic failure.

The literature survey reveals that the influence of matrix properties such as toughness still has to be fully understood. Also, little information is available on the effects of the interface on fatigue damage mechanisms of both unidirectional and cross-ply laminates.

The failure processes proposed are in general based on post failure macro and micro level fractographic analysis. Very limited investigation is supported by online damage monitoring methods.

The damage mechanisms of composite materials are complex and depend on many material, load and environmental parameters. The generalised damage mechanisms may not be unique for all composites. It is necessary to develop a damage monitoring method that can define just the damage on the ordinate. That is, the complex damage mechanisms should be simplified to just one damage parameter.

3

ELECTRICAL RESISTIVITY MEASUREMENTS

This chapter is concerned with the literature survey of electrical resistivity measurements of carbon fibre reinforced composites (CFRP). In recent years, investigations have been made to use the electrical properties of CFRP as a tool to investigate the internal state of the structure. The Electrical Resistivity Measurement (ERM) technique is a relatively new technique, and there is only very limited research work on the use of electrical properties for damage monitoring of CFRP. ERM has great potential to be used as an in-service damage monitoring technique. The damage sensing and 'smart' capabilities have not been explored. It has not even been considered as a non-destructive testing technique. However, there is an extensive information available on the electrical properties of CFRP and its constituents, though studied in a different context to damage monitoring (Summerscales 1990).

This chapter is organised as follows. The physics of electrical conduction for metals, semiconductors and insulators is described in section 3.1. Physics of conduction mechanisms of graphite and polymers are given with special reference to carbon fibres and epoxy resin. Sections 3.2 and 3.3 detail the electrical resistivity measurements of carbon fibre and epoxy resin that are relevant to the resistivity measurement of CFRP. The structure, electrical properties, temperature dependent electrical properties, piezo-resistance behaviour of carbon

fibres, effects of additives and moisture in epoxy resin are described. The electrical resistivity measurements concerned with carbon/epoxy composites are presented in section 3.4. The electrical properties, electrode effects, simulation of damage and effects of mechanical loading are described. Section 3.5 presents the theoretical electrical models to predict the electrical properties of CFRP. The parallel resistance, mechanics of material, effective medium theory, lattice and finite element models are reviewed.

3.1 PHYSICS OF ELECTRICAL CONDUCTION

To use electrical properties as a tool to investigate the internal state of the material or structure, it is necessary to understand the fundamental physics of electrical conduction. This section is compiled from excellent sources of books on physics of electrical conduction and material science (e.g., Jones 1957; Ziman 1960, Blatt 1968; Saunders 1970; Schmitz 1965; Shackelford 1992), as one source is not enough to cover all the materials presented in this section.

Electrical resistivity is one of the fundamental physical properties of materials and is related to the atomic level. The electrical conduction in materials is due to individual atomic scale species called charge carriers. Electrons, electron holes and ions are the three main charge carriers. While the conduction in materials is due to the movement of charge carriers, the resistivity is due to the scattering of charge carries in crystal lattice, crystal imperfection, defects and grain boundaries.

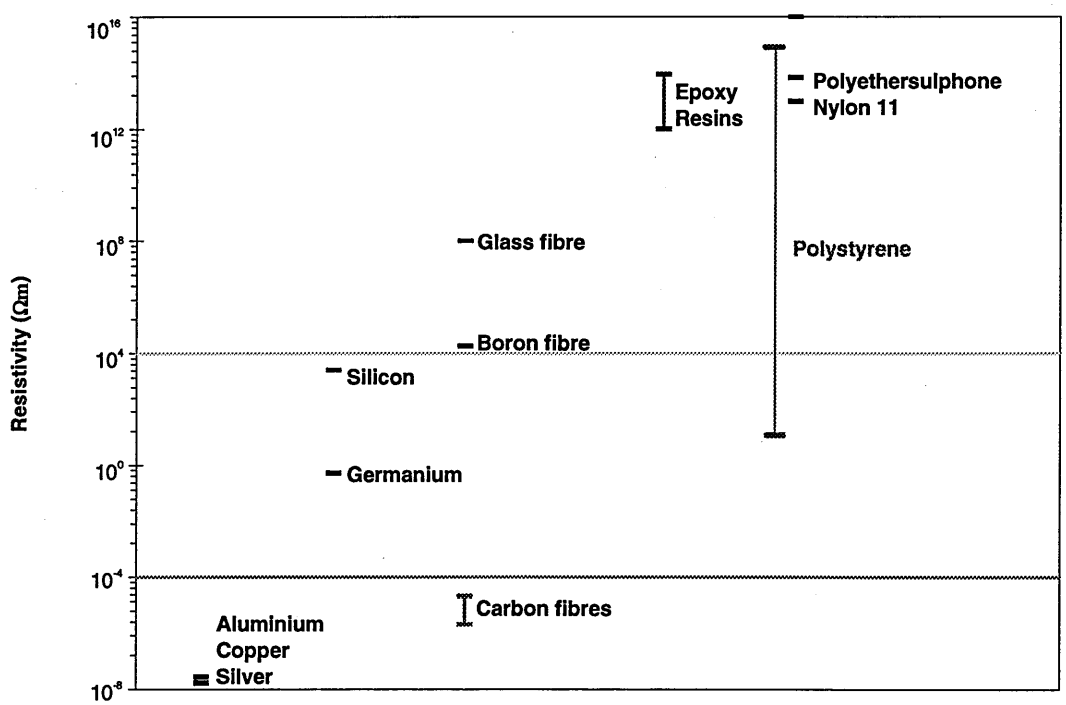

Figure 3.1. The resistivity plot.

The electrical conductivity or resistivity is one of the physical properties of materials that has a very wide range. The resistivity ranges from 10^{-6} Ωm for a conductor to 10^{20} Ωm for an insulator. The resistivity plot of various categories of materials is shown in Figure 3.1. This figure demonstrates the wide spectrum of resistivity of materials, and the resistivity of different types of carbon fibre and epoxy resin in comparison with other materials.

3.1.1 Electrical parameters

The elemental unit of electricity is the absolute charge on a single electron or proton. The commonly used unit of resistance is the ohm, which is the resistance of a conductor in which a potential difference of 1 volt causes a current flow of 1 ampere. Electrical resistance is the basic parameter generally measured by an electrical resistivity measurement technique. The resistivity, volume resistivity, surface resistivity, and their reciprocals' conductivity, volume conductivity and surface conductivity are derived from the basic parameter.

The resistance, *R*, is related to the magnitude of current flow, *I*, and voltage, *V*, of a circuit by Ohms law.

$$V = I R \qquad (3.1)$$

The resistance value depends on the specific sample geometry. So, the resistivity, independent of specimen geometry is defined as follows,

$$\rho = \frac{R A}{L} \qquad (3.2)$$

where, *A*, is the cross sectional area and, *L*, is the length of the sample.

In metals and semiconductors, the resistivity means the bulk resistivity of the sample. The resistivity measurements of an insulator with very high magnitude of resistivity can be influenced by the current flow along the surface and through the volume. So, care should be exercised when measuring the resistivity of an insulator. Volume resistivity is defined as the resistivity of the sample when the current flow is confined to the volume of the sample. Similarly, the surface resistivity is defined as the resistivity confined to the surface of the sample.

3.1.2 Conductivity equation

The conductivity of materials is determined by the number of charge carriers available for conduction and by the rate at which they move. The conductivity, σ is given by the following equation.

$$\sigma = n \mu q \qquad (3.3)$$

Where, *n*, is the number of charge carriers, μ, is the mobility of the charge carriers and, *q*, is the

charge in coulombs. The equation 2.3 is the general conduction equation. In metals the conduction is mainly due to electrons and hence the variables in the above equation can be substituted for the values of electrons.

If the conduction is due to two charge carriers as in semiconductors, the following equation can be used.

$$\sigma = n_n \mu_n q_n + n_p \mu_p q_p \qquad (3.4)$$

Where, subscripts' n and p denote the negative and positive charge carriers or electron and electron holes, respectively. In semiconductors both electron and electron hole take part in the conduction process.

The conduction in an insulator can be due electrons or ions. If the conduction is due to electrons the equation 3.3 can be used. However, if the conduction is due to ions the conductivity equation 3.5 can be used. This equation is known as the Einstein relation, originally proposed for crystal ionic conductivity (Blatt 1968).

$$\sigma = \frac{nq^2D}{kT} \qquad (3.5)$$

where, D, is the diffusion constant of mobile ions, k, is the Boltzmanns constant, and T, is the absolute temperature.

3.1.3 Band theory

Conduction mechanisms in materials are generally explained using band theory. The band theory provides with the background, with which the conduction mechanisms of the constituents of CFRP can be reasonably explained.

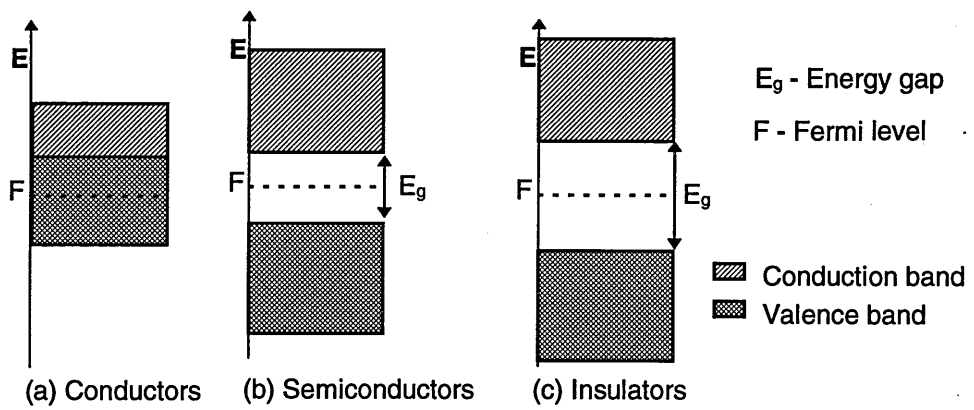

Figure 3.2. The band structure of materials.

The band theory of conduction was originally developed to explain the conduction mechanisms in solids. This is based on extending the models of bond between two atoms over a whole crystalline solid. The electron orbitals in a single atom have discrete energy levels. As these atoms are brought together to form a solid, the levels are broadened to bands that may overlap. The overlap of electron orbitals of atom produces high and low energy level bands. The lower energy band, filled with valence electrons, is known as valence band. The higher energy band is known as conduction band. The energy gap, E_g, between conduction band and valence band is known as the forbidden energy band. For electrical conduction in materials electrons are required to increase their energy to an energy level just above the Fermi level, E_F. The Fermi level is defined as the energy of the highest filled state in the energy band.

The nature of electrical properties is determined by the extent of the energy bands and the magnitude of the energy gap between them. The band structure and the Fermi level for the three main categories of materials are shown in Figure 3.2. In metals the energy gap is zero and the valence band is only partially filled (Figure 3.2 (a)). This means that there are more orbitals available for conduction. Metals are generally good conductors and the Fermi level is just above half way in the valence band at absolute zero temperature. In a semiconductor the energy gap is less than 2 eV. The Fermi level is between valence and conduction band (Figure 3.2 (b)). For electrical conduction the electrons are to be promoted to just above the Fermi level and into the conduction band. Thermal excitation can promote the electrons into the conduction band. This puts electrons in the conduction band and leaves electron holes in the valence band. In an insulator the energy gap is more than 2 eV (Figure 3.2 (c)). Since the energy gap is much larger, the electrons are not promoted into the conduction band by thermal excitation. The electronic conduction in an insulator is extremely low.

3.1.4 Temperature dependence

The conduction mechanism of materials can be understood better by studying the influence of temperature. Study of temperature dependent resistivity in materials can provide better information about the nature of electrical conduction in materials. The electrical classification of materials is based on temperature dependence of resistivity. For some materials, the electrical classification based on magnitude of resistivity can be misleading.

In metals the resistivity, ρ, increases quite linearly with temperature. Hence, a temperature coefficient of resistivity, α, can be defined. The resistivity equation for temperature dependence of metals is given below.

$$\rho = \rho_{rt} \left[1 + \alpha(T - T_{rt})\right] \qquad (3.6)$$

where, ρ_{rt}, is the room temperature resistivity, T, the temperature and, T_{rt}, the room temperature. The increase in resistivity with temperature in metals is due to decreases in electron mean free path with temperature. This increases the probability of electron collision with other electrons and the resistivity sources.

In semiconductors and insulators the resistivity decreases exponentially with increasing temperature. The resistivity dependence of temperature is given by the following equation.

$$\rho = \rho_o e^{\left(\frac{E_c}{kT}\right)} \qquad (3.7)$$

where, ρ_o, is a temperature independent constant, E_c, is the activation energy for the electrical conduction process, k, is Boltzmanns constant and, T, is the absolute temperature. In semiconductors the increase in temperature promotes additional electrons into the conduction band. These electrons leave holes or electron holes in the valence band that can also conduct. The number of charge carriers increases with temperature and hence the resistivity decrease exponentially with temperature.

3.1.5 Graphite and carbon

Study of the electrical conduction mechanism of graphite was pioneered by Kinchin (1953). Saunders (1970) reviewed the electrical transport properties of graphite and carbon. The electrical properties of graphite and carbon are anisotropic, i.e., the conductivity is different along and orthogonal to the layer axis (For a brief description of the structure of graphite and carbon fibres, refer section 3.2.1). Along the layer axis the electrical behaviour is like semi-metal, i.e., the properties are between metals and semiconductors. According to band theory, in a single crystal of graphite the energy gap overlaps and is 0.03 eV. This small overlap leaves a few electrons and electron holes for conduction, and hence graphite always conducts along the layer axis regardless of temperature. The conduction mechanism perpendicular to the layer axis is relatively complex. According to the magnitude of conductivity, perpendicular to the layer axis graphite can be classified as a semiconductor. The simplified band theory states that the conduction is due to hopping of charge carriers between the layer planes. Also, defects can play a critical role in electrical conduction perpendicular to the layer axis.

Different grades of carbon fibres are available and a general description of conduction mechanisms based on band theory would be futile. Mrozowski and his co-workers as reported by Robson et al. (1972) have made extensive studies on the effects of heat treatment temperature of soft carbon conductivity. This can be used to explain the general conduction mechanisms of carbon fibres, as the production route of carbon fibres also goes through these

heat treatment temperatures. Also, Robson et al. (1972) have suggested that these models are valid for polyacrylonitrile (PAN) based carbon fibres treated above 1750°C. The results of Mrozowski and his co-workers are shown in Figure 3.3. It is found that the energy gap decreased with increase in heat treatment temperature and then finally disappeared. The resistivity is also found to decrease drastically with heat treatment temperatures up to 1700°C and then more gradually decrease. Similar changes in resistivity are also observed in PAN based carbon fibres with heat treatment temperature (Konkin 1985). It is suggested that the band model shown in Figure 3.3 (d) and (e) are suitable for polycrystalline and well graphitised materials, respectively. (Saunders 1970; Robson et al. 1972).

3.1.6 Polymers and epoxy resin

The conduction mechanisms of polymers have not yet been studied in detail relative to metals and semiconductors. The recent investigations of conduction mechanisms of polymers are due to advances in conducting polymers (Przyluski 1991). A general description of electrical properties of polymers and conduction mechanisms can be found elsewhere, e.g., Seanor (1982). In general, polymers are insulators and of non-crystalline nature. The magnitude of conductivity is generally much lower. The available literature suggests that the conduction can be electronic and or ionic. Therefore the conduction mechanisms and the reasons for lower conductivity of polymers based on both electronic and ionic conduction mechanisms are given below.

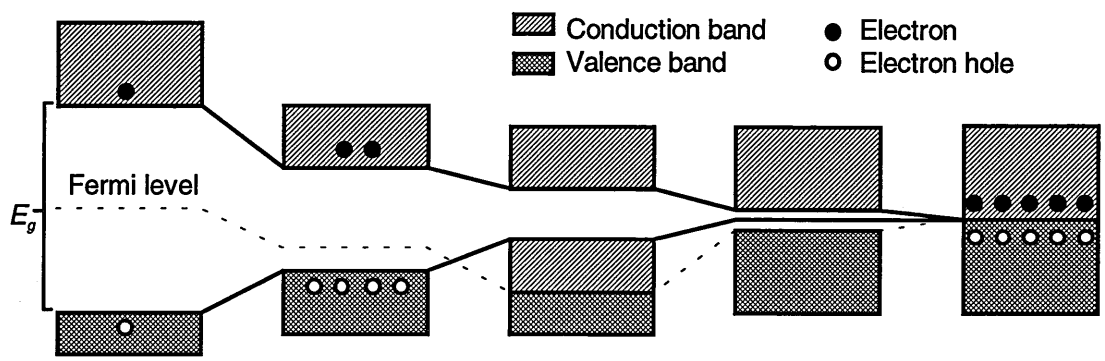

	(a) Molecular solid	(b) Raw coke	(c) Baked carbon calcined coke	(d) Polycrystalline graphite	(e) Natural Graphite
HTT	< 600°C	500° - 700°C	900° - 1700°C	> 2200°C	Natural
E_g	> 0.3 eV	0.5 - 0.2 eV	0.15 - 0.03 eV	< 0.01 eV	≤ 0.01 eV
ρ	> 10^3 Ωm	10^5 Ωm	5 x10^{-5} Ωm	≤ 10^{-5} Ωm	≤ 5 x10^{-7} Ωm

Figure 3.3. The band structure of carbons after different heat treatment temperature (Redrawn from Robson et al. 1972)

According to band theory, in an insulator there are very few free electrons available for electronic conduction. The energy band gap is also higher and is more than 2 eV. So, thermal excitation of electrons into the conduction band at reasonable temperatures is difficult, and hence the magnitude of conductivity is very low. Moreover, band theory only applies to a crystalline solid. The conduction mechanisms of non-crystalline materials such as polymers are explained using suitably modified band theory. It is suggested that noncrystalline materials will have similar band widths and energy gaps to their crystalline counterpart. However, it is found that the band edges become smeared out into the band gap and that the mobility becomes much slower. This disorder causes localised states, which act as traps or defects. These traps or defects delay the transit of charge carriers.

On the other hand, investigations of polymers such as epoxies suggests that the conduction is mainly ionic (Warfield 1965). The ions come from uncured monomers, additives and plasticisers. Continuous chains of these sources of ions may not be available and hence conduction may be due to hopping of charge carries. The mass of ions is much higher than the mass of electrons, and hence the mobility of charge carriers is slower (Blatt 1968). This results in a lower magnitude of conductivity of polymers. To the author's knowledge, the conduction mechanisms of epoxy resins are not available in the literature. The reason may be that epoxy resins are insulators with higher magnitudes of resistivity than that required for a general insulator. Also, it is difficult to measure the resistivity of insulators above 10^{16} Ωm (Kroschwitz 1988).

3.2 ERM OF FIBRES

The electrical properties of carbon fibre has been known for a long time. Edison's first use of carbon fibre in an electrical lamp, is a good example that demonstrates the electrical conductivity of carbon fibres. The recent electrical resistivity measurement of advanced carbon fibres can be found along with the invention and development of carbon fibre itself. Earlier resistivity measurements on carbon fibres correlated the electrical resistivity of carbon fibres with their structure and other mechanical properties. The structure, electrical properties, temperature dependence, piezo-resistance and other miscellaneous properties of carbon fibres are reviewed in this section.

3.2.1 The structure of carbon fibre

The structure of graphite crystals was first established by Bernel (1924). It consists of layers of carbon atoms as shown in Figure 3.4. In each layer, carbon atoms are bonded to their neighbours in a two-dimensional hexagonal network formation, 0.142 nm apart. These layers

are stacked with a separation of 0.335 nm. In graphite there is a definite relationship between the atoms in adjacent layers.

Many researchers used X-ray diffraction, transmission electron microscopy and field-ion-microscopy methods to study the structure of the carbon fibres (e.g., Reynolds 1973; Coyle and Wicks 1974, Johnson 1985). The atomic structure of carbon fibre consists of ribbon like layer planes. In general, these layer planes are several thousands of nm long and only 6 nm wide. Guigon et al. (1984) defined a basic structural unit (Figure 3.5) that appears as a wrinkled aromatic carbon layer sheet. This is characterised by three parameters, a length, thickness and a radius of curvature of wrinkles or folds. The three-dimensional representation of carbon fibre structure (Figure 3.6.) shows that numbers of ribbons group together to form a wrinkle micro fibril with high degree of preferred orientation parallel to fibre axis. The micro-fibrils branch and form needle shaped voids between the micro-fibrils.

The mechanical and electrical properties of carbon fibre depend on the structure of carbon fibre. There are three major structural parameters, orientation, crystallinity and defect content. In general, all these structural parameters affects the final properties of carbon fibre.

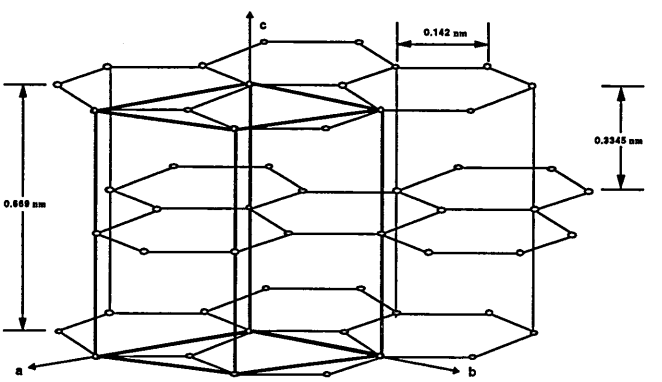

Figure 3.4. The graphite lattice structure (Delmonte 1981).

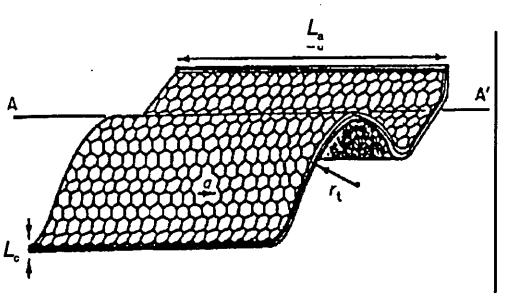

Figure 3.5. Schematic representation of basic structural unit of a carbon fibre (after Guigon et al. 1984).

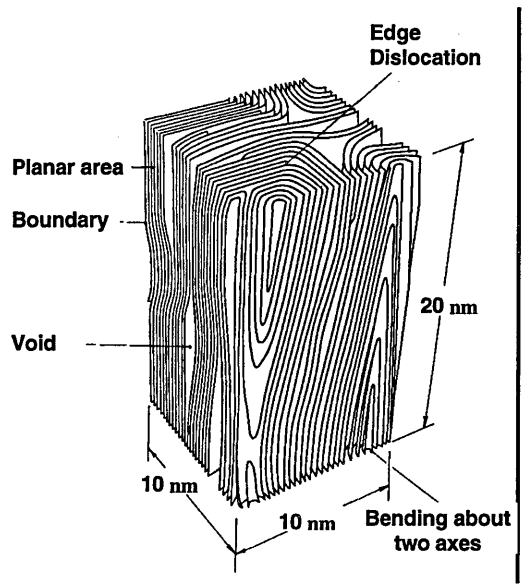

Figure 3.6. The schematic three-dimensional model of a carbon fibre (after Coyle and Wicks 1974).

3.2.2 Electrical resistivity

Shindo (1961) was the first to report the higher electrical resistivity of carbon fibre made from PAN precursor. He studied the change in resistivity of carbon fibre upon pyrolysis of a precursor. He reported that the resistivity changed from 5000 μΩm for fibres heated up to 700°C, to 20 μΩm after heating up to 1000°C. It was suggested that this change is due to carbonisation of the PAN precursor and the development of length and preferred orientation of crystallites. Watt and Johnson (1966) have also noted the higher resistivity of carbon fibres compared to that of single crystal graphite. It was suggested by them that the higher resistivity is due to the small crystallite size and predominant scattering effects of crystalline boundaries. Owston (1970) reported the resistivity of seven batches of carbon fibres heat treated at temperatures in the range of 1000 to 2500°C. The resistivity value ranged from 5.8 to 31 μΩm.

After the initial invention, investigations of the structure and the effects of processing variables of carbon fibres over the past thirty years lead to the development of carbon fibres with consistent physical properties (Lovell 1986). Now, there is a variety of carbon fibres available on the market with a wide range of properties. The resistivity varies over a wide range from above the precursor values to close to the value of single crystal graphite. The electrical resistivity of commercial carbon fibres is shown in Table 3.1. The electrical property of a single crystal graphite and bulk graphite is shown in Table 3.2. The resistivity of carbon fibres is determined by the precursor, manufacturing route and the heat treatment temperature. For commercial

PAN based fibres the resistivity ranges from 6 to 20 μΩm and for pitch based fibres the resistivity ranges from 2 to 14 μΩm. These values are comparable with the resistivity of bulk graphite, 6.97 μΩm. However, they are approximately 5 to 50 times higher than those of single crystal graphite.

Almost all the electrical resistivity measurement investigations on carbon fibres were concentrated mainly on longitudinal resistivity. To the author's knowledge, there are no investigations of transverse electrical resistivity of carbon fibres. The possible reason could be difficulties in making electrical contact on relatively small size samples with a diameter of 7 μm. However, there are limited investigations available on transverse electrical properties of single

Table 3.1. Electrical properties of carbon fibres.

Trade name/Grade	Type	Resistivity μΩm	Modulus GPa	References
Torayca T300	PAN	18.0	230	Lovell (1991)
Torayca T300J	PAN	20.0	230	Lovell (1991)
Celion GY-80	PAN	6.0	572	Lovell (1991)
Celion G50-300	PAN	10.0	358	Lovell (1991)
Celion G30-600	PAN	15.0	234	Lovell (1991)
Type I 303/B	PAN	8.5	319	Knibbs et al. (1971)
Type II 341/B	PAN	13.9	235	Knibbs et al. (1971)
P100	Pitch	2.5	690	Jaworske (1987)
Thornel P120S	Pitch	2.2	827	Lovell (1991)
Thornel P100S	Pitch	2.5	724	Lovell (1991)
Thornel P75S	Pitch	7.0	520	Lovell (1991)
Thornel P55S	Pitch	8.5	380	Lovell (1991)
Thornel P-25	Pitch	13.0	160	Lovell (1991)

Table 3.2. Electrical properties of single crystal graphite and bulk graphite.

Material	Longitudinal resistivity μΩm	Transverse resistivity μΩm	References
Graphite crystal	0.4 (∥ to layer planes)	40 to 30 000 (⊥r to layer planes)	Saunders (1970)
Bulk graphite	6.97 (∥ to grain direction)	21.87 (⊥r to grain direction)	Delmonte (1981)

crystal graphite (Saunders 1970). These investigations can provide the background with which the transverse properties of carbon fibres can be presumed. The transverse resistivity of bulk graphite is 20 μΩm and the anisotropic ratio is 4. The measured transverse resistivity of single crystal graphite ranges from 40 to 30000 μΩm. The anisotropy ratio of resistivity ranges from 10^2 to 10^5. From these values it can be postulated that the transverse resistivity values of carbon fibre can also have values ranging from 10^2 to 10^5 times higher than that of longitudinal resistivity. Similar derivation of transverse resistivity of carbon fibres from the transverse resistivity of CFRP is described in section 3.4.1.

The other electronic properties of carbon fibres such as the electron spin resonance, thermo electric power and magnetoresistance, and its correlation with structure and mechanical properties can be found else where, for example, the work of Robson et al. (1972), Dillon et al. (1989) and Bright and Singer (1979).

3.2.3 Dependence on temperature

The temperature range of interest is from room temperature to a maximum of 200 °C. This is the maximum operational temperature of CFRP, which is limited by the resin used. The studies on carbon fibre are at higher temperature often of the order of 1000 °C (Watt and Perov 1985).

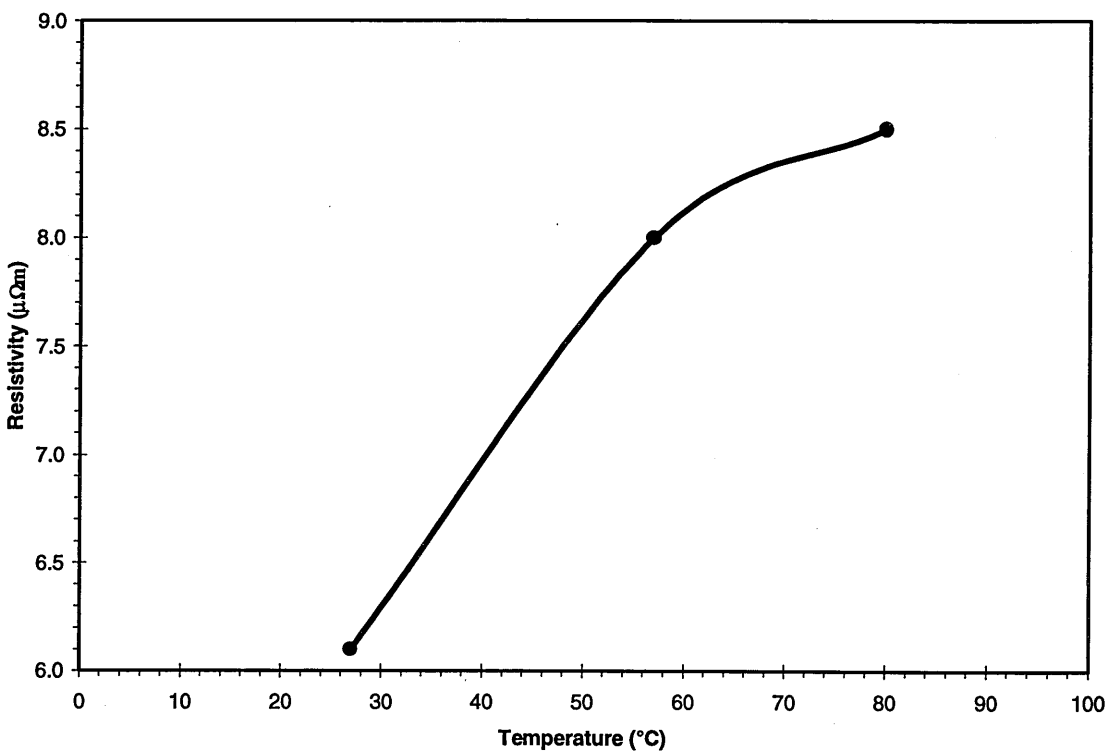

Figure 3.7. Temperature dependent resistivity of a typical carbon fibre (data from Yasin et al. 1987).

The objective of the temperature dependence studies was to understand the structure of the carbon fibre heat treated at various temperatures. In general, for a given heat treatment temperature the resistivity decreases with increase in temperature. This suggests that the behaviour of carbon fibres is like semiconductors. However, increase in resistivity with temperature and anomalies are also observed. The temperature dependence studies of carbon fibre with properties close to that one used in this investigation is shown in Figure 3.7. (Yashin et al. 1987). In this case, the resistivity increases with temperature.

3.2.4 Piezo-resistance

Piezo-resistance is defined as the change in electrical resistance with applied stress or strain. This effect is of great importance in the context of the present work. The piezo-resistance or, stress-strain behaviour of the carbon fibre should be understood first, as these can influence the resistivity measurements of CFRP to sense strain and or damage. Any anomalies in the carbon fibre can be expected to reflect in its composite.

The change in resistance due to applied stress or strain of carbon fibre was first reported by Conor and Owston (1969). Later Owston (1970) investigated in detail the piezo-resistance effects of seven batches of PAN based carbon fibres. He observed a linear increase in

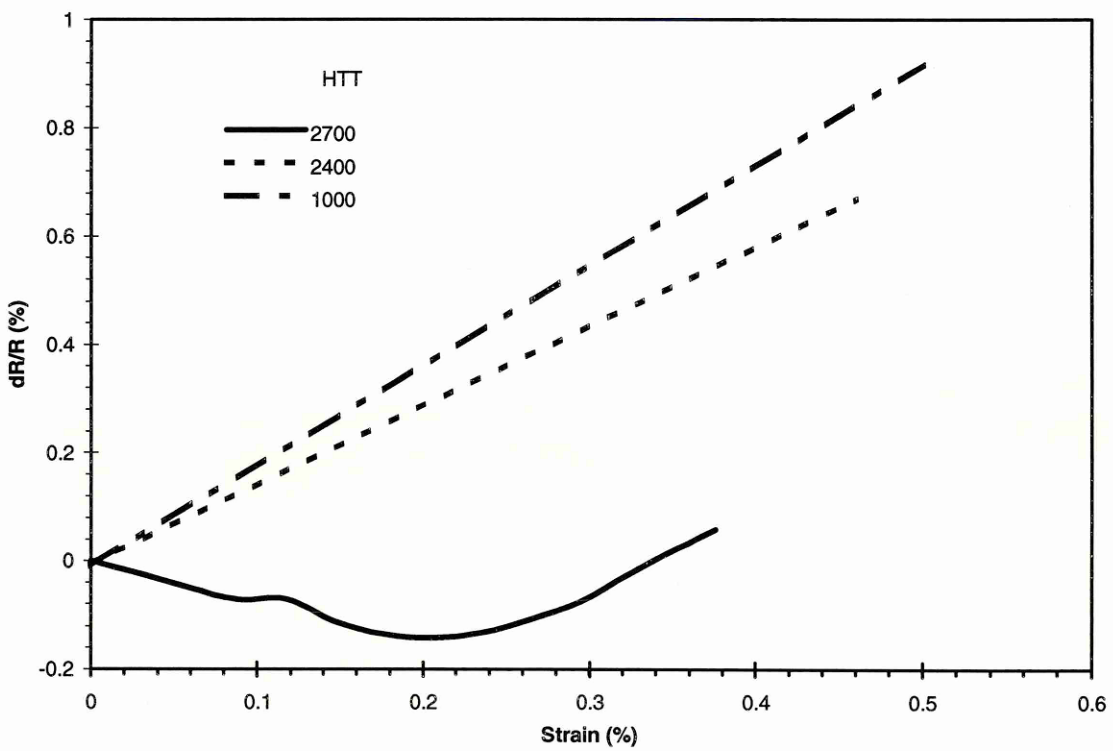

Figure 3.8. Piezoresistance behaviour of PAN based carbon fibres (Redrawn after Fischbach 1980).

resistance above 0.1% strain on most of the fibres. He also observed some initial non-linearity in some of the fibres at strain level below 0.1%. Owston suggested that the initial non-linearity and the change in resistance are due to variation in the contact resistance between the rope like fibril structure of carbon fibre and the contact.

Fischbach and his co-workers (Fischbach and Komaki 1977; Fischbach 1980) also studied the piezo-resistance of PAN, pitch and rayon based carbon fibres treated at various heat treatment temperatures. The results of PAN based carbon fibres are shown in Figure 3.8. In most of the fibres heat treated up to temperature 1000°C and 2400°C, they observed linear and positive increases in the ratio of change in resistance and resistance with strain. Fischbach also observed negative ratios at lower strains and positive at higher strains of carbon fibres treated at 2700°C. He suggested that this may be due to the dependence of carrier density and mobility on applied strain.

3.2.5 Resistivity and other properties

It has long been recognised that electrical resistivity measurements can give vital information about the structure of carbon fibre. Electrical resistivity measurements were used to study the structure changes occurring during production of carbon fibres from the pre cursor. Konkin (1985) reported the resistivity of carbon fibres as a function of heat treatment temperature. He has observed sharp decrease in resistivity with heat treatment temperature up to 1000-1100°C and then only slight change up to 3000°C. He commented that the sharp decrease in resistivity is sufficient proof of the aromatizatation of carbon and of the formation of the planes of graphite. A slow decrease in resistivity during graphitisation was suggested to indicate that the structure gradually becomes perfect.

Different types of carbon fibres are produced with a range of strength and stiffness by varying the heat treatment temperature. Heat treatment of carbon fibres is the principle process to obtain different strength and stiffness. The mechanical as well as the electrical properties are influenced by heat treatment temperature. Yashin et al. (1987) observed increase in electrical resistivity with elastic modulus of PAN based Celion 6000 carbon fibres. This behaviour was attributed to the reorientation of the c-axes of the graphite crystals during heat treatment. The relationship between resistivity and other mechanical properties are available in the literature (e.g., Watt and Perov 1985).

3.3 ERM OF EPOXY RESIN

The invention of bakelite and the disclosure of its dielectric property by Baekelund in 1907 (as

reported by Warfied 1965), can be considered as the first resistivity measurement on polymers. Though the history starts in 1907, there was no detailed investigation on this subject until 1940. After that the extensive use of polymers in structural applications and in composites, necessitated the need for such investigations. Electrical resistivity measurements of polymers were used to monitor the state of cure, degree of polymerisation, effects of additives and plasticisers, environmental effects and thermal ageing. The investigations of epoxy resin whose data influence electrical resistivity measurements of CFRP are described below.

3.3.1 Electrical properties

For reasons mentioned previously, the electrical resistivity properties of epoxy resin have not been studied in detail. The available investigations on epoxy resin are due to their use in advanced composites. These investigations were mainly to monitor the cure status. Limited investigations are available on the influence of the formulation, hardener and additives on the electrical properties of epoxy resin. The resistivity values of some of the commercial resin are shown in Table 3.4.

3.3.2 Effects of additives

Fuoss (1939) investigated the effects of internally or externally plasticised polymers. Plasticisers are added to lower the glass transition temperature and to make the solid more rubbery. In recent years, plasticisers are added to increase the toughness of brittle resin. Fuoss observed reduction in magnitude and the temperature dependence of resistivity of polymers with increases in plasticiser content. He suggests that the reduction is due the conductive nature of most of the plasticisers.

3.3.3 Temperature dependence

Polymers usually exhibit exponential decrease in resistivity with increase in temperature, see section 2.2.3. Warfield (1965) studied the temperature dependent resistivity of a number of resin systems including two epoxide systems. He observed non-linear decrease in resistivity with increase in temperature. He suggested that the deviation from linear behaviour is an

Table 3.3. Electrical properties of epoxy resin.

Type	Resistivity Ωm	References
MY750	$> 2.0 \times 10^{6}$	Knibbs et al. (1971)
HYSOL 4366	9.0×10^{13}	Dixon (1960)
HYSOL 4754	1.25×10^{12}	Dixon (1960)

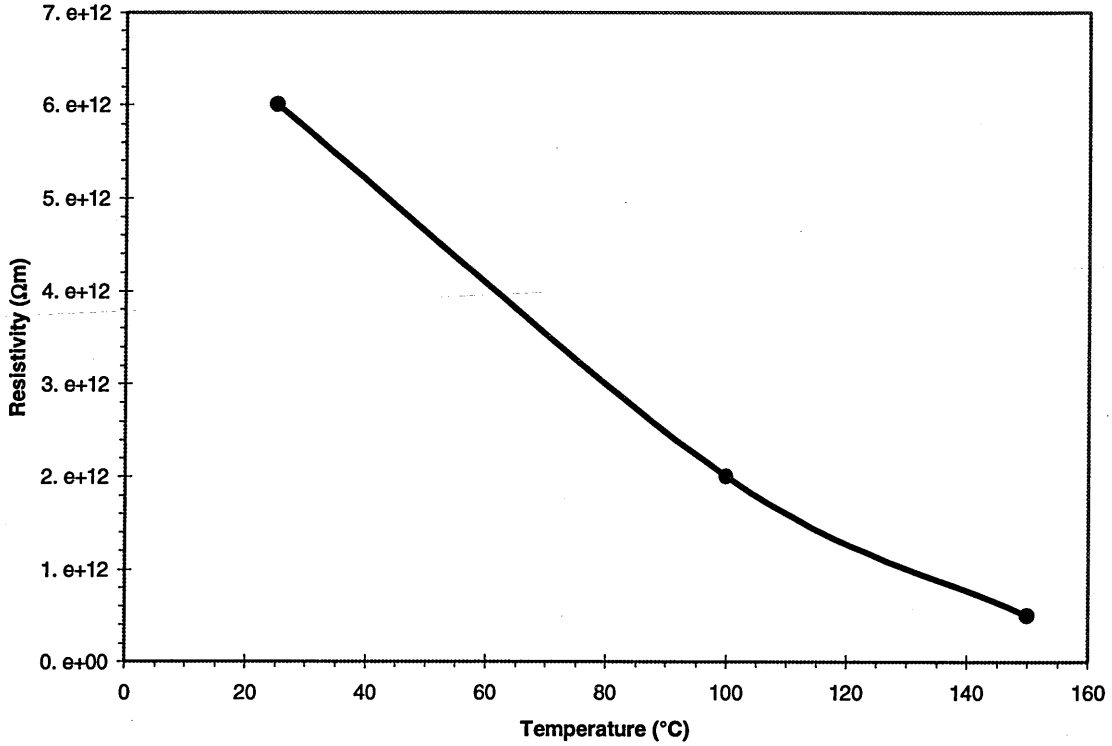

Figure 3.9. Temperature dependence of resistivity of a typical epoxy resin (data from Dixon 1960).

indication of the extent of plasticization. Also, he observed abrupt change in slope at glass transition temperature. He has commented that the activation energy for electrical conduction, which can be derived from temperature dependence plots, can be useful to compare the temperature dependence of resistivity of polymers.

3.3.4 Cure monitoring

Warfield and his co-workers in a series of papers reported the investigations of resistivity characterisation of cure status of thermoset polymers. Their results are summarised in a review by Warfield (1965) himself. In brief, he used electrical resistivity to study the rate and degree of polymerisation and estimation of microviscosity. He observed increased resistivity and electrical activation energy for highly cross linked polymers. He suggests that this information can be used to estimate the fundamental structural parameter such as microviscosity. He also proposed a relationship between rate of polymerisation and logarithmic change in resistivity with time as shown below.

$$\text{Rate of polymerisation} = \frac{[d \log \rho]}{dt}. \qquad (3.8)$$

He suggested that the resistivity changes are due to variations in the mobility of the current carriers caused by the progressive increase in the microviscosity of the system during polymerisation.

Martin (1977) discussed the effects of cure cycle variables such as the temperature, degree of polymerisation, viscosity and applied pressure on electrical resistivity. His discussion was based on data from an earlier experimental work. Magee and Rotariu as reported by Warfield (1965) have shown that during isothermal polymerisation of an epoxide polymer, the logarithm of the resistivity changed in proportion to the disappearance of the epoxide groups.

3.3.5 Moisture ingress

Recently, Singh et al. (1988) studied the effects of moisture on epoxy laminates. Their investigation was not on pure resin but on an epoxy laminate reinforced with glass fibre. However, this investigation can provide us with information on the dependence of resistivity on moisture content of epoxy resin. They observed an increase in conductance (decrease in resistance) with exposure time of samples exposed to different relative humidities. Also, they observed an increase in conductance for the same time of exposure with increase in relative humidity. They suggest that the increase may be due the increase in vapour pressure with relative humidity. The increase in conductivity with moisture content was attributed to the interaction of water molecules with epoxy resin. They also reported that the moisture effects on resistivity are reversible, i.e., no chemical change on sample.

3.4 ERM OF CARBON/EPOXY COMPOSITES

The available investigations of electrical resistivity measurement techniques to monitor damage non-destructively are mostly concentrated on delamination crack growth. There are also investigations to monitor other damage mechanisms such as fibre breaks. The available investigations are more demonstrations than detailed investigations. More recent investigations have used electrical resistivity to monitor impact damage and high strain rate loading effects.

The electrical resistivity measurements concerned with damage sensing in CFRP laminates may be limited. However, the electrical properties of CFRP are relatively well known and available in the literature , though studied in a different context than damage monitoring.

3.4.1 Resistivity measurements

There are a myriad of investigations available on electrical properties of CFRP, which are very useful for the present investigation and the future of the electrical resistivity measurement technique. The earlier investigations on electrical properties of CFRP have been made because of the following reasons.

- Use of CFRP in electrical applications,
- To improve the electromagnetic shielding capabilities of CFRP (Gajda 1978; Volpe 1980),

- To understand the effects of lightning strikes (Kung and Amason 1978),
- Interest in conductive fibre filled conductive polymers (Przyluski 1991),
- Effects of carbon fibre released from damaged CFRP structures on electronic equipments (Delmonte 1981; Springer 1979) and
- Use of carbon fibre as warfare materials to disable electronic equipments.

The resistivity of unidirectional CFRP, as reported by earlier investigators is shown in Table 3.4. As expected the resistivity is different in the longitudinal and transverse fibre directions. The reported longitudinal resistivity ranges from 5 to 150 μΩm. The transverse resistivity ranges from approximately 2000 to 600 000 μΩm. The anisotropic ratio, the ratio of transverse resistivity to longitudinal resistivity, also ranges from 20 to 4000. In general, the electrical properties of CFRP are determined by the properties of the constituents, the fibre and matrix and its volume fraction. Other factors that can influence the electrical properties are specimen dimensions and electrode type.

The longitudinal properties are fibre dominated, therefore, the variation in longitudinal resistivity may be due to the properties of the fibre used. For example, the resistivity of PAN based carbon fibre (Type I) reinforced CFRP is approximately three times higher than that of pitch based carbon fibre (P100) reinforced CFRP for a same volume fraction, (see Table 3.4). This

Table 3.4. Electrical resistivity of unidirectional CFRP reported by previous investigators.

Sl. No.	Material Type Fibre /Resin	V_f %	Longitudinal resistivity ρ_L, μΩm	Transverse resistivity ρ_T, μΩm	ρ_T/ρ_L,	References
1	Type I/Epoxy	40	22	4347	198	Knibbs et al. (1971)
2	Type I/Epoxy	50	19	2703	142	Knibbs et al. (1971)
3	Type I/Epoxy	60	15	1961	131	Knibbs et al. (1971)
4	Type II/Epoxy	40	40	8333	208	Knibbs et al. (1971)
5	Type II/Epoxy	50	29	3226	111	Knibbs et al. (1971)
6	Type II/Epoxy	60	24	1724	72	Knibbs et al. (1971)
7	CF/Epoxy	40	110	15000	136	Owston (1973)
8	CF/Epoxy	50	90	5000	56	Owston (1973)
9	CF/Epoxy	60	75	2000	27	Owston (1973)
10	CF/Epoxy	70	65	1500	23	Owston (1973)
11	CF/Epoxy	65	25	10000	400	Lodge (1982)
12	P100/Epoxy	63	5	5280	1056	Jworske (1987)
13	XAS/Epoxy	65	154	600000	3896	Kaddour (1984)

variation in resistivity can be directly related to the fibre properties. The longitudinal resistivity ratio for type I and P100 fibre is 3.4, (refer Table 3.1 on electrical properties of carbon fibre). Similarly, comparison of type I and type II carbon fibres and their composite results in a figure of approximately 0.6 times. This suggests that the longitudinal properties of CFRP are mainly determined by the fibre properties.

Similar comparison of the effects of fibre properties on transverse electrical properties of CFRP can not be made at present be made, as the transverse properties of carbon fibre are not available. However, with the available results on the transverse resistivity of CFRP, it can be suggested that the transverse electrical properties of CFRP of pitch based carbon fibre is higher than that of PAN based carbon fibres. If we assume a fibre dominant property, then we can suggest that the transverse electrical resistivity of pitch based fibres is higher than that of PAN based fibres. The higher degree of graphite alignment in pitch based carbon fibre may be responsible for this higher resistivity (Saunders 1970).

It was observed by many researchers that longitudinal and transverse electrical resistivity decreases with increase in fibre volume fraction (see Table 3.4). The increase in volume fraction increases the number of fibres available for electrical conduction and hence, decreases the resistivity. This effect is very prominent for both longitudinal and transverse resistivity.

The electrical properties in the through thickness direction were measured by Lodge (1982). The through thickness and transverse resistivity are expected to be same, because unidirectional CFRPs are transversely isotropic. However, Lodge reported a through thickness resistivity of 2500 $\mu\Omega m$, which is 2.5 times higher than the transverse resistivity. This suggests that the through thickness and transverse properties of CFRP are different. It was commented by Lodge that the higher through thickness resistivity may be due to increase in resin content or on the other hand reduction in the fibre distribution between the laminate plies.

The resistivity of unidirectional CFRP as a function of fibre orientation angle was measured by Knibbs and Morris (1974), Tse et al. (1981) and, Belani and Broutman (1978). Knibbs and Morris observed a linear increase in resistivity with the square of the secant of fibre orientation angle. They observed at 90° fibre orientation angle (transverse resistivity), a ten percent higher resistivity than other fibre orientation angles. Belani and Broutman used a single sample to study the effects of fibre orientation on resistivity. They measured the resistance between two electrodes on a single sample at different locations. Their measurement was not really representative of the effects of fibre orientation. However, that was one of the earlier investigations and gave some idea about the resistivity changes with fibre orientation. Tse et al.

studied the effects of sample dimension also, on the electrical resistivity of samples with different fibre orientation angles. They observed a nonlinear decrease in conductivity with fibre orientation angle. They also reported that increase in resistance with increases in length of samples with a constant width deviated from linear behaviour. They suggested that wide, short samples should be used for measuring conductivity to confine the applied field to the direction of resistivity measurement.

3.4.2 Electrode effects

Resistivity is generally measured by passing a constant current or voltage into the sample and monitoring the potential or current, respectively. This requires electrodes to be attached to the specimen to allow the current to flow in and out of the sample. In an isotropic material the current flow is essentially same in all directions and the electrical properties are homogeneous. Therefore the electrodes do not play a critical role in measuring the resistivity of isotropic specimens. However, CFRP is anisotropic and the current flow depends on the fibre orientation. Therefore when measuring resistivity of CFRP it should be ensured that the measured resistivity is due to the current flow in the required direction. Also, it is essential to make sure that the measured resistivity is due to the material and is not influenced by the electrode. If the measured resistivity is significantly influenced by the resistivity of electrode then necessary corrections have to be made to account for the electrode resistivity.

All the researchers who have measured the electrical resistivity of CFRP reported difficulties in making proper electrodes. For example, Knibbs and Morris (1974) reported that their accuracy of resistivity measurement are ± 7%, because of the difficulties in making proper electrodes. The fabrication of electrodes involves two major steps, one to expose the carbon fibres and the other to attach measuring leads or strips to the exposed area. The methods employed to expose the carbon fibres and the electrode types used by the previous investigators are described below.

- Knibbs and Morris (1974) polished the specimen edges using diamond powder. Their electrode involves a mercury bath at each end of the polished specimens.
- Belani and Broutman (1978) polished the electrode area on a grinding wheel and then coated the area with silver paint. They then used metal clamps to inject current into the sample.
- Bull et al. (1981) exposed the carbon fibres by polishing in stages, first using a medium-fine grade glass paper and then using a fine grade carborundum paper. They copper coated the exposed surface using direct electroplating and electroless plating methods.
- The method used by Tse et al. (1981) is different from that used by other investigators.

First, like the others they sanded the surface, they then attached a thin layer of indium by ultrasonic soldering. The current and potential leads were then again attached to the indium.

- Robinson (1987) and Rask and Robinson (1988) used silver paint to attach brass strips to the sample. They did not mention about surface preparation. They covered the electrode area with an epoxy resin coating to protect the electrodes.
- Jaworske et al. (1987) sanded the surface and then used wire wrapped pinch clamps.
- Schulte and Baron (1989) polished the electrode area using 3μ aluminium oxide powder. The copper strips soldered with measuring leads were then attached to the sample using silver paint.
- Gaier et al. (1991) suggested that sand blasting can damage fibres and hence just used silver paint.
- Fischer and Arendts (1993) coated the electrode area with silver paint and then attached the wires using metal clamps.
- Williamson et al. (1994) and Kemp (1994) lightly grit blasted the electrode area and then attached the enamelled copper strips using silver paint.
- Finally, Kaddour et al. (1994) abraded the electrode area with emery paper and then glued silver plates using silver paint.
-

Invariably, all the researchers used some form of abrasion to expose the carbon fibres. The effectiveness of abrasion as against just an ordinary saw cut on the measured electrical resistivity is not reported. The influence of electrodes on measured electrical resistivity and the magnitude of the electrode resistivity are also not reported. The good quality of the electrode, in the first instance, is that it should be ohmic, that means the current should flow freely in and out of the sample without any perturbation. Investigations are not available to prove that the electrodes are ohmic.

3.4.3 Simulation of damage

Damage such as fibre breaks and crack growth were simulated by many researchers to demonstrate that the electrical resistivity measurement technique can be used to monitor damage. These simulation studies were also used to establish base line experimental data and to gain some knowledge about the expected experimental results, prior to subjecting the sample to mechanical loading. Prabhakaran (1989) simulated crack growth by cutting a compact tensile specimen sample across the width. Schulte and Baron (1989) simulated fibre breaks on a unidirectional specimen by cutting across the width of the sample. Both observed increases in resistance with depth of cut. These simulation studies proved that the damage can be

measured using electrical resistivity measurement.

More recently, Kemp (1994) simulated fibre breaks by drilling a hole and damage growth by cutting the sample on a cross-ply laminate. He used a network of sensors to map the change in potential distribution due the effects of damage. He observed a notable change in voltage distribution for the drilled hole and also an increase in potential distribution with increase in slot length. From these results, he suggested that the detection limit of electrical resistivity measurement technique is a function of damage and electrode spacing.

3.4.4 Effects of mechanical loading

The available investigations of the effects of mechanical loading on electrical resistivity of CFRP are concentrated more on delamination crack growth studies. Therefore delamination crack growth studies are described in a separate section. The investigations on using electrical resistivity measurement to characterise damage during static and fatigue loading conditions are described in the following paragraphs.

Robinson (1987) and Rask and Robinson (1988) studied the electrical resistance of unidirectional carbon composite as an indicator of strain in undamaged composites and as an indicator of fibre breaks in damaged composites. Their specimen consists of two strips of CFRP separated and insulated at the middle by a strip of GFRP. They studied and reported the strain response and the strain sensitivity of the above specimens using a three-point bend test. They observed that the change in resistance up to a certain strain level is reversible in a cyclic testing. They detected fibre breaks by increasing the strain levels and by observing irreversible changes in the resistance.

Schulte and Baron (1989) studied the effects of mechanical loading in detail. They studied the dependence of electrical resistivity on temperature and cross sectional area in an unloaded specimen. They studied the electrical resistivity response of a unidirectional sample due to static tensile loading. They found a linear change in resistivity up to 0.7% strain and nonlinear after 0.7% strain. Above 1.2% strain they observed stepwise increases in resistance and suggested that this was due to fibre fracture. They studied resistivity response of a cross ply sample under fatigue loading conditions by varying fatigue load levels at different stages of life and have observed increases in resistance at initial life and at different stress levels. They reported that erratic increases in resistance occurs only during fibre breaks. Also during the fatigue life they observed a reduction in resistance and explained that this was due to increases in temperature. In their temperature dependence study, they observed a decrease in resistance due to increase in temperature.

Recently, Kaddour et al. (1994) used ERM to detect failure in balanced angle-ply CFRP under high strain rate tensile testing. They applied this technique to monitor the expansion of CFRP tubes subjected to internal explosive loading and compared the results to conventional strain gauge measurements. They suggested that the ERM is a very useful tool to detect and monitor the onset of damage growth. From their experimental results, they suggested that matrix cracks can also be detected using ERM.

More recently, Williamson et al. (1994) and Kemp (1994) used ERM to detect effects of impact damage on a crossply laminate. They used both a.c and d.c resistivity measurement techniques. They attached a network of electrodes on one side of the laminate to form a 6X6 square arrangement. The current was injected through four electrodes located at the central edge of the four sides. They compared the potential distribution before and after impact damage and observed an increase in potential distribution with increase in level of impact damage. The results were presented as surface plots of potential difference. They reported that the potential difference plot superimposed over a c-scan showed clearly the correlation between damage and potential change. They concluded that the initial measurements are very promising for the future development.

3.4.5 Delamination crack growth

Prabhakaran (1990) used the electrical resistance method to measure crack growth under static and fatigue loading conditions using a compact tensile specimen. Also, he proposed that composite materials can be modelled as a bridge of resistors connected in parallel. He applied this model to compare his experimental results on specimens made up of laminates with different orientation of plies. He found that the theoretical results show the same trend but it deviates from the experimental results. The reason is that the off axis plies cannot be modelled as above. The off-axis plies should be modelled by giving appropriate consideration to the transverse conductivity. However his model provides a basic concept with which the off-axis laminates can be modelled.

Almost at the same time Moriya and Endo (1990) studied crack growth measurements on double cantilever beam (DCB) specimens made from unidirectional and crossply laminates. They glued eleven pairs of electrodes to the top and bottom of the sample. The first pair of electrodes were used as current input leads. The other pairs were used to monitor the potential. They observed a linear increase in resistance with increase in crack length on both unidirectional and crossply samples. In crossply samples the crack inserted on the midplane at the 90/90 interface suddenly jumped to the 0/90 interface and was shown as a transition region on the linear electrical resistivity change. From their results they suggest that the sensitivity

decreases as the electrode is set away from the delaminated region. They also modelled the transverse conductivity and the delamination crack growth using a random network model and a finite element model, described in section 2.6.2. They observed excellent correlation between experimental and numerical results.

Recently, Fischer and Arendts (1993) used ERM to study the temperature dependence of fracture toughness of CFRP using DCB specimens. Basically, ERM was used to measure the crack growth and the subsequent results to calculate the fracture toughness in the temperature range of -55°C to 120°C. They reported that the crack growth measured by ERM were in excellent agreement with optical and analytical methods.

3.4.6 Environmental effects

There are few investigations available in the literature on the dependence of environmental effects such as moisture absorption and temperature on electrical resistivity. In general, it has been found that transverse properties are more significantly influenced by environmental effects than longitudinal properties.

Belani and Broutman (1978) investigated the effects of moisture absorption on resistivity of CFRP. They measured the longitudinal and transverse resistivity of specimens exposed to different level of moisture. They observed no increase in longitudinal resistance with increase in moisture content. It was suggested by them that the moisture absorbed by resin or the interface did not affect significantly the longitudinal resistance. However, they observed up to 50% increase in transverse resistance and suggested that this is due to an increase in fibre to fibre contact pressure in the transverse direction.

3.4.7 Summary

Though there are myriad of investigations on the resistivity of CFRP, the effects of specimen size and the reasons for the wide variation in reported resistivity are not fully investigated. Despite the fact that the electrodes are an important part of electrical resistivity measurement, they are the least studied. The effect of electrodes on the measured resistivity, methods to obtain proper ohmic contacts, influence of the electrodes on damage monitoring are the major areas to be addressed. The literature survey reveals that crack growth can be measured. Limited amounts of initial work on the detection of fatigue damage such as fibre breaks, is available. Most of the research work is on crack growth measurements. The significance of resistivity change with respect to damage is not explained. In general, it has been demonstrated that ERM can be used to monitor damage, but no investigations are available to quantify

damage. Detailed studies to understand the fatigue damage mechanisms like fibre breaks, matrix cracks and transverse splitting by electrical resistivity measurements are not available.

3.5 ELECTRICAL CONDUCTION MODELS

Electrical models have been developed to predict the resistance of composite materials. These models can then be used to predict the effect of damage on resistivity. The ultimate aim is to predict the electrical response of composite structures due to mechanical loading and or damage. The electrical modelling of composite materials is not straight forward due to its anisotropic and non-homogeneous properties. The available models are derived from mechanics of materials and electrical circuit analysis methods.

3.5.1 Longitudinal conduction

Longitudinal conduction in unidirectional CFRP is fibre dominated. The conduction is mainly due to carbon fibres. The resin, in general does not play a critical role. However if the resin is filled with conductive filler or additives, it can play a role in longitudinal conduction. The longitudinal properties are relatively simple and can be predicted using rule of mixtures and the parallel resistance model, as described below.

3.5.1.1 Parallel resistance model

The current flow along the fibre direction can be modelled by considering the fibres as electrical resistors connected in parallel. In the parallel resistance model it is assumed that the conducting carbon fibres are surrounded by insulating matrix materials. The carbon fibres are connected at the ends to the electrodes to measure the electrical resistance. This forms a parallel arrangement of all the carbon fibres bridged by the two edges. The resistance of the composite, R_c, is simply the resistance of fibres divided by total number of fibres.

$$R_c = \frac{R_f}{N} \qquad (3.9)$$

Where, R_f, is the resistance of a single fibre, N, is the total number of fibres. The detailed derivation of parallel resistance model is described in section 5.1.

Liebmann and Miller (1963) used the parallel resistance model to predict the longitudinal electrical properties of two phase solids, the single crystal rods of Sb in a matrix of single crystal InSb. Prabhakaran (1990) proposed that the CFRP laminates can be modelled using a parallel resistance approach. However, he applied this model to simulate crack growth behaviour in compact tensile specimens made of multidirectional laminate as stated previously in section 3.4.5. The parallel resistance model is not suitable for multidirectional laminates.

3.5.1.2 Mechanics of materials approach

In general the properties of the composites are average of the properties of the constituents, the so called 'property averaging' or 'rule of mixtures' (Jones 1975). This can be used to calculate the effective properties of the composites. For two phase material systems, the longitudinal resistivity, ρ_c, can be calculated by knowing the properties of the individual phases and the fibre volume fraction, V_f, as shown below:

$$\frac{1}{\rho_c} = \frac{1}{\rho_f} V_f + \frac{1}{\rho_m}(1 - V_f) \qquad (3.10)$$

where, ρ_f, is the fibre resistivity and, ρ_m, is the matrix resistivity. The details are described in section 5.1.

Knibbs et al. (1971) used the rule of mixtures to predict longitudinal electrical properties of unidirectional CFRP. They observed that the rule of mixture prediction is 5% lower than the experimentally measured resistivity. They suggested that this may be due to misorientation of fibres. It is the author's opinion that this is highly unlikely, the major reason may be due the electrode (see chapter 5 and chapter 7).

3.5.2 Transverse conduction

The transverse resistivity, i.e., the resistance to the current flow orthogonal to the fibre direction is a relatively complex process. This is an important factor in characterisation of electrical properties and use of electrical resistivity measurements as a damage monitoring technique. The modelling of the transverse conduction process is also a relatively complex process. Effective medium theory, percolation theory and finite element based models have been used to study transverse conductivity.

3.5.2.1 Effective medium theory

Effective medium theory was first introduced in of classical theory of conduction of mixtures to calculate the conductivity of two or more phases by Bruggeman (1935). Kerner (1956) extended the effective medium theory to composite materials. The effective medium theory states that the average effects of random resistors may be represented by an effective medium. This is defined as the medium in which the effects of external fields applied to a random resistor network are assumed to be equal to internal fields (Miller 1969). The mathematical details of effective medium theory can be found in the literature (Kerner 1956a, 1956b; Hashin 1968).

Effective medium theory is generally used to predict the lower and upper bounds of electrical

conductivity. These models do not take into account the contact between fibres. In theory, the transverse conductivity of a composite laminate reinforced with fibre insulated by a matrix is zero. However, the measured transverse electrical conductivity of CFRP is non-zero (see Table 3.4). The fibre to fibre contact is an important parameter in transverse conductivity. Effective medium theory fails to predict transverse conductivity and percolation processes in CFRP. This is due to the larger mismatch between conductivity of the individual phases (conductive fibre and the insulating matrix) (Ueda and Taya 1986). Hence, effective medium theories without modifications are not suitable for predicting the electrical properties of CFRP. However, this theory provides a strong mathematical background with which future models can be built by giving appropriate consideration to the fibre to fibre contact.

3.5.2.2 Lattice model

In CFRP, the transverse electrical conduction is due to conduction through the carbon fibres distributed randomly in the composite. That is, the conduction is due current flow along random electrical networks. The electrical conductivity of random resistor networks has been studied as an idealised lattice conduction model (Kirkpatrick 1973). The insulator to conductor transition of random resistor network is known as the percolation phenomenon. The percolation model in general is defined as the collection of points distributed in space and certain pairs of which are said to be adjacent or linked. These models are applied to solve many engineering problems and hence there is an extensive literature on this subject, for example, Essam (1980).

Percolation theories have been applied to composite materials to study the conductivity behaviour. These models are often called random resistor network models. Figure 3.10 illustrates the percolation phenomenon in composite materials. The effect of fibre volume fraction on composite electrical conductivity is studied using site and bond percolation models (Ruschau and Newnham 1992). 'Site' percolation assumes that lattice sites are randomly filled until a continuous linkage is formed and adjacent filled sites are assumed to be conducting. 'Bond' percolation assumes that the lattice sites are filled but the adjacent sites do not necessarily form a continuous linkage, but rather are randomly connected. Percolation theory is more critical for short fibre reinforced and particulate composites, therefore, extensive information is available in the literature (Boissonade et al. 1983; Ueda and Taya 1986; Carmona 1989; Bridge 1989).

The random resistor network models applied to continuous fibre reinforced composites, essentially uses a square or hexagonal lattice fibre arrangement. The fibres are assumed to be of circular cross section. A random number generator routine is generally employed to fill the fibre lattices. The details of random number routine are not provided. The fibre to fibre contact

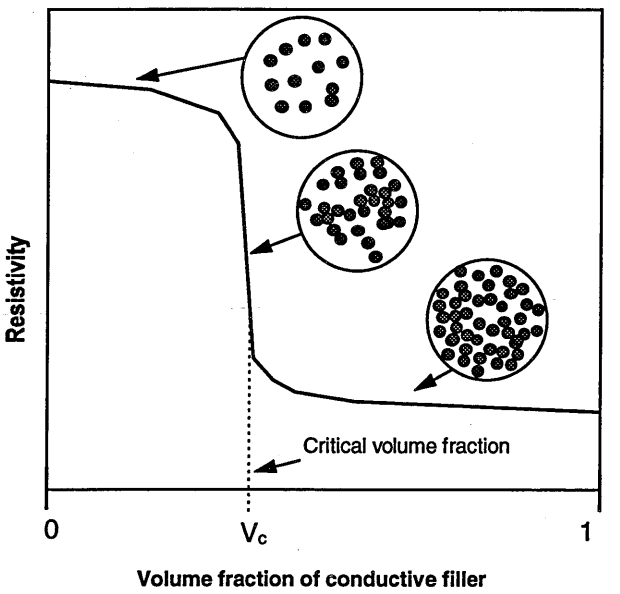

Figure 3.10. Percolation theory as applied to composites (Ruschau and Newnham 1992).

conductance is assumed to be constant. In a square lattice, a site filled with a fibre makes a maximum of four contacts with neighbouring filled sites. Similarly a hexagonal lattice makes a maximum of six contacts. The details of lattice models that are of present interest are as follows.

Joy and Strider (1979), and Joy et al. (1980) studied the conduction and percolation phenomena of single ply unidirectional composites. They have used both square and hexagonal arrangements of fibres to calculate the effect of lattice thickness on the critical fibre fractions for percolation. Both models suggest that the transverse electrical conductivity of single ply unidirectional composite should increase with decrease in thickness.

Li et al. (1982) studied the lattice conductivity at various fibre fractions and lattice thickness values using square and hexagonal lattice models. Good agreement was observed between experimental results and the dependence of thickness on conductivity. Monte Carlo lattice conductivity calculations are also reported.

Tse et al. (1981) presented a theoretical treatment based on Kirkpatrick's (1973) random resistor network model. Theoretically the transverse conductivity is zero, because the epoxy resin is a non-conductor. They assumed that the transverse conductivity is a result of touching fibres due to an irregular arrangement. The possible transverse conductance values were determined from the number of fibre contacts in a given sample thickness. The fibre contacts

are assumed to be distributed according to the binomial probability law. They presented detailed comparison of the predictions of this theory with experimental results.

Recently, Moriya and Endo (1990) used lattice models to study transverse conductivity. They have used square and hexagonal lattice to form the random resistor network. The potential distribution of every fibre site and the overall conductivity were obtained by solving Kirchhoff's equations for this random resistor network model. They used this model to explain the resistance changes due to delamination crack growth.

3.5.2.3 Finite element model

The electrical conduction behaviour can be modelled using finite element method also. If we assume that the electrical behaviour of CFRP on a macroscopic scale is homogenous then the electrical conduction behaviour can be modelled as an electrical field problem. The formulation of a physical problems governed by 'quasi harmonic' equations such as the electrical potential distribution can be found elsewhere (e.g., Zienkiewich and Taylor 1989).

Moriya and Endo (1990) modelled the transverse conduction behaviour using finite element method. Based on their lattice model results, they assumed that transverse conductivity was homogeneous and could be formulated as orthotropic field problem. They have shown that the crack growth predicted using the finite element model agrees well with lattice model results.

3.5.3 Summary

The longitudinal properties of unidirectional composite materials can be predicted using a `rule of mixtures' or parallel resistance model. Transverse properties are not in general predicted accurately by this method. The effective medium theory is not suitable for predicting the electrical properties of composites. However, it is useful for prediction of the upper and lower bounds. Lattice models can explain the percolation phenomenon observed in conductive composites. All the researches agrees that the confinement of fibres to square or hexagonal arrangement is a simplification of the real fibre distribution. The lattice models are shown to predict the thickness dependent resistivity of CFRP laminas.

Most of the models deal with the percolation phenomena. The volume fraction of the laminates used in this investigation and in practical structural applications is around 0.6. At this volume fraction, the composites are generally above the percolation threshold. Moreover, a relatively good source of experimental information on the electrical properties is available. So, the present models are not of much use to the present application.

A good model should be able to predict the three dimensional electrical behaviour as well as the effects of damage and environmental effects. Limited investigations are available which report damage simulation. There is only one lattice model that deals with damage simulation.

The effects of damage in real structures is three dimensional in nature. So, it is necessary to have three dimensional models to simulate the effects of damage. To the author's knowledge, there is no model at present that is capable of predicting the effect of damage in three dimensions.

PART II

EXPERIMENTAL AND THEORETICAL WORK

4

MATERIALS AND METHODS

This chapter is concerned with the materials, specimen fabrication, experimental setup and test programme. The electrical conduction mechanisms should be understood first to exploit the potential of electrical resistivity measurement technique. This requires resistivity measurements of CFRP samples with different widths, lengths and thicknesses together with temperature dependent investigations. Extensive experimental tests are needed to investigate the static and fatigue damage mechanisms of CFRP. This chapter describes the test details to establish the electrical properties and to investigate the electrical conduction mechanisms. This chapter also presents details of test programmes to investigate the behaviour and electrical response of unidirectional and cross-ply samples under static and fatigue loading conditions.

This chapter is organised as follows: The properties of carbon fibre are described in section 4.1. Similarly, the epoxy resin and conductive adhesive details are described in section 4.2 and 4.3, respectively. The laminate fabrication methods are presented in section 4.4. This section also includes the quality control test details of the laminates. The specimen design details including tabs and electrodes are described in section 4.5. The experimental setup details are given in section 4.6. Section 4.7 describes the details of static and fatigue test programme. This section also includes the test programme used for characterising electrical properties.

4.1 THE CARBON FIBRES

Carbon fibres have been in use since the time of Edison as mentioned previously. However, the origin of high strength and high modulus carbon fibres can be found in the 1960's, for example, the published work of Shindo (1961) and Watt et al. (1966). Since then, carbon fibres have become the predominant reinforcement for advanced composite structures. The origin and development of carbon fibres from Edison's time to the present can be found else where. Delmonte's (1981) book is a good source of information, which includes all the patents and papers on carbon fibre.

Carbon fibre is produced by the controlled oxidation and carbonisation of precursors in the fibre form. Polyacrylonitrile (PAN), cellulose and pitch, are the three major precursors. PAN is most commonly used and it has very high carbon content. Different grades of carbon fibres are produced by varying the heat treatment temperature. The fibre is then treated with suitable sizing agents for ease of handling and for better bonding with matrix materials.

Various types of carbon fibres are available commercially. The recent grouping of carbon fibres is based on modulus range (Lovell 1988), as follows,

Ultra high modulus (UHM - Greater than 440 GPa)
High modulus (HM - 320 to 440 GPa)
intermediate modulus (IM - 265 to 320 GPa) and
Standard modulus (SM - less than 265 GPa).

The fibre used in this investigation is carbon Torayca T300. As regards the modulus and strength, T300 belongs to the standard modulus and high strength (HS) type, respectively. The properties of carbon T300 fibre are shown in Table 4.1

Table 4.1. Properties of Torayca T300 carbon fibre.
(Source: Manufacturers data sheet Torayca)

Properties	ll to fibre axis
Tensile Modulus (GPa)	230.00
Tensile Strength (MPa)	3530.00
Elongation (%)	1.50
Resistivity (μΩm)	18.00
Thermal conductivity (W/mK)	6.50
Coefficient of thermal expansion (10^{-6}/°C)	-0.70
Specific heat (cal/g °C)	0.17
Density (g/cm^3)	1.75

4.2 THE EPOXY MATRIX

The so called standard epoxy, diglycidyl ethers of bisphenol A, were developed in the late 40's. Epoxy based resin systems have been widely used for a long time in the aerospace industry due to their high heat resistance, environmental stability and wetablity with advanced fibres. Epoxies are versatile two part resin systems. Plasticisers, flexiblisers, dilutents and fillers are added to the resin system to modify the properties. Background information on the available materials and systems can be found in standard hand books on epoxy resins. Lee's (1967) book on epoxy resins is a good source of information. The resins used in this investigation are Epoxy-914 and Epoxy-920. The properties of the epoxy resins are shown in Table 4.2.

4.2.1 Epoxy-914

Epoxy-914 is a modified epoxy resin system with a high operational temperature. It is one of the resin systems most widely used in structural applications. The characteristics of 914 as described by the manufacturer are, high melt viscosity giving easy processing characteristics, latitude for medium or high-pressure laminating and moulding processes, medium tack level giving excellent drape characteristics and longer shelf life. Epoxy-914 is a mixed tetra and tri functional epoxy polymer, dicyandiamide (DICY) hardner and polyethersulphone (PES) viscosity modifier system.

4.2.2 Epoxy-920

Epoxy-920 is one of toughest epoxy based resin systems. The characteristics of epoxy-920 as described by the manufacturer are, impact resistance, good hostile environment resistance and flexible cure cycle. The details of constituents are not available in the open literature. However,

Table 4.2. Properties of epoxy resin .
(Source: F914 Characterisation report- Dr. M Fischer - Ciba Marly)

Properties /Materials	Epoxy -914	Epoxy-920
Tensile modulus (GPa)	3.90	3.76
Tensile strength (MPa)	48.00	34.90
Failure strain (%)	1.50	8.40
Poisson's ratio	0.41	0.39
Compression yield strength (MPa)	177.00	289.00
Fracture toughness- K_{Ic} (MPa $m^{1/2}$)	0.70	1.41
Fracture toughness- G_{Ic} (J/m^2)	103.00	462.00
Glass transition temperature (°C)	190.00	107.00
Cured density (g/cm^3)	1.29	1.21

It was reported by Jaussaud (1992) that epoxy-920 contains thermoplastic particle for toughness enhancement.

4.3 CONDUCTIVE ADHESIVE

The purpose of conductive adhesive is two fold, one is to form an ohmic contact with carbon fibres and the other is to have good adhesive properties. Electrically conducting adhesives are generally made by mixing conductive filler particles in a general adhesive. The details of electrode materials used for the investigations of the influence of the electrode on resistivity is described in chapter 6. The details of adhesives used for bonding electrodes for resistivity measurements and fatigue and static damage characterisation are described below. The electrical and mechanical properties of the adhesives used in this investigation are given in Table 4.3.

4.3.1 Silver loaded epoxy adhesive

The conductive silver epoxy adhesive (IONACURE 650) is a two component pure silver filled epoxy adhesive. It is available from RS components ltd. IONACURE combines the adhesive properties of the epoxy and the electrical properties of pure silver. The chemical composition of epoxy in IONACURE is based on a diepoxide resin of Bisphenol A and a polymide hardener. The silver loaded epoxy adhesive was primary adhesive used to bond the electrodes of specimen used in mechanical loading.

4.3.2 Silver paint

Silver paint is pre silver filled electrically conductive acrylic paint. The formulation is based on cello-solve acetate, Xylene, silver pigments and methyl methacrylate. It is good conductor, however the adhesive properties are relatively poor. Electrodes made using silver paint adhesive could be satisfactory for steady state measurements. In static and fatigue loading situations, the electrode failed before the sample. It is easy to use and bonds well with CFRP, however the bonding with copper is poor. Due to its low viscosity it was difficult to apply on both surfaces, it generally has the tendency to flow out of the bonding area and so leads to the

Table 4.3. Properties of conductive adhesives.
(source: RS components, Chemence data sheet)

	Silver Epoxy	Silver Paint
Resistivity (μΩm)	5	1
Joint Strength (MPa)	0.7 to 1.4	-
Working temperature (°C)	-60 to 175	-50 to 150

formation of voids. It can be a good electrode on an exposed surface, because it sets by solvent evaporation. However, application of silver paint as adhesive between two parts, may result in poor contact.

4.4 LAMINATE FABRICATION

The combination of carbon fibre and epoxy matrix is widely used in advanced structural applications, since 1970. Two resin systems, brittle (epoxy-914) and tough (epoxy-920) reinforced with Torayca-T300 carbon fibre were used in this investigation. An important link in combining the fibre and matrix in laminate production is prepregs. The above combinations are available as prepregs 914C-TS(6K)5-34% (Fibredux-914) and 920CX-TS-133-42% (Fibredux-920) respectively from Ciba-Geigy.

The laminates were fabricated using the prepregs. The prepreg was cut to the required dimensions and laid up to the required stacking sequences using hand lay-up technique. The stacked laminate was then vacuum bagged and cured in an autoclave using the optimum cure cycle recommended by the manufacturer. The components of the autoclave curing process is shown in Figure 4.1. The technical details of the autoclave curing process can be found elsewhere (Purslow and Childs 1986). Three major types of laminates with stacking sequences as shown in Table 4.4 were made.

The unidirectional and cross-ply CFRP laminates were made for mechanical testing and resistivity measurements. The cross-ply GFRP was made to use as tabs for the specimens and to insulate the specimen from the grips during testing. Initial laminate for the tabs was 2 mm thickness. The tapering was made by machining after fabrication. To avoid the machining costs and defects associated with machining, a 3 mm thick laminate was made with built in taper. Special tooling was made to make the GFRP laminate with taper. Additional unidirectional laminates with artificial flaws such as fibre breaks, delaminations, resin rich areas and foreign inclusions were made for the ultrasonic studies.

4.4.1 Fibre volume fraction

The Fibredux-920 prepreg was supplied with fibre volume fraction less than Fibredux-914 prepreg. For comparison of fatigue and electrical behaviour, the volume fraction should be the same. Investigations were carried out on the 920 prepreg to establish how to remove excess resin. Six laminates were made with different peel plies to assesses the effectiveness of resin removal. After fabrication, the amount of resin removed was calculated by weighing the resin in

the peel ply. The laminates were also examined microscopically to asses the quality of the laminate and the fibre distribution.

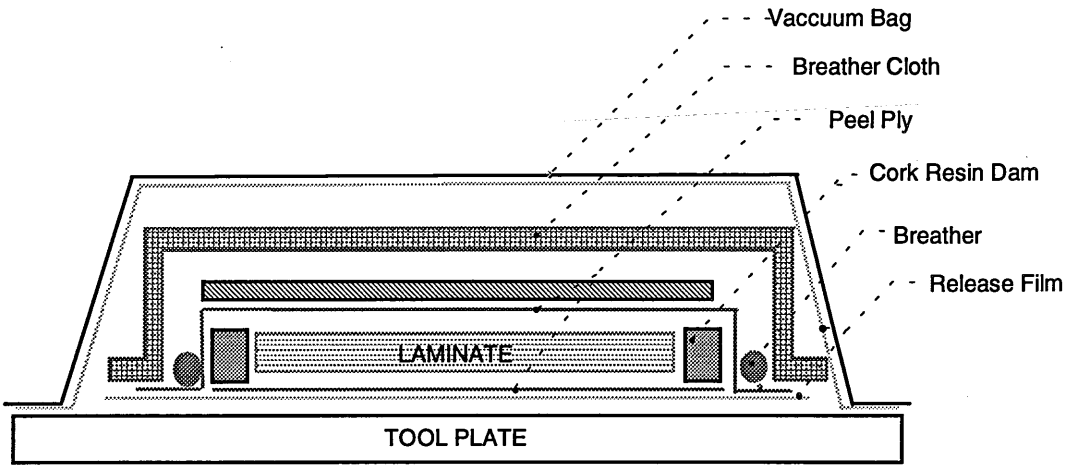

Figure 4.1. Components of autoclave curing.

Table 4.4. Types of laminate fabrication.

Sl. No.	Type	Materials	Stacking Sequence
1	Unidirectional	T300/Epoxy 914	$[0]_{16}$, $[0]_1$
2	Unidirectional	T300/Epoxy 920	$[0]_{16}$, $[0]_1$
3	Cross ply	T300/Epoxy 914	$[0,90]_{4s}$, $[0,90]_{6s}$
4	Cross ply	E-glass/Epoxy 913	$[0,90]_{4s}$, $[0,90]_{6s}$

The fibre volume fraction was calculated using image analysis and thickness measurement methods. For image analysis 10 samples were cut from representative parts of the laminate. The samples were then polished and analysed using an image analyser. The fibre volume fraction was then calculated at ten different random locations on each sample. Thickness measurement methods were also used to find the fibre volume fraction. Based on these results, the laminates of Fibredux-920 prepreg were fabricated using polypropylene peel ply to yield a volume fraction close to 0.60. The nominal fibre volume fraction of all the laminates used in this investigation is 0.60.

4.4.2 Quality control

Fatigue testing usually requires a large number of specimens. Approximately two hundred samples were prepared for fatigue and static testing alone in this investigation. This requires fabrication of laminates in batches. The quality of the laminates should be consistent for reliable and repeatable test results. The laminates should also be free of any manufacturing defects. It is a necessity to check the quality of the laminates. Various quality control test methods are available for assessing the quality of CFRP laminates. In this investigation ultrasonic C-scan and interlaminar shear strength tests were used.

4.4.2.1 Ultrasonic scanning

All the laminates were scanned using the ultrasonic C-scan technique in pulse-echo immersion mode using the double transmission technique (for a brief introduction refer section 4.6.10). The laminates were scanned to asses the manufacturing quality of the laminates and to detect any manufacturing defects such as foreign inclusions, delamination and voids. An ultrasonic immersion tank using aluminium sheets was fabricated to accommodate the specimens in the immersion tank and to provide a coupling medium. Initially the laminates with artificial defects were scanned to select a suitable ultrasonic probe, frequency and scanning method to characterise different type of manufacturing defects. Defects such as delaminations and resin rich areas were successfully detected. Fibre breaks were detected using an ultrasonic backscattering technique. The laminates scanned showed high quality of manufacturing. There were no ultrasonically detectable defects in the laminates.

4.4.2.2 Inter laminar shear strength (ILSS)

The inter laminar shear strength and flexural test are popular quality control tests of laminated composite materials (Tarnopol'ski and Kincis 1985). The shear test requires only basic testing fixtures and uses a very simple specimen configuration. In this investigation, the short beam inter laminar shear strength test was chosen to assess the quality of the laminates. This test uses a three-roller jig and specimens with a small span to width ratio. The specimens were prepared and tested according to the CRAG 100 standard. After mechanical testing the specimens were examined using an optical microscope to confirm the failure pattern. The specimens with other than shear failure patterns were eliminated from the calculations. The results of the different batch laminates are shown in Figure 4.2. These results shows that the quality of the unidirectional laminate is more consistent than the cross-ply laminate. The results also show that the overall quality of the laminates is good.

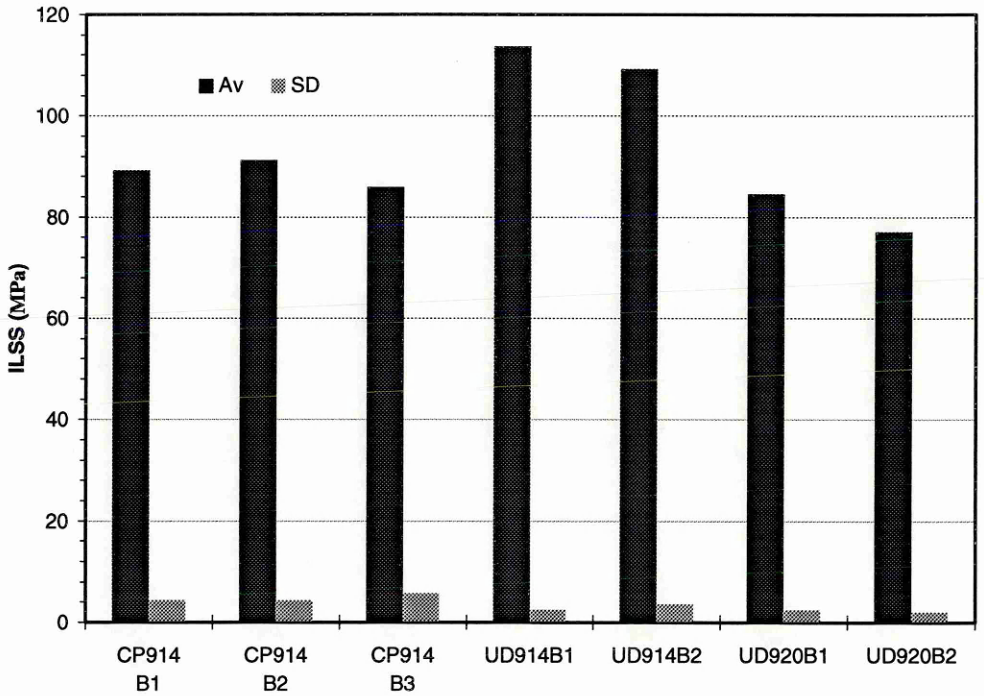

Figure 4.2. Inter-laminar shear strength test results.

4.5 SPECIMEN DESIGN

A suitable representative specimen had to be designed to generate sensible mechanical data. A good starting point for specimen design is standard test methods. The ASTM D3039 and D3479 standards describe the details of static and fatigue test procedures, respectively. As a starting point specimens were prepared according to the ASTM standard for static and fatigue testing. However, the pilot fatigue testing results, indicated a need to modify the specimen tab for unidirectional specimens. Also, the specimen ends need to be modified to introduce current injection points for electrical resistivity measurements. The details of specimen design and preparation are described below.

4.5.1 Specimen preparation

The specimens were prepared from the postcured laminates. An electroplated diamond wheel with a grit size of 44-60 μm, was used to cut the specimens for different tests from the laminates. For a smooth finish, a wheel with grit size of 100-120 μm was used. To remove the cutting marks and other related defects, the specimens were ground polished on a surface grinder using an aluminium oxide wheel. The geometry of the specimens as shown in Figure 4.3, was used for the initial investigations.

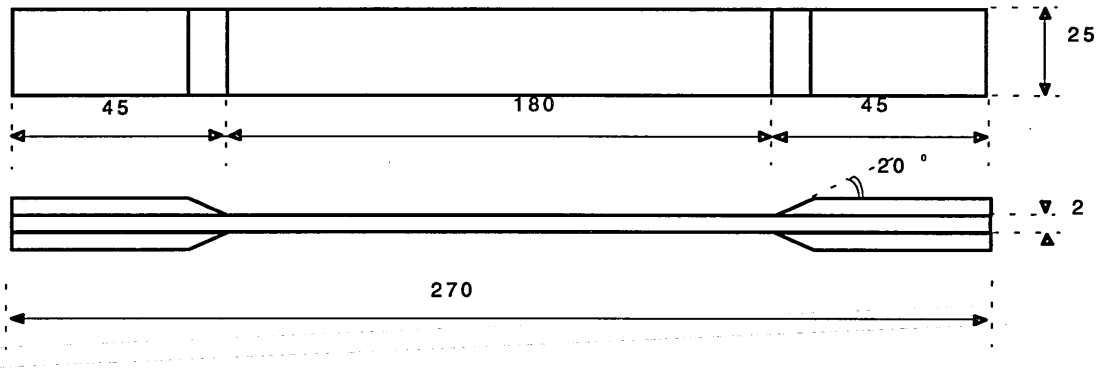

Figure 4.3. The details of mechanical test specimen geometry.

For static and fatigue testing, the specimens were prepared according to ASTM standard D3039. The specimens were 2 mm thickness with 25 mm width and 270 mm length. A gauge length of 180 mm was maintained throughout this work. The tolerance on specimen geometry recommended by the ASTM is ±1% on width and ±1% on thickness with no tolerance on length. For the present case this is equivalent to ±0.25 mm on width and ±0.04 mm on thickness. A tolerance of ±0.05 mm (0.2%) on width and ±0.05 mm (2.5%) on thickness was adopted.

The tabs to the specimen were prepared from the cross plied GFRP laminates. The specimens prepared according to ASTM standards were found suitable for static testing of unidirectional specimens, and static and fatigue testing of cross ply specimens. However, unidirectional samples with the above tab configuration failed within the tab area on fatigue testing. This stressed the need to modify the tab design to promote failure within the gauge length. The strong anisotropic properties of unidirectional laminates and the biaxial stress state at the grip area further complicated the specimen tab design. The stress conditions should be known before the tab can be modified. A finite element model was developed using IDEAS. The details and the results of finite element analysis (FEA) are given in appendix B. Based on the FEA results, different tab configurations and bonding methods were formulated as described below.

The tab design involves seven combinations of specimen geometry and bonding methods as shown in Table 4.5. The tab geometry details are shown in Figure 4.4. The two methods of bonding of tabs are almost same. The main difference is the method used to control the adhesive thickness. In method I, the adhesive thickness was controlled using a bonding jig. This method does not allow much control over the applied pressure. In method II, a vacuum bag technique was used to control the adhesive thickness. The vacuum bag technique allows control of pressure. Unless otherwise stated, the tabs were bonded to the specimens using Redux-410-NA adhesive and cured at 50^{o}C for 4 hours. The other minor modification details are shown in Table 4.5.

Type 1 was used for initial investigations. Two samples were prepared for each type of tab. These samples were then subjected to fatigue loading and Type-5 was found satisfactory. So, the later specimens were prepared with tab configuration and bonding method of type-5.

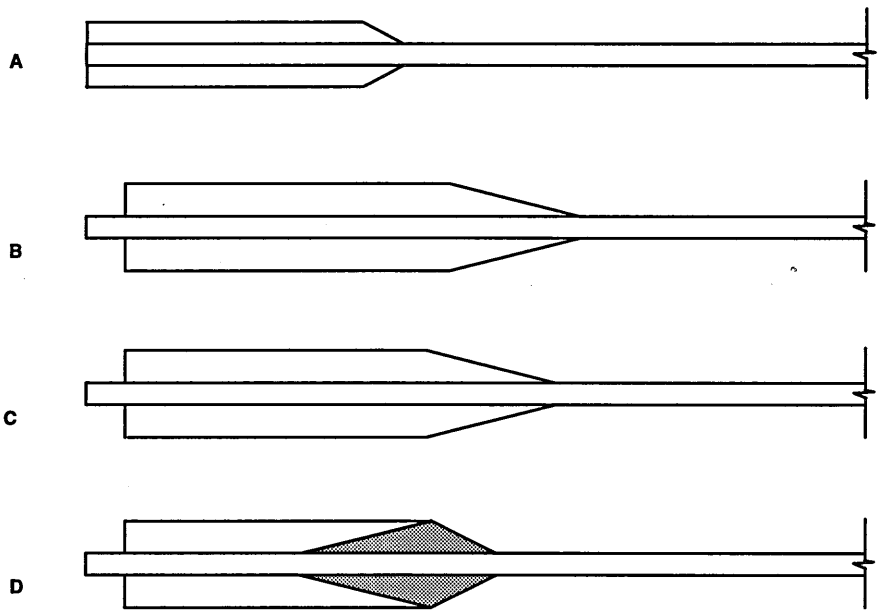

Figure 4.4. Types of tab geometry.

Table 4.5. The details of tab design.

Types of tabs	Tab geometry (Figure 4.4)	Bonding methods (for full description see text)
Type 1	A	As per ASTM standard, Method I
Type 2	B	Method I.
Type 3	B	Method II, scrimp to control adhesive thickness, 1 atmospheric pressure.
Type 4	B	Method II, No scrimp, 0.5 atmospheric pressure. different release film, abrading of glass tags
Type 5	C	Method II, Different Release Film
Type 6	C	Method II, Film adhesive
Type 7	D	Method II, Radical configuration

4.5.2 Electrode preparation

The main purpose of the electrode is to provide current injection and potential measurement points on the samples. The electrode is an important factor in resistivity measurement. Any problem with the electrodes may lead to erroneous results.

Three types of electrodes (Type I, II and III) as shown in Figure 4.5 were used for all the samples used for resistance measurements. Electrodes other than the above three types were used for investigating the influence of the electrode on electrical resistance. This electrode formation method and details are described in chapter 6. The type I electrode was mostly used for resistance measurements of samples used in mechanical testing and other resistance measurements. So, unless otherwise stated type I electrodes were used for all the samples. The details of electrode type I, II and III are described below.

Electrode type I, involves copper strips and silver epoxy conductive adhesive. Copper strips of 0.5 mm thick with soldered leads were bonded to the specimen using silver loaded epoxy adhesive. Prior to bonding, the specimen electrode locations and the copper strips were abraded using different grade of abrasive paper. The specimen was again polished using aluminium oxide powder of 3 μm to erode only the epoxy resin and to expose the maximum

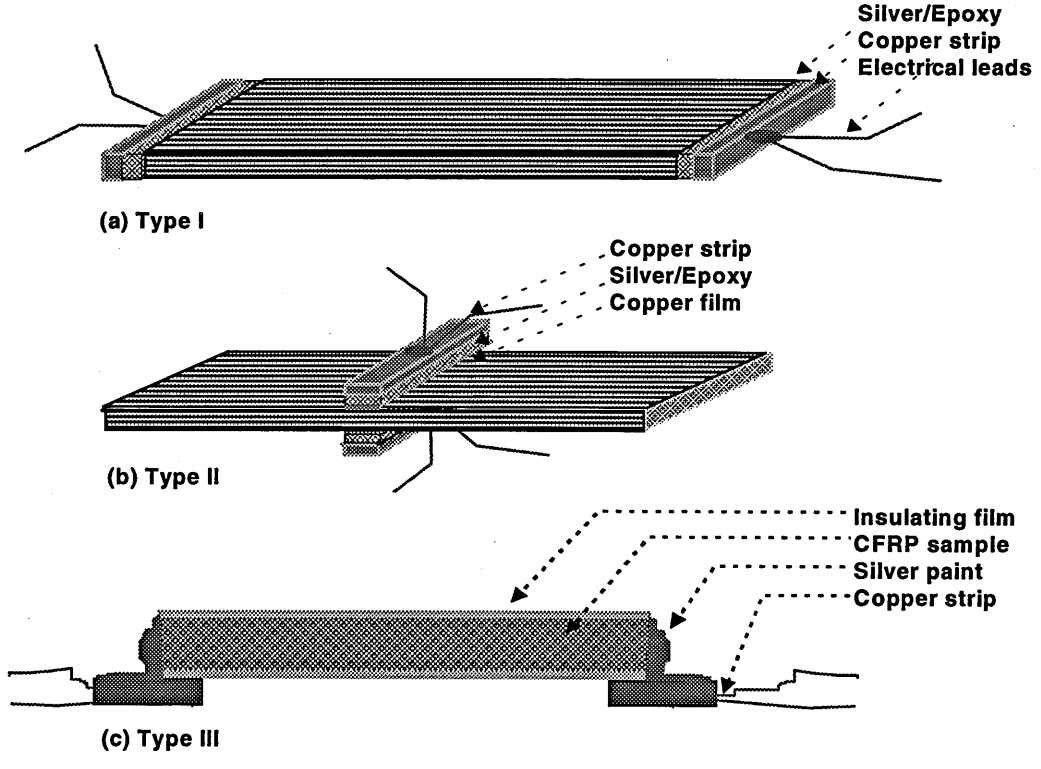

Figure 4.5. Types of electrode used for resistance measurements.

number of carbon fibres (Schulte and Baron 1989). After making the connections the electrodes were coated with quick setting epoxy adhesive to avoid any possible damage during handling and to insulate the electrodes to avoid any possible contacts with testing machine grips. A special jig and silicone inserts were made to apply pressure and to position the electrode on the specimen edges.

Electrode type II, was used for through-thickness resistance measurement of laminates. Type I electrode was found more difficult to form on the specimen surface than on the edges. Hence, the Type II electrode formation method was used. This electrode involves copper sputtering, silver epoxy adhesive and copper strips. The electrode area was first abraded using a suitable abrasive paper. Sufficient care was taken just to remove the epoxy layer and not to damage the fibres. Thin copper film was sputtered over the electrode area, masking the other areas. The copper strips with soldered leads were then bonded to the sputtered copper film using silver epoxy adhesive. The electrode area was coated with quick setting epoxy adhesive.

The type III electrode was mainly used for measuring the electrical properties of a lamina. The thickness of the laminae used in this investigation is only 0.125 mm. It was found difficult to use type I and II electrodes for the relatively thin lamina samples. In order to form the electrode to these smaller samples, after several initial investigations with different electrode configuration and formation methods, the electrode configuration as shown in Figure 4.5 was used. The electrode area was first abraded using emery paper. The copper strips were than glued as shown in the figure using colloidal silver compound. The sample surface other then the electrode area was covered with a thin insulating film to avoid any possible short circuits. It is necessary to take sufficient precautions to avoid short circuits as formation of short circuits is easier because of the smaller sample dimensions and the flowing tendency of the silver paint. Electrical leads were soldered to the copper strips, prior to bonding. After gluing the copper strips the electrode area was coated with commercial grade quick setting epoxy adhesive to avoid possible damage to the electrode during handling.

The geometry of the specimen with the electrode connection used in mechanical testing is shown in Figure 4.6. As stated previously, the type I electrode was used for all the samples used in mechanical testing. The tab design was slightly modified to isolate the electrode from the tabs and to facilitate the use of special inserts to align the electrodes over the specimen electrode area. The geometry of the tab configuration was modified as shown in the figure. Types A and B were used for initial investigations. The Type C configuration was used to isolate the electrodes completely from the tabs, so as to positively make sure that the electrodes are not disturbed during mechanical loading.

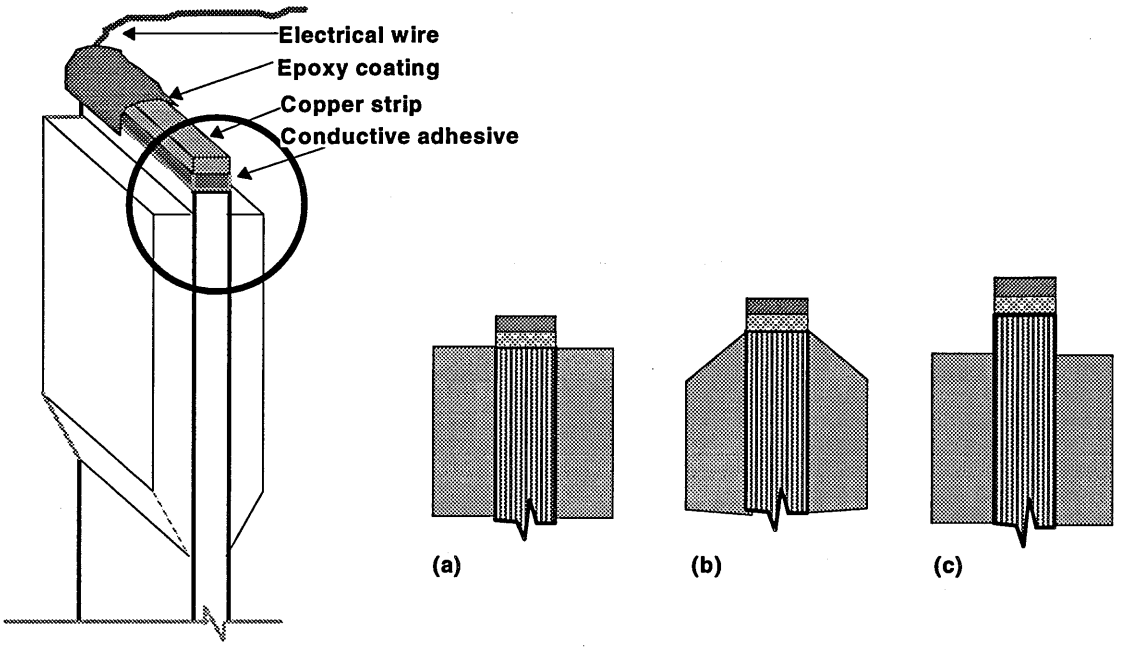

Figure 4.6. Electrode-tab geometry of samples used for mechanical testing (Electrode Type I).

4.6 EXPERIMENTAL SET-UP

A schematic illustration of the experimental set-up is shown in Figure 4.7. The main function is to measure the electrical resistance changes caused by mechanical loading. The fatigue test set-up involves measurement of resistance or voltage, load, strain, position, acoustic emission and temperature. The main components of the ERM test set-up are constant current source, back-off unit and signal conditioner. All the measurement parameters were acquired and recorded using a PC based data acquisition system. The details of the equipment used, the parameters measured and their significance are discussed below.

4.6.1 Constant current source

The function of the constant current source is to deliver a constant current through the specimen. The constant current source limits the amount of current flow and allows any amount of voltage to be drawn. In the case of a constant voltage source, the voltage is limited, but the current flow is unlimited. The advantage of using a constant current source is that the current flow through the specimen can be limited, thereby limiting resistive heating due to Joule's effect. However, the voltage drawn should not exceed the break down voltage of CFRP samples. The breakdown voltage of CFRP in the longitudinal direction is about 300 V/m and in the transverse direction is 3000 V/m (Kaddour et.al 1994). The above limits are well above the voltage level drawn by CFRP specimens used in this investigation. More over the maximum voltage range of the constant current source is 15 V and any overload situation is revealed by a voltage limit indicator.

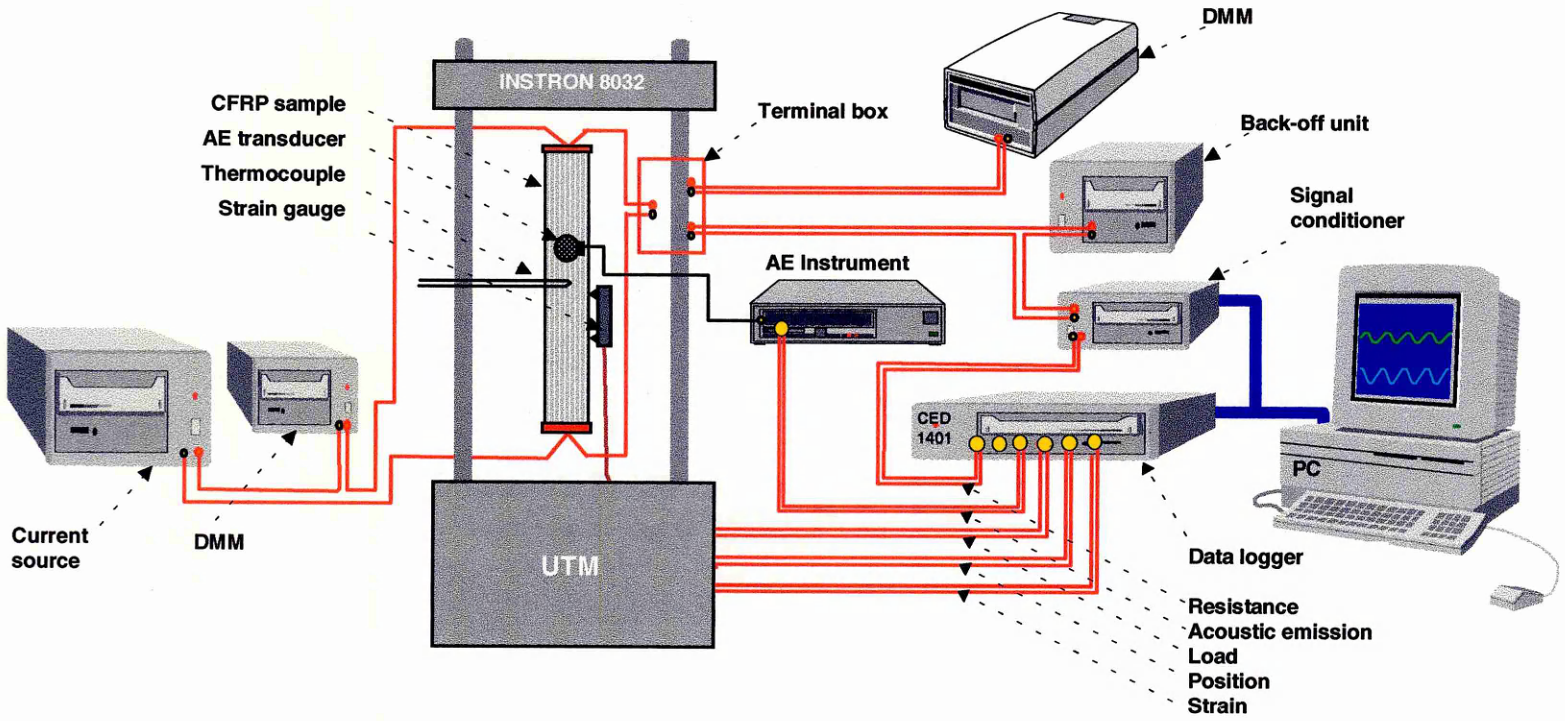

Figure 4.7. Schematic illustration of experimental set-up.

The selection of current level to flow through the samples depends on many parameters, such as sensitivity and resistive heating effects. The resistive heating will increase with increase in current. The sensitivity to damage, i.e. the change in voltage due to mechanical loading will also increase with increase in current. An optimum current level should be chosen that should minimise heating effects and improve the sensitivity.

The resistive heating should be minimised because, already there is a temperature rise due to fatigue damage. A 50 mA current was used by Schulte and Baron (1989) and they reported no increase in temperature due to this relatively small current. Most of the investigation is concerned with fatigue loading so a constant current of 30 mA was used throughout this study. For static loading conditions the current level could have been increased to increase the sensitivity. However, for comparison purposes and to eliminate any unknown current effects, the current level was kept constant. However, in 90^0 samples the current source was unable to drive sufficient voltage at 30 mA, instead a constant current of 1 mA was used.

A current calibrator, model 609N, manufactured by Time electronics ltd, was used as a constant current source. The relevant specification of the instrument is as follows:

Output	0-100 mA in 5 ranges.
Accuracy	±0.02% of setting, ±0.005% of range, ±0.2 nA
Voltage capability	15V
Output noise:	less than 5 ppm of full scale.

The accuracy of the current source for set current output of 30 mA is 6 μA. The instrument is equipped with a switch that enables selection of the output polarity and to zero the current output. The polarity switch enables change of the current direction in the samples. This is very useful in measuring the contact resistance of the samples. The zero current output switch allows setting of the current to zero and thereby facilitates the measurement of voltage due thermal emf.

4.6.2 Back-off unit

The function of the back off unit is to suppress the initial voltage of the sample. Therefore, only voltage changes due to mechanical loading are amplified and processed. This system enables exploitation of the full measurement precision of the data acquisition system. In most cases amplifying the entire signal would result in exceedance of the maximum range of the recording equipment. The back-off unit is essentially a negative voltage source, which is connected in series with the measuring signal. The voltage source, model 2003N, manufactured by Time

electronics ltd was used as back-off unit. The relevant specification of the instrument is as follows:

Output	0-10 V in 5 ranges.
Accuracy	±0.02% of setting, ±0.005% of range, ±0.2 nA
Output noise:	less than ±0.2 mV.

4.6.3 Signal conditioner

The function of the signal conditioner is to suppress noise in the circuit and to amplify the changes in voltage due to mechanical loading. A programmable signal conditioner, the 1902, manufactured by CED was used. The input signal was amplified by 1000 times to increase the resolution. The resolution of the measured signal with the present setup is equal to 0.005 mV.

Electrical noise is a common source of problems with any electrical measurements. Initial measurement signals were mixed with spurious noise signals. At an early stage of research, it was hard to distinguish between the original signal and the noise. Suitable signal conditioning is vital to eliminate any unwanted signal. The general noise sources (external) and inherent noise associated with electrical resistivity measurements are given below. The methods employed to eliminate noise are also discussed.

Mains electricity is probably the largest single source of noise pickup. The noise from the mains is mainly due to 50-60 Hz signals and transient signals. The 50-60 Hz noise pick-up is generally caused by close proximity of unscreened mains cables. Transient signal pickup is caused by heavy load switching on the mains from equipment such as electric motors, light fixtures, electric ovens, etc. Use of shielded leads, earthing and filters on the common mains source minimised the noise pickup from the mains. Some of the noise could be due to the equipment used for measurement, for example, the constant current source, DMM, Back-off unit and data acquisition system. All these items of electronic equipment will have inherent noise due to their circuitry. The signal conditioner was used to filter unwanted signals.

The intrinsic noise associated with electrical resistivity measurements comprises thermal noise (Johnson 1928), contact noise (Ott 1988) and magneto-mechanical noise (Bardal et al. 1981). Thermal noise is due to thermal agitation of electrons in carbon fibres. This noise sets the minimum noise level in the circuit. The contact noise is due to non uniform conductivity at the improper contacts. This noise can be eliminated by forming ohmic contacts. The magneto mechanical noise is due to the movement of electrical leads in magnetic field. This could be eliminated by arresting the movement of wires using clamps.

4.6.4 Data acquisition system

The data acquisition system comprises a PC-386 and CED 1401 data logger. The CED 1401 has a 4 MHz (12 bit) processor and a 12 microsecond analog to digital converter (ADC). This enables sampling of up to 16 channels. The standard full scale input range is ± 10 V with a resolution of 5 mV. The maximum sample rate is around 82.5 kHz. The PC is used to control the 1401 and record data. The main function of the 1401 is to sample data. The application software, Chart, supplied with the system, was used for data capturing and recording.

The recorded data were analysed using Chart, MS-Excel and custom made C programs. Each of the above programs has its advantages and drawbacks in analysis of data. Chart program data are stored in customised CFS format. The CFS files have to be converted into text format to use with popular spread sheets. The fatigue testing normally required an average of five days of data recording at a frequency of 50 Hz. This needs a large amount of hard disk memory to store all the data. The stored data are often too big, and so data retrieval and further analysis are time consuming. A suitable data discrimination method is required. The chart program could be used to record the data at timed intervals. This has the draw back of missing some vital information. The ideal software should have the following qualities.

- sampling at highest maximum possible rate
- recording only if the sampling parameters changes other than pre-set values or
- record at prescribed linear or log interval and
- dynamic recording sample rate.

But, Chart does not have the above capabilities. Development of software for controlling and recording needed a minimum of three months work. Software development was not the main aim of this work. Therefore, it was decided to use the existing software with some compromise. The entire data were recorded for samples with unexpected behaviour. After the test, external data discrimination methods were used to free up the hard disk memory. For established test results the timed interval was used. Once the data were recorded and discriminated, static data were analysed using desktop spread sheets. Fatigue data were analysed using custom built software.

4.6.5 DMM

Digital multimeters convert analog signals to digital information. Most DMM's are capable of measuring basic electrical parameters. The DMM, model 195A, manufactured by Keithley Instruments were used. The sensitivity and versatility of this DMM enabled measurement of the resistance, voltage and current to higher accuracy. The DMM was used to calibrate the output

of all the equipment and to cross check the measuring instruments. It was also used to eliminate any artefacts in the electrical resistance measurement circuit and the data acquisition system.

4.6.6 Mechanical testing equipment

An Instron 8032 servo hydraulic testing machine was used for fatigue and static testing. The maximum dynamic load carrying capacity was 100 kN (±1%). It was equipped with self aligning wedge type hydraulic grips. Despite the fact that the maximum frequency of the test machine is 100 Hz, a frequency of 6 Hz was used for most of the samples, a practical maximum frequency for the magnitude of load used.

Most of the fatigue tests were carried out on the Instron. However, some of the fatigue testing was carried on a similar servo hydraulic, Mayes testing machine. Static tests of 90^{0} laminates and inter-laminar shear strength tests were carried out using an Instron 1195, screw driven static testing machine. The load cell of this test machine and extensometer were calibrated before every testing.

4.6.7 Strain measurement

The strain was measured using a dynamic extensometer, model 2620-602 manufactured by Instron. The maximum strain at 50 mm gauge length was 5%. The frequency response was 150 Hz. Most of the strain measurements were measured using the dynamic extensometer. Some strain gauges were also used for strain measurement during static testing. In fatigue testing, for most of the samples, the strain gauge failed before the specimen. After the initial investigation extensometers were used to measure and record strain throughout this investigation. The measurement of the LVDT transducer output defining the position of the actuator, also proved to be very useful in measuring the secant modulus of the fatigue samples. Changes in the position of the actuator for a given load is due to overall change in the specimen compliance, and therefore may be a good measure of damage.

4.6.8 Resistance measurement methods

There are several methods and instruments available for resistance measurement. The simple ohm meter is a quick and inexpensive way to measure resistance, however, the range and accuracy are limited. Resistance measurements can also be made using various types of bridge circuits, which operates on the principle of comparing an unknown with a known resistor. The Whetstone bridge is one of the most common items of laboratory equipment, and is mainly used for strain measurement.

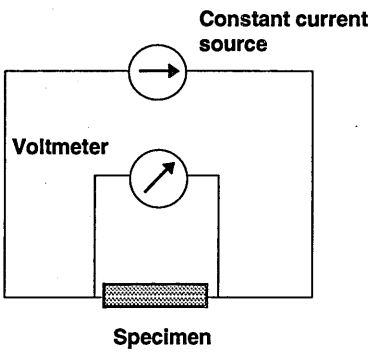

Figure 4.8. Four-point resistance measurement method.

The four point resistance measurement method was used in this investigation. This mainly involves a constant current source and a voltmeter. The experimental set up for four point measurement is shown in Figure 4.8. A known current is passed thorough the sample and the voltage drop across the sample is measured using a voltmeter. The resistance is then calculated using the Ohms law. This method measures the sample resistance and eliminates the resistance of measurement leads.

The resistance of samples in all the resistance measurement investigations was measured using the four point resistance measurement. The resistance was measured by averaging the voltage for reversal of direction of current. This can eliminate the contact resistance. Necessary corrections were made for thermal emf by measuring the voltage at zero current.

4.6.9 Acoustic emission

Acoustic emission (AE) of specimens during mechanical loading was also monitored. A single channel AE system, 1200A, manufactured by Physical Acoustics Corp. was used to monitor AE. The AE transducer, model R15 was used. The operating range of the transducer was 50 to 200 kHz. This transducer is particularly suited for monitoring emission from CFRP samples, which generally emits signal with a frequency range between 100 and 200 kHz (Fuwa et al. 1975). The AE output was monitored and recorded in terms of AE counts.

4.6.10 C-scan

Ultrasonic testing is based on the interaction of sound waves passing through the materials with the structure of the materials. Using ultrasonic techniques, it is possible to derive information concerning features within the material by observing either the attenuation or the scattered or reflected sound waves. The ultrasonic test details specific to composite materials can be found elsewhere (Thiagarajan 1989).

In this thesis, ultrasonic C-scanning was used for assessing the quality of the laminates and to measure the damage level of samples subjected to mechanical loading prior to final failure. A model PA1020, ultrasonic flaw detector manufactured by Baugh and Weeden ltd with home built scanning arrangement was used. Scanning of the samples was carried out using double transmission technique in pulse-echo immersion mode. A frequency of 5 MHz was used using a R10 type transducer. This system provides a C-scan image based on the attenuation of sound waves. The output of sound attenuation is converted into electrical voltages, i.e., one volt of electrical signal corresponds to the maximum signal amplitude of the A-scan.

4.6.11 X-ray radiography

The X-ray radiographic tests are based on the principle of differential absorption of penetrating X-rays, i.e., the intensity of the penetrating radiation is modified through material and by defects in the materials. The details of X-ray tests related to CFRP laminates can be found elsewhere, e.g., Stone (1971).

In this thesis, the X-ray tests were mainly used for damage characterisation of samples subjected to mechanical loading. The X-ray tests were carried out at Department of Mechanical and Process Engineering, Sheffield university. These investigations were carried out using Hewlett Packard Faxitron, Model 43855A type X-ray cabinet. Zinc iodide solution was used as penetrant. The penetrant was brushed on faces and edges and left to penetrate overnight. The x-ray film was exposed at 22 kVe, 3 mA for 90 seconds.

4.6.12 Grip and grip pressure

The Instron test machine used in this investigation was equipped with wedge action hydraulic grips. The grip pressure is very critical for unidirectional samples because of the strong anisotropic properties. The grip pressure of samples tested in this investigation was set based on the recommended grip pressure by Instron (Figure 4.9). The recommended grip pressure in MPa is approximately equal to the applied maximum load in kN. This grip pressure is the pressure pumped into the hydraulic system and may not necessarily be the pressure applied on the specimen sides. This recommended grip pressure was found suitable to avoid slippage at the grips. However, the grip pressure was varied to find the lowest grip pressure to avoid excessive pressure on the sample and the failure of the samples with in the gripping area.

A grip pressure of 8.5 MPa (85 bar) was found suitable for unidirectional samples and maintained for all the 0° unidirectional static samples. Similarly, a grip pressure of 4 MPa (40 bar) was maintained for all the cross-ply static samples. The grip pressure for fatigue samples

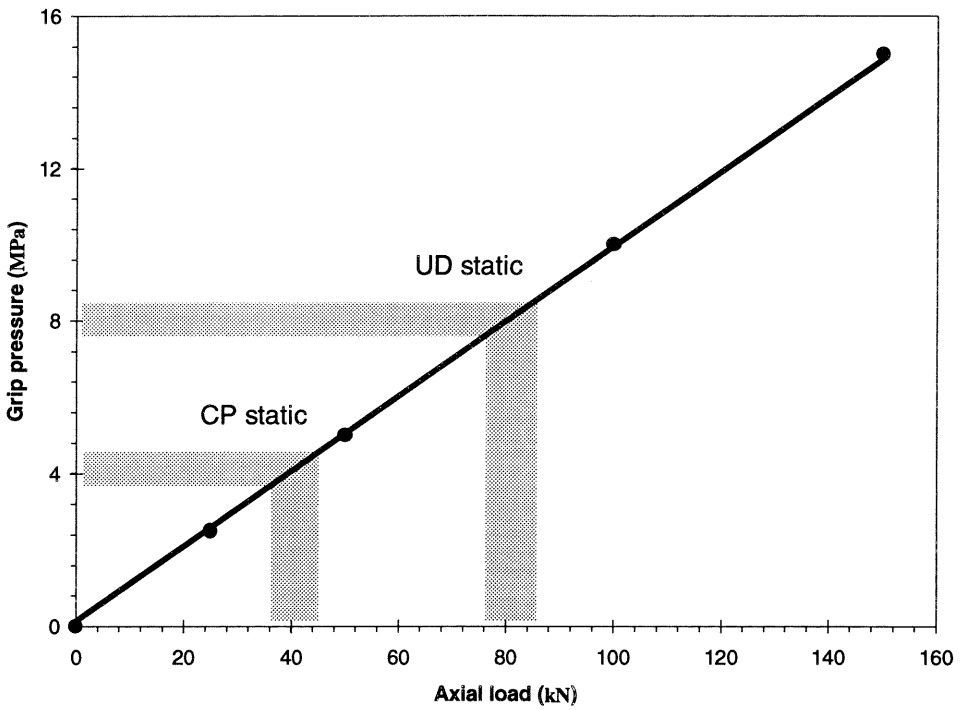

Figure 4.9. The relationship between grip pressure and sample axial load.

was set according to the maximum load level of the samples. The 90° unidirectional samples were tested in an Instron machine with manual wedge action grip. So, the grip pressure was manually controlled by trial and error method to avoid slippage at the grips and promote failure outside the gripping area.

4.7 TEST PROGRAMME

The sample code, laminate and constituent material details of samples used for fatigue and static testing are shown in Table 4.6. The same sample code was used for samples used for resistivity measurements including temperature dependence. Figure 4.10 illustrates the co-ordinate system used for a unidirectional laminate.

4.7.1 Static testing

Static testing was carried out in a displacement control mode at a rate of 1 mm/min for all the samples according to ASTM D3039. The tensile modulus, tensile strength and failure strain were measured for 0° and 90° unidirectional and cross-ply samples. A minimum of 10 and a maximum of 20 samples were tested for each category. The electrical resistance of the samples was also measured to detect the onset of damage initiation and growth. The acoustic emission counts were also measured for some of the samples.

Table 4.6. Sample code and material details of samples.

Sample code	Laminate type	Fibre/Matrix	Types of test
UD914L	0° unidirectional	T300/914	Static/Fatigue/Resistance
UD920L	0° unidirectional	T300/920	Static/Fatigue/Resistance
UD914T	90° unidirectional	T300/914	Static/Resistance
UD920T	90° unidirectional	T300/920	Static/Resistance
CP914	Cross-ply	T300/914	Static/Fatigue/Resistance

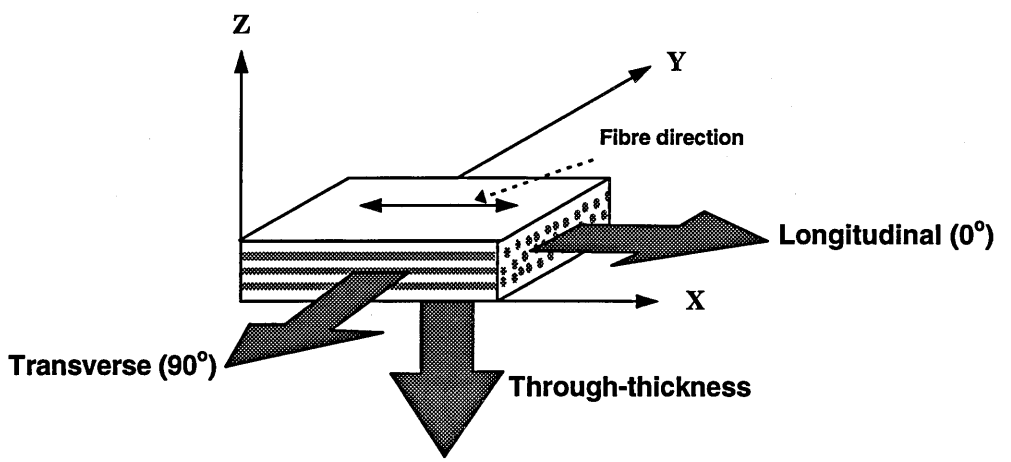

Figure 4.10. Schematic representation of a unidirectional laminate illustrating the co-ordinate system used in this investigation.

In order to characterise the damage level of samples subjected to static tensile loading, some of the cross-ply samples were stopped at intermediate stress levels (25%, 50%, 75% and, 94% of UTS) prior to failure. Two samples were used for each stress level. The electrical resistance was measured during loading and unloading also. The electrical resistance measurement results were compared with C-scan and X-ray results. The results are presented in chapter 9.

4.7.2 Fatigue testing

Fatigue samples of UD914 and UD920 were subjected to 7 different peak stress levels. All the samples were subjected to tensile fatigue loading in a load control mode with a 'R' ratio of 0.1. These stress levels were chosen based on the conceptual fatigue life diagram proposed by Talreja (1987) and pilot static and fatigue test results. These stress levels were chosen to characterise the damage mechanisms at each stress level and to demonstrate the damage sensing capabilities of electrical resistivity measurement technique.

The fatigue stress levels of samples are shown schematically in Figure 4.11, superimposed over the conceptual fatigue life diagram. The details of the fatigue test programme and stress levels for UD914 and UD920 samples are shown in Table 4.7. In general, 1 or 2 stress levels in the horizontal scatter band, 2 to 3 stress levels within the sloping band below the horizontal scatter band and 3 stress levels below the fatigue threshold of epoxy resin were tested. The 6% stress level (i.e., 6% of UTS) was chosen to demonstrate that the observed electrical resistance change is not due to any magneto-mechanical effects.

At stress levels above 50%, a minimum of three samples to a maximum of 8 samples were tested at each stress level. At stress levels below 50% of UTS a minimum of 2 samples and a maximum of 5 samples were tested at each stress level. Samples tested above 50% of stress level were taken up to the failure. Some of the high stress level samples were stopped at intermediate cycles prior to failure for further non-destructive testing. Samples tested below 50% are all stopped at around 4 million cycles. One of the sample tested below 50% was taken up to 12 million cycles to characterise the damage growth rate using electrical resistance measurement technique. Samples tested at stress level around 75% were sprayed with white acrylic paint to enhance visual observation.

Most of the samples were tested at a frequency of 6 Hz. The samples tested below 50% of UTS were tested at a frequency of 10 Hz. The load, electrical resistance (voltage), position, strain, temperature and acoustic emission counts during fatigue testing of samples were monitored and recorded as described in section 4.6. For more than 90% of the samples, all the above parameters were monitored, however, for some of the samples some of the above parameters

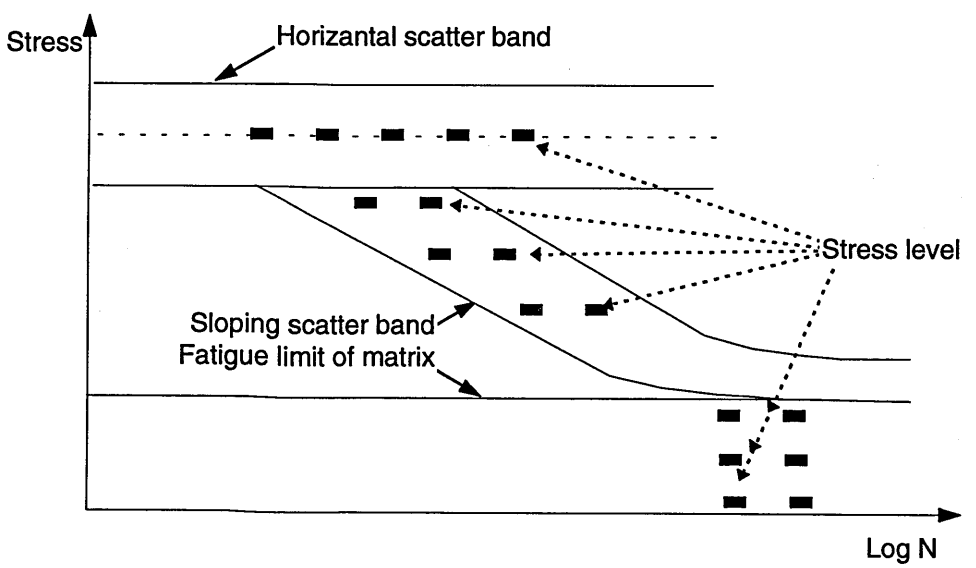

Figure 4.11. Schematic illustration of fatigue test programme.

Table 4.7. Details of fatigue test programme.

	UD914		UD920		Remarks
	Max. Stress (MPa)	% of UTS	Max. Stress (MPa)	% of UTS	
1	1481	92%	1400	88%	SL close to the UTS (horizontal scatter band)
2	1348	88%	1300	82 %	SL just below the horizontal scatter band
3	1265	82%	1200	75%	SL below the horizontal scatter band (sloping band)
4	1157	75%	1000	63%	SL at Intermediate SL . (sloping band)
5	750	48%	750	48%	SL just below the fatigue threshold of epoxy resin
6	500	32%	500	32%	SL below the fatigue threshold of epoxy resin
7	100	6%	100	6%	To demonstrate no magneto-mechanical effects.

were not monitored because of various reasons such as non-availability or malfunction of the equipment.

After fatigue testing the runout samples were tested non-destructively using C-scan and X-ray techniques to measure the damage level. The residual tensile strength of runout-UD920 samples was also measured.

Three UD914 samples with drilled circular holes were prepared to investigate the longitudinal split growth rate. The split growth rate was measured using optical and electrical resistance measurement methods. These specimens were also sprayed with white acrylic paint for better observation. The fatigue results are presented in chapter 10.

4.7.3 Electrical resistivity measurements

The purpose of resistivity measurement is to establish the resistivity of CFRP independent of specimen geometry and electrode formation method, and to understand the conduction mechanism of CFRP. The resistance of the sample was measured using various sample configurations and electrode formation method to establish the electrical properties of CFRP without the influence of specimen geometry and electrode. Four point resistance measurement methods were used as described in section 4.6.8. The temperature and specimen geometry

dependent resistance investigations were designed mainly to yield more information about the conduction mechanism. The results are presented in chapter 7.

4.7.3.1 Electrical properties

Many samples were prepared to measure the electrical properties of unidirectional and cross-ply CFRP laminates. In order to compare the electrical properties of laminates used in these investigations, independent of specimen geometry and electrode configuration, samples of similar specimen geometry and electrode configuration were used. Samples with a length and width of 25 mm and a thickness of 2 mm were used. The resistance was measured for three types of laminates (UD914, UD920 and CP914) and six samples per configuration (see Table 4.6) and the directions of measurement were used. The Type I electrode configuration was used.

This thesis work mainly involves measurement of resistance. So, the electrical properties measured in any other context of testing can also be used to establish the electrical properties of CFRP. The samples used in mechanical testing involves measurement of resistance of more than two hundred samples. This can be used to establish the statistical distribution of electrical properties of CFRP. Similarly, the electrical properties of samples used to characterise the influence of electrode, specimen geometry and temperature dependence can also be included.

4.7.3.2 Influence of electrode

The electrode is an important parameter in the electrical resistivity measurement technique. In order to understand the influence of the electrode on electrical properties, various electrode formation methods were developed. The influence of electrode was investigated mainly using 50x25x2 mm UD914L samples. This investigation involves more than 10 electrode formation method and 50 samples. The details and the results are described in chapter 6.

4.7.3.3 Influence of specimen geometry (length)

The influence of specimen geometry (length) on electrical properties of unidirectional samples was investigated using three sets of experimental measurements as follows.

For the dependence of longitudinal resistance on length, UD914 samples were used. Samples with a width of 25 mm, thickness of 2 mm and with a variable length from 10 mm to 600 mm were used for this investigations. The lengths of the samples are 10, 20, 30, 40, 50, 100, 200, 300, 400 and 600 mm. The Type I electrode configuration was used.

The dependence of transverse resistance on sample length was investigated using UD920 samples. This investigation was carried out on samples with a width of 25 mm, thickness of 2 mm and a variable length of 10 mm to 300 mm. The length of the samples was 10, 20, 30, 40, 50, 100, 200, 300 mm. A minimum of two samples was used for each sample length. The Type I electrode configuration was used.

The dependence of through-thickness resistance on length was investigated using UD914 samples. Four samples with a dimension of 300x25x2 mm were used in this investigation. The electrodes were attached to the samples at the middle of the length, i.e., the Type II electrode configuration was used. The dependence of length was investigated by reducing the sample length, in steps of 10 mm.

4.7.3.4 Influence of specimen geometry of a lamina

Composite laminates are generally fabricated by stacking individual lamina, thus lamina are the basic building block of a laminate. Electrical resistivity measurements of a lamina can be a vital tool to understand the electrical conduction mechanism of CFRP laminates. Moreover, these experimental results are necessary for the 3D model to determine the properties of the unit cell, as the model is based on three-dimensional linkage of unit cells.

The main aim of this experiment is to investigate the effects of specimen geometry on the transverse electrical resistivity of a lamina. This investigation was carried out using both UD914 and UD920 lamina samples and the Type III electrode configuration. The nominal thickness of the lamina samples used is 0.125 mm. In order to investigate the influence of specimen geometry, samples of various widths and length ranging from 2 to 20 mm were used. For a given width, the length was varied from 2, 5, 10, 15 and 20 mm and vice versa. Three samples per configuration were used and that adds up to a total of 150 samples.

4.7.3.5 Temperature dependence

Temperature plays a critical role in electrical conduction of materials. The temperature dependent resistivity investigations will yield information about the physics of the conduction mechanism in the material. So, the main purpose is to understand the conduction mechanism of CFRP. The other purpose is to establish a correlation curve or coefficient of resistance for specimens used in mechanical testing. This will aid in differentiating the observed resistance change from damage and from temperature effects during mechanical loading.
The temperature dependent resistivity measurement was carried out on samples of length and width 25 mm and a thickness of 2 mm. Three samples per configuration and per direction of

measurement was used. The temperature dependent resistivity measurement to establish the temperature coefficient of resistivity of samples used for mechanical testing was carried out on samples of similar size to those used for mechanical testing. The details of sample dimension and laminate are shown in table 4.5.

These investigations were carried out on a Techne-500 series environmental enclosure equipped with a RT type temperature sensor. The electrical resistance was measured using the four point resistance measurement method with current reversal for eliminating thermoelectric effects. The temperature dependent resistivity was carried out for a temperature range of 200 °K to 360 °K. The temperature coefficient of resistivity of samples used in mechanical testing were carried out for a temperature range of 273 °K to 360 °K

Table 4.8 Details of samples used for temperature dependent experiments

Sl. No.	Sample code	Dimensions LxWxT (mm)
1	UD914L	25x25x2
2	UD920T	25x25x2
3	CP914	25x25x2
4	UD914TT	5x25x3
5	UD914L (mechanical test samples)	330x25x2
6	UD920L (mechanical test samples)	330x25x2
7	CP914 (mechanical test samples)	270x25x2
8	Silver/epoxy adhesive	5x25x2

5

THEORETICAL AND COMPUTATIONAL MODELS

Electrical conduction models are essential to exploit the quantitative damage sensing potential and to achieve the ultimate goal of smart capabilities in the resistivity measurement technique. The models in the first instance should have the capability to predict the electrical resistivity. Furthermore, these models should be able to predict the effects of mechanical loading, damage and environment on electrical resistivity. It is evident from the literature survey that new models are essential to achieve the above goal, though some preliminary models are available for predicting the electrical resistivity.

This chapter presents the details of the formulation and development of the two new electrical conduction models, a random resistor network model (2D) and a proposed new three-dimensional (3D) unit cell assemblage model. Results that illustrate the importance of these models are also presented. The details of a parallel resistance model and the lattice models are also described. Details of other miscellaneous models are also described.

The approach in developing these proposed new electrical models are inspired by the ethics of Spinoza, the 16th century Dutch philosopher. He states that 'Nothing in nature is random... A thing appears random only through the incompleteness of our knowledge.'

5.1 LONGITUDINAL CONDUCTION

The longitudinal conduction models are simple models to predict the longitudinal electrical properties of CFRP (chapter 3).The longitudinal conduction of a unidirectional CFRP is mainly due to current flow along the fibres. This can be predicted using a simple electrical circuit and mechanics of materials approach. These models can predict fairly accurately the longitudinal resistivity of unidirectional CFRP from the constituent properties and the volume fraction. The longitudinal electrical properties are not significantly influenced by the size, shape and distribution of the fibres as the conduction is mainly due to current flow along the fibres. Moreover, the transverse resistance of fibres is 10^2 to 10^5 times higher than the longitudinal resistivity. So, the transverse fibre to fibre contacts do not significantly influence the longitudinal resistance of the unidirectional CFRP.

5.1.1 Parallel resistance model

This model is based on the assumption that the conducting carbon fibres are surrounded by insulating matrix materials. The carbon fibres are connected at the ends by the electrodes. This forms a parallel arrangement of all the carbon fibres bridged by the two edges as shown in Figure 5.1. This is equivalent to resistors connected in parallel and hence the resistance of the composite, R_c, is simply the resistance of a single fibre, R_f, divided by total number of fibres, N.

i.e. $$R_c = \frac{R_f}{N} \qquad (5.1)$$

The resistance of the single fibre, R_f, can be calculated from fibre resistivity, ρ_f, cross sectional area, A_f, and the length, L, using the following relation.

$$R_f = \frac{\rho_f . L}{A_f} \qquad (5.2)$$

The number of fibres, N, in the composite can be calculated using the fibre volume fraction, V_f, cross sectional area of the composite, A_c, and cross sectional area of the fibre, A_f, as shown

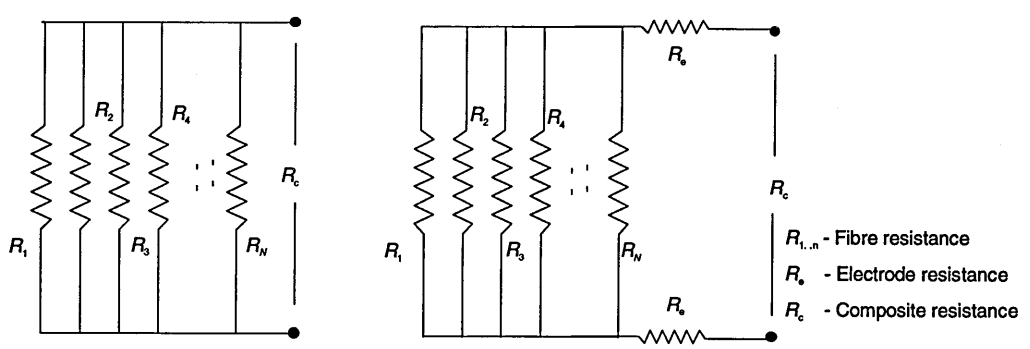

Figure 5.1 Parallel resistance model

below.

$$N = \frac{A_c . V_f}{A_f} \qquad (5.3)$$

Substituting equation 5.2 and 5.3 in 5.1.

$$R_c = \frac{\rho_f . L}{A_c . V_f} \qquad (5.4)$$

The above equation predicts the longitudinal resistance of the composite from the fibre resistivity, volume fraction and the specimen dimension. If we assume that the electrodes are connected in series with the existing parallel arrangement of fibres, then the resistive components of electrode, R_e, can be included in the equation 5.4. The electrode resistance includes the resistance of the conducting adhesive R_{ad}, copper strips R_{cu}, and the electrical leads R_{le}.

$$R_c = \frac{\rho_f . L}{A_c . V_f} + 2\, R_e \qquad (5.5)$$

5.1.2 Rule of mixtures

The resistance of the composite can also be predicted by mechanics of materials approach using the rule of mixtures. The resistivity of the composite can be expressed in terms of the constituent materials property and volume fraction relation, as follows.

$$\frac{1}{\rho_c} = \frac{1}{\rho_f} V_f + \frac{1}{\rho_m} V_m \qquad (5.6)$$

$$\frac{1}{\rho_m} \approx 0$$

$$\therefore \quad \rho_c = \frac{\rho_f}{V_f} \qquad (5.7)$$

Thus, $R_c = \frac{\rho_f . L}{A_c . V_f}$. (5.8)

The final equation of both approaches results in the same equation. This is because the fibre plays major role and the matrix is completely eliminated.

5.2 TRANSVERSE CONDUCTION (2D MODEL)

The transverse conduction is a relatively complex process and is mainly due to current flow orthogonal to fibre direction. The transverse conduction orthogonal to fibre direction predominantly depends on the fibre to fibre contact and the contact distance. The conduction can be due to direct ohmic contact between the adjacent fibres or due to other complex

conduction mechanisms. For example, even if the fibres are separated by few hundred nm the conduction could continue due to electron tunnelling and or electron hopping.

The lattice models have constrained the fibres in a square or hexagonal arrangement (refer section 3.5). The earlier researchers agreed that the confinement of fibres is for computational simplicity and is an approximate representation of a real fibre distribution. This simplification can lead to vital information being missed. This section describes the development of a new random resistor network model. The main objective of this model is to simulate the fibre distribution as close to the real composite and then use this as a basic building block to extend this model to simulate electrical behaviour of the real laminates and then the structures. There is a possibility that the simplification at micro-level itself can manifest errors during integration of this model into real structure.

5.2.1 New random resistor network model

The various steps involved in this model are shown in Figure 5.2. This new random resistor network model involves the following major steps,

- Simulation of fibre distribution
- Transformation of the fibre distribution data into electrical topological data
- Generation of a conductance matrix from the above topological data
- Solution of this conductance matrix or the electrical network.

The development of this model is demonstrated in the following sections for a square area of a typical CFRP unidirectional laminate of 100 μm width and a fibre volume fraction of 0.60.

5.2.1.1 Simulation of fibre distribution

The fibre distribution in a real composite is a complex and random distribution. The fibre distribution depends on the fibre volume fraction and manufacturing process. The laminates generally used for structural application have volume fractions around 0.60 and at this volume fraction the optimum material properties are realised (Garcia et al. 1987). In a real laminate at this volume fraction the fibre distribution can be square, hexagonal or random. In theory, at very high fibre volume fraction the fibres tend to pack themselves into hexagonal arrangement. This is possible only at very high volume fraction at around 0.90. Similarly, square regions were found at volume fractions around 0.78. At volume fractions around 0.60 the fibres are distributed randomly (Kelly and Parkhouse 1993; Garcia et al. 1987). Moreover, the volume fraction of the laminates used in this experimental investigation is 0.60. A micrograph of laminates used in this investigation shows irregular fibre distribution. This is clearly illustrated in

Figure 5.3. Therefore, the main aim is to simulate the fibre distribution as close to the real laminate.

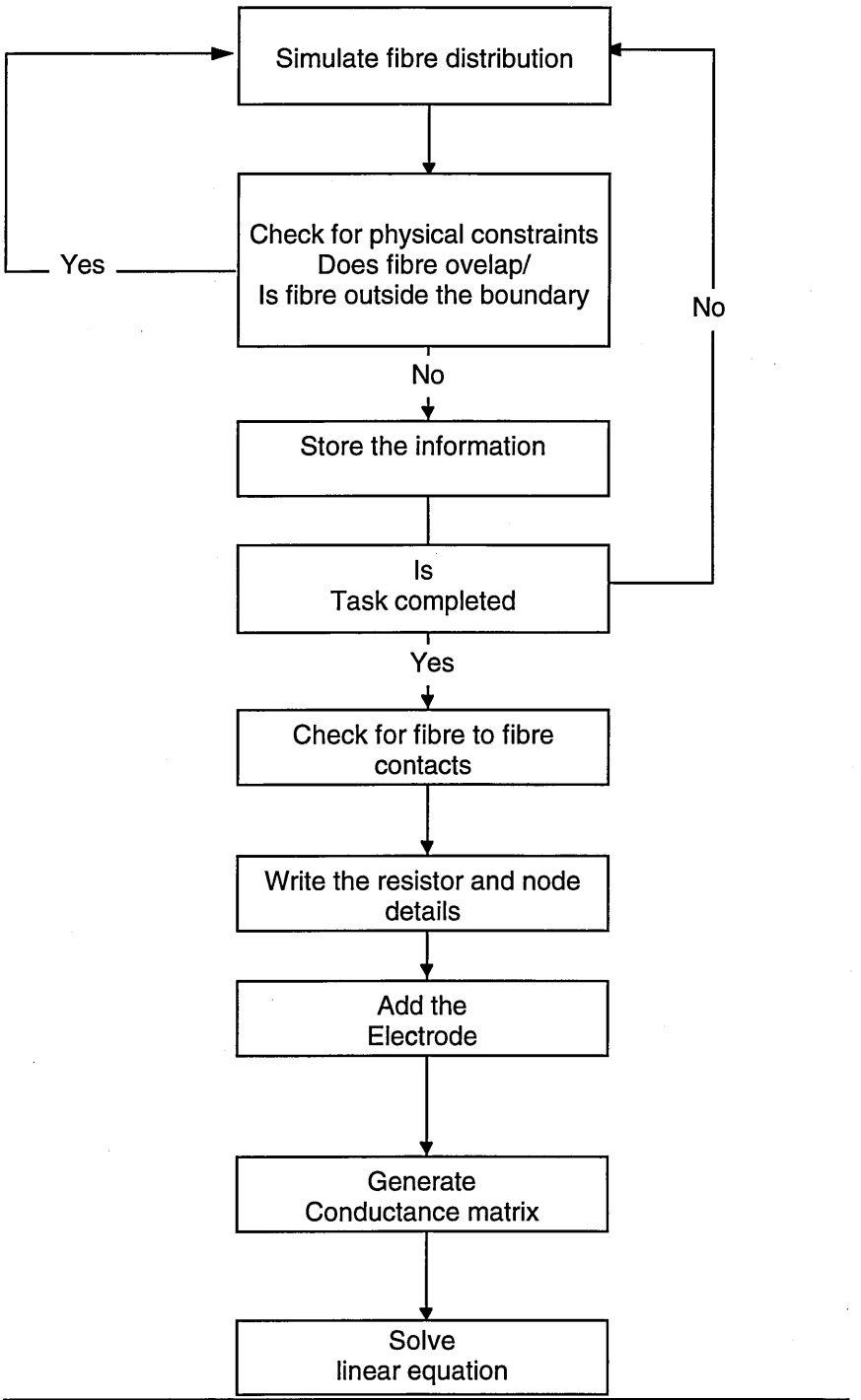

Figure 5.2. Flow diagram illustrating the major steps involved in the proposed new random resistor network model.

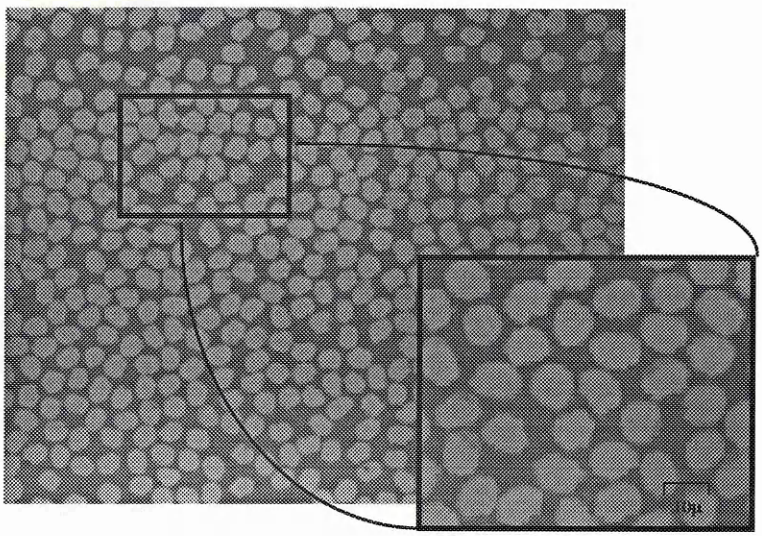

Figure 5.3. Fibre distribution in a typical unidirectional laminate.

The fibre location, i.e., the *x* and *y* co-ordinates of the fibre in a Cartesian square was simulated using a random number generator routine. This random number routine generates consecutive sets of *x* and *y* co-ordinates, i.e., the fibre locations. The simulated fibre locations were stored in a two dimensional matrix. The details of random number routine used are described in section 5.2.1.2. This procedure was repeated till the required number of fibres were simulated. The required total number of fibres, *N*, distributed in a given cross-sectional area, A_c, was calculated using the following relation.

$$N = \frac{A_c . V_f}{A_f} \qquad (5.9)$$

where, V_f, is the fibre volume fraction and, A_f, is the area of a single fibre. Thus, the total number of fibres in a CFRP laminate of square area with a 100 μm width and a fibre volume fraction of 0.60 equals 156.

The only physical restriction in fibre distribution simulation is that the adjacent fibres should not overlap. Each fibre location generated by the random number generator routine is checked for fibre overlap. To avoid overlap the fibre positions should be outside the circumference. However for an ohmic contact, the fibre location should lie on the circumference. The fibre used in this investigation is of circular cross-section with a diameter of 7 μm. An algorithm was developed to check the fibre overlap and is described in the following paragraphs.

In the case of a fibre with circular cross-sectional area and with a radius of *r*, a fibre can overlap other fibres only if the centre lies within the boundary of the circle with centre of the first circle

with a radius of 2*r*. Let the fibre locations of two adjacent fibres be x_1, y_1 and x_2 and y_2 respectively. The fibres can overlap only if the distance, *l*, between them is less than the fibre radius, 2*r*.

$$\text{i.e.} \quad l = \sqrt{(x_2 - x_1)^2 - (y_2 - y_1)^2} \qquad l < 2r \quad \Rightarrow Overlap \qquad (5.10)$$

Therefore, the physical constraint to avoid overlap of fibres is that the distance between the fibre should be equal or greater than the other adjacent fibres. An algorithm based on the above criterion was developed and implemented in the model. This algorithm checks for fibre overlap. If the fibre overlaps then that fibre location is ignored and a new set is generated. This is then continued till the required number of fibres are simulated.

Another constraint in simulating the fibre distribution is that the fibres should lie within a given area. In this model, the fibre centres are simulated and hence the fibre centres close to the boundary can protrude the given area. To implement this boundary condition in the model, the fibre centres with any one of the co-ordinates less than radius of the fibre or greater than the width of the side minus the radius of the fibre were ignored.

5.2.1.2 Random number generation

The selection of the random number generator is an important element in the fibre distribution simulation. In this model the fibres are not constrained to a predetermined square or hexagonal arrangement. Every fibre location is allowed to take any position in the given area, other than satisfying the fibre overlap and boundary conditions. The fibre locations generated by the random number routine should not cluster around a small region in the given area. The fibres should be distributed uniformly throughout the area, as in a real laminate. The random numbers should not form clusters in one small region. In order to optimise the computer time, the random number generator should not repeat the same number again, i.e., in this case the same fibre locations. The repetition rate of the random number should be greater than the required number of fibres.

There are numerous random number routines available in the literature (Essam 1980). Also, there are standard routines supplied with the compilers. In recent years, quasi-random number generator routines have been used to generate random numbers. These quasi-random number generators facilitate the writing of compact, efficient and faster computer codes. In this model, Sobol's quasi-random sequence was used to generate random numbers. Sobol's quasi random number generator is very suited to this application. The uniformity property of this generator, generates random numbers distributed uniformly (Sobol' 1976). It never generates the same

number again. The random sequence repeatation rate is very high. This is particularly suited for simulation of fibre distribution in CFRP. Sobol's random number generator is based on the theory of 'primitive polynomials of modulo 2'. It is beyond the scope of this thesis to discuss the mathematical theory. The mathematical theory, uniformity and distribution properties are described by Sobol' himself in his excellent papers (Sobol' 1967; 1976, 1979). The algorithm for computer implementation is given by Bratley and Fox (1988).

5.2.1.3 Transformation into electrical network

This section describes the transformation of fibre distribution data into electrical topology data. Topology, in electrical circuit theory means the details of interconnection of components of an electrical circuit. The topology of the electrical network was formulated based on the fibre to fibre contact distance. The fibre to fibre contact distance represents an electrical resistor, i.e., a 'branch' and the fibre location represents a 'node' in the electrical circuit. So, the transformation of fibre distribution in to electrical topological data involves finding out the number of fibres in contact with each other.

In order detect the fibre to fibre contacts, an algorithm was developed to scan the adjacent fibres from a given fibre location. The scan area was determined depending on the requirements, i.e., parameters to be added to the fibre to fibre contact resistance. For example, for ideal ohmic contact of fibres with circular cross section, the fibre centres should lie at the circumference of the centre of the first fibre with a radius equal to twice the radius of the fibre. In this case, the scan area is limited to the circle area with a radius equivalent to twice the radius of the fibre. This scanning was repeated for all the fibres to determine the fibre to fibre contact information.

5.2.1.4 Generation of conductance matrix

After generating the information about the fibre to fibre contacts (topological data), the next step is to convert this information in such a way that the electrical circuit analysis methods can be used to obtain potential distribution at every node (every fibre location) and the overall resistance. The nodal method of circuit analysis was used to form the circuit equations from the topological information. This method is widely used in electrical circuit simulation programs. The details of this method and the associated algorithm for computer implementation are described elsewhere (Chua and Lin 1975). The methods used in this model are described below.

The nodal method of circuit analysis involves choosing a 'common' or 'reference' node and assigning the unknown nodal voltages with respect to this reference. Kirchoff's current law

equations (KCL) are then used to complete the analysis. For an n node circuit there are n-1 independent KCL equations. Also every branch (resistor) is connected between two nodes. The Kirchoff's voltage law (KVL) can be used to express each branch voltage as the difference of the two node voltages between the branch that is connected. Thus, every unknown branch current could be expressed as a function of branch voltage and the branch voltage could be expressed in terms of nodal voltage. The Kirchoff's current law equations of all the nodes can be written in matrix form as follows.

$$[G]\{V\}=\{I\} \qquad (5.11)$$

where, ***G***, is the conductance matrix, ***V***, is nodal voltage vector and, ***I***, is source vector.

The main task in this section is to generate the conductance matrix from the topological information. The step in our algorithm to generate the conductance matrix, ***G***, is explained using Figure 5.4.

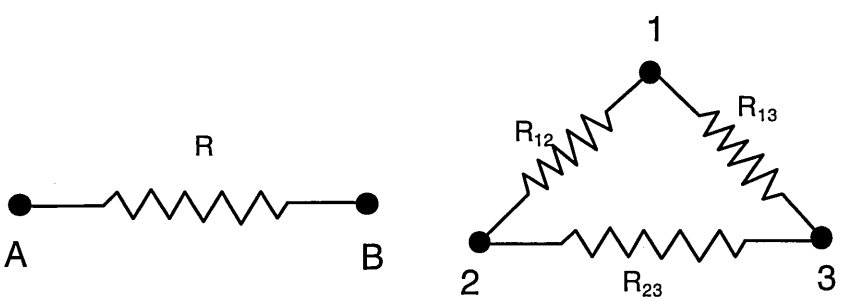

Figure 5.4 A typical resistor network

Consider the resistor connected between nodes A and B (Figure 5.4). The current leaving the node A through R is $(V_A-V_B)/R$ and the current leaving node B through R is $(V_B-V_A)/R$. Thus, in the matrix ***G*** (equation 5.12) in row A $1/R$ is added in column A and $1/R$ is subtracted from column B. Similarly, in row B $1/R$ is added in column B and $1/R$ is subtracted from column A.

$$[G] = \begin{array}{c} \\ A \\ B \end{array} \begin{array}{c} \begin{array}{cc} A & B \end{array} \\ \begin{bmatrix} \frac{1}{R} & -\frac{1}{R} \\ -\frac{1}{R} & \frac{1}{R} \end{bmatrix} \end{array} \qquad (5.12)$$

The overall conductivity matrix is assembled by applying the above equation to all the conductors. The conductivity matrix for a three node circuit (Figure 5.4) is shown on the next page.

$$[G] = \begin{array}{c} \\ 1 \\ 2 \\ 3 \end{array} \begin{array}{c} \begin{array}{ccc} 1 & 2 & 3 \end{array} \\ \begin{bmatrix} \frac{1}{R_{12}}+\frac{1}{R_{13}} & -\frac{1}{R_{12}} & -\frac{1}{R_{13}} \\ -\frac{1}{R_{12}} & \frac{1}{R_{12}}+\frac{1}{R_{23}} & -\frac{1}{R_{23}} \\ -\frac{1}{R_{13}} & -\frac{1}{R_{23}} & \frac{1}{R_{13}}+\frac{1}{R_{23}} \end{bmatrix} \end{array} \qquad (5.13)$$

If the current source, I_m, is connected between two nodes, the value of the current in the current source is added to the corresponding node in the source vector, $\boldsymbol{I}$, if the current flows into the node, and subtracted if it flows out.

Once the conductivity matrix and source vector are assembled then the problem is reduced to the solution of equation 5.11. This is a simple linear simultaneous equation. Various methods are available to solve this linear algebraic equation. The LU decomposition method with forward and backsubstitution was used to solve this linear equation.

5.2.2 Lattice models

Lattice models (square and hexagonal) were also developed to compare with the proposed new model. In lattice models, the fibres are assumed to be distributed in a predetermined square or hexagonal arrangement. The fibres are placed in the square or hexagonal lattice by filling the lattice sites randomly. In this case, the total number of fibre sites equals the total number of fibres. The total number of fibres was calculated using the equation 5.9. The lattice sites that are not filled with fibres are assumed to be filled with matrix material of zero conductivity.

Once the fibre sites are filled, the next step is to determine the number of fibres in contact to generate the electrical topological information. It is assumed that the fibres occupying adjacent sites in a lattice will contact at a point and that is represented as a resistor between two adjacent fibre centres. The unoccupied fibre site is filled with matrix material. So, there is no conductance between a fibre site and an unoccupied fibre site. The diagonal fibre sites in a square lattice are not in contact and hence there is no conduction between diagonal fibre sites. In a square lattice there can be maximum of four fibre contacts. Similarly, in a hexagonal lattice there can be a maximum of six fibre contacts. This fibre to fibre contact information is transformed into electrical topological information. The topological information is then used to form the conductance matrix. The detail of formation of conductance matrix from topological information is described in section 5.2.1.4. The solution of this equation will provide the overall resistance and the potential distribution at every fibre site.

5.3 3D MODEL

The electrical conduction mechanism of CFRP is a three-dimensional process. This is demonstrated in chapter 7. 2D models are not suitable for simulation of the 3D conduction process of CFRP. 3D models are essential to simulate the effects of damage. This section details the development of the proposed new model.

The main objective is to first model the fibre arrangement or the resistive components of the laminate as an assemblage of unit cells. Once the basic model is developed, then the next step is to introduce the effects of electrode, damage mechanisms and environment. The major steps involved in this model are shown in Figure 5.5.

The formulation of the 3D model is based on the assumption that the laminate is madeup of repeated linkage of a unit cell. Consider the parallelepiped unit cell of length *L*, width *W*, and thickness *T*, as shown in Figure 5.6. The fibres are oriented along the X-axis, i.e., the length of the unit cell. In order to include effects of anisotropic electrical properties of CFRP, the unit cell is modelled as homogenous cell with orthotropic electrical properties. Let, the electrical resistivity of the unit cell along the three axes be ρ_x, ρ_y and ρ_z.

The properties of these unit cell are determined by the properties of the constituent materials and the volume fraction. The properties of the unit cell along the three different axes can be calculated using the previous models. For example, the resistivity along the fibre direction can be calculated using the parallel resistance model. Similarly, the transverse and through thickness resistivity can be calculated using the lattice models and the proposed new random network model.

The assumption of unit cell linkage is valid only if the size of the unit cell is large enough to avoid the nonhomogenity of CFRP. Moriya and Endo (1990) have shown that the transverse conductivity of CFRP for similar materials used in this investigation can be considered as homogeneous over thickness of 0.14 mm. So, If we assign a thickness and width of the unit cell more than 0.14 mm then the unit cell linkage assumption is valid. This sets the minimum width and thickness of the unit cell. This minimum size of the unit cell for a particular type of laminate can be calculated using the transverse conduction models.

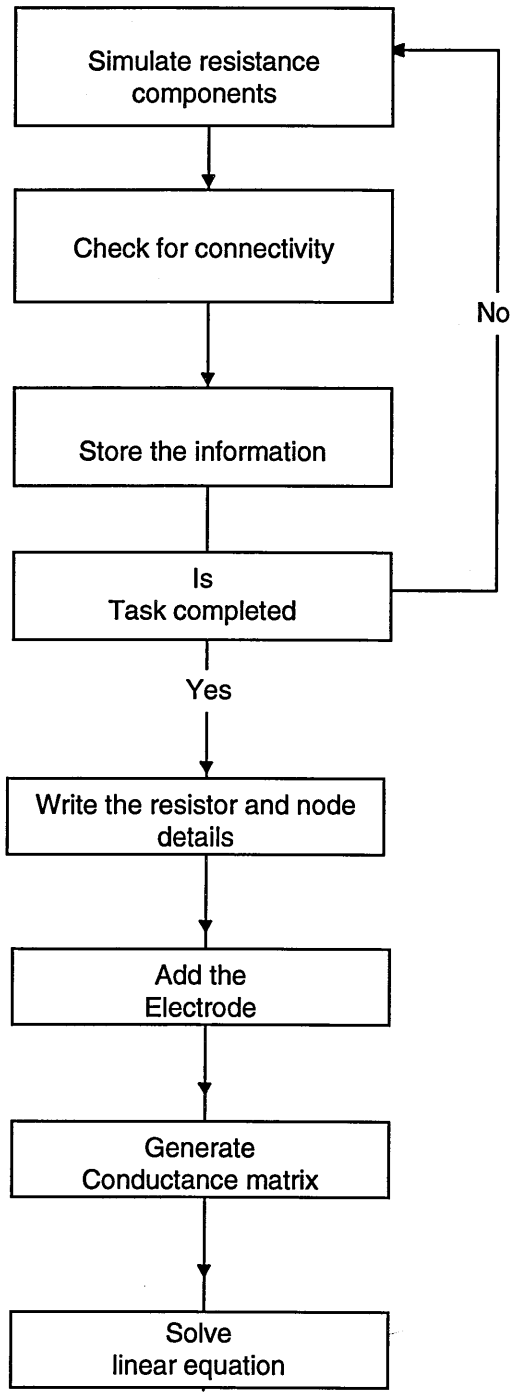

Figure 5.5. Flow diagram illustrating the major steps involved in the proposed 3D model.

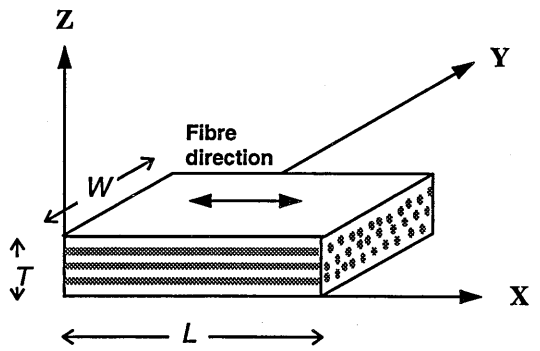

Figure 5.6. The parallelepiped unit cell.

The size of the unit cell is mainly determined by the structural parameters of the laminate. The other main factor is computing power. The sensitivity of the model will increase with decrease of the size of the unit cell. It is possible to model the unit cell with size equivalent to the size of the individual fibre itself. There are around 600 000 fibres in a laminate with a cross sectional area of 50 mm^2. Modelling at fibre level will need supercomputing power though the sensitivity will be very high. So, a compromise had to be made to optimise between sensitivity and computing power. This consideration is very important when we have to model the entire structure.

The main objective, as regards this thesis, is to demonstrate the importance of the 3D model and to understand the effects of damage mechanisms on electrical resistivity. These models have to be solved using the available computing power. So, it is important to determine the size of the unit cell that can demonstrate the model capabilities, and compromises between sensitivity and computing power.

The thickness can be modelled as equal to the thickness of a lamina. The laminate is made-up of individual lamina and sets the physical constraint in selecting the thickness of the unit cell. The fibre to fibre contacts are higher within the laminae than between the lamina. This model facilitates modelling of through thickness effects in a laminate.

The width of the cell can be assumed to be equal to the width of the strand. The CFRP prepregs are made by mixing fibre strands and not of individual fibres. When placing the fibre strands, the thickness is predetermined by the thickness of the lamina and so the strands can spread out on the width direction. It is possible that the fibres are not distributed uniformly over the entire lamina. The fibre volume content is more in the strand and less between the strands than the average volume content of the lamina. So, it is reasonable to assume that the width of the unit cell is equivalent to the spread out width of the fibre strands.

Along the fibre direction, the fibres are continuous. In order to introduce the effects of fibre breaks and other damage mechanisms, it is assumed that the fibres along the fibre direction are continuous linkages of fibres connected in series at the nodes. The length of the unit cell is assumed to be equal to 800 μm. This is equivalent to the approximate length where two fibres touch (Paluch 1994). In 3D model, the fibre breaks are simulated as broken linkage of a unit cell. Therefore, the fibre break simulation represents the breakage of all fibres distributed in a unit cell.

The topological information describes the details of the unit cell inter connections. The details of inter connection between the cells is shown in Figure 5.7. This figure shows the possible connection of a single cell. This also shows the resistive components of the cell in all the three directions. This interconnection detail is then transformed as topological information for circuit analysis. This procedure is similar to the transformation of fibre distribution data into electrical topological data as described in the previous section 5.2.1.3. The conductance matrix generation and the solution procedure are described in section 5.2.1.4.

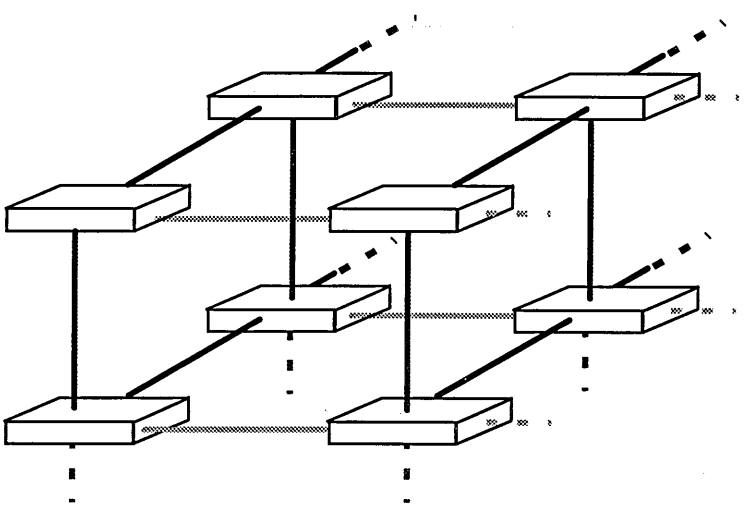

Figure 5.7. Illustration of the unit cell assemblage and its connectivity.

5.4 COMPARISON OF TRANSVERSE CONDUCTION MODELS

Figure 5.8 shows the simulated fibre distribution in a square area of a CFRP laminate with a side width of 100 μm and a fibre volume fraction of 0.60 for square, hexagonal and the proposed new random network model in comparison with the real laminate. This figure clearly demonstrates the closeness to reality of the fibre distribution simulated by the proposed new model.

Figure 5.9 shows the electrical network simulated from the fibre distribution data. The fibres at the top and bottom or left and right are connected to the electrode through which a constant current source is connected. The electrode at the bottom is considered as the reference point. The electrical solution of this network provides the potential distribution at every fibre site and the overall resistance. This figure clearly shows the effects of fibre to fibre contact distance in forming the electrical network. It is clear that the number of conductive paths are higher in the proposed new model and this can be modified according to the conduction mechanism.

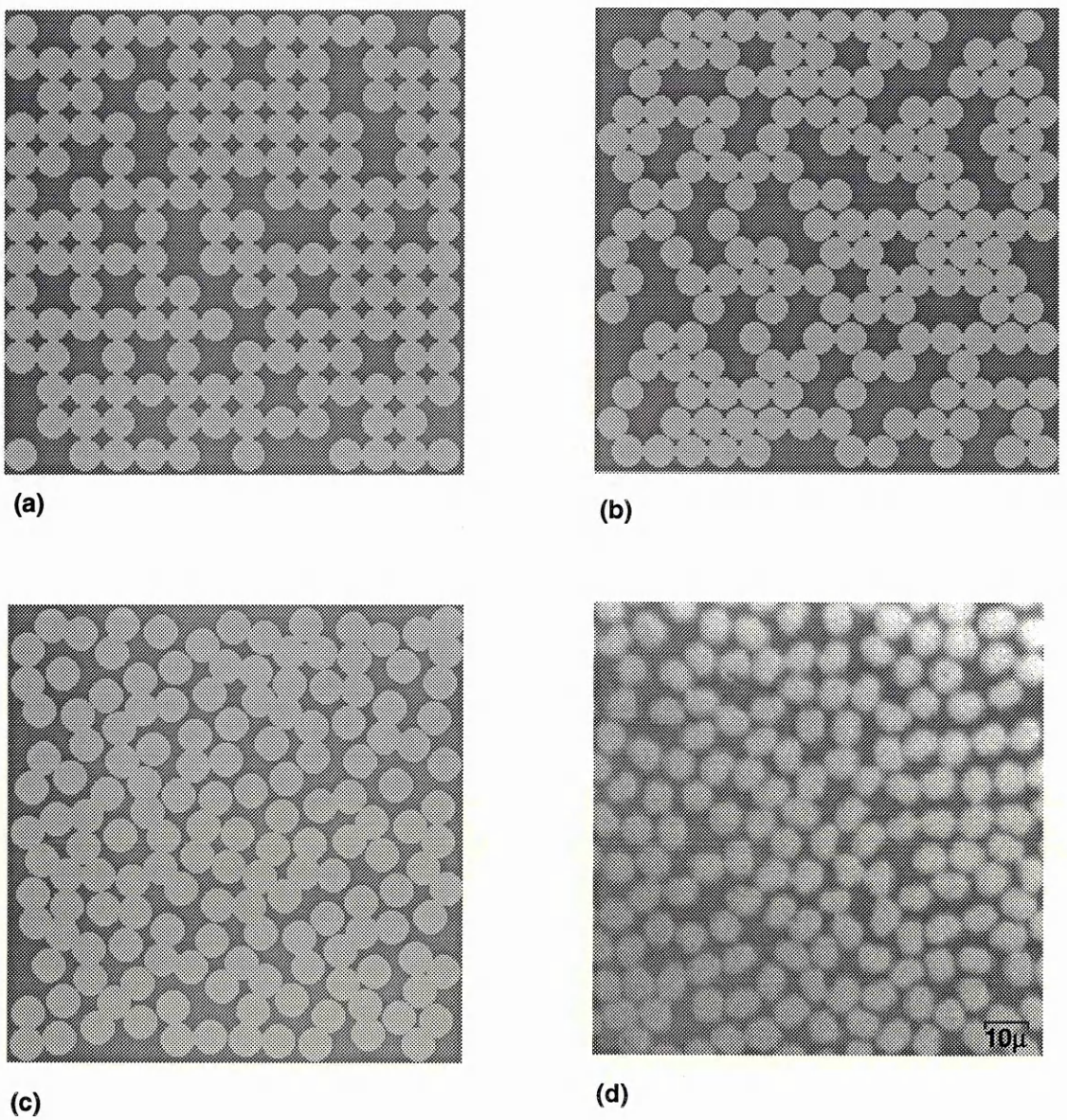

Figure 5.8. Comparison of fibre distribution simulated by, (a) square, (b) hexagonal and (c) proposed new random resistor network model in comparison with (d) the real laminate.

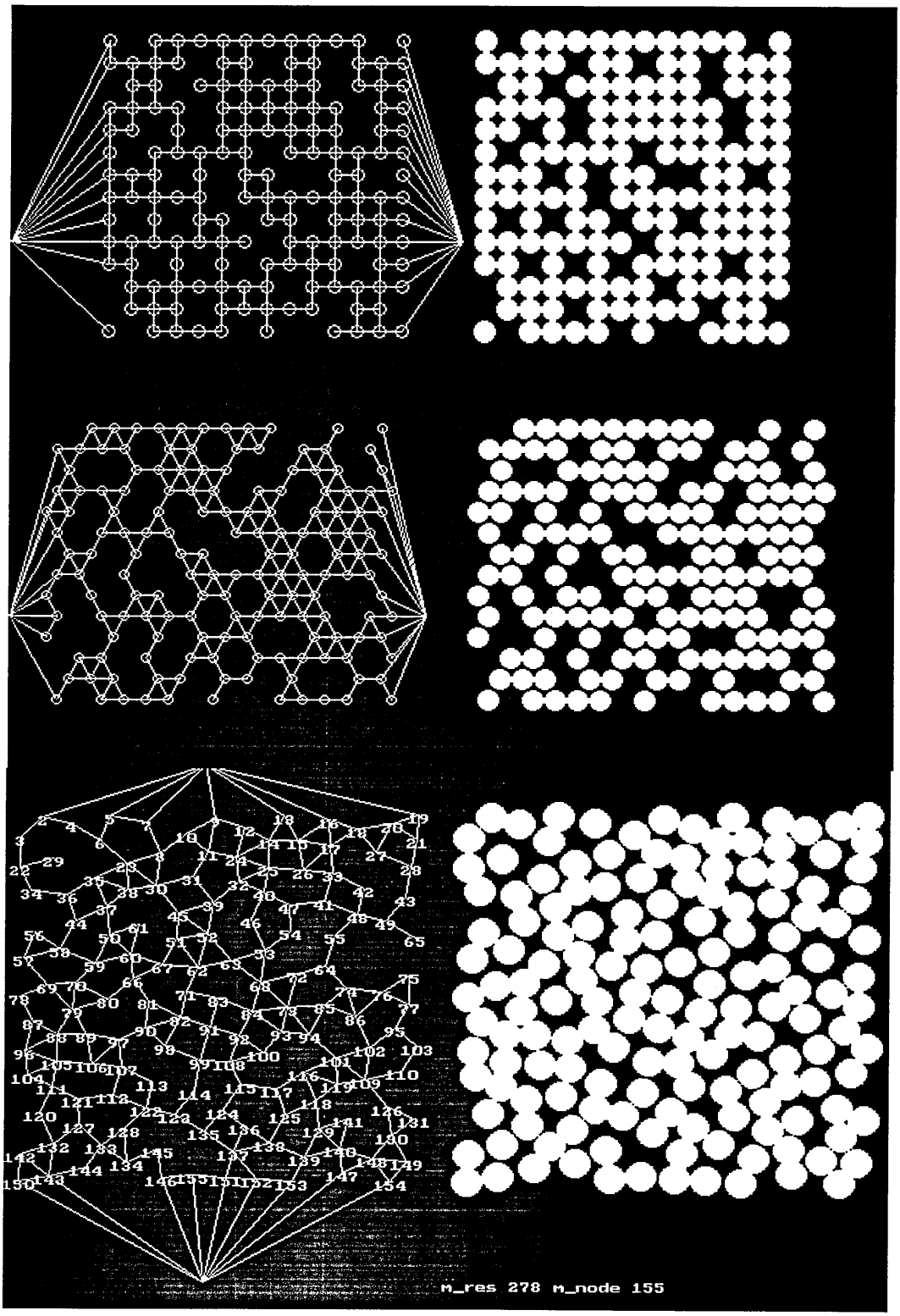

Figure 5.9. Electrical network transformed from fibre distribution data.

5.5 STRAIN SENSOR

The piezo-resistance property of carbon fibre can be used to measure the strain in the CFRP. This section describes the derivation of equation that relates the strain and the resistance. This can be used to measure the strain directly from the changes in the resistance. The resistance of a single fibre, R_f, of resistivity, ρ_f, length, L, and a cross sectional area of, A, can be written as follows.

$$R_f = \rho_f \frac{L}{A} \qquad (5.14)$$

If the fibre is stretched then the resistance will change because of dimensional change. The change in resistance of the fibre, dR_f, can be calculated by differentiating equation 5.14. Lets, assume that the fibre resistivity is constant. Partial differentiation of equation 5.14 yields :

$$dR_f = \rho_f \left[\frac{A.dL - L.dA}{A^2} \right] \qquad (5.15)$$

Area of a single fibre,

$$A = \frac{\pi D^2}{4}; \qquad (5.16)$$

The rate of change in area, dA, can be obtained by differentiating equation 5.16.

$$dA = \frac{\pi}{2} D \,.\, dD \qquad (5.17)$$

The transverse strain, ε_2, is equal to ratio of change in diameter, dD, and diameter, D.

$$\therefore \frac{dD}{D} = \varepsilon_2 \qquad dD = D \,.\, \varepsilon_2 \qquad (5.18)$$

The transverse strain, ε_2, and longitudinal strain, ε_1, can be written as follows using Poisson's ratio, μ,.

$$\varepsilon_2 = -\mu\varepsilon_1 \qquad (5.19)$$

Substituting the value of ε_2 in equation 5.18,

$$dD = -D\mu\varepsilon_1 \qquad (5.20)$$

Substituting the value of dD in equation 5.17,

$$dA = -\frac{\pi D^2}{2} \mu \varepsilon_2$$

$$dA = -2A\mu\varepsilon_1 \qquad \Theta\ A = \frac{\pi D^2}{2} \qquad (5.21)$$

The longitudinal strain ε_1,

$$\frac{dL}{L} = \varepsilon_1 \qquad \therefore dL = \varepsilon_1 . L \qquad (5.22)$$

Substituting the values of *dD* and *dL* from equation 5.20 and 5.22 respectively in equation 5.15.

$$dR_f = \frac{\rho_f L}{A} \varepsilon_1 (1+2\mu)$$

$$dR_f = R_f \varepsilon_1 (1+2\mu) \qquad (5.23)$$

The equation 5.23 can be used to predict the strain from resistance measurements of a fibre. Similar, derivation can be made for a unidirectional CFRP as shown below,

$$dR_c = R_c \varepsilon_1 (1+2\mu) \qquad (5.24)$$

where, R_c, is the resistance of the composite, dR_c is change in resistance. This equation can be used to predict the strain from the resistance measurements of a unidirectional CFRP.

PART III

RESULTS AND DISCUSSION

6

ON THE EFFECTS OF ELECTRODE

The electrode is an important part of the electrical resistivity measurement technique. Most of the earlier investigators (refer the literature survey, section 3.5.2) have identified the problems with the electrode, however, no one has addressed it in detail. This is because most of the available investigations are qualitative. In qualitative electrical resistivity measurements the effect of the electrode is not critical, as they are only concerned with the change in resistance. Even in this case, it is necessary to know the behaviour of the electrode in order to understand the behaviour of the samples. For quantitative use of the electrical resistivity measurement technique and to achieve the ultimate goal of smart capabilities, the resistance, behaviour, and characteristics of the electrode should be known.

Conduction in CFRP is established mainly through the conductive carbon fibres. The electrodes used to pass the current should make maximum contact with the fibres to make better conductivity. It is more critical that this problem should be addressed first in order to study and characterise damage using electrical resistivity measurements.

This chapter presents the investigations of the different electrode formation methods and its effect on the resistivity measurements of unidirectional CFRP. The main objective is to

investigate the electrode formation method that results in the lowest possible or close to the theoretically predicted resistance of the sample and also, the lowest scatter, i.e., consistent results. This chapter also describes the electrode details, factors that influence the resistance and presents the relevant results.

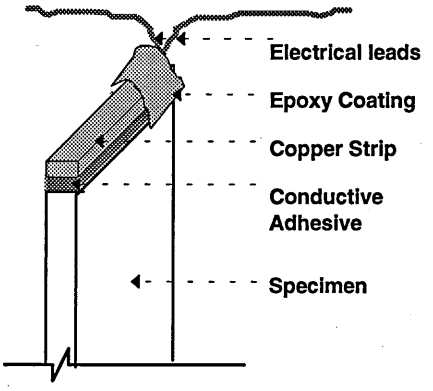

Figure 6.1. A typical electrode.

6.1 ELECTRODE DETAILS

An electrode, according to the Oxford Dictionary, is a conductor through which electricity enters or leaves a conducting medium. This is a general definition and it includes all forms of electrodes. For example, in metals, even a point probe can be considered as an electrode. In CFRP, use of point probe can be misleading as the resistance can be different according to the place of contact. So, a plate probe is generally used. Plate probes are glued to the samples using some conductive adhesive. This facilitates keeping many of the electrode variables constant and is hence helpful in standardisation. Therefore, we are concerned with the electrode that can be permanent and can act as an electrical sensor for the present specimens and the future smart structures. In this thesis, electrode means the combined form of the conductor (copper strips with soldered electrical leads), and the conductive adhesive. The details of a typical electrode connection are shown in the Figure 6.1.

6.2 FACTORS INFLUENCING THE RESISTANCE

The resistance of the sample can be influenced by many factors. Prior to the experimental measurements, it is necessary to know the factors that can influence the measured resistance. This theoretical understanding can provide us with the information for designing better experimental methods for the characterisation of electrode effects. The scatter in the measured resistance of CFRP samples can be due the inherent anisotropic and inhomogeneous nature of CFRP itself. The other factors are from the external electrode configuration and the physical properties of the conductive adhesive. Some of the important factors that are critical are summarised below.

6.2.1 Material properties

In general, the properties of a composite will be the average of the properties of the individual components, the so called `property averaging' (Agarwal and Broutman 1990). Therefore, the

measured resistance is influenced by the electrical properties of the fibres, matrix and also the electrode materials. In unidirectional CFRP the properties are the average of the constituents and hence can be predicted using rule of mixtures. The knowledge of the properties of the constituents is necessary to predict the properties of the composites. This will aid in quantifying the resistance of the electrode.

6.2.2 Geometry of the sample

The geometry of the sample also influences the resistance. This is true for all materials and that is why resistivity is generally used and is independent of specimen geometry. However, changes in resistivity with thickness and width have been observed for unidirectional CFRP (Joy et al. 1980; Belani and Broutman 1978). This is critical for off-axis unidirectional laminates, as the conduction is mainly due to current flow along the fibres.

6.2.3 Fibre volume fraction

Fibre volume fraction of the composite itself can vary from sample to sample. The fibre volume fraction is an average measure of fibre content over the entire laminate. The volume fraction of samples that are cut from the bulk laminate can vary from the average volume fraction of the laminate. The volume fraction determines the number of fibres involved in the conduction process. If the volume fraction is less, then that means less fewer fibres for electrical conduction and that leads to higher resistance in unidirectional CFRP, and vice versa with high volume fraction. The simplest method to measure the fibre volume fraction for each sample is the thickness measurement method. This is relatively simple, non-destructive and does not need additional sample preparation.

6.2.4 Misorientation of fibres

Misorientation of fibres is a manufacturing defect, and can be due to fabrication or machining process. Misorientation of fibres will affect the longitudinal electrical resistance of the unidirectional CFRP. Misorientation causes two effects, first the effective length of the fibre increases, furthermore some of the fibres are eliminated from the conduction process. This effect is clearly shown in the Figure 6.2. The former increases the resistance of the fibres due to increase in length and hence the resistance of the sample. The latter removes the fibre from the conduction process. This will lead again to

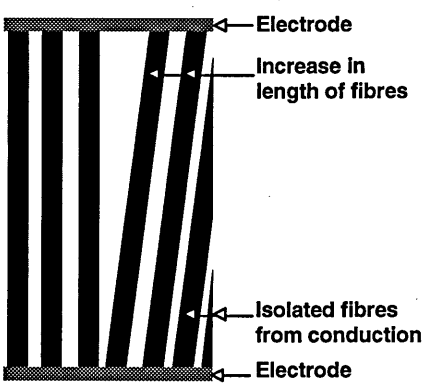

Figure 6.2. Schematic illustration of the effects of fibre misorientation.

increase in resistance of the sample due to the parallel arrangement of fibres. The above misorientation is an ideal case, i.e., the misorientation effects are uniform throughout the sample. However, in a real case there may be local misorientation that can overlap with other fibres, etc. This can cause short circuits and different conduction paths as against the oriented fibres. This will alter the current flow pattern and hence the resistance. Similar effects can also be expected for fibre waviness also.

6.2.5 Conductive adhesive

Conductive adhesive is an important part of the electrode. Conductive adhesives are generally made by mixing conducting filler particles in an adhesive, for example, silver or gold particles are generally mixed in an epoxy resin (Ruschau and Newnham 1992). The electrical properties of conductive adhesives are again complex, as is almost same as the composites. The inherent factors and parameters that influence the conductive adhesive can then influence the resistance of the CFRP. The properties of the conductive adhesive are determined by the particle size, volume fraction, properties of the matrix material, etc. The percolation phenomena are more critical in the conductive adhesive. The other external parameters such as the thickness, cure, etc., of the conductive adhesive can also affect the resistance of the sample.

6.2.6 Surface preparation methods

The surface preparation method includes the methods employed to expose the carbon fibres and other usual preparation methods of bonding two surfaces. The extent and the nature of fibre exposed by various methods can influence the resistance. On the other hand the process chosen to prepare or expose the electrode area should not alter the properties of the sample. For example, fibre exposure by abrasion is known to damage the fibres (Gaier et al. 1991). The damaged fibres are isolated from the main conduction process and hence will influence the electrical properties. So, it is necessary to ensure that the electrode formation methods are not going to alter the properties of the sample or influence the measured resistance.

6.3 EXPERIMENTAL WORK

The details of the experimental work are shown in Figure 6.3. As regards the direction of resistance measurement and basic electrode formation method, in this investigation the type I electrode was used. In order to make better electrodes, the first step is to expose more carbon fibres. Therefore, two methods were selected to expose the carbon fibres namely, mechanical polishing and plasma etching. Once the carbon fibres were exposed then the next step is to connect the copper strips with soldered electrical leads to the sample. Conductive adhesives such as silver paint and silver epoxy adhesives were used. Prior to bonding the copper strips,

some of the samples were coated with thin copper film by a copper sputtering technique. Where possible the resistance was measured after every process to compare the effects of each process on the sample resistance. For comparison purposes samples as obtained from the laminate, i.e., saw cut samples, referred here as unpolished samples, were also used in this investigation. These samples were subjected to all the electrode formation methods other than the carbon fibre exposure methods. The details of the process are described in the following sections.

Experiments such as dependence of the sample resistance on length and width were made to quantify the electrode resistance. In these experiments similar electrode formation methods were applied to samples of different length. In theory, the dependence of length study should aid in quantifying the electrode resistance.

Specimens for resistivity measurements were fabricated using UD914L samples. The laminate fabrication and sample preparation methods are described in section 4.4. Specimens with a length of 50 mm, width of 25 mm and a nominal thickness of 2 mm were used. A minimum of five samples per category were prepared. After initial investigation, for some of the selective category ten samples were prepared. The electrical resistance was measured using the four point method as described in section 4.6.8.

6.3.1 Mechanical polishing

The main aim of mechanical polishing is to subject the samples to different levels of abrasion to

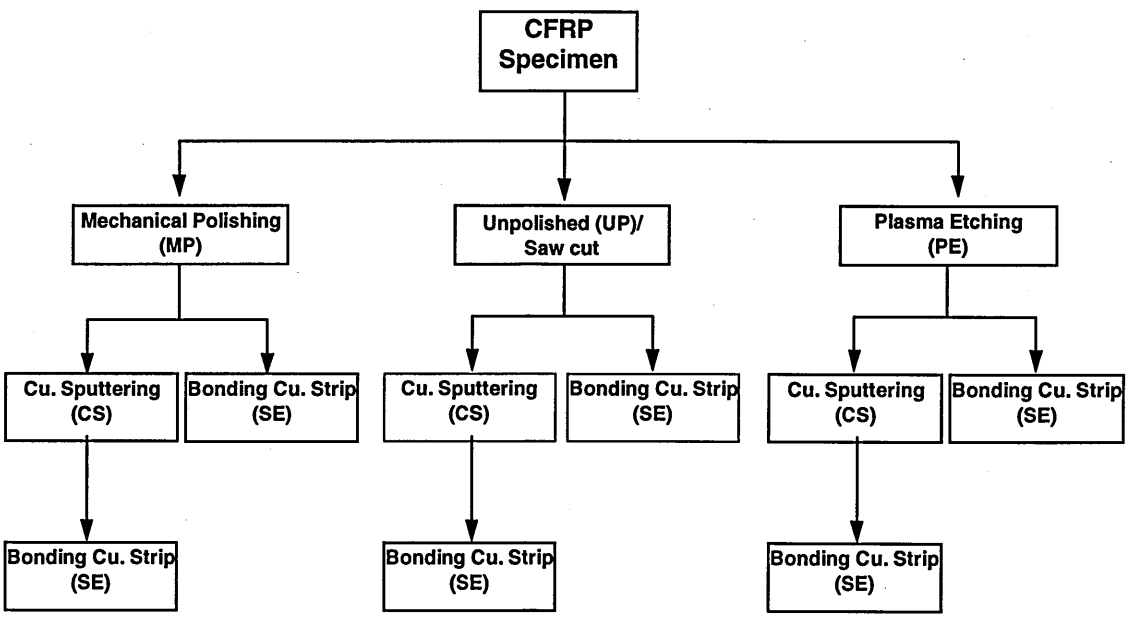

Figure 6.3. Flow chart illustrating the experimental programme.

expose only carbon fibres and abrade epoxy resin. It was suggested by Schulte and Baron (1989) that use of 3 μm diameter aluminium oxide powder can abrade epoxy resin and protrude the carbon fibres. This is possible in theory due to the difference in hardness level of carbon and epoxy. In practice, it was suggested by the metallography laboratory staff that this is difficult to achieve. To the author's knowledge the effect of differential material removal due to mechanical polishing is not described in the literature. It is understood that this procedure is by trial and error and there are no established procedures or equations to calculate the amount of pressure and the time of polishing. After the initial trial investigations, a jig, a rectangular block with a 2 mm thick slot, to hold the samples in position was made. This improved the handling of samples and so it was easy to polish the samples flat. The automatic polishing machine was not used because of the unusual sample size and configuration. Therefore, the time and applied pressure were manually controlled. However, it was found that it is difficult to control the pressure manually. Four stages of abrasion were used. The first three were to remove the cutting marks and to remove any associated damage due to the cutting of the samples from the laminate and to prepare the sample surface for the final polishing. The final stage is to subject the samples to differential erosion. The four stages are listed below.

- P80 grade silicon carbide paper for two minutes.
- P500 grade silicon carbide paper for two minutes.
- P1200 grade silicon carbide paper for two minutes.
- 3 μm aluminium oxide powder for one minute.

The micrograph of a typical unidirectional sample subjected to various stages of mechanical polishing is shown in Figure 6.4.

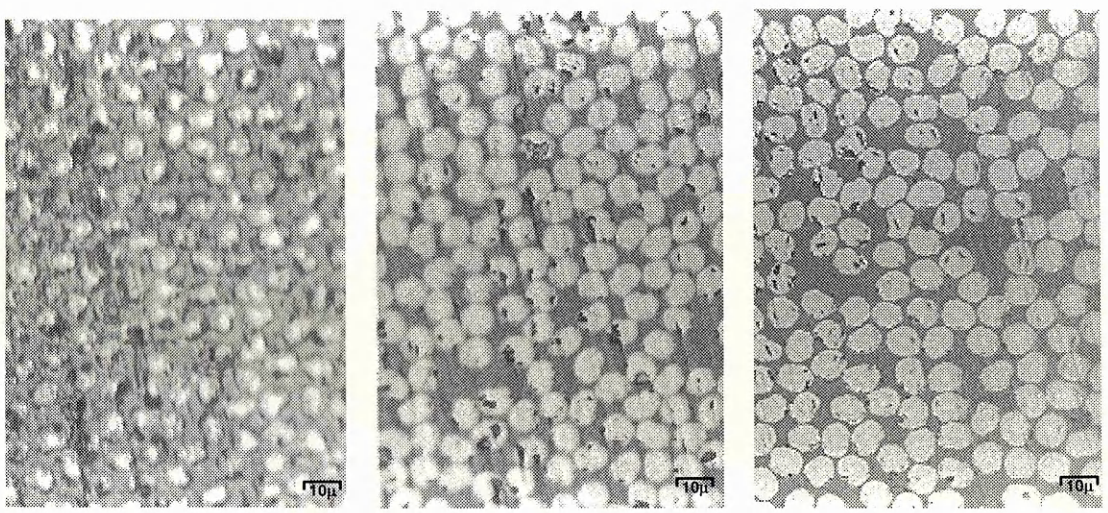

(a) (b) (c)

Figure 6.4. Optical micrograph of a typical unidirectional sample subjected to different levels of mechanical polishing, (a) P500, 2 minutes, (b) P1200, 2 minutes and (c) Al_2O_3 powder, 1 minute.

6.3.2 Plasma etching

Plasma etching is a dry etching process of material removal. In this case, plasma etching was used to etch the epoxy resin and so the carbon fibres are the resist. The physics and experimental principles of this technique can be found elsewhere (e.g., Thomson et al. 1994; Till et al. 1985). In a typical plasma etch operation, first the sample is loaded in to the etch chamber followed by vacuum pull down. The gases are then bled into the chamber and the rf power is turned on, resulting in a glow discharge that produces the reactive etch plasma. A 'gas plasma' is simply a form of the specific gas mixture that contains atomic and ionised species when the rf energy couples with it. The plasma is really a breakdown process caused by the rf energy breaking the bonds of the supplied gas molecules into atoms of the same molecules. A constant etch rate is maintained by metering in a predetermined amount of the etching specie. All volatile products of the reaction are removed by the vacuum pump.

Plasma etching was carried out at British Aerospace, Sowerby Research Centre, Bristol (BAe) in an Electotech ET425 parallel plate etcher. This machine was used in plasma etch mode, i.e., sample table grounded. The gas used was pure oxygen at pressure of 300 mT. The plasma was generated by a 300 KHz power supply operating at a current of 2 amperes. The SEM micrograph of a typical unidirectional sample after 100 minutes in plasma is shown in Figure 6.5.

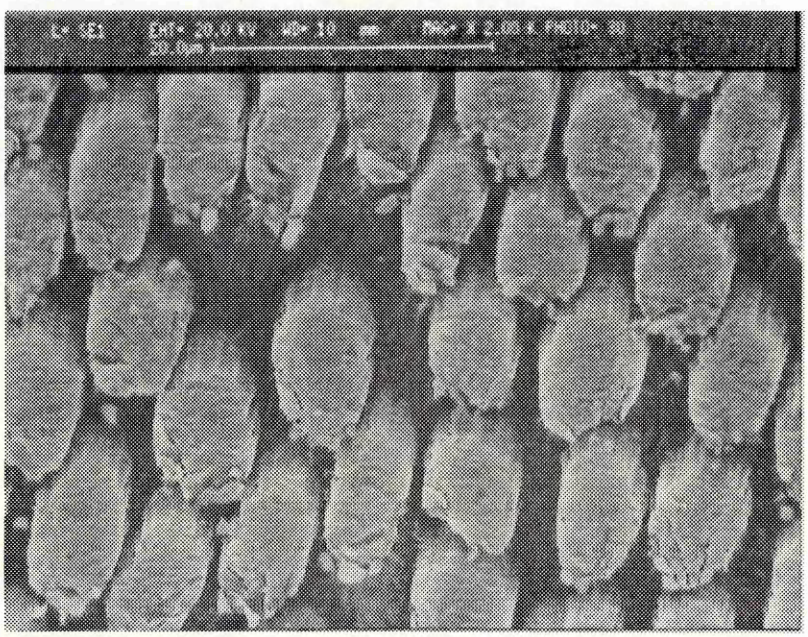

Figure 6.5. SEM micrograph showing the protruded carbon fibres of a typical unidirectional laminate after 100 minutes in plasma.

6.3.3 Copper sputtering

Sputtering is a versatile tool in that many materials can be deposited by this technique. Copper sputtering is a process of applying thin film or 'metallising' the samples using copper. Sputtering is done by ionising inert gas particles in an electric field producing a gas of plasma. This is then directed toward the source or target, where the energy of these gas particles physically dislodges, or 'sputter off,' atoms of the copper or other source materials.

Sputtering was also carried out at BAe, in a diffusion pumped Nordiko NM2000 sputter deposition equipment. The substrate was sputter etched at 500 W rf and 20 mT of argon to enhance adhesion prior to DC sputtering of 99.99% pure copper from a magnetron high rate sputter source. A total thickness of 5 μm of copper was deposited. Simple adhesive tape peel tests showed the film had adhered well and four point probe measurements on calibration samples showed the resistivity to be the same as bulk copper.

6.3.4 Bonding copper strips

Copper strips of 0.5 mm thick were glued to the samples using conductive adhesives. Initially silver paint was used for gluing the sample. The electrodes were debonded even during handling itself and hence were not suitable for use with specimens subjected to mechanical loading. Hence, after the initial investigations the silver paint was excluded from further investigations. Silver epoxy was the primary adhesive used for bonding the copper strips to the electrode.

The initial investigations and the scatter in the measured resistance suggested that the bonding method had to be standardised. The conductive adhesive should only be applied to the electrode areas, if other areas are contaminated then that can form different conductive paths and hence can introduce errors in the measured resistance. A special jig and silicone guides were made. This facilitated application of uniform pressure and alignment of samples and electrode in position. After this procedure, the scatter in the measured resistance was under control, the standard deviation was reduced from 12 to a maximum of 0.2.

Prior to bonding, the copper strips soldered with electrical leads were abraded using emery paper of grade P1200. Some of the samples were treated in nitric acid to remove the tarnish film. Finally samples were cleaned using acetone. The electrical leads were soldered to the samples prior to bonding to avoid damage to the samples and electrodes by soldering heat. After making the connections the electrodes were coated with commercial grade quick setting epoxy adhesive to avoid any possible damage during handling and to insulate the electrodes.

6.4 RESULTS AND DISCUSSION

The electrical resistance of the samples measured using different types of electrode is shown in Figure 6.6. This includes only the main results, other results are shown in Table 6.1. The lowest resistance and standard deviation were observed for PE/CS/SE configuration. The highest resistance and standard deviation were observed for MP/SE. From the electrical sensor point of view, what we see from the results is the electrode formation method that results in lower resistance and with very little scatter. According to this view, PE/CS/SE configuration results in lower resistance and standard deviation. Also, the electrode formation method has to be simple and must not require specialised techniques or complicated process. According to this view, UP/SE is the best. Though, this results in higher resistance the standard deviation is relatively less than the mechanically polished samples.

At this point, it is useful to recall the parallel resistance model to quantify the electrode resistance and to explain the effects of different electrode formation methods. According to the parallel resistance model, the unidirectional CFRP samples can be modelled as a parallel network of resistors. If we assume that the electrodes are connected to the sample as series of resistors, using simple electrical circuit theory, the resistance of the electrode alone can then be derived. This equals the measured resistance minus the predicted resistance of the sample

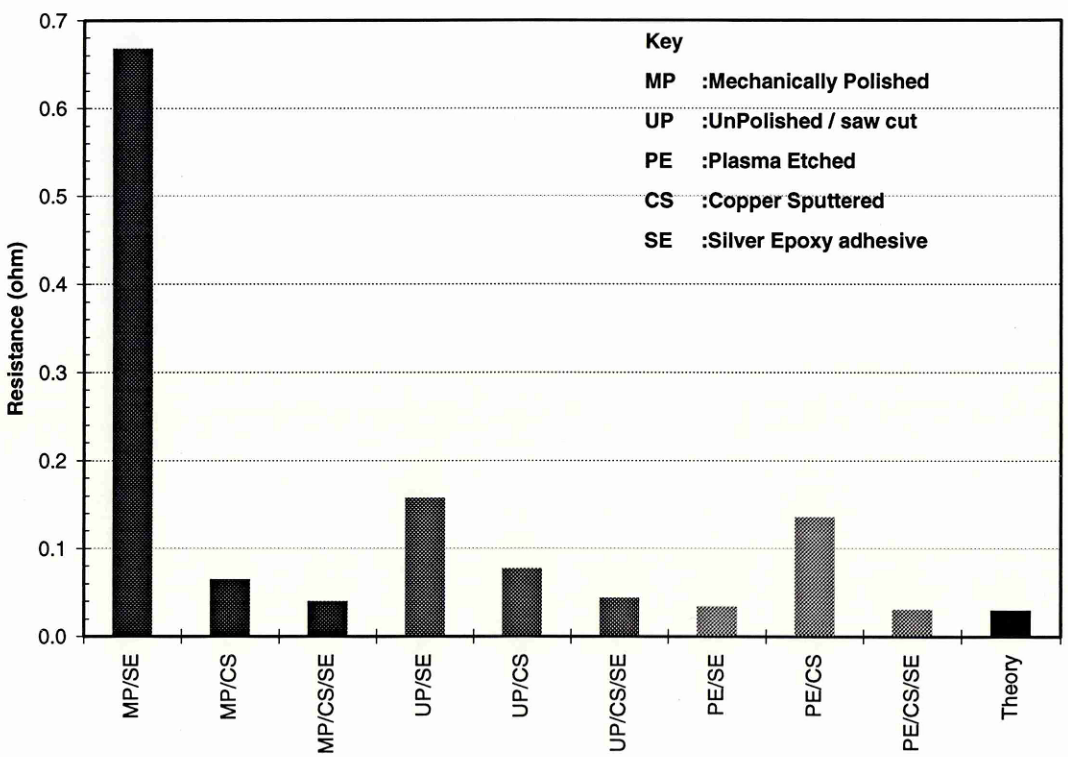

Figure 6.6. Bar chart illustrating the results on the influence of electrode on sample resistance.

using the parallel resistance model. The theoretical resistance of the samples used in this investigation is 0.03 ohm. The electrode resistance calculated is shown in the last column of Table 6.1.

From the results, it is clear that the plasma etching exposed more carbon fibres. Mechanical polishing did not expose more carbon fibres compared with plasma etching (refer Figure 6.4 and 6.5). The results prove that differential abrasion is difficult to achieve by mechanical polishing.

However, mechanically polished samples with a copper sputtered film minimised the electrode resistance. For all mechanically polished samples the standard deviation is higher, i.e., the results are scattered and not centred around the mean. This is true even if we compare the mechanically polished samples with unpolished samples. Though, the polishing time was maintained constant for all the mechanically polished samples, the contact pressure was not maintained uniform due to practical difficulties as mentioned earlier. This could have introduced non-uniform level of abrasion and may be the main reason for the scatter in measured resistance. The main aim of mechanical polishing was to introduce differential abrasion. The results show that this is not the case. The mechanical polishing introduced additional problems.

Table 6.1 Results of electrode effects

Electrode detail	Average resistance (Ω)	Standard deviation	Sample variance	Electrode Resistance (Ω)
MP/SE	0.668	0.146	2.1E-02	0.6378
MP/CS	0.065	0.003	8.0E-06	0.0348
MP/CS/SE	0.040	0.007	4.8E-05	0.0010
UP/SE	0.158	0.003	8.9E-06	0.1275
UP/CS	0.078	0.011	1.3E-04	0.0476
UP/CS/SE	0.044	0.002	3.9E-06	0.0135
PE/SE	0.034	0.002	3.4E-06	0.0040
PE/CS	0.136	0.002	5.9E-06	0.1059
PE/CS/SE	0.031	0.001	3.3E-07	0.0006
UP/CS/SE_B	0.034	0.002	3.1E-06	0.0041
UP/SE/920	0.098	0.003	8.3E-06	0.0679
UP/SP/SE/920	0.405	0.057	3.3E-03	0.3750

For example, for better bonding, the bonding surface has to be rough. The mechanical polishing actually made the surface smooth. Therefore, the quality of the mechanical bonding should be poor. However, the copper adhered well to the mechanically polished surface, possibly due to chemical bonding. This is evident from the results of MP/SE and MP/CS.

If we compare the results of XX/CS and XX/CS/SE, the resistance of the latter is less than the former. In this section, XX, denotes the surface preparation methods such as plasma etching, mechanical polishing and saw cut. In this case after copper sputtering another electrode formation process is added, i.e., we are adding additional resistance components in to the electrode configuration. In a simple series resistor electrical circuit, this is equivalent to addition of two more resistors in series with the existing three resistors. In theory, this has to increase the resistance, however, the experiment shows decrease in resistance. The resistance of XX/CS samples was measured using a plate probe. This result demonstrates that a permanent electrical attachment method is necessary for reliable electrical resistance measurements.

It is evident that copper sputtering reduces the electrode resistance. If we compare the results of XX/CS and XX/SE, XX/CS results in lower resistance for mechanically polished and unpolished samples. Copper sputtering forms a thin copper film over carbon fibre and that is continuous. In XX/CS samples, if the carbon fibres make contact with the copper film then that is sufficient to ensure a complete conduction path to the copper strip soldered with electrical leads. In silver epoxy conductive adhesive the conduction is due to current flow along the millions of silver particles. So, in XX/SE samples, for conduction from carbon fibre to the copper strip, first the fibre has to make a contact with a silver particle and furthermore this silver particle has to form a complete conduction path to the copper strip. The possibility of forming a complete conduction path is more straightforward in XX/CS samples than in XX/SE samples and is clearly illustrated in Figure 6.7. Moreover, the resistance of silver epoxy is higher than copper film, though the bulk resistivity of silver is slightly lower than copper.

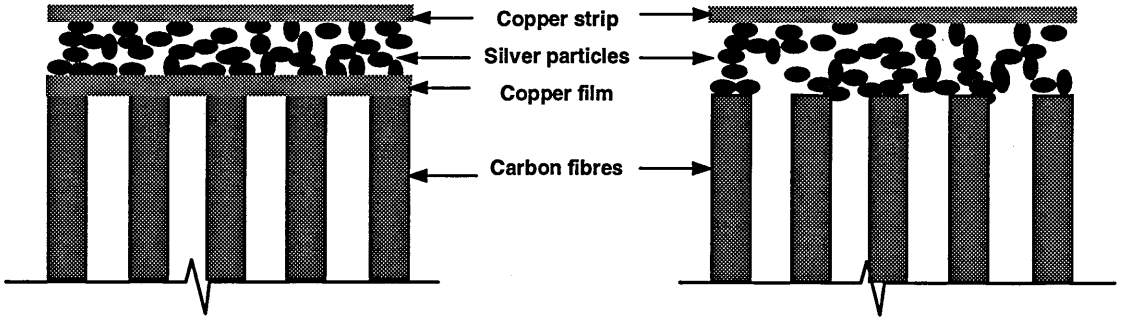

Figure 6.7. Schematic illustration of the effect of copper sputtering over silver epoxy.

The copper sputtering process did not reduce the electrode resistance of plasma etched samples. In fact, the resistance of PE/CS samples is higher than all the XX/CS samples and PE/SE and PE/CS/SE samples. It is strange in comparison with mechanically polished and unpolished samples that the resistance of PE/CS/SE is five times lower than the PE/CS samples. The copper film was sputtered over the carbon fibres protruded by plasma etching. The results suggest that the copper film did not form proper coating with the carbon fibres. During the resistance measurements of PE/CS samples the resistance decreased with increase in contact pressure. This again supports the above claim that the copper sputtering did not make contact with all the fibres. So, the contact pressure should have increased the number of fibres in contact and hence the decrease in resistance. Again a plate probe was used that can only apply uniform pressure over the copper film and hence the fibres that were on the same plane only could have made the contact. The use of silver epoxy during the formation of the electrode must have penetrated or pushed the copper film to make more fibre contacts and hence the resistance of PE/CS/SE is lower than the PE/CS samples.

It is obvious from the results that the proper copper sputtering reduces the electrode resistance. It was understood that this is because of the continuous conduction path provided by the copper film. The last two rows of the Table 6.1 show the results of the effect of silver paint coating. Epoxy-920 resin was used for these two batches of samples. The UP/SP/SE/920 samples were first coated with silver paint and then the usual electrode formation methods were employed. This in comparison with UP/SE/920 samples suggests that the silver paint coating did not improve the contact and reduce the contact resistance. This is evident from the observed higher resistance and standard deviation of these samples.

The results of UP/CS/SE_B demonstrate the repeatability of the results of electrode formation method that are carried out at other laboratories. The UP/CS/SE_B samples were fabricated at BAe, Sowerby Research Centre. These results compare well with the results of UP/CS/SE samples.

Figure 6.8 shows the resistance of samples of different length for two types of electrode configuration. The experimental points include the resistance of 100 mm, 200 mm, 300 mm, 400 mm and 600 mm length samples. This figure also shows the linear-fit of experimental points extrapolated up to zero length. In theory, at zero length the resistance of the sample should be zero and if we observe any other value other than zero then that is the electrode resistance. According to this, the electrode resistance is 0.1534 and 0.0712 Ω for MP/SE and MP/CS/SE samples, respectively.

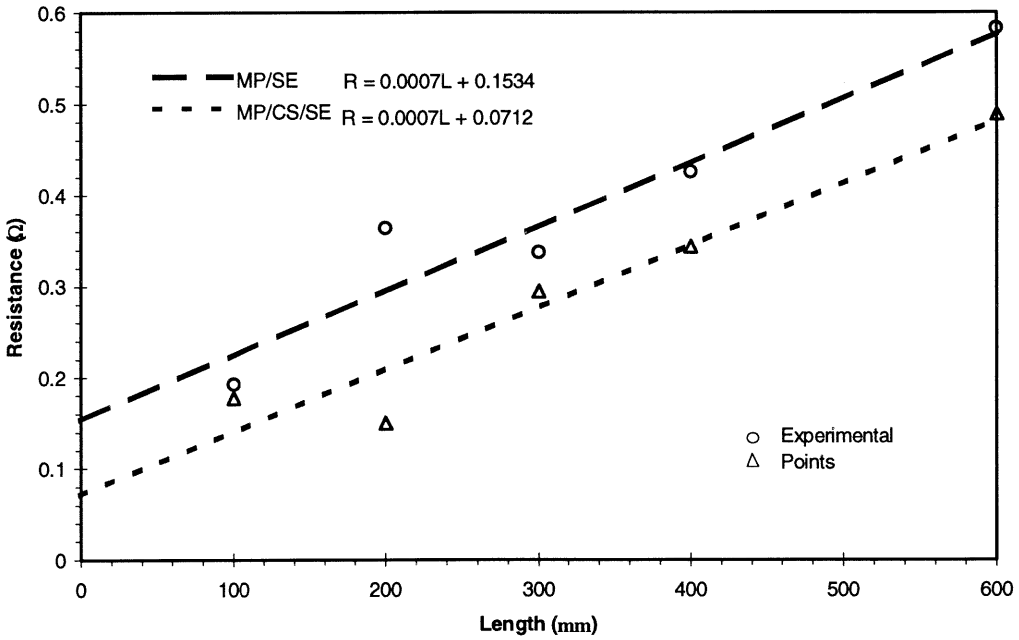

Figure 6.8. Results of the electrode resistance quantification experiments.

7

ELECTRICAL PROPERTIES

This chapter presents the results pertaining to specimen geometry and temperature dependent electrical properties of CFRP. The electrical resistivity values reported in the literature ranges over a wide spectrum. The resistivity of CFRP depends mainly on the properties of the constituents and their volume fraction. The resistivity is also influenced by the type of electrode and specimen geometry. The influence of electrode on the measured resistivity was investigated only in this thesis (refer chapter 6). So, it is necessary to measure the actual electrical properties of CFRP without the influence of the electrode. It is necessary to investigate the dependence of electrical properties of CFRP on specimen geometry because of the heterogeneous behaviour of CFRP.

The dependence of resistivity of CFRP samples on specimen geometry is investigated and reported in this chapter. The influence of electrode on electrical resistivity is reported in chapter 6. The electrical properties of unidirectional and cross-ply samples are presented in this chapter. The influence of specimen length, width and thickness on longitudinal and transverse resistance is also reported. The results presented in this chapter are viewed within the framework of the physics of electrical conduction.

The temperature dependence of electrical resistivity is another important property of CFRP that is vital for damage sensing using the electrical resistivity measurement technique. The temperature of the specimen or the structure can change during the measurement of resistance while characterising the damage. The measured resistance may be influenced by the temperature. In order to differentiate the measured resistance from the damage and temperature, it is necessary to know the effects of temperature on electrical resistance. There are no previous temperature dependent resistivity investigations of unidirectional and cross-ply CFRP laminates, hence, a detailed investigation was conducted. This can provide the calibration curve that can be used to differentiate the observed temperature change from that of the damage during mechanical testing. Further more, this investigation will give more information with which to understand the physics of electrical conduction of CFRP.

The details of sample preparation, electrode configuration, resistance measurement methods are described in chapter 4. Unless otherwise stated the electrical resistivity of the samples presented in this section was calculated using equation 3.2 from the resistance measurements.

7.1 ELECTRICAL PROPERTIES

Table 7.1 shows the summary of the electrical properties of UD914 and UD920 unidirectional samples measured using different types of specimen geometry. Figure 7.1 shows the electrical properties of 0° and 90° unidirectional and cross-ply samples of similar specimen geometry and electrode configuration. The statistical summary of the electrical properties is shown in appendix C (Table C.1 and C.2).

The results presented in Figure 7.1 provide direct indication of the electrical properties of samples used in this investigation. These results can be used for direct comparison of the magnitude of expected experimental electrical properties of the laminates.

Table 7.1. Summary of electrical properties of CFRP samples measured using different type of samples.

	UD914		UD920	
Resistivity (mΩm)	LR	TR	LR	TR
25x25x2 samples	0.2468	163.73	0.2829	34.29
Mechanical testing	0.0396	182.21	0.0486	37.06
Dependence of length	0.1880	-	-	35.06
Lamina samples	-	285.94	-	129.37
Parallel resistance model	0.0300	-	0.0300	-

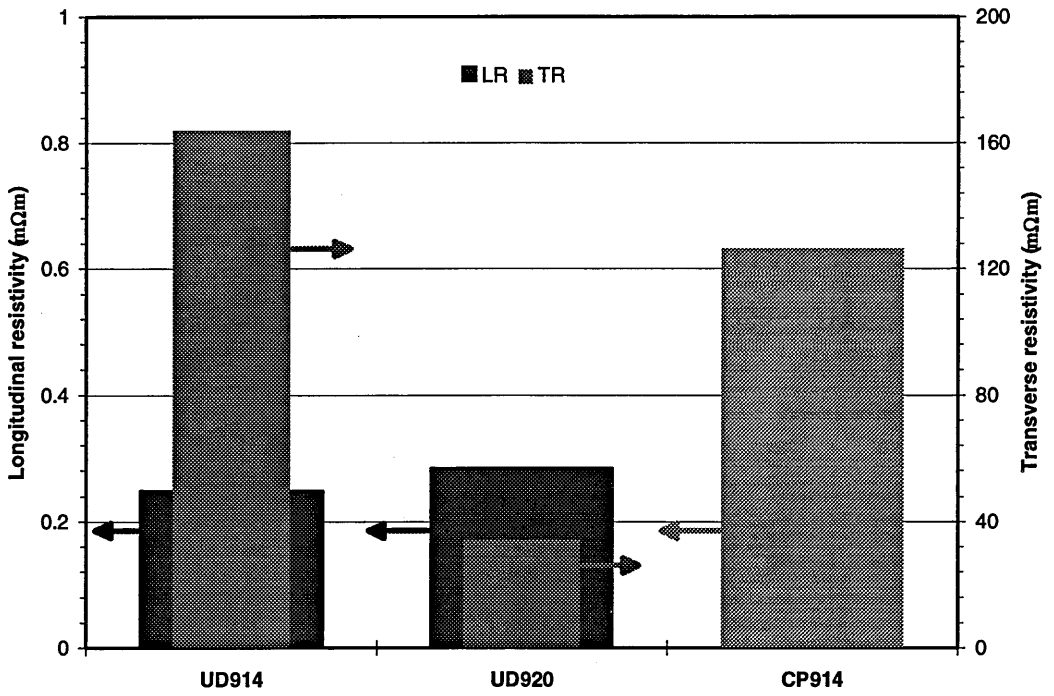

Figure 7.1. Electrical property of CFRP laminates of similar specimen geometry and electrode configuration.

7.1.1 Longitudinal resistivity

The statistical summary of the longitudinal electrical properties of UD914 and UD920 samples is shown in the appendix C. It can be seen from these tables that the mechanical test samples show lowest resistivity and standard deviation for both UD914 and UD920 samples. More over, these results are supported by a large population of samples. Therefore, these values can be taken as the actual longitudinal properties of CFRP laminates. Moreover, these values are close to the theoretical prediction. Therefore, in the subsequent sections, these values will be used for further discussion and comparison. The longitudinal resistivity of UD920 samples is higher than UD914 samples.

The theoretical longitudinal resistivity of unidirectional CFRP can be evaluated using the parallel resistance model or the 'rule of mixtures'. This is simply equivalent to fibre resistivity divided by fibre volume fraction (refer section 5.1). According to the above, the theoretical longitudinal resistivity of 0° unidirectional sample is 0.03 mΩm. The measured longitudinal electrical properties are higher than the theoretical values (refer Table 7.1). Experimental values of longitudinal resistivity of unidirectional samples close to the theoretical prediction have been measured using a different electrode configuration (refer chapter 6). This leads us to the

conclusion that the difference between the theory and the experiment is mainly due to the electrode contact resistance.

7.1.2 Transverse resistivity

Table 7.1 shows the statistical summary of the transverse electrical properties of UD914 and UD920 samples. The average transverse resistivity of UD914 and UD920 laminate samples measured using different specimen geometries is 173 mΩm and 35 mΩm, respectively. The transverse resistivity of lamina samples of UD914 and UD920 is 286 mΩm and 129 mΩm, respectively.

The anisotropic ratio, i.e., the transverse resistivity divided by longitudinal resistivity, of UD914 and UD920 samples is 4601 and 763, respectively (mechanical test samples). That is, the transverse resistivity of UD914 and UD920 samples are approximately 760 to 4600 times higher than the longitudinal resistivity.

The results also show that the transverse resistivity of UD914 laminate samples is approximately five times higher than the UD920 samples. Similarly, UD914 lamina samples are approximately two times higher than UD920 samples. These results are unexpected, because the UD914 and UD920 samples are almost the same, i.e., same fibre and volume fraction. It has been suggested that the transverse conduction is due transverse fibre to fibre contacts (Schulte and Baron 1989). For a given volume fraction it is expected that the number of fibre to fibre contacts would be the same. Therefore, the transverse resistivity is also expected to be the same. However, the five fold differences in resistivity suggest that the transverse conduction mechanism of CFRP is non-conventional and complex. This opens up an interesting discussion on the transverse conduction mechanism of CFRP.

7.2 DEPENDENCE OF SPECIMEN GEOMETRY

This section presents the results related to the influence of specimen length on longitudinal, transverse and though-thickness resistance of CFRP laminate. The laminate, test, electrode, and resistance measurement details are described in chapter 4. Some of the results presented in this section can be inferred from the effects of electrode location on damage sensing.

7.2.1 Dependence of longitudinal resistance on length

Figure 7.2 shows the results of the dependence of longitudinal resistance on sample length. The sample resistance is expected to increase linearly with increase in sample length. The linear fit extrapolated through the experimental points indicates that the resistance increases

linearly with increase in sample length. This is in excellent agreement with the theoretical prediction predicted using the parallel resistance model, i.e., the slopes are almost same. If we extrapolate the linear fit to the zero sample length, then the sample resistance should be zero. However, the extrapolated resistance at zero length is a positive value of 0.014 Ω. This indicates that this is the average contribution of electrode resistance. The y-axis intercept of this linear fit gives the value of the electrode resistance.

It is clear from Figure 7.2 that the deviation of experimental values from linear behaviour and the theoretical prediction is higher for samples of shorter length. This may be because, if we assume a constant electrode resistance for each sample then the contribution of electrode resistance to the sample resistance for shorter samples is higher. This behaviour can be better understood if we consider the dependence of resistivity on sample length. In theory, the resistivity of unidirectional CFRP is expected to be constant. Moreover, at the fibre level the electrical properties of CFRP are heterogeneous but at sample level with dimensions used in this investigation the electrical properties are expected to be homogeneous (Moriya and Endo 1990). So, the longitudinal resistivity for various sample lengths should be constant. The experimental result shows (Figure 7.3) that the apparent resistivity decreases with increase in sample length. This experimental behaviour was found to follow a power type decrease. It can be shown that this non-linear behaviour is due to the effect of the electrode and is not the property of the CFRP (see discussion).

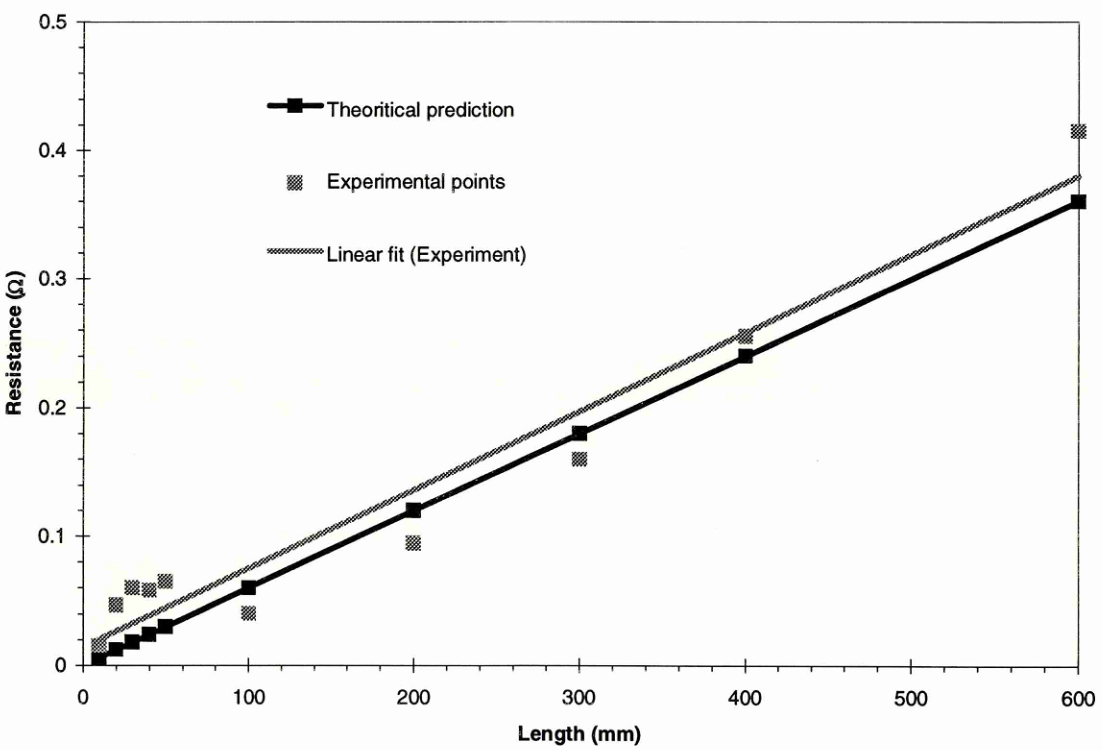

Figure 7.2. Dependence of longitudinal resistance on length.

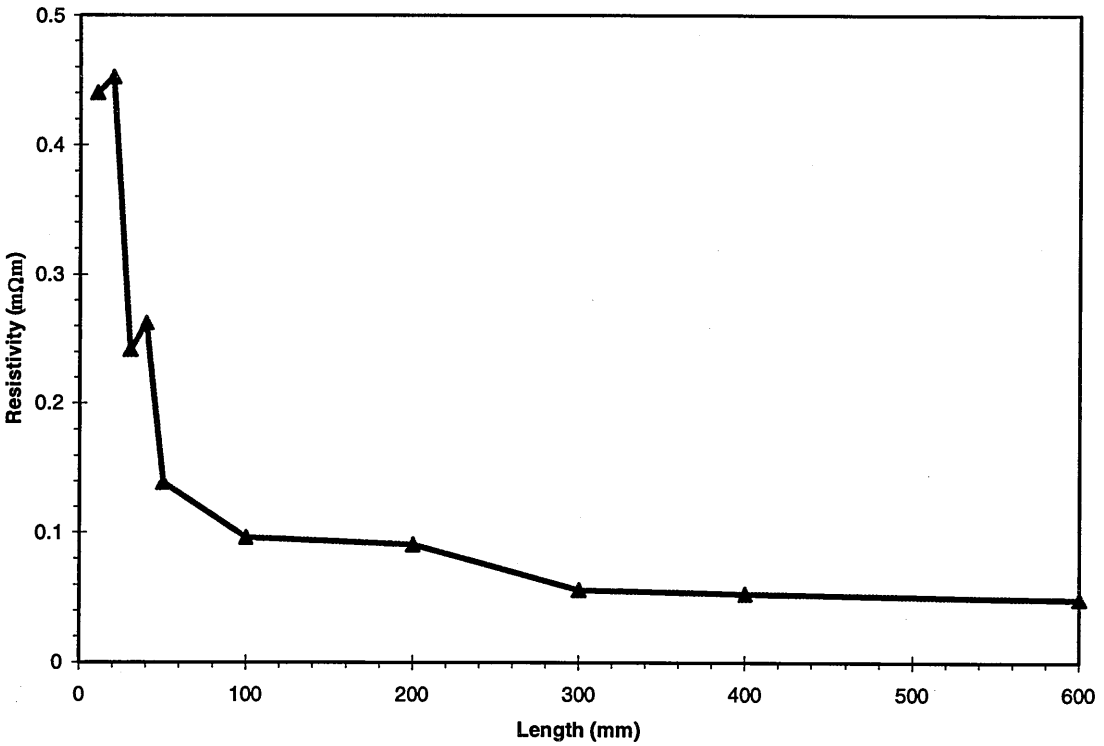

Figure 7.3. Dependence of longitudinal resistivity on length.

7.2.2 Dependence of transverse resistance on length

Figure 7.4 shows the results of the influence of sample length on transverse resistance. This figure shows that the transverse resistance increases linearly with increasing sample length, as expected. The electrode resistance was calculated from the y-axis intercept of the linear fit to the experimental data. Then the resistivity was calculated from the measured experimental resistance of the sample minus the electrode resistance, and is shown in Figure 7.4 on the second y-axis. The resistivity for varying sample length is constant, though the scatter in experimental measurements is high, i.e., a standard deviation of 8.1.

7.2.3 Dependence of through-thickness resistance on length

Figure 7.5 shows the influence of sample length on through-thickness resistance. The sample length was reduced in steps of 10 mm on each side of the electrode and then the resistance was measured. This figure includes the results of four samples. The result shows that the resistance increases non-linearly with decreasing sample length. It is a surprising result for the first look, as the resistance increases with decrease in sample length. This behaviour may be due to the 3D conduction mechanism of the CFRP (refer discussion, section 7.5.5).

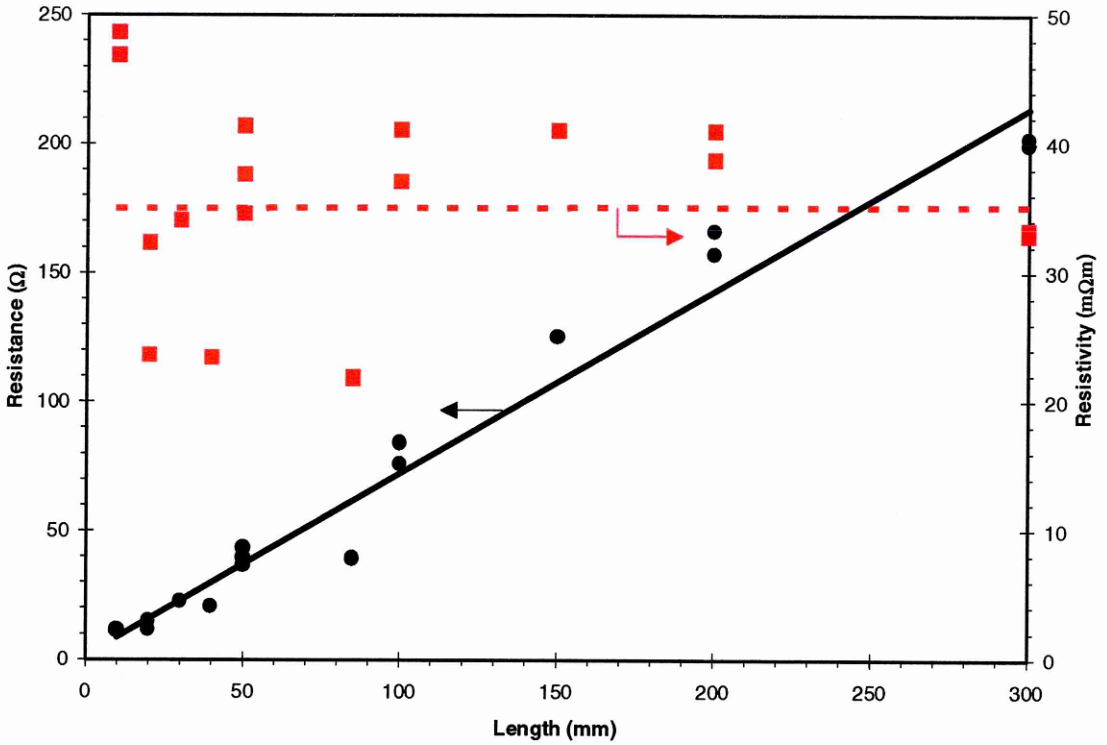

Figure 7.4. Dependence of transverse resistance and resistivity on sample length.

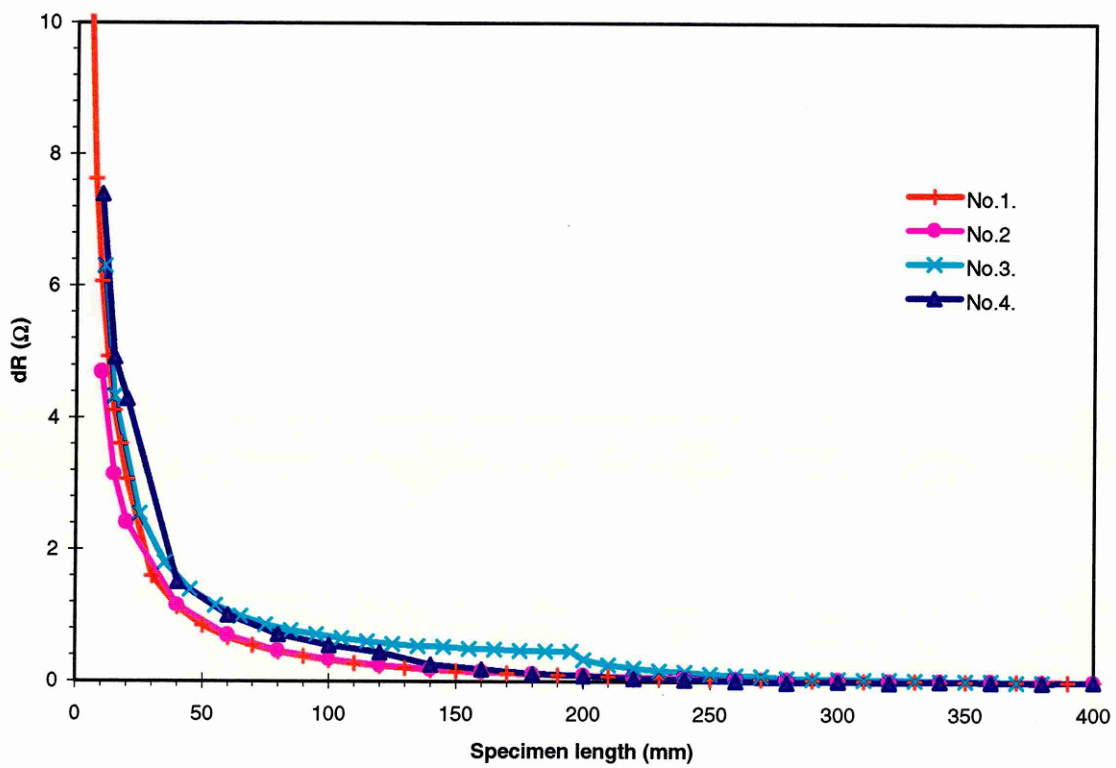

Figure 7.5. Dependence of through-thickness resistance on sample length.

These results also show the influence of electrode location on sample length. Moreover, this result is very important from the damage sensing point of view. The reduction in sample length is equivalent to fibre break simulation at locations away from the electrode. This result suggests that the damage that is happening at a location away from the electrode can be detected. The sensitivity to detect such a damage happening at a location increases exponentially with the distance of the location. The significance of the results and the details of the experiments for damage sensing is described in section 8.2.1.

7.3 TRANSVERSE RESISTIVITY OF LAMINAE

The results of the influence of specimen geometry on transverse electrical resistivity of UD914 and UD920 lamina samples are shown in Figure 7.6 and Figure 7.7, respectively. The results presented in these figures show that for a given width the resistivity decreases with increasing sample length. The slope of the resistivity change for increasing sample length, decreases with increase in width. This behaviour is similar for both UD914 and UD920 samples. The only exception to this behaviour is the UD914 samples of width 2 mm. The results also demonstrate that the resistivity converges to a constant magnitude with increasing sample dimension, i.e., both length and width. The statistical summary of the transverse resistivity data is shown in appendix C (Table C.3 and C.4). It is clear from these tables that the scatter in the measured resistivity is high. Also, the scatter is relatively higher for UD914 samples than for UD920 samples.

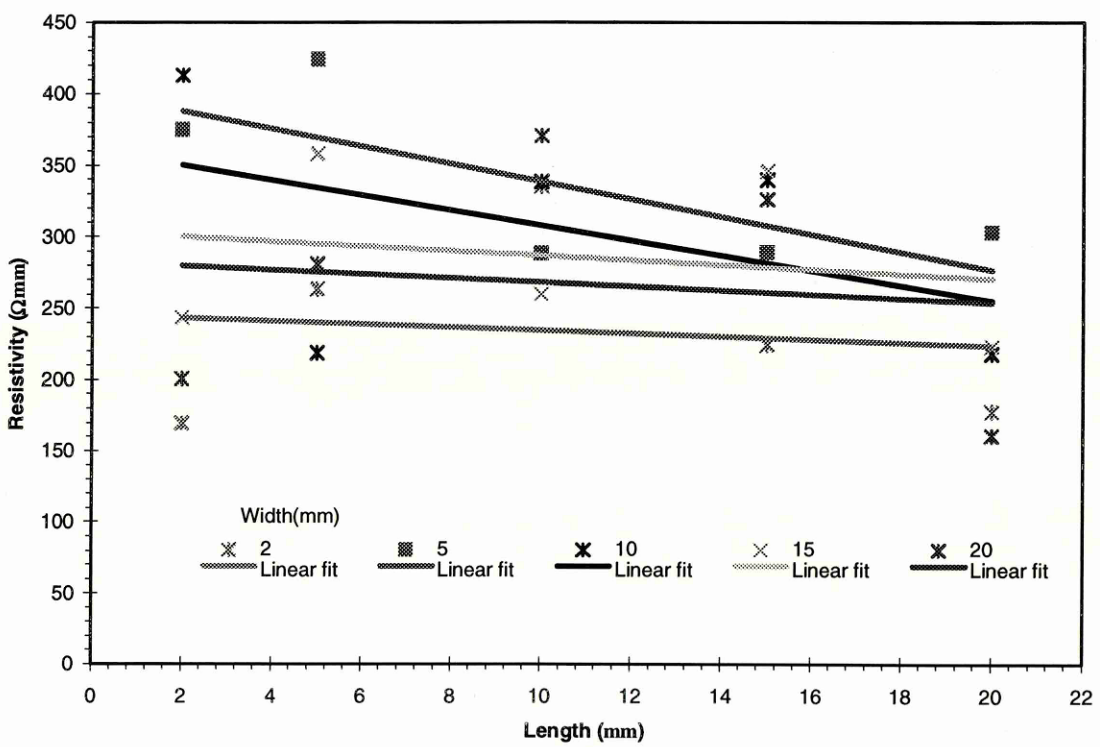

Figure 7.6. Dependence of transverse resistivity on specimen geometry (UD914).

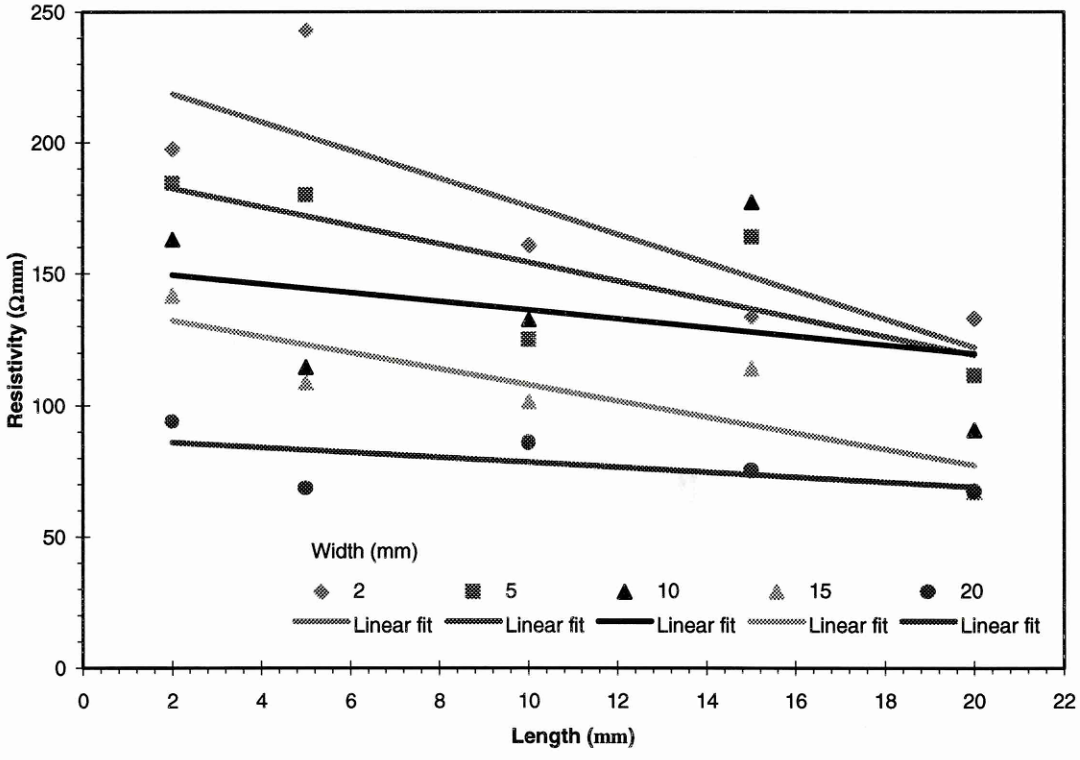

Figure 7.7. Dependence of transverse resistivity on specimen geometry (UD920).

7.4 TEMPERATURE DEPENDENCE

The temperature dependent resistivity results are presented in Figure 7.8-14. The temperature coefficient of resistivity of samples used in mechanical testing are shown in Figure 7.14-17. A word of caution is necessary in interpreting the results presented in this section. The author has demonstrated that the measured electrical resistivity of CFRP samples is influenced by the type of electrode configuration used (refer chapter 6). The effect of electrode has been over looked by previous researchers who investigated the electrical behaviour of CFRP laminates (refer section 2.5.2). Therefore, the results presented in this section should be viewed as the behaviour of the CFRP samples including the electrode. This is critical for temperature dependent studies because the electrode was also exposed to temperature.

In order to make sure that the observed behaviour is only of the CFRP, it is necessary to investigate the temperature dependent resistivity with various electrode configurations. This type of investigations is necessary for the physicist for developing more insight into the physics of the problem. In the context of the present thesis and the electrical resistivity measurement

technique for damage sensing, the temperature dependent studies are necessary to establish the temperature coefficient of resistivity. Moreover, at the moment we are interested only in the results of samples with electrode configuration similar to the samples used for the mechanical testing. Furthermore, the results presented in this section are first of its kind and can aid in developing more insight into the electrical conduction mechanisms and property of CFRP laminates. This can provide a strong background with which future investigation can be extended.

7.4.1 Longitudinal resistivity

The normalised longitudinal temperature dependent resistivity of UD914 and UD920 samples is shown in Figure 7.8 and Figure 7.9, respectively. The resistivity increases gradually from lower temperature to room temperature and increases exponentially above room temperature. This behaviour is similar for both UD914 and UD920, though the magnitude of resistivity change is different

7.4.2 Transverse resistivity

The normalised transverse temperature dependent resistivity of UD914 and UD920 is shown in Figure 7.10 and Figure 7.11, respectively. The resistivity decreases linearly with increasing temperature for UD914 samples. This behaviour is similar to intrinsic semiconductors (Jaros 1989). For UD920 samples, the resistivity decreases linearly with increasing temperature for the range of 200 to 310 °K and increases above 310 °K with increasing temperature. The behaviour of UD920 samples within the temperature range of 200 to 310 °K is like a semiconductor, and above 310 °K UD920 samples behave like metals. The magnitude of normalised transverse resistivity change is relatively less than the longitudinal resistivity change.

7.4.3 Through-thickness resistivity

The temperature dependent through thickness resistivity of UD914 samples is shown in Figure 7.12. The resistivity decreases linearly with increasing temperature. This result is similar to the temperature dependent transverse resistivity of UD914 samples. The behaviour and magnitude of resistivity changes are in good agreement with each other. This is expected because of the transverse isotropy of unidirectional CFRP, i.e., the transverse and through-thickness properties are same. The electrode configuration used for through-thickness measurements were slightly different from the electrode configuration used for transverse resistivity measurements (type I). The electrode configuration type II was used for through-thickness measurements. This indicates that the temperature dependent transverse resistivity is not critically influenced by the electrode.

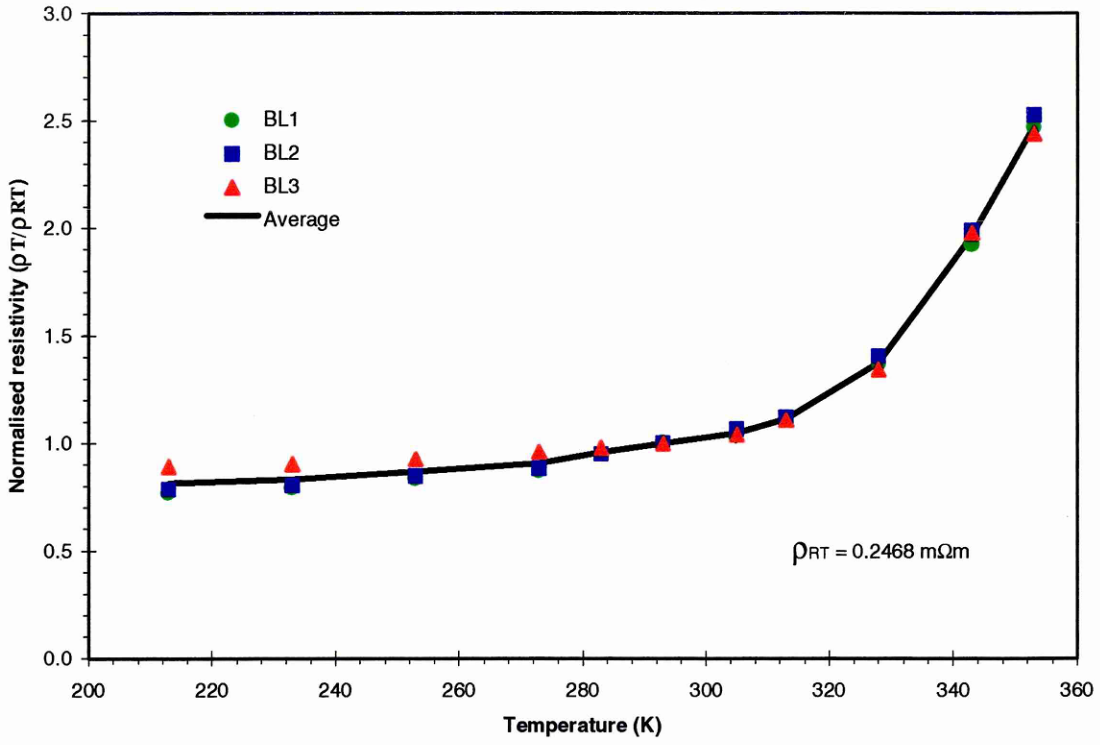

Figure 7.8. Temperature dependent longitudinal resistivity of UD914 samples.

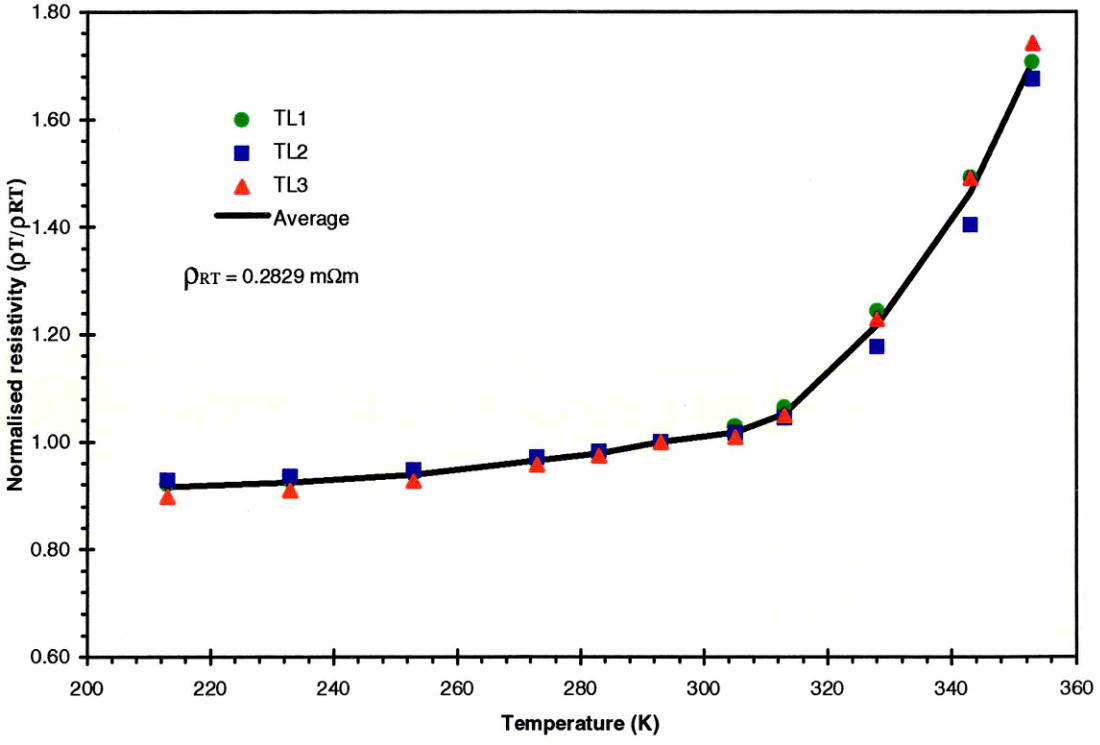

Figure 7.9. Temperature dependent longitudinal resistivity of UD920 samples.

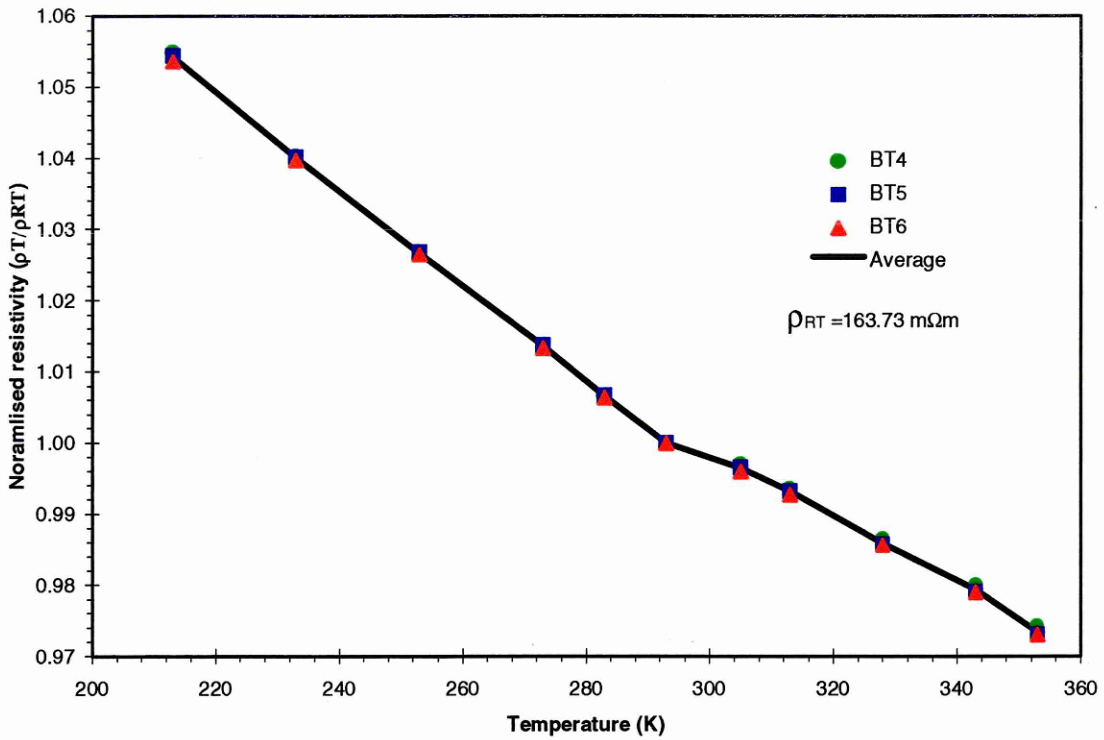

Figure 7.10. Temperature dependent transverse resistivity of UD914 samples.

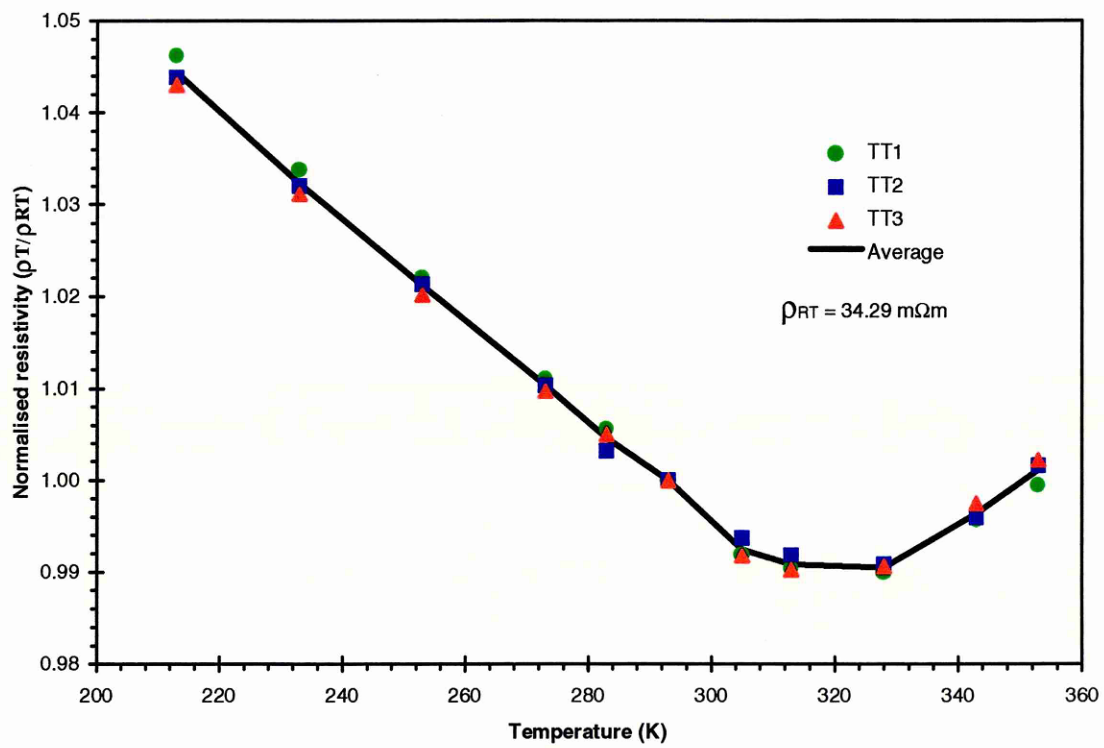

Figure 7.11. Temperature dependent transverse resistivity of UD920 samples

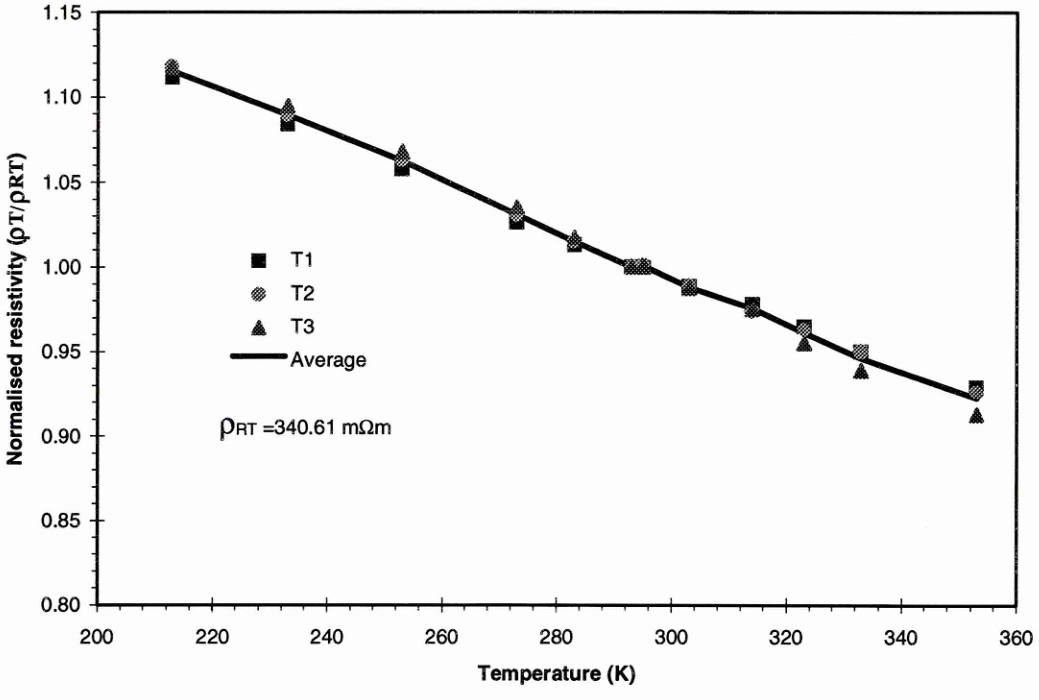

Figure 7.12. Temperature dependent through-thickness resistivity of UD914 samples.

7.4.4 Cross-ply

The temperature dependent resistivity results of CP914 samples are shown in Figure 7.13. This figure shows three behaviours within the temperature range tested. The first region is from 200 °K to room temperature (295 °K). In this region, CP914 samples shows a gradual increase in resistivity with increasing temperature. In the second region, i.e., from room temperature and up to 345 °K the resistivity increases drastically with increasing temperature. Again at temperatures above 345 °K and up to 360 °K, the third region, the rate of resistivity change decreases with temperature. The rate of change of resistivity with temperature in the third range is less than the second range. The behaviour of CP914 samples is similar to UD samples in the temperature range ranging from 200 K to 345 °K.

7.4.5 Conductive adhesive

Figure 7.14 shows the temperature dependent resistivity behaviour of silver epoxy conductive adhesive. The silver epoxy adhesive was used for gluing the copper strips to all the samples used in this temperature dependent investigation. Moreover, the silver epoxy and copper strip electrode configuration is the standard electrode formation method employed for 90 percent of the samples used throughout this thesis work. The silver epoxy adhesive is also a composite

and the properties are determined by the constituents. It is necessary to know the temperature dependent resistivity behaviour of the adhesive and this can be useful to make sure that the adhesive does not have any non-conventional behaviour. If there are any anomalies in the behaviour of the adhesive then that anamaly could manifest into another anomaly in the behaviour of CFRP samples. The result shows that the resistivity of silver epoxy adhesive increases linearly with increasing temperature. This figure also shows that there are no anomalies in the behaviour of silver epoxy adhesive. This linear behaviour is similar to metals. Silver epoxy adhesive is made my mixing fifty percent each of silver particles and epoxy adhesive. The result shows that the behaviour of silver epoxy adhesive is dominated by the silver particles. This is evident from the lowest magnitude of resistivity and the linear and positive temperature dependent resistivity.

7.4.6 Temperature coefficient of resistivity

The temperature coefficient of resistivity (TCR) results are shown in Figure 7.15-17. It may be noted that the apparent linear behaviour shown in these figures is due to forced linear fit. These investigations were made only for the samples used in mechanical testing. The figure shows that the TCR of unidirectional samples is almost same. The magnitude of the TCR is higher for UD samples than CP samples. This can be used to correct for the temperature dependent resistivity change of samples used in mechanical testing

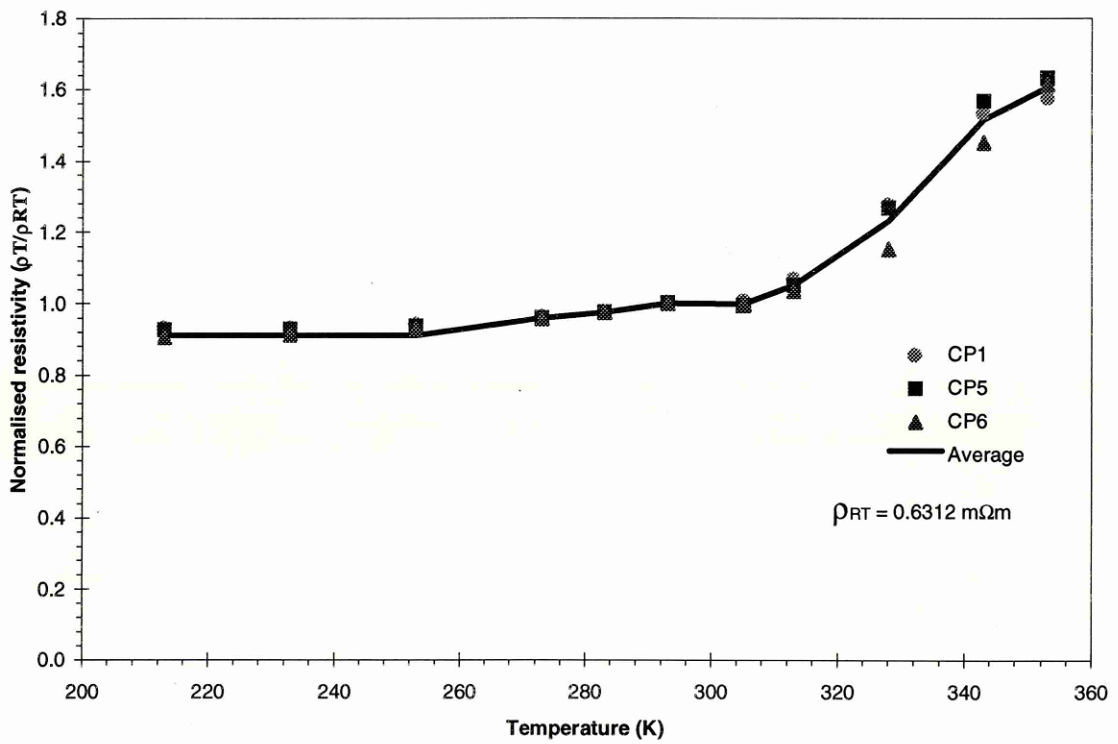

Figure 7.13. Temperature dependent resistivity of CP914 samples.

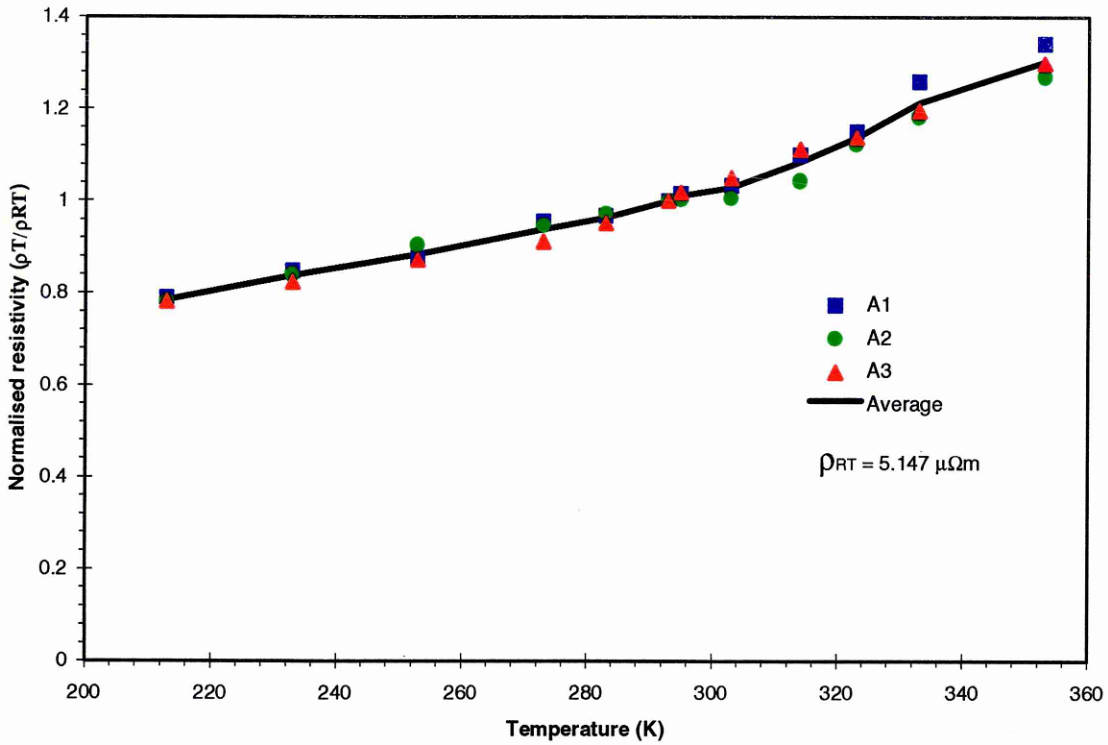

Figure 7.14. Temperature dependent resistivity of silver/epoxy conductive adhesive samples.

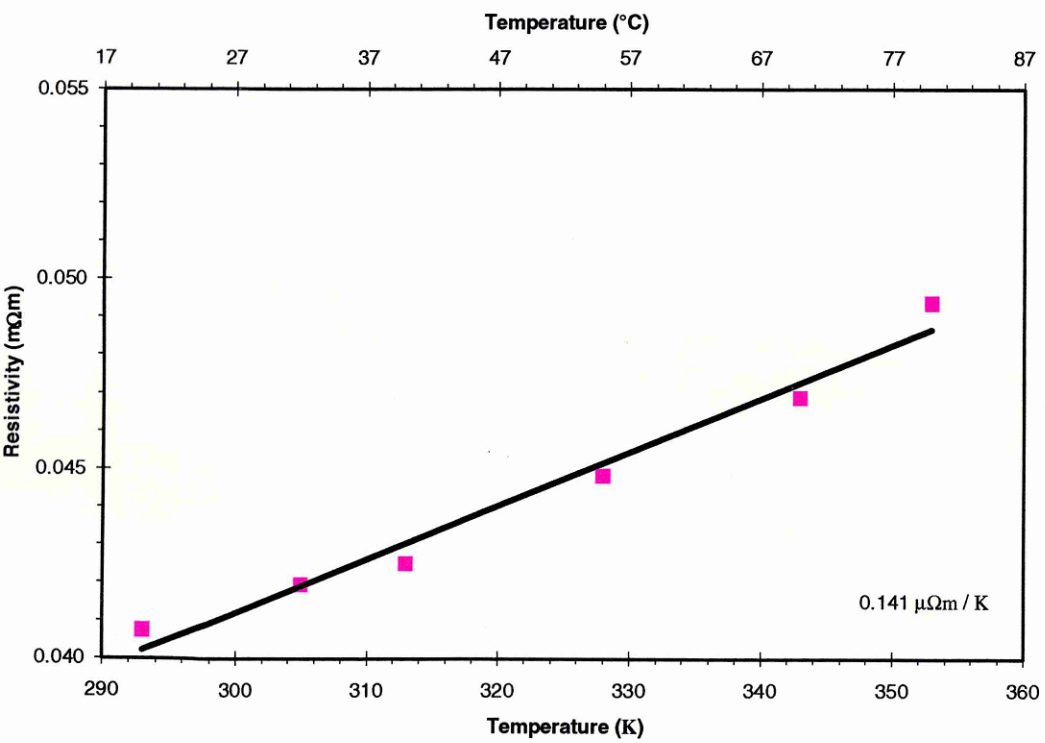

Figure 7.15. Temperature coefficient of resistivity of a typical UD914 sample.

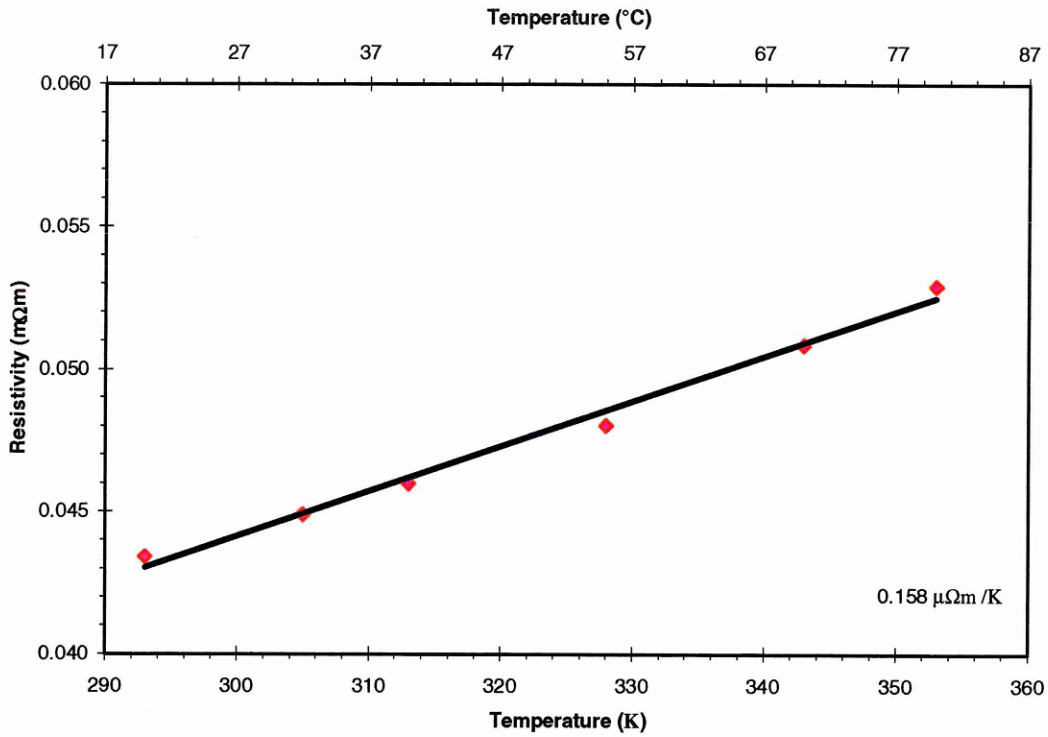

Figure 7.16. Temperature coefficient of resistivity of a typical UD920 sample.

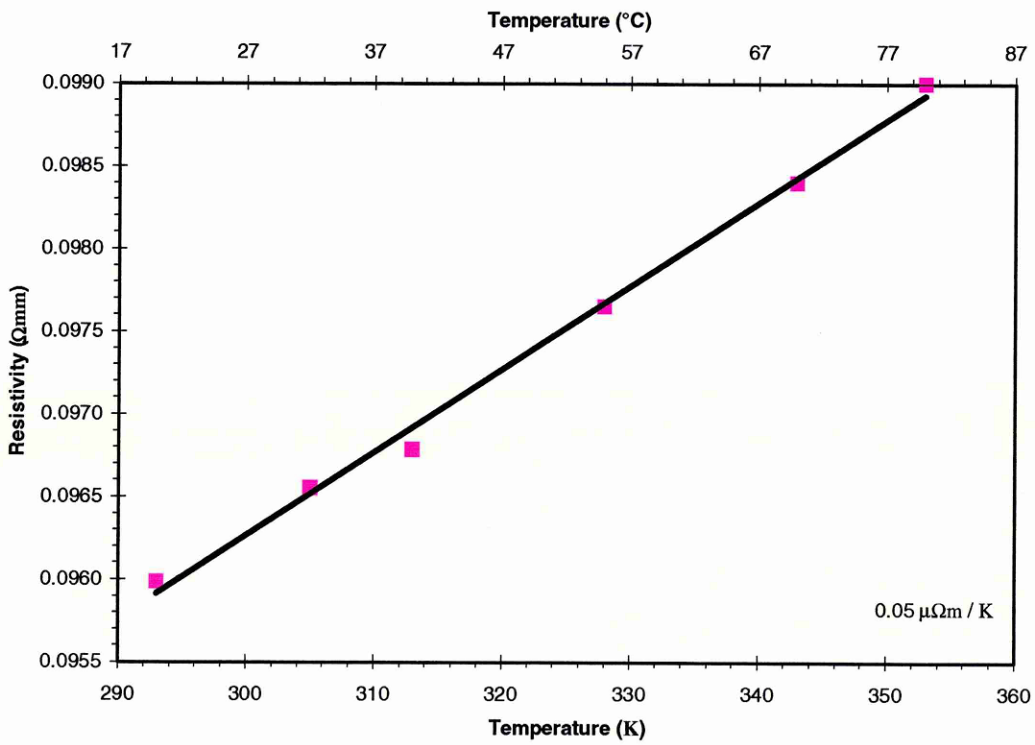

Figure 7.17. Temperature coefficient of resistivity of a typical CP914 sample.

7.5 DISCUSSION

7.5.1 Longitudinal electrical properties

If we compare the longitudinal electrical resistivity of UD914 and UD920, the magnitudes of resistivity are almost same. This is because the longitudinal properties of unidirectional CFRP are fibre dependent. The matrix does not play a critical role. The resistivity of the matrix is 10^{10} times higher than the fibres. So, when the current flows along the fibre direction in a unidirectional laminate, the current tends to flow along the lowest resistive paths, i.e., along the fibres. The contribution of current flow through the matrix is negligible. Both the above laminates are made-up of same fibre and hence the longitudinal electrical resistivity is same.

If we compare the longitudinal electrical resistivity of unidirectional and cross-ply CFRP, the cross-ply CFRP is more than two times higher than the unidirectional CFRP. Cross-ply CFRP is made-up of fifty percent fibres oriented along the longitudinal direction and the remaining fifty percent of fibres in the transverse direction. There are only fifty percent of main current carriers along the fibre direction. Hence, the resistivity of CFRP is more than twice the longitudinal resistivity of unidirectional CFRP. However, the current flow along the 90° layers will also contribute to the resistivity of cross-ply CFRP. The properties of cross-ply laminates in the longitudinal and transverse direction will be same because of the symmetry of fibre orientation.

7.5.2 Transverse electrical properties

The transverse property of unidirectional CFRP shows that the properties are influenced by the type of matrix along with the type of fibres used. The order of experimental values of transverse resistivity of CFRP in comparison with the constituent matrix material suggests that the transverse conduction mechanism of CFRP is non-conventional. Under these circumstances, the measured electrical properties suggest that one single conduction mechanisms may not be responsible for the transverse conduction.

The transverse electrical resistivity of CFRP may be due to the following mechanisms,

- Conduction through the transverse direction of the fibres,
- Conduction through the matrix material due to electron tunnelling and
- Conduction along the fibre direction of fibres.

In the following paragraphs, the possibilities and contributions of the above mechanisms for transverse conduction will be discussed.

It has been suggested previously that the transverse conduction may be due to transverse fibre touching (Schulte and Baron 1989 and Tse et al. 1981). The transverse fibre touching in CFRP laminates may have originated from the production process. The inter fibre sticking or fusing of PAN based carbon fibres (Figure 7.18) that occurred during the spinning or thermal processing (Thorne 1985) may be responsible for the transverse conduction between the fibres.

In general, continuous conduction chains of fibre sticking observed in the fibre strands may not be observable in a laminate. The laminates are made of fibre strands and fibre sticking between the fibre strands may not be possible. Moreover, a size is applied to carbon fibres that is generally an insulator (Ehrburger and Donnet 1985). Therefore, for transverse conduction between carbon fibres the electrons have to tunnel through this insulator. The transverse conduction is expected to be due to conduction through the thin film of the matrix or size. According to classical electron theory, conduction through an insulator is zero. This theory state that the electrons cannot penetrate this insulating barrier. On the other hand, quantum mechanics states that if the insulating barrier is thin then the electron can tunnel through the barrier and the conduction can continue due to these tunnelled electrons (Simmons 1984). The effect of tunnelling of electrons on thick and thin barriers is illustrated in Figure 7.19. This figure illustrates the work function of electrons on a thick and thin insulating barrier. Therefore, it can be suggested that the transverse conduction of CFRP laminates may also be due to the conduction between fibres due to electron tunnelling.

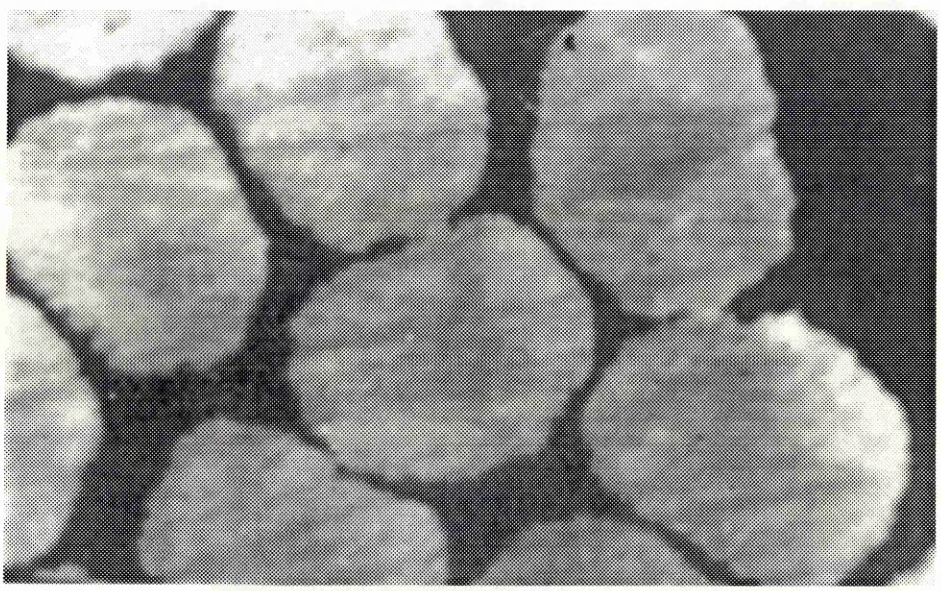

Figure 7.18. Cross-sectional view after oxidation of PAN based carbon fibres showing points of inter-fibre sticking or fusing (Thorne 1985).

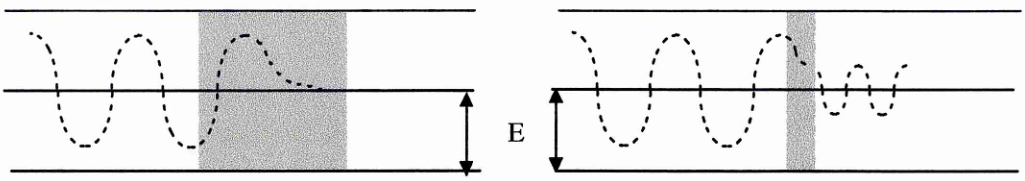

(a) Thick barrier (b) Thin barrier (<10 nm)

Figure 7.19. Schematic representation of tunnel effect at a thick and thin barrier (Simmons 1984).

If we consider the fact that the electrical properties of carbon fibres are anisotropic and the transverse resistivity is 10^2 to 10^4 times higher than the longitudinal resistivity (Blackman 1970), then, it can be postulated that the current flow along the fibre direction can also contribute to the transverse electrical conduction of CFRP.

The transverse electrical properties of CFRP are macroscopically homogeneous (Moriya and Endo 1990). The scatter in the measured electrical properties may be due to the electrode. The overall resistance of the sample can be influenced by the electrode depending on whether the electrode makes the first contact with the fibre or the matrix. The ideal electrode should make ohmic contact with the fibre. If the electrode contacts the matrix first then that can introduce scatter depending on the thickness of the matrix between the immediate fibre and the electrode. Though the transverse conduction mechanism of CFRP and the conduction mechanism of the electrode to the sample are similar and depend on electron tunnelling through the matrix, it is critical for the electrode because the electrical properties of the CFRP are homogeneous at macroscopic level.

The transverse resistivity of UD920 is approximately five times less than UD914. The only known variable in UD920 is the matrix. The observed relatively lower resistivity of UD920 is mainly due to the matrix because that is the only variable. Jaussaud (1988) reported that epoxy 920 contains thermoplastic particles of diameter 7 to 9 μm. This particles are added to the resin system for toughness enhancement. These thermoplastic particles may be the prime component responsible for the observed lower resistivity of UD920 than UD914. In general, the resistivity of thermoplastics is lower than the epoxy thermosets. The investigations carried out by Warfield et.al (1965) indicates that the addition of plasticisers to thermoset polymers reduces the electrical resistivity. From the available information it can be concluded that the lower resistivity of UD920 is mainly because of the formulation and the constituents of the matrix.

7.5.3 Dependence of longitudinal resistivity on length

As discussed earlier, the longitudinal resistivity should be constant for all sample lengths. Figure 7.3 shows that the experimental resistivity decreases drastically with increasing sample length. However, it can be shown that this behaviour is not the property of CFRP using Figure 7.20. The third resistivity in this figure was evaluated from the experimental sample resistance minus the electrode resistance. The electrode resistance was calculated from the y-axis intercept of the linear fit of experimental points (refer Figure 7.2). The deviation from the linear behaviour and the theoretical prediction is less for this curve. This gives a hint that the observed experimental resistivity is influenced by the electrode resistance. If we assume a constant electrode resistance then the contribution of the electrode resistance to the sample resistance is higher for samples of shorter length. This may be the predominant reason for the observed power type experimental resistivity decrease of samples with increasing length. To demonstrate that the observed behaviour is due to the electrodes, a constant electrode resistance of 0.1 ohm was added to the theoretical resistance of the sample and then the resistivity was calculated and is shown in the fourth resistivity curve. This closely follows the behaviour of the experimental results (second curve). This explains the overall power type decrease of experimental resistivity with increasing length and demonstrates that this is mainly due to the contribution of electrode resistance.

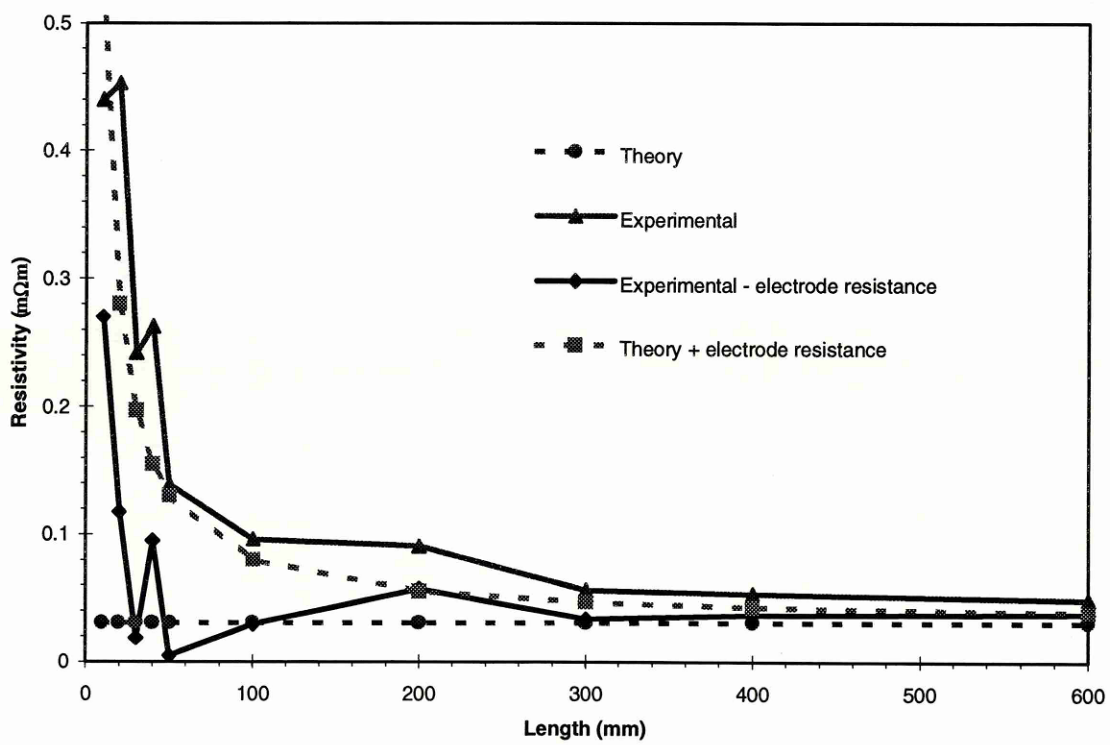

Figure 7.20. Dependence of longitudinal resistivity on sample length (electrode effects).

7.5.4 Dependence of transverse resistivity on length

This dependence of transverse resistivity on sample length suggests that the transverse conductivity of unidirectional CFRP is homogeneous. The non-linear behaviour observed in the dependence of transverse resistivity on sample length is in contrast to the longitudinal resistivity. The transverse resistivity is constant. The transverse resistivity is 760 times (UD920 samples) higher than the longitudinal resistivity, i.e., the magnitude of transverse resistivity is higher. Moreover, the sample resistance is significantly higher than the electrode resistance and hence the effect of electrode is not very critical for transverse resistivity. The influence of electrode resistance is very critical for longitudinal resistivity because of the comparable magnitude of the resistance of the sample and the electrode. This is not critical for transverse resistivity of the samples because of the relatively insignificant resistance of the electrode.

7.5.5 Dependence of through-thickness resistance on length

The behaviour depicted in Figure 7.5, can be expected for isotropic materials, if the sample length, i.e., the cross-sectional area of sample in which the current flows decreases. In order to understand the exponential increase in resistance with decrease in length of CFRP samples, consider the well-known resistance equation of materials,

$$R = \frac{\rho L}{A}$$

In this case, for a given constant resistivity, ρ, sample length, L, and for a decreasing cross-sectional area, A, of the sample then the resistance is expected to increase with decreasing cross-sectional area. If we look at our results with this point of view there is nothing of surprise in the results presented in the figure. However, if we take into account the fact that the electrodes did not cover the entire surface area and occupied only a 3 mm width over the sample area, this then highlights the non-conventional electrical behaviour of unidirectional CFRP.

The observed behaviour is similar to the isotropic case, even though the electrodes were only 3 mm in width. This demonstrates that in a unidirectional CFRP, first the current flows along the fibre direction as the longitudinal resistivity is much lower than the transverse or through thickness resistivity and then percolates through the thickness. The electrical conduction is not only confined just below the electrode area, the current flows in the in-plane direction and then percolates through the thickness direction. The magnitude of current flow along the in-plane direction decreases with increase in sample length, this is evident from the exponential increase in resistance with decreasing sample length.

The dependence of longitudinal, transverse and through-thickness resistance on sample length demonstrates that the electrical conduction process in a unidirectional CFRP is a three-dimensional process.

7.5.6 Dependence of transverse resistivity on specimen geometry (lamina)

The overall scatter in the measured resistivity of lamina samples may due to the sample dimension. The dimension of samples used in this investigation may not be sufficient to form proper electrical contacts. The probability of formation of electrical contacts between the electrode and the sample may be less. That is the probability that the electrode can make contact with the fibre is limited because of the smaller sample dimension. The higher scatter in UD914 samples than UD920 samples may due to the formulation of the matrix. The transverse conduction is mainly due to interaction between the fibre and matrix, i.e., the fibre to fibre contact distance is the predominant factor. The epoxy 920 matrix contains non-dispersed thermoplastic particles (Jaussaud 1992). The thermoplastic particles may assist in maintaining the fibre to fibre contact distance. The UD914 samples do not have such inclusions and the fibre to fibre contact distance may be relatively inconsistent. This may be the possible reason for the relatively higher scatter in the UD914 samples.

If we compare the magnitude of transverse resistivity evaluated from the resistance measurements of laminate and lamina samples, the magnitude of lamina sample is higher. The scatter in the measured resistivity of lamina is also relatively higher than the laminates. The possible reason may be that the probability of electrode to fibre contacts is higher for laminates than the lamina.

7.5.7 Temperature dependence

The similarity in longitudinal resistivity behaviour of UD914 and UD920 samples suggests that the longitudinal properties are fibre dominated. Therefore, the observed temperature dependent properties of unidirectional CFRP should also be fibre dominated. The behaviour depicted in Figure 7.8 and Figure 7.9 is similar to metals (Blatt 1968). The increase in resistivity with temperature is predominantly due to drop in electron mobility. As the temperature increases the electron scattering increases with lattice and with other electrons. In unidirectional CFRP the resistivity increases exponentially above the room temperature with increasing temperature. This exponential increase in resistivity may be due to additional electron scattering in the carbon fibres. The diameter of the carbon fibres is comparable with the mean electron free path and hence this can introduce additional electron scattering at the boundaries of carbon fibre (Ziman 1960). As the temperature increases the electron scattering increases in carbon fibre due to the

decrease in electron mobility and increase in scatter at the boundary of carbon fibres. There is additional electron scattering in carbon fibres in comparison with bulk metal or graphite. This may be one of the primary reason for the observed exponential increase in the resistivity with increasing temperature. The resistivity change is almost constant from lower temperature to room temperature. Below room temperature, the electron mobility is less and there is no thermal energy to activate the electrons and hence the electron scattering is less. So, below room temperature the resistivity does not vary drastically with temperature. The gradual increase in resistivity from lower temperature to room temperature may be due scattering of electrons by phonons (Ziman 1960).

The longitudinal electrical properties of CFRP are fibre dominated. The electrical behaviour of carbon fibre along the fibre direction is similar to semi-metal (Blackman 1970). The results presented in the figure supports the metal like behaviour of UD CFRP samples along the fibre direction.

The temperature dependent transverse resistivity results intensify the fact that the transverse electrical conduction mechanism of CFRP is due to both fibre and the matrix and their interaction. The behaviour of UD914 and UD920 are different, and the only known variable in them is the matrix. Therefore, it can be suggested that the observed temperature dependent resistivity of UD920 may be due to the matrix. The increase in resistivity above 310 K may be due to the thermoplastic particles added to the resin system for toughness enhancement (Jaussaud 1992). The glass transition temperature of epoxy 920 is lower than the epoxy 914. At temperatures above 310 K the thermal behaviour of epoxy 920 may be non-linear and this may have introduced non-linear expansion of the matrix (Nicodemo et al. 1978, Littlewood and Briggs 1978). This non-linear expansion may have increased the fibre to fibre contact resistance and hence the overall increase in resistivity with increasing temperature.

8

DAMAGE MECHANISMS - EXPERIMENTAL AND COMPUTATIONAL SIMULATION

This chapter presents the details and the results of the effects of damage on electrical resistance simulated by experimental and computational methods. This chapter provides a framework within which the resistance change observed during the mechanical testing (chapter 9 and 10) can be explained and predicted. Results presented in this chapter demonstrates the smart capabilities of the electrical resistivity measurement technique.

This chapter is organised as follows. The schematic illustrations of different damage modes, their electrical analogy and electrode locations are described in section 8.1. The experimental simulation details of fibre breaks and longitudinal splits are described in section 8.2. Section 8.3 deals with the computational simulation. This section first examines the applicability of the parallel resistance model. The results related to the validation of the proposed three-dimensional unit cell assemblage model are presented. This section also presents the computational simulation results of damage modes such as fibre breaks, longitudinal splits and delamination. These simulation results are presented for two types of laminate (UD914 and UD920) and three types of electrode location.

8.1 DAMAGE MECHANISMS AND ELECTRICAL ANALOGUE

The measured quantity in an electrical resistivity measurement technique is the resistance. The change in resistance is mainly due change of conductivity paths in the material due to the effect of damage. It is necessary to understand at the concept level the analogy between damage mechanisms and electrical resistivity. This analogy is very important for quantitative measurement of damage. Moreover, the electrical properties of unidirectional CFRP are orthotropic. The change in electrical resistivity can vary with the direction of current flow and the direction of resistance measurement. This is a major factor in determining the sensitivity of electrical resistivity measurement technique for characterising different damage mechanisms. Also, this is very important in determining the location of the electrode for current injection and measuring the potential distribution.

Composite laminates can have complex failure modes such as fibre fracture, splits, delaminations and intra and inter laminar cracks. All these damage mechanisms whether caused by impact, fatigue or any other loading conditions affect the longitudinal and or the transverse conduction process. It is necessary to understand the effects of damage from the electrical circuit point of view. This analogy between the damage mechanisms and electrical circuits can provide more information to investigate the effects of damage mechanisms on electrical resistivity. In the following paragraphs, the electrical analogy between major damage mechanisms such as fibre breaks, matrix cracks and delamination are described.

8.1.1 Fibre breaks

Figure 8.1 shows the electrode configuration for characterisation and the electrical analogy of fibre breaks. In the electrical resistivity measurement technique, fibre breaks are easily detected when the current flows along the fibre direction. The electrodes should be glued to the ends of the fibres to facilitate the current flow along the fibres. This arrangement has carbon fibres as resisters connected in parallel. In this case, a fibre break is equivalent to a broken resistor. This analogy is illustrated in Figure 8.1. The number of fibre breaks may be quantified from the measurement of resistance change.

8.1.2 Matrix cracks

In an electrical resistivity measurement technique, the matrix cracks may be detected when the current flows orthogonaly to the fibre direction. Matrix cracks affect the transverse conduction process. Figure 8.2 shows the electrode configuration for characterisation and the electrical analogy of matrix cracks. In a 2D representation, the matrix cracks effectively remove the fibre to fibre contacts that are responsible for transverse conduction process. The matrix crack

crack removes the fibre to fibre contact resistance and hence alters the conduction path. Effectively, this changes the resistance and hence facilitates quantification of matrix cracks.

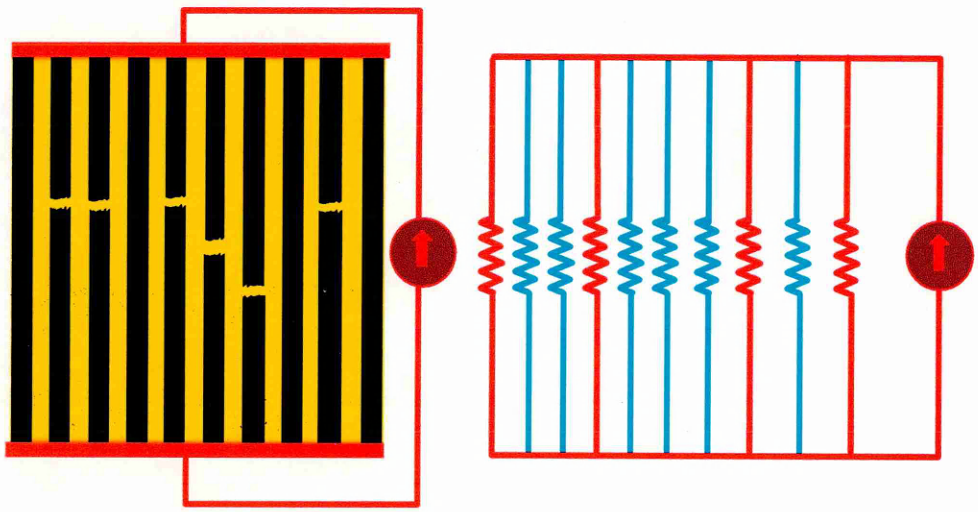

Figure 8.1 Schematic illustration of damage mechanism of a unidirectional CFRP laminate and its electrical analogue (fibre breaks)

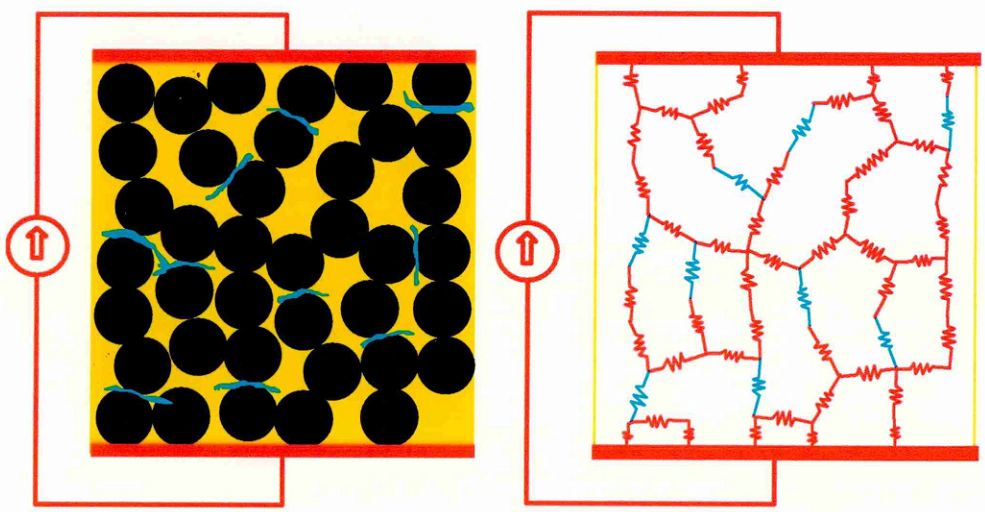

Figure 8.2. Schematic illustration of damage mechanisms of a unidirectional CFRP laminate and its electrical analogue (matrix cracks).

8.1.3 Longitudinal splits

Figure 8.3 illustrates the electrical analogy and electrode configuration of longitudinal splits. Longitudinal splits are a form of matrix or interfacial damage. The fibre resistance is much lower than the fibre to fibre contact resistance. Therefore, it is expected that the current will flow along the fibre direction first and then percolate across the fibre direction. The longitudinal splits, from an electrical circuit point of view, remove the fibre to fibre contact resistance along the fibre direction as shown in the figure. This can lead to a change in resistance due to the changes in the conduction paths.

8.1.4 Delamination

Figure 8.4 shows the electrode configuration for measuring delamination crack growth and the electrical analogy. Delamination crack in a unidirectional CFRP is governed by the transverse conduction process. In the electrical resistivity measurement technique, the effect of a delamination crack is similar to that of a matrix crack. In this case the crack growth is continuous. The delamination crack removes the fibre to fibre contacts, i.e., the resistors in an electrical circuit. In simple two-dimensional electrical analogy, the crack propagation increases the conduction path because of the broken resistors. The resistance change with respect to the electrode is indicative of the delamination crack growth.

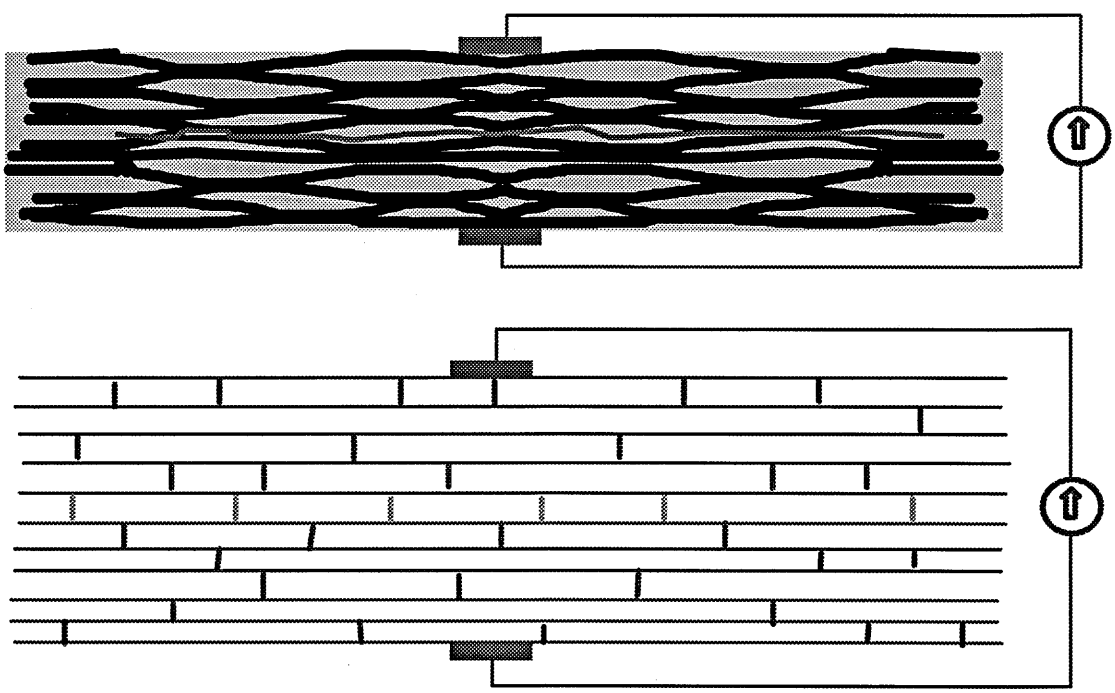

Figure 8.3. Schematic illustration of damage mechanism of a unidirectional CFRP laminate and its electrical analogue (longitudinal splits)

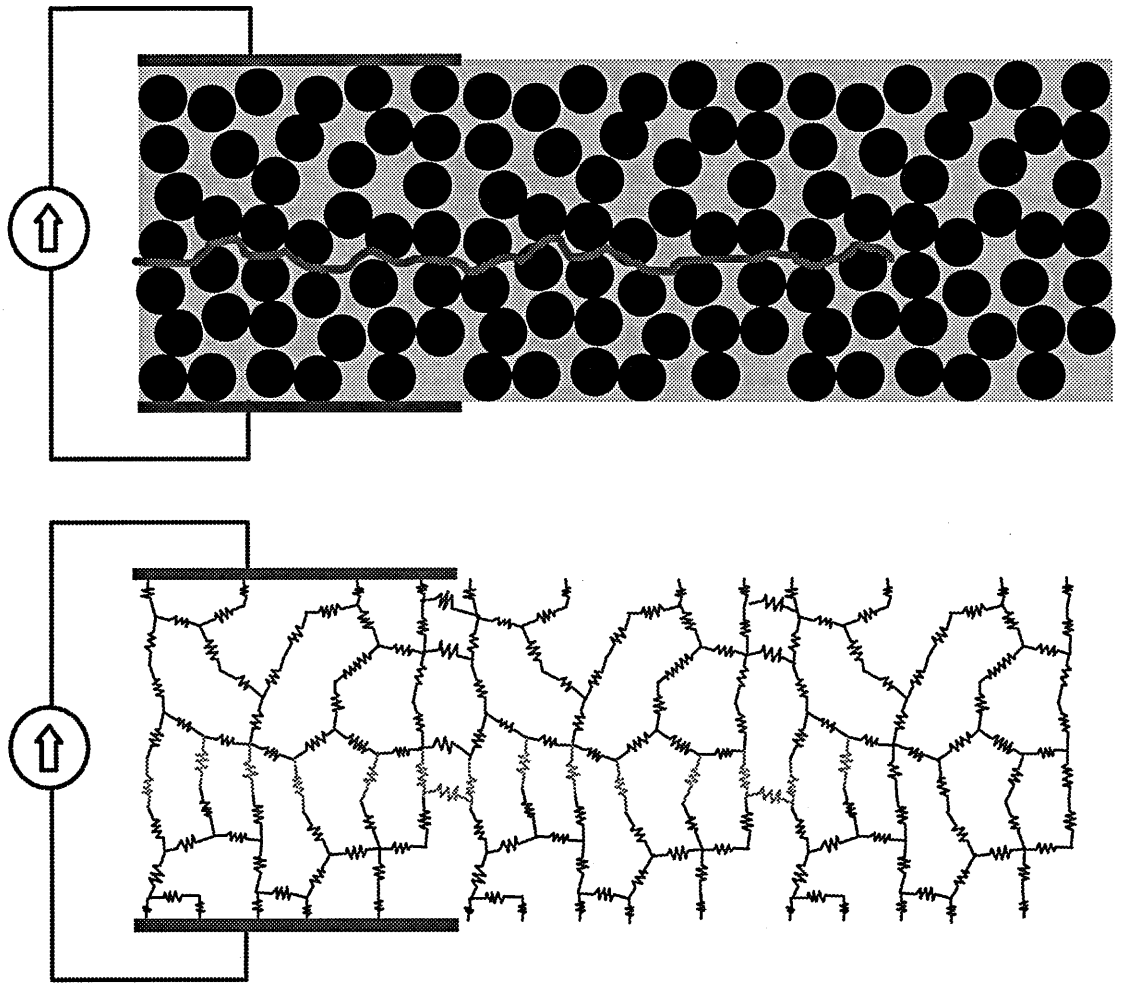

Figure 8.4. Schematic illustration of damage mechanisms of a unidirectional CFRP laminate and its electrical analogue (delamination).

8.2 EXPERIMENTAL SIMULATION

This section presents the results of damage mechanisms simulated experimentally. In an electrical resistivity measurement technique the measured resistance is a direct consequence of the effects of complex damage mechanisms. The change in resistance is a measure of all types of damage. In order to understand the resistance change from complex damage mechanisms and to distinguish the effects of individual damage mechanisms, experimental simulations are essential. In this section, experimental simulation means simulating the damage mechanisms in an unloaded specimen. For example, fibre breaks can be simulated by simply cutting the laminate using a sharp knife or a thin saw. These simple investigations can provide better information for designing specimens and the electrode location for injection of current into the specimen and the measurement of resistance. The earlier investigations on experimental simulations by other researchers are described in section 3.5.3.

8.2.1 Fibre breaks

Fibre breaks were simulated by cutting the sample across the width at the centre of the sample length using a hack saw. Fibre breaks are mostly sensitive when the current flows along the fibre direction. Hence, the electrodes were attached at the ends of the sample, i.e., type I electrode configuration was used. The experimental simulation details are shown in Figure 8.5. In most of the experiments, samples with dimensions similar to the one used for mechanical testing were used. The fibre break simulation results are shown in Figure 8.6 - 8.8.

The fibre break simulation results for a typical sample used in mechanical testing is shown in Figure 8.6. It is clear from the figure that the resistance increases non-linearly with increase in depth of cut, i.e., fibre breaks. This behaviour is in good agreement with the previously published results of similar material and configuration (Schulte and Baron 1989). This simple result proves that the fibre breaks can be detected using this technique. The non-linear behaviour is mainly due to the parallel arrangement of fibres. It is evident from the figure that the sensitivity to fibre breaks increases with increase in number of broken fibres. Therefore, sensitivity to fibre breaks is a function of total number of fibres and the broken fibres.

Figure 8.7 shows the fibre breaks simulation of samples of various lengths. The fibre break was simulated at the middle of the sample of length of 100, 200, 300, 400 and 600 mm. The UD914 laminate samples were used for this simulation. Figure 8.7 shows that the resistance change is higher for samples of longer length than the shorter length samples. The resistance change decreases with decrease in sample length. This highlights that the change in resistance for a similar depth of cut (i.e. fibre breaks) is a function of sample length. The overlap of resistance change behaviour of some of the samples may be due to the fibre misorientation.

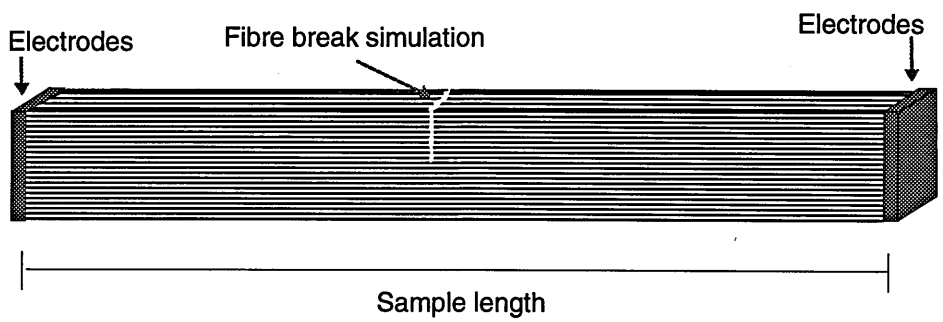

Figure 8.5. Experimental details of fibre break simulation.

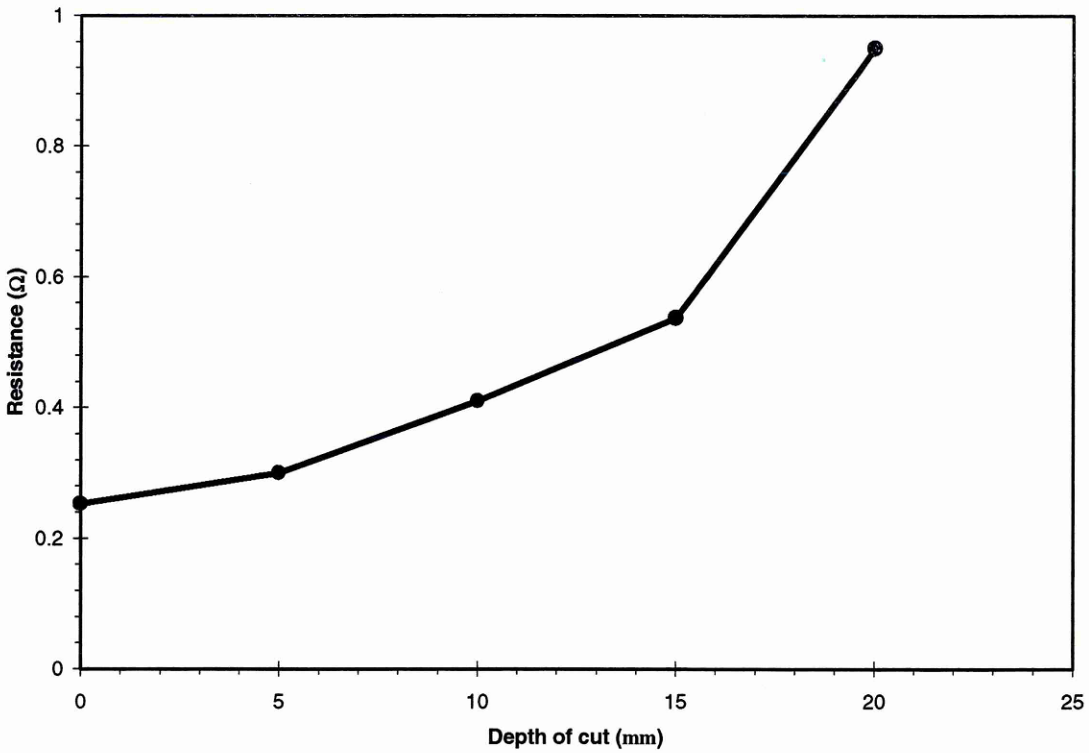

Figure 8.6. Experimental simulation results of fibre breaks when the current flows along the fibre direction.

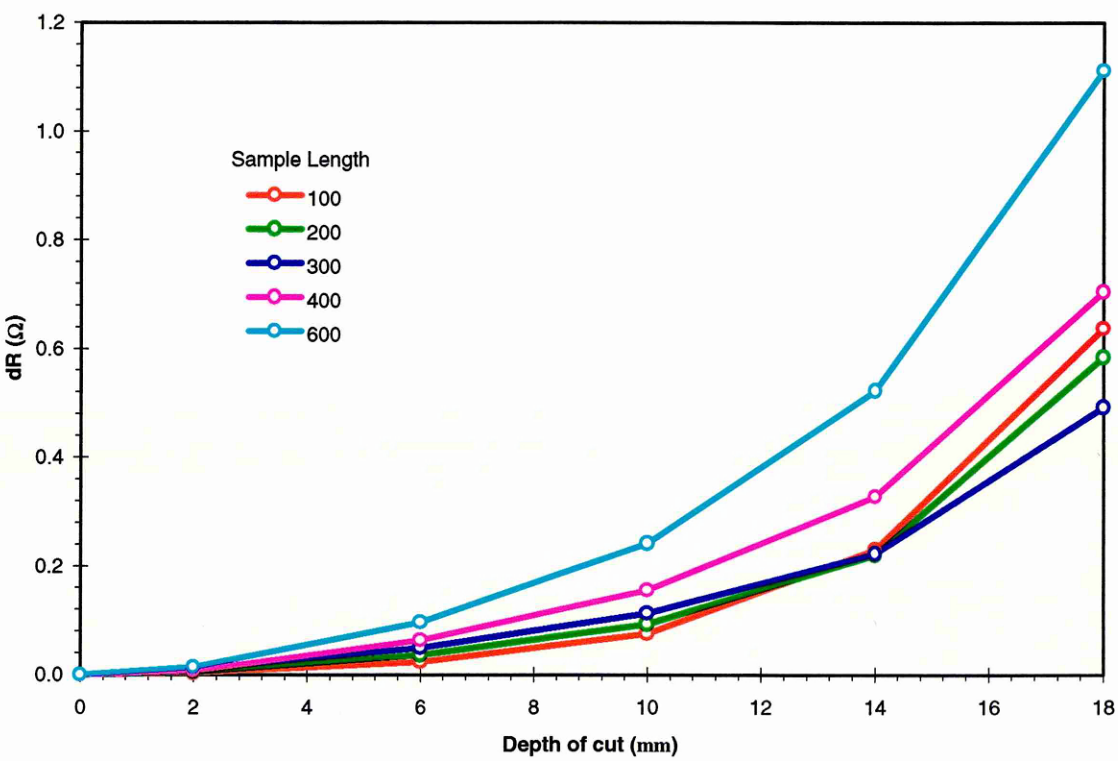

Figure 8.7. Experimental simulation of fibre breaks of samples with various length.

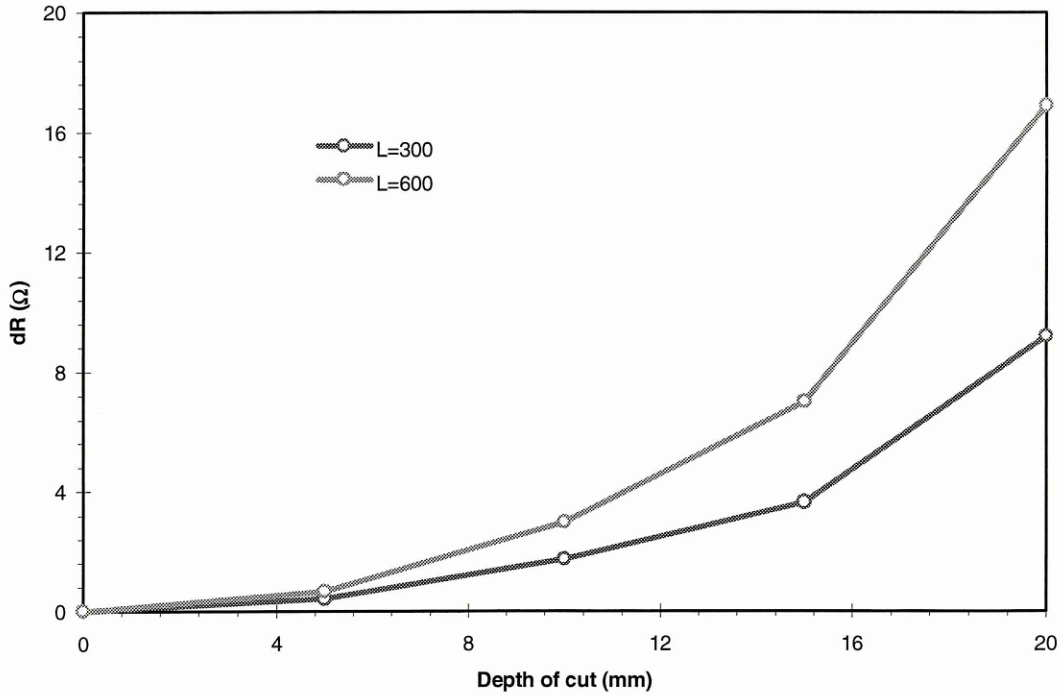

Figure 8.8. Experimental simulation of fibre breaks of UD920 lamina samples.

Figure 8.8 shows the fibre break simulation results of UD920 lamina samples. This simulation is similar to the previous one. The results are also similar. The resistance change with depth of cut of 600 mm length sample is higher than the 300 mm length sample. The above two experiments were carried out to evaluate the applicability of parallel resistance model, besides investigating the influence of sample length on fibre breaks.

The parallel resistance model does not take into account fibre touching, i.e., the conduction is assumed to be mainly due to current flow along the fibres. However, it is evident from the other experimental results that the conduction is a three-dimensional process (refer chapter 7). These simulation studies can aid in understanding the conduction process and to check the bounds of the parallel resistance model.

Figure 8.10 shows the results of fibre breaks simulated when the current flows transverse to the fibre direction. The electrode configuration and the specimen details are shown in Figure 8.9. Fibre breaks were simulated at different lengths, i.e., four cuts were made across the width, along the length as shown in the figure. The cut 1 and cut 2 reduces a total of 75 mm of the sample length. The cut 3 and cut 4 reduces 20 mm of the sample length. If we compare cut 1 and cut 2, the magnitude of resistance change is higher for cut 2 than cut 1. Similarly, the magnitude of resistance change of cut 4 is higher than cut 3. The behaviour depicted in the figure shows the combined effect of reduction in sample length and fibre breaks.

magnitude of resistance change of cut 4 is higher than cut 3. The behaviour depicted in the figure shows the combined effect of reduction in sample length and fibre breaks.

The results depicted in Figure 8.10 are very important. First, they demonstrates that the fibre breaks can be detected even if the current flows transverse to the fibre direction. Moreover, this result demonstrates that the conduction is a three-dimensional process. The fibre breaks could not have been detected if the fibre were not touching. This highlights that the fibres are touching or there is a transverse conduction between the fibres and the conduction is a three-dimensional process. The computational simulation results of this experiment are described in section 8.3.2.

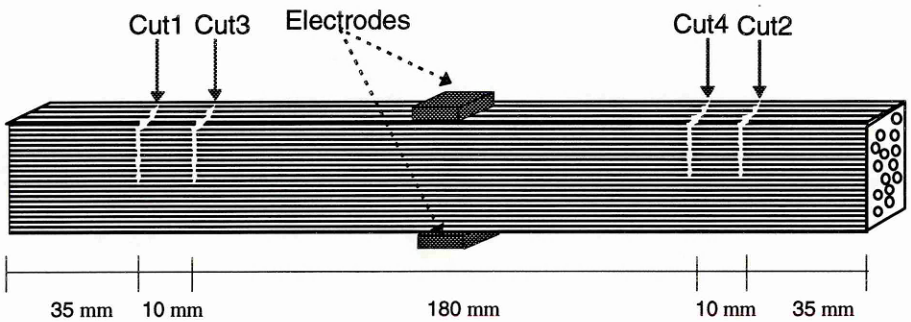

Figure 8.9. Experimental details of transverse fibre break simulation.

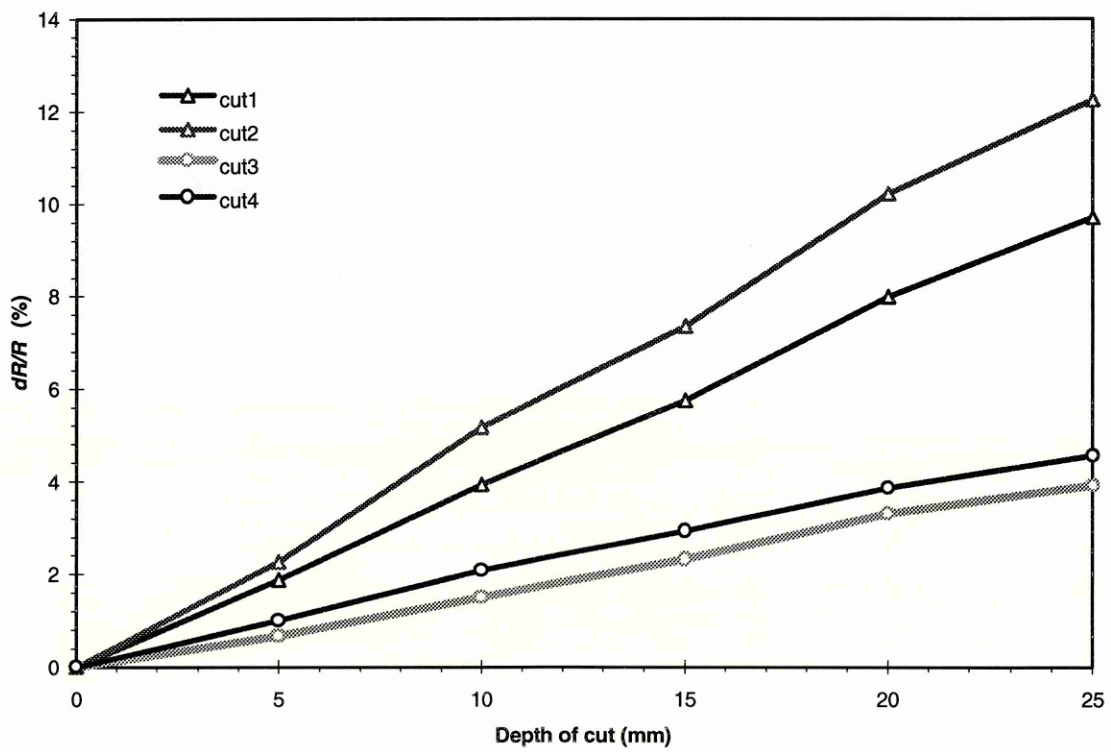

Figure 8.10. Experimental simulation results of fibre breaks when the current flows transverse to the fibre direction.

8.2.2 Longitudinal splits

Longitudinal splits are critical damage mechanisms of unidirectional CFRP and are mainly due to debonding between fibres. This mainly affects the transverse conduction process. The electrode configuration and specimen details of longitudinal split growth simulation are shown in Figure 8.11. The current was injected through electrode set A and the resistance was measured on all the three sets of electrode A, B and C. A longitudinal split was simulated by cutting the sample along the length as shown in the figure. Initially a 1 mm diameter hole was drilled to facilitate cutting. The longitudinal split was then simulated from this hole. The resistance was measured at steps of 10 mm length of split.

Figure 8.12 shows the longitudinal split simulation results. The resistance increases with

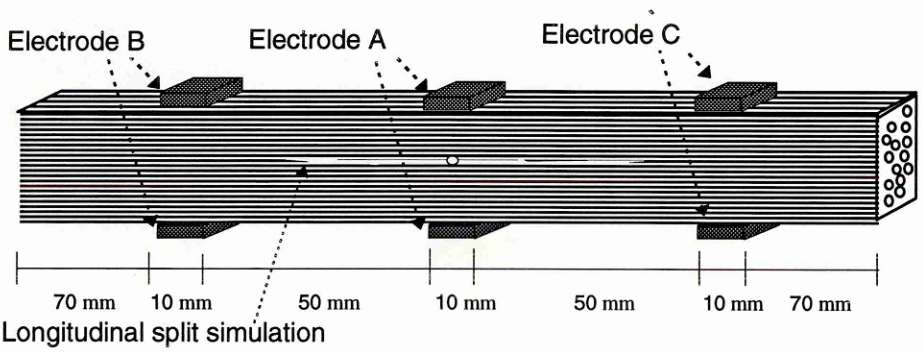

Figure 8.11. Experimental simulation details of longitudinal split.

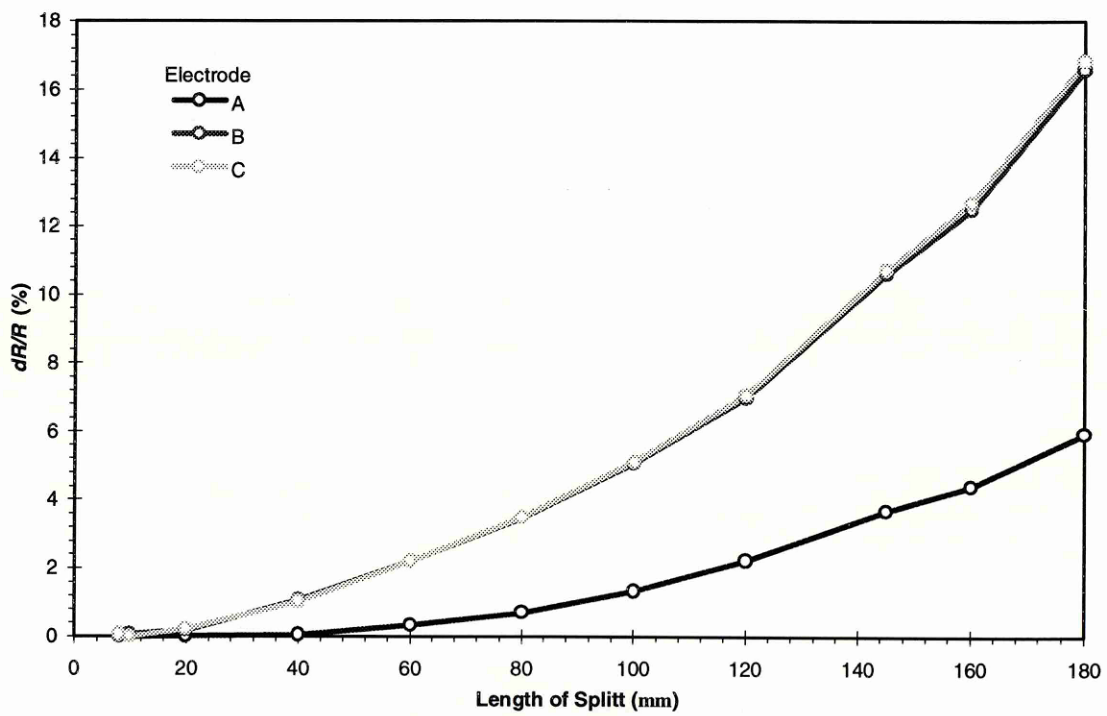

Figure 8.12. Experimental simulation of longitudinal split.

increase in the length of the split. The change in resistance increases nonlinearly with the length of split. The nature of resistance change was found to follow a second order polynomial behaviour. The importance of the result is that the longitudinal split can also be detected using this technique. The measured resistance from the electrode sets B and C, indicates that the change in resistance for a given split length will be the same if the electrodes are located at the same distance away from the damage. This suggests that the longitudinal split detection is a function of electrode location. In other words, if we have two sets of electrodes then the location of the damage can be detected.

8.3 COMPUTATIONAL SIMULATION

The 3D model developed in section 5.4 was used for simulating effects of damage mechanisms computationally. The parallel resistance model was also used for simulating fibre breaks. Firstly to validate the 3D model, experiments described in section 8.2 were simulated computationally. The details and the comparison results are presented in section 8.3.2.

The electrode location is a major factor in detecting the damage. There are many variables that can influence the measured resistance during the mechanical testing. The main aim is to measure the resistance change associated with the damage. Therefore, it is necessary to minimise or eliminate other variables as much as possible. One of the critical components of ERM that can introduce as an artefact is the electrode. It was observed that the noise level was very high for samples with electrodes attached at the middle, during mechanical testing.

These electrodes were also subjected to mechanical loading and therefore the measured resistance was influenced by the electrode. It is difficult to differentiate the resistance change due to the electrode from that due to damage. The main objective is to study the effects of damage of the sample and not of the electrode. This problem can be avoided if we attach the electrodes at sample locations where it is not subjected to mechanical loading. Moreover, the damage sensing capability depends on the electrode location. Therefore, after validation of the 3D model, the effects of damage were simulated for different types of electrode configuration. In these computation simulation studies the effects of electrode on sensing different type of damage was investigated. This investigation was carried out for both UD914 and UD920 samples.

The 3D model is based on the linkage of unit cells, as described in chapter 5. The size of the unit cell used in these simulation studies is 10 x 2.5 x 0.125 mm. The laminate dimension used in these studies is 300 x 25 x 2 mm. The number of unit cells for this laminate is 4800. This is equivalent to a three-dimensional network of electrical resistor circuit with 4800 nodes. This is

the maximum number of nodes that can be handled using the available computing power. The electrical properties of the unit cell are assumed to be of orthotropic. The longitudinal property of the unit cell along the fibre direction was calculated using the parallel resistance model (section 5.1). The transverse and through thickness properties of the unit cell was obtained from the experimental measurements (chapter 7).

Damage mechanisms such as fibre breaks, matrix cracks and delaminations were simulated for three types of electrode configuration. Each electrode configuration is sensitive to a particular type of conduction process and the associated damage mechanisms. For example, the electrode configuration E1 facilitates the current flow along the fibre direction and hence is sensitive to the damage mechanisms that influence the longitudinal conduction process. The electrode configurations used in this investigation are shown in Figure 8.13. The electrode configurations were chosen in such a way that the results obtained from this computational simulation can be correlated with samples used in mechanical testing. Initial investigations were concerned only with individual electrode configurations and the associated damage mechanisms. Using the individual electrode configuration results as guidelines, in later investigations, combinations of electrodes was considered. The combination of electrodes E2 and E3 was considered.

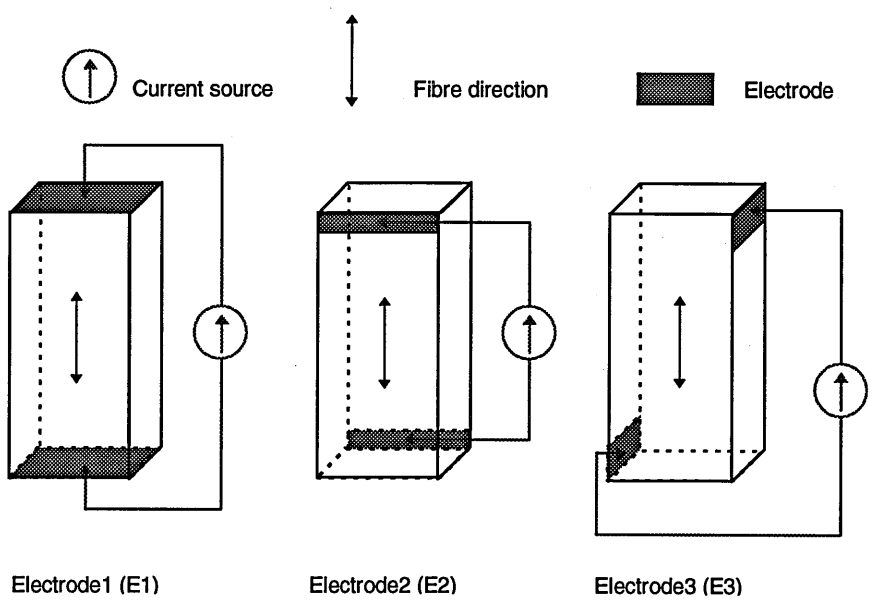

Figure 8.13. Electrode configuration used for computational simulation.

8.3.1 Applicability of parallel resistance model

Figure 8.14 and Figure 8.15 show the fibre break simulation results of UD914 laminate and UD920 lamina samples, respectively. The fibre break was simulated using the parallel

resistance model. In the parallel resistance model, a single fibre break is equivalent to a broken resistor (refer Figure 8.1).

Figure 8.14 shows fibre break simulation results of UD914 samples predicted using the parallel resistance model. The parallel resistance model also shows similar behaviour as observed in the experimental simulation. However, if we compare both the results (Figure 8.7 and 8.14) then the experimental results are higher than the theoretical results. Figure 8.15 also shows that the parallel resistance model predicts the fibre break simulation behaviour. In UD920 lamina samples, the resistance change predicted using parallel resistance model is higher than the experimental simulation.

These results demonstrate that the parallel resistance model predicts the trend of the resistance change behaviour due to fibre breaks. The parallel resistance model assumes that the broken fibres are eliminated from the conduction process. The comparison result shows that this is not true. The broken fibre may also be involved in the conduction process depending on the sample length and material properties. These results also implies that the conduction along the fibre direction is not only due to current flow along the fibres. The transverse fibre to fibre contacts are also involved in the conduction process.

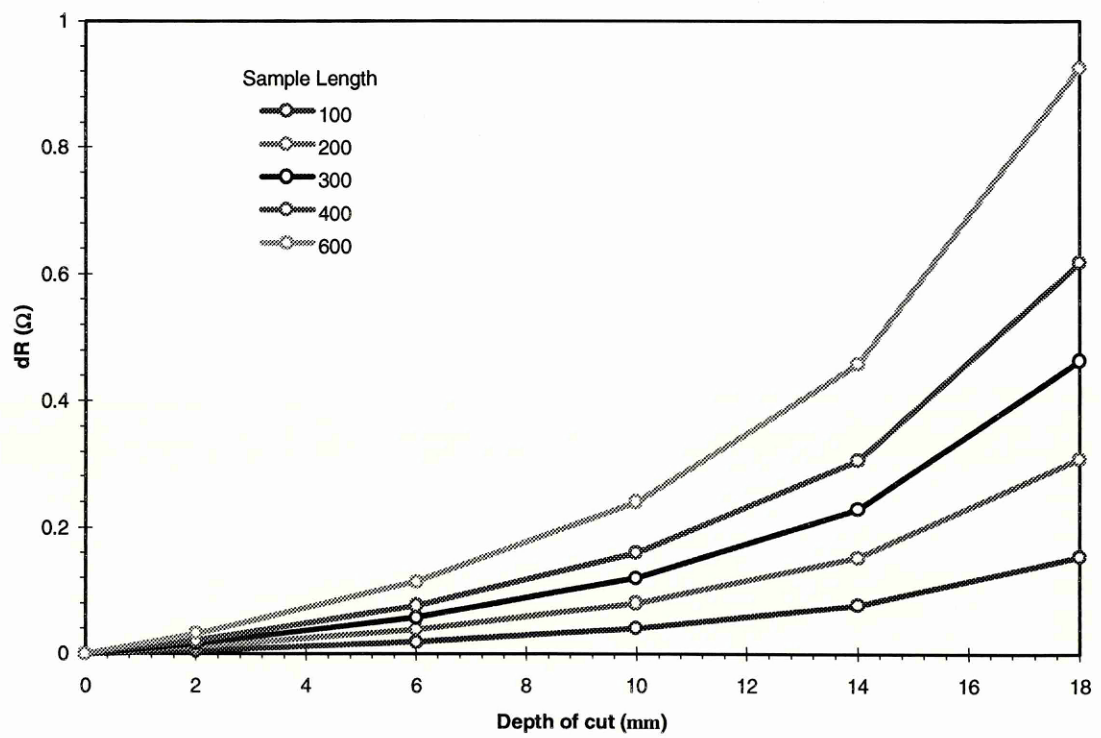

Figure 8.14. Computational simulation of fibre breaks of UD914 laminate samples of various length using parallel resistance model.

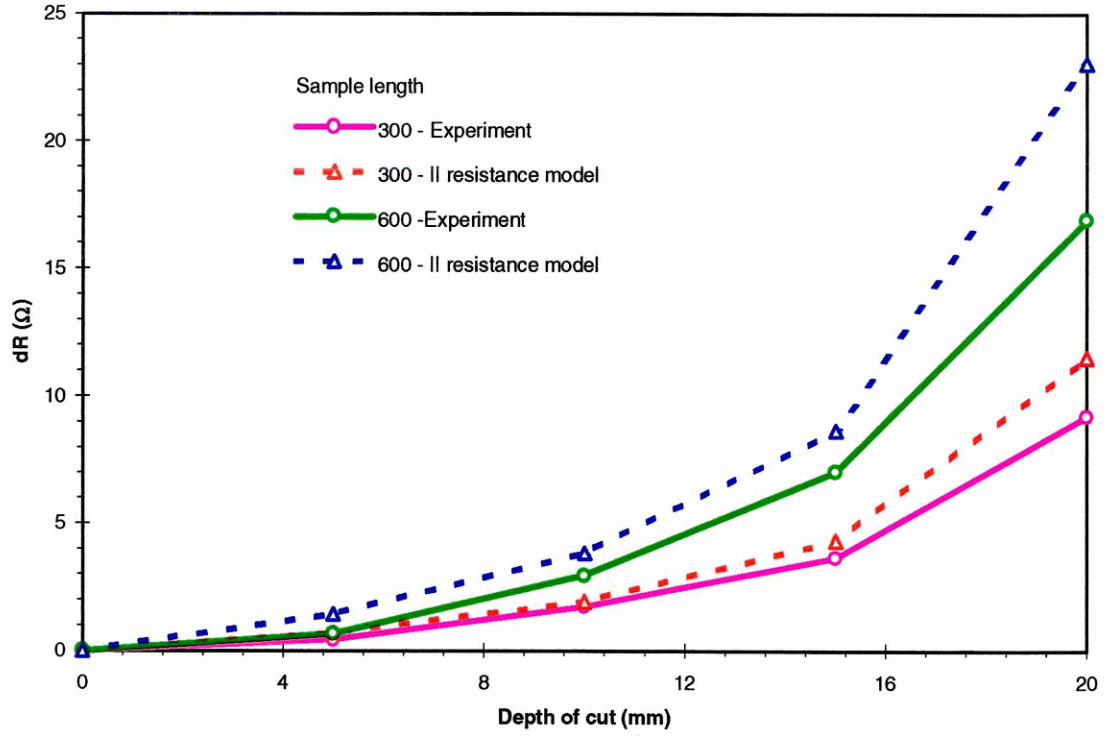

Figure 8.15. Computational simulation of fibre breaks of UD920 lamina samples of various length using parallel resistance model.

8.3.2 Validation of the 3D model

Figure 8.16 shows the computational simulation results of fibre breaks simulated when the current flows transverse to the fibre direction. As stated previously, the experimental simulation was carried out using UD914 samples. Therefore, the 3D model was simulated using UD914 properties. The electrode location and the experimental damage simulation were simulated exactly in the computational model. The comparison of Figure 8.16 and Figure 8.10 demonstrates that the 3D model predicts accurately the behaviour observed in experimental simulation.

Figure 8.17 shows the comparison of longitudinal split growth simulated using both experimental and computational methods. For comparison purpose only electrode A was simulated. The computational simulation agrees excellently with the experimental results. These results validate the 3D model. This also demonstrates that the conduction mechanism of a unidirectional composite is a three-dimensional process and 3D models are essential to investigate the effects of damage on unidirectional laminates.

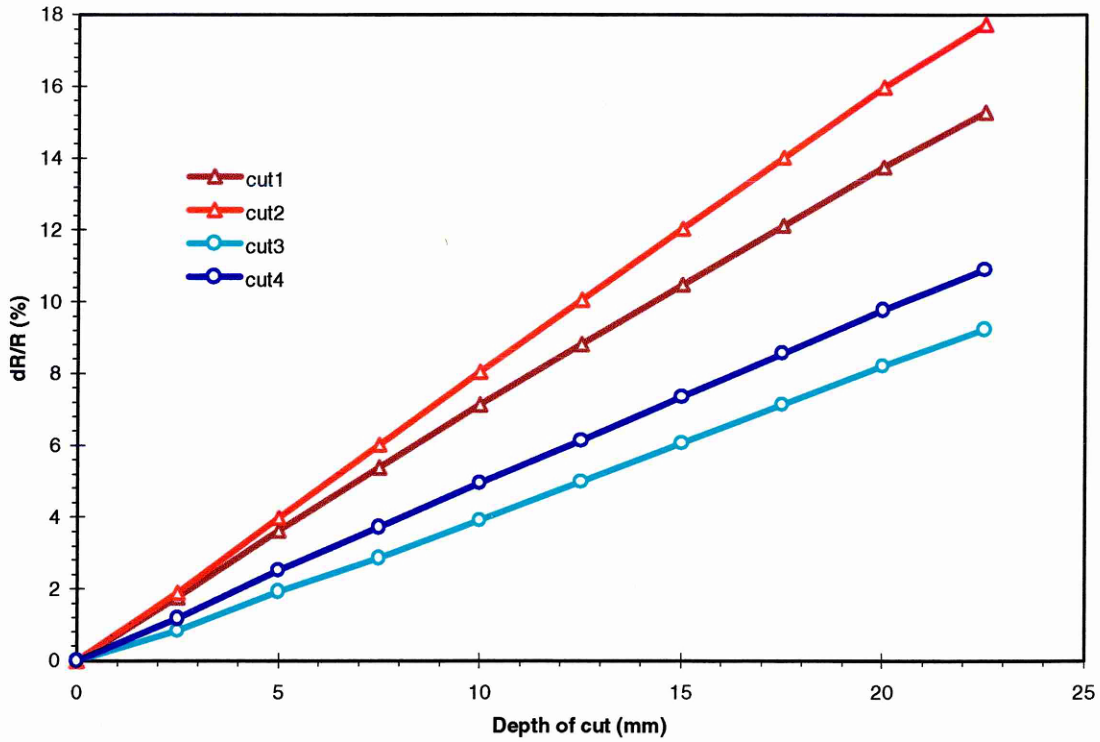

Figure 8.16. Computational simulation results of fibre breaks when the current flows transverse to the fibre direction.

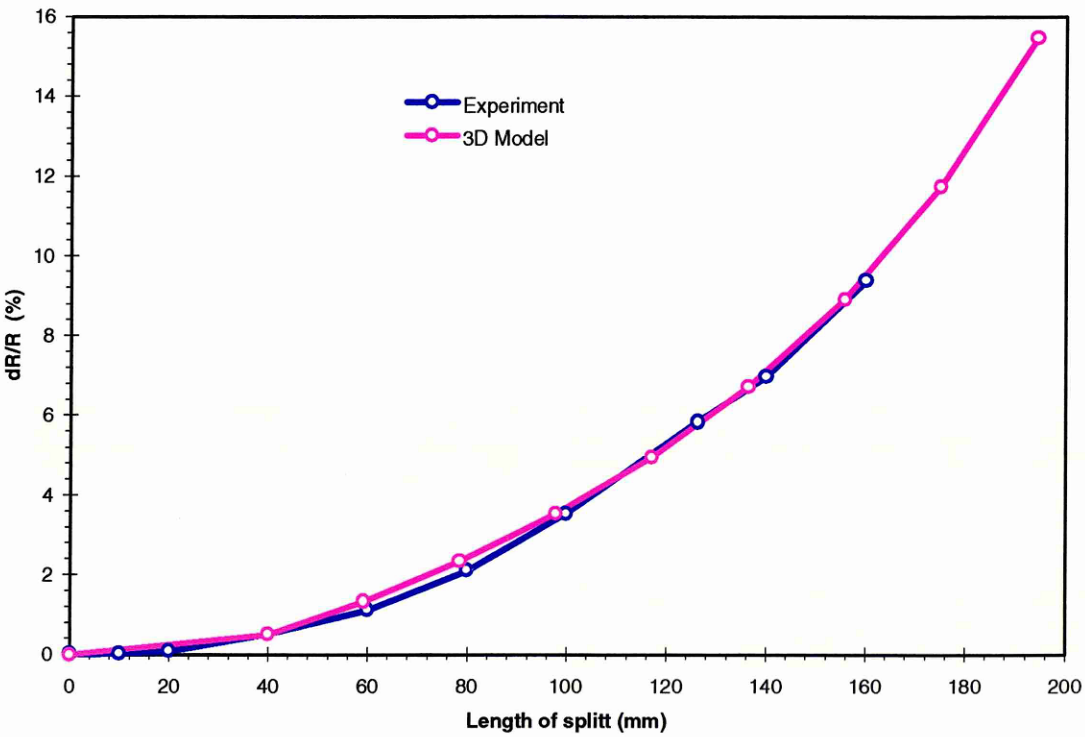

Figure 8.17. Comparison of experimental and computational simulation results of longitudinal splits.

8.3.3 Fibre breaks

Figure 8.18 shows the influence of fibre breaks on resistivity of samples made with different type of fibres. The resistivity value of the fibres used in this simulation ranges from 0.01 mΩm to 0.05 mΩm, including carbon Torayca T300 fibre which is used in experimental, theoretical and computational investigations. This figure clearly illustrates that the change in resistance increases with increasing resistivity of the fibre for a given number of fibre breaks. This result shows that the resistivity of the fibre is a major factor in detecting fibre breaks.

Figure 8.19 and Figure 8.20 shows the fibre break simulation results of UD914 and UD920 samples for three types of electrode configuration, respectively. This figure depicts that the fibre breaks can be detected and are sensitive to all the three type of electrode configuration. It is noteworthy that the behaviour, i.e., the change of resistance with fibre breaks is similar for electrode types E1 and E2. The behaviour of UD914 and UD920 samples are almost similar, though the magnitudes of resistance changes are different. It can be seen that the resistance increases with fibre breaks for all the three types of electrode. This highlights that the fibres are the major current carrying members in a unidirectional CFRP. The fibre breaks are sensitive to all the three type of electrode configuration because they affect the conduction process, whether the current flows in the longitudinal, transverse or through thickness direction.

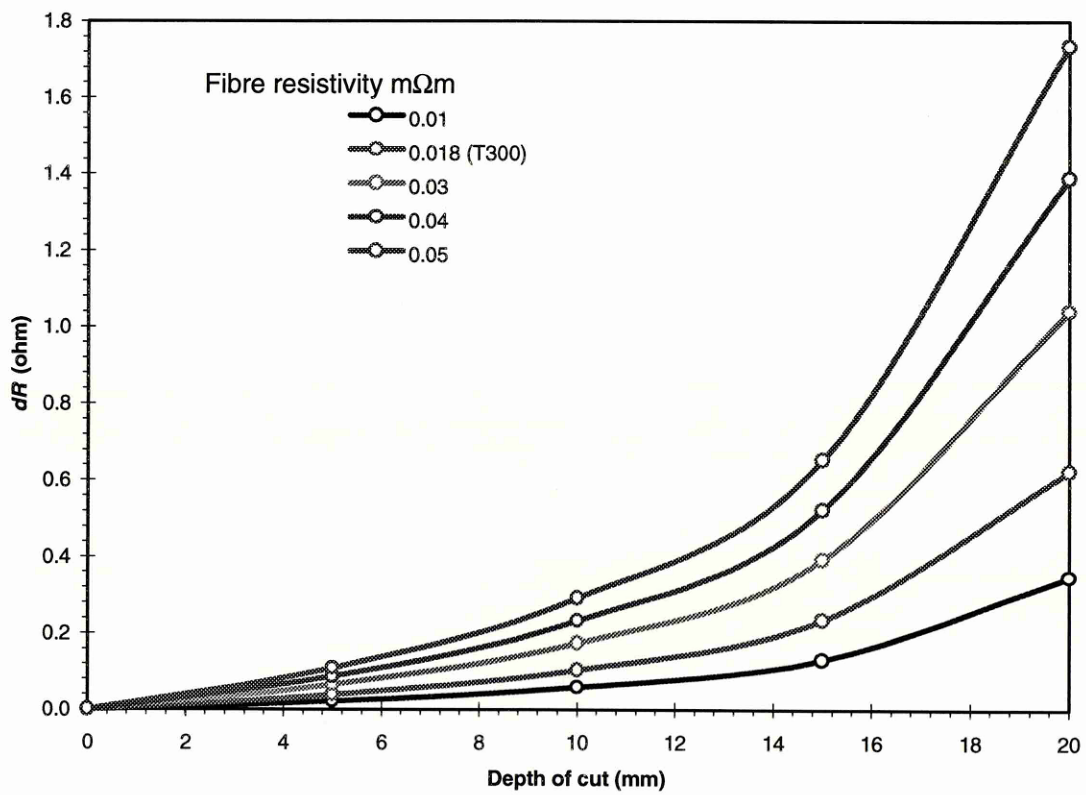

Figure 8.18. Results of computational simulation of effects on fibre resistivity of fibre breaks.

8.3.4 Longitudinal splits

Figure 8.21 and Figure 8.22 show the simulation results of the effects of longitudinal split growth in UD914 and UD920 samples for three types of electrode configurations. This figure clearly illustrates that the longitudinal splits are only sensitive to electrode E3. The electrodes E1 and E2 are not sensitive to longitudinal splits, i.e., longitudinal splits can not be detected. These results demonstrate that the damage can be detected only if the damage growth is perpendicular to the direction of current flow. The damage can be detected only if the damage mechanism alters the conduction process. It is clear from the results that the longitudinal splits did not alter the longitudinal and the through thickness conduction process. This behaviour is similar for both UD914 and UD920 samples.

8.3.5 Delamination

Figure 8.23 and Figure 8.24 show the results of the effects of delamination crack growth simulated for three types of electrode configurations of UD914 and UD920 samples, respectively. This figure clearly illustrates that the delamination crack is only sensitive to electrode E2. The electrodes E1 and E3 are not sensitive to delamination cracks, i.e., delamination cracks can not be detected. This result again demonstrates that the damage can be detected only if the damage growth is perpendicular to the direction of current flow. The damage can be detected only if the damage mechanism alters the conduction process. It is clear from the results that the delamination crack did not alter the longitudinal and the transverse conduction process.

8.3.6 Damage location

Figure 8.25 and Figure 8.26 show the effect of damage location (fibre breaks) for UD914 and UD920 samples, respectively. The electrode configuration E3 was used for this simulation. These figures show the effect of a single fibre break that was simulated at different locations on the sample. These surface plots represent resistance on the z-axis and damage location on the x-y plane. These results demonstrate that the magnitude of resistance change for a single fibre is a function of both length and width of the sample. This behaviour is similar for both UD914 and UD920 samples, however, the magnitudes of resistance change are different.

The implications of these results are very important. These results infer that the damage can be located using the electrical resistance measurement technique. In the previous section we have seen that sensitivity of each electrode is different for different type of damage. These results also infer that the combination of two electrodes can be used to characterise the type of damage and location.

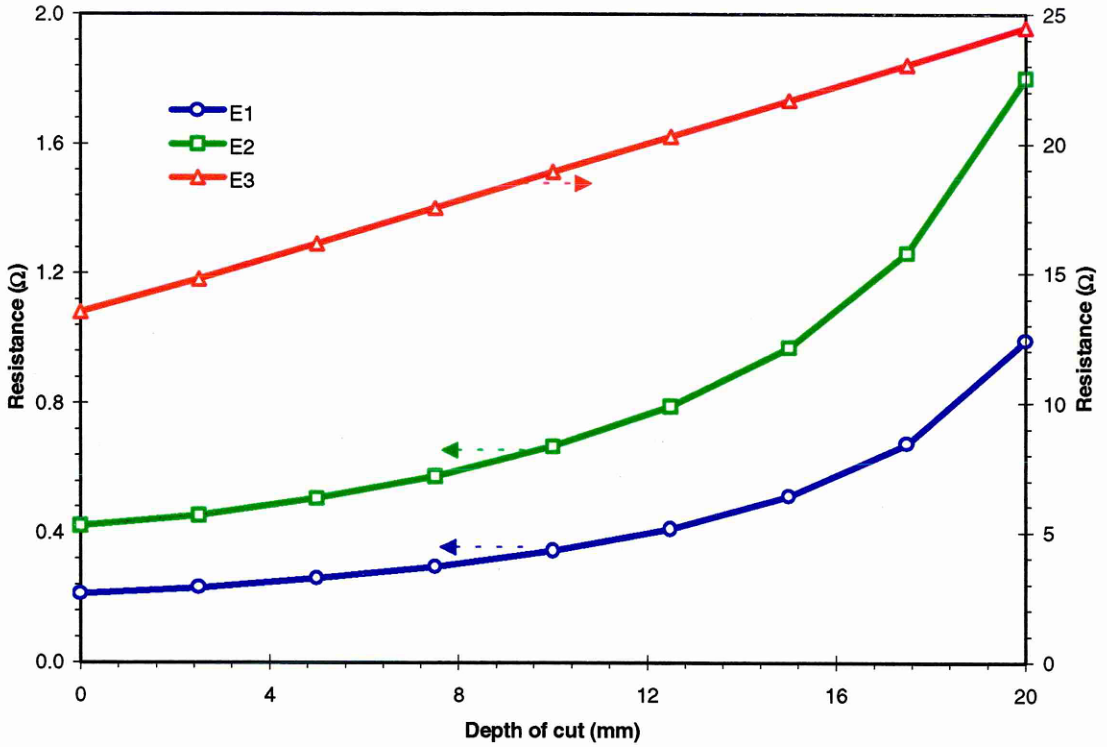

Figure 8.19. Computational simulation results of fibre breaks for three types of electrode configurations (UD914).

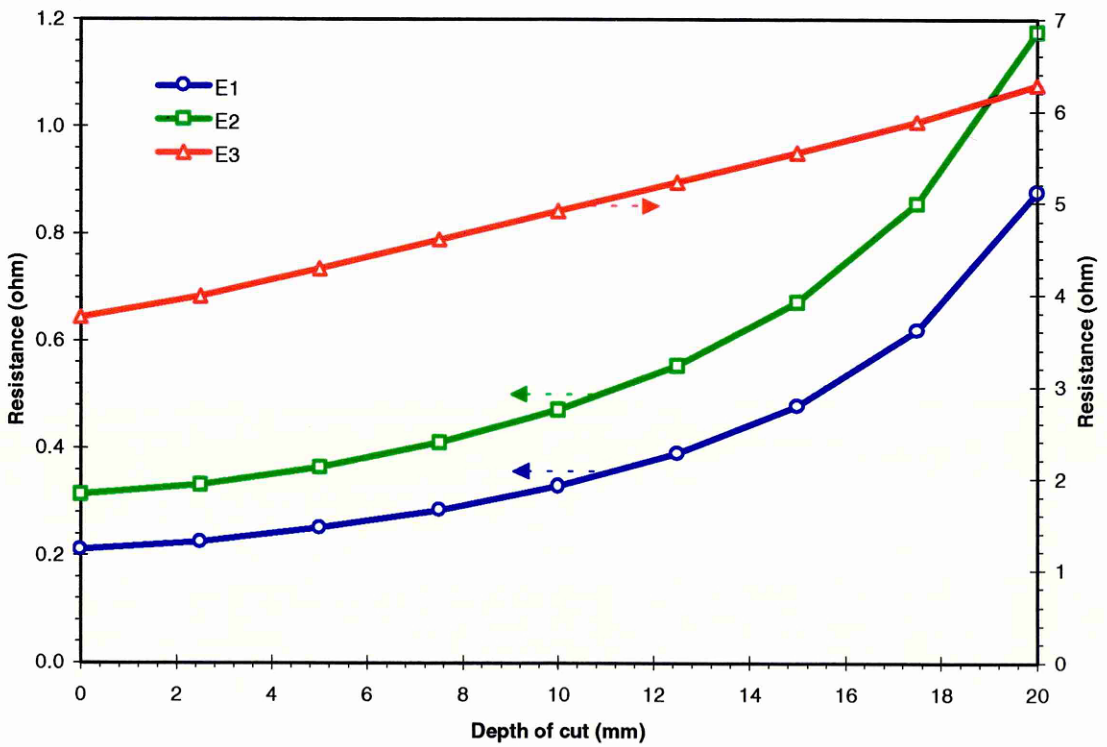

Figure 8.20. Computational simulation results of fibre breaks for three types of electrode configurations (UD920).

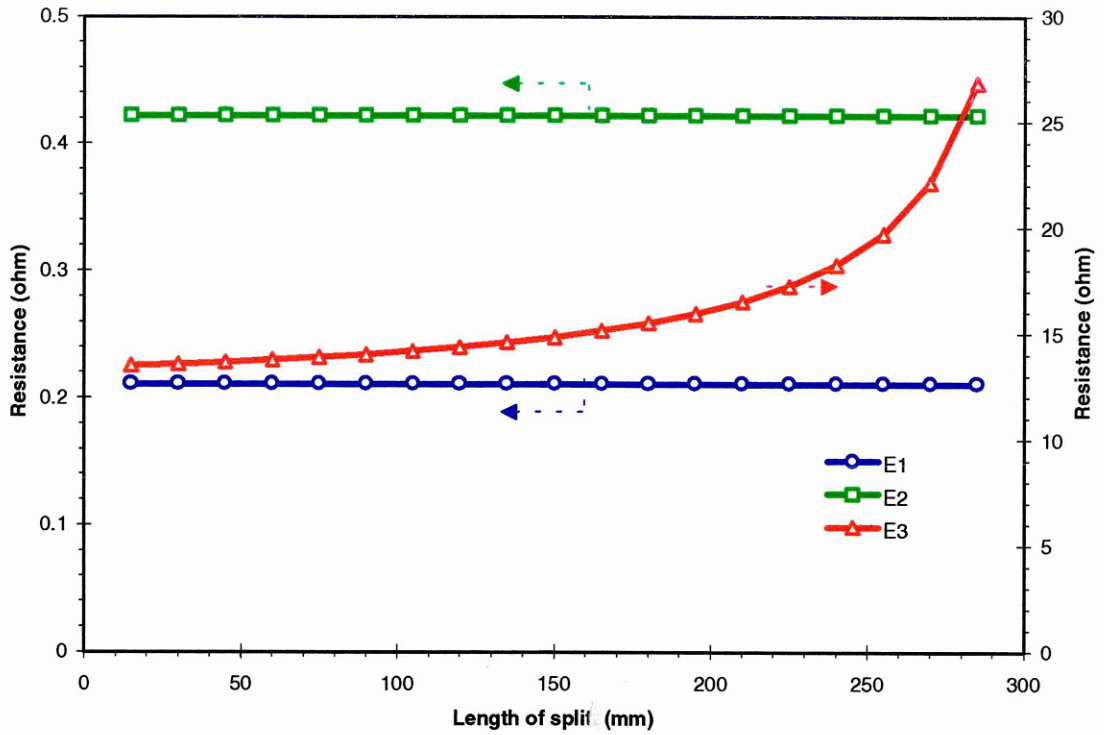

Figure 8.21. Computational simulation results of longitudinal split growth for three types of electrode configuration (UD914).

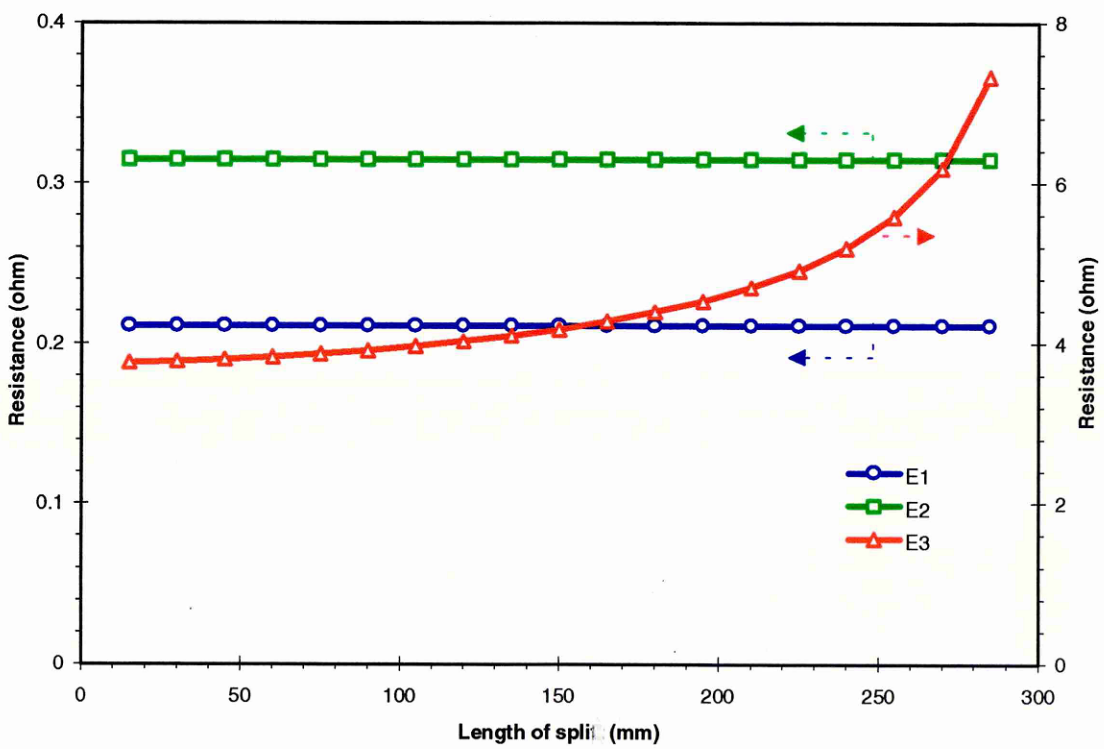

Figure 8.22. Computational simulation results of longitudinal split growth for three types of electrode configuration (UD920).

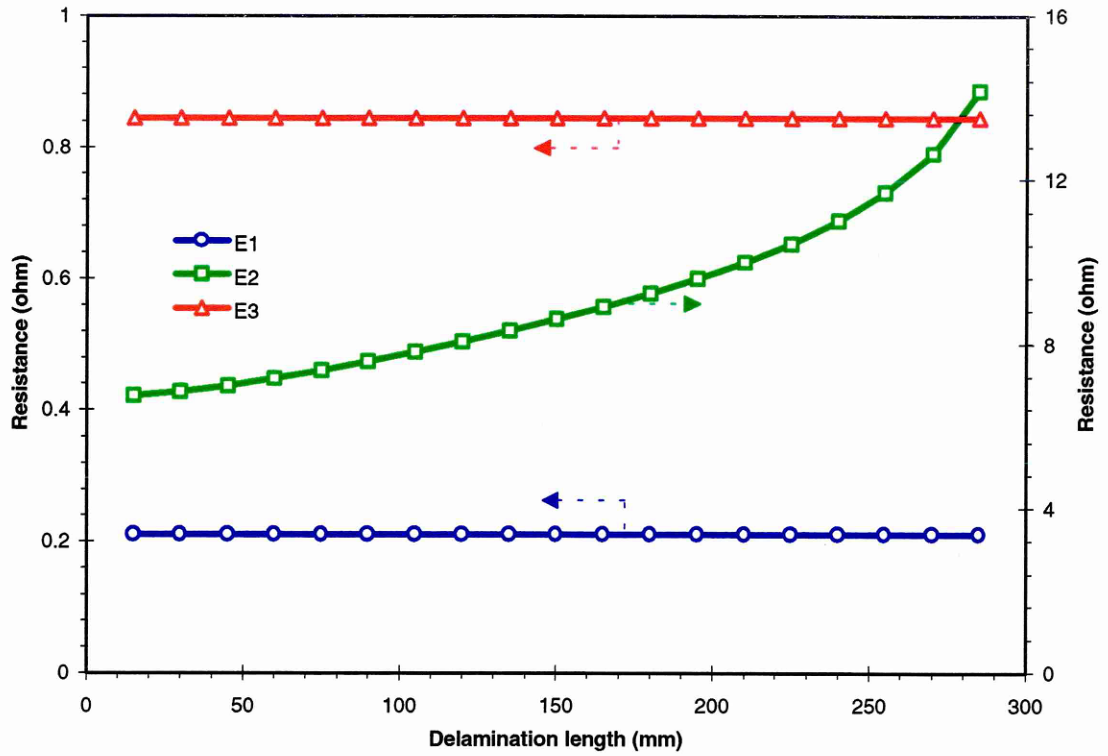

Figure 8.23. Computational simulation results of delamination crack growth for three types of electrode configuration (UD914).

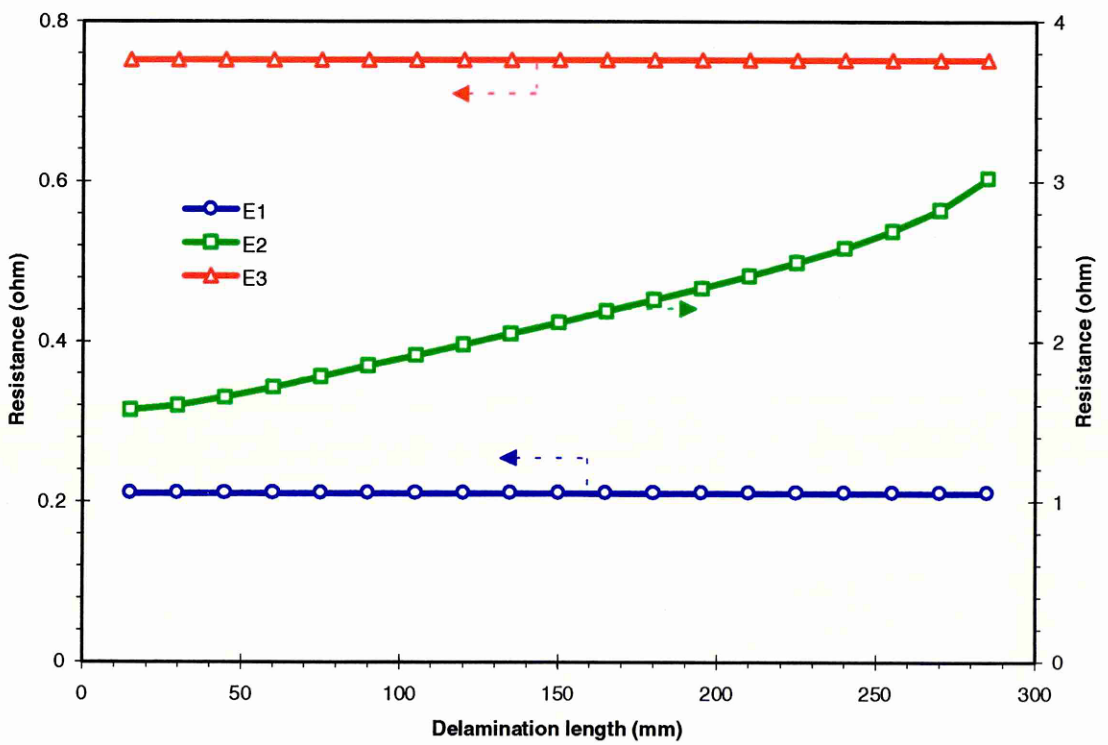

Figure 8.24. Computational simulation results of delamination crack growth for three types of electrode configuration (UD920).

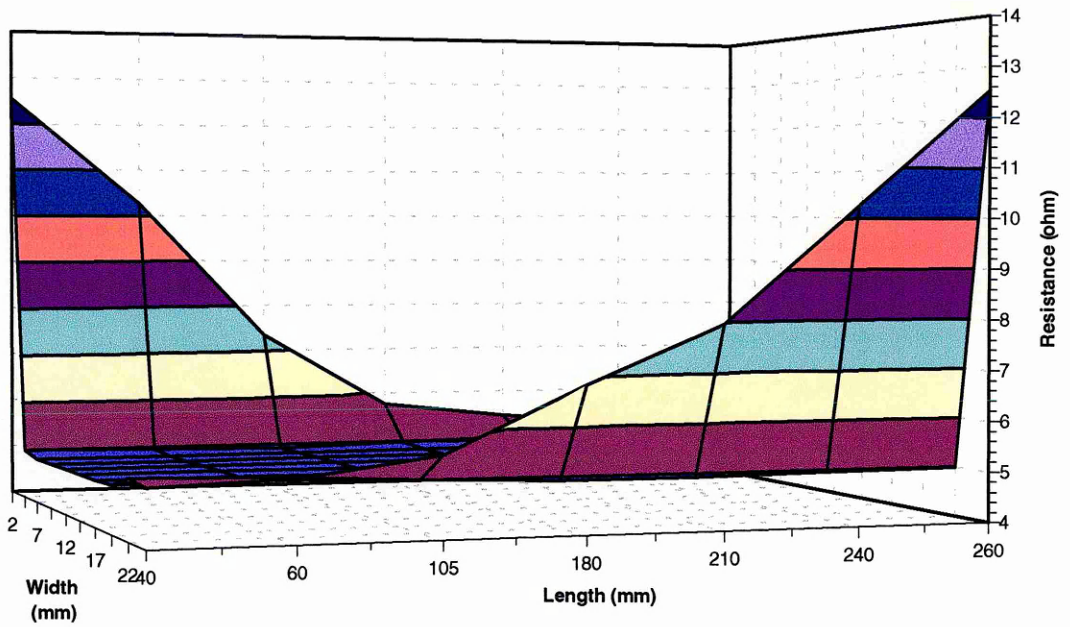

Figure 8.25. Computational simulation results of the effect of fibre break location (UD914, electrode E3)

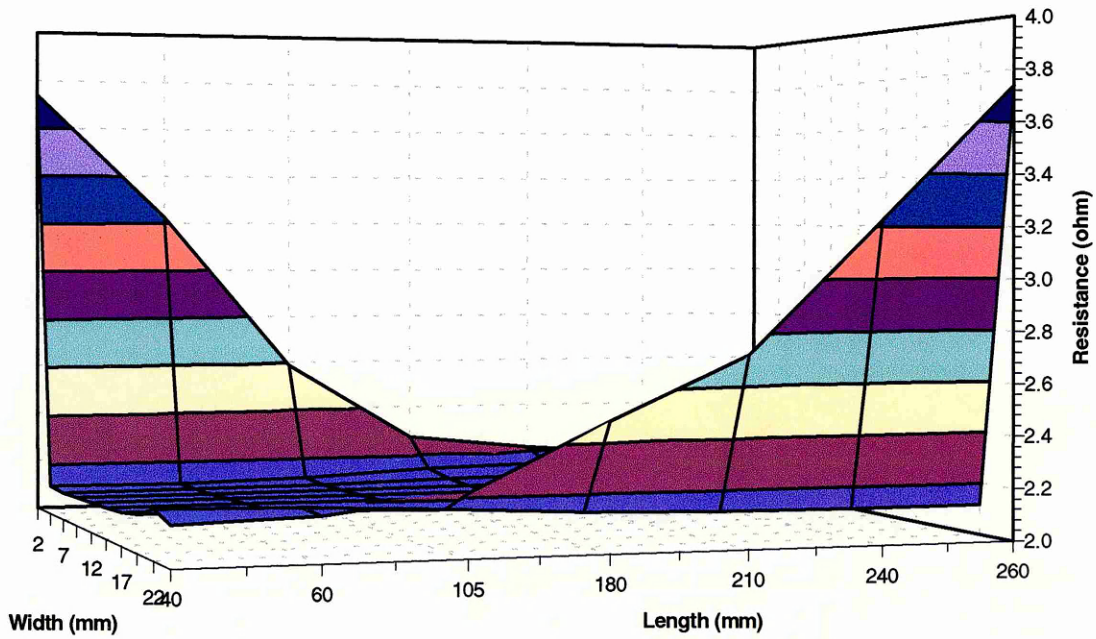

Figure 8.26. Computation simulation results of the effect of fibre break location (UD920, electrode E3)

9

TENSILE FAILURE MECHANISMS

This chapter presents the results related to the longitudinal and transverse tensile behaviour and damage mechanisms of unidirectional and cross-ply CFRP laminates and the associated electrical resistivity measurements. The electrical resistivity measurement results are viewed to highlight the following,

strain sensing,
damage sensing and
smart capabilities.

This chapter is organised as follows. The tensile properties, stress-strain behaviour and failure modes of the samples are presented in section 9.1. The electrical response of samples to tensile loading is presented in section 9.2. Section 9.3 examines the strain sensing capabilities of electrical resistivity measurement technique. The damage sensing capabilities are presented in section 9.4. This section also presents the acoustic emission, C-scan and X-ray radiography results compared with electrical resistance.

Most of the figures presented in this chapter shows experimental lines rather than experimental data points in order to enhance the clarity of presentation. Each line includes a minimum of one hundred to a maximum of one thousand data points.

9.1 TENSILE BEHAVIOUR

9.1.1 Tensile properties

The summary of the tensile properties of the laminates is shown in Table 9.1. The statistical summary of the properties is shown in the appendix C (Table C.4-8). The reported values are in accordance with the previously published results (Harris et.al. 1990, Curtis 1988). The mechanical properties of composite laminates can be predicted using rule of mixtures and classical lamination theory (Jones 1975, Agarwal and Broutman 1990). The theoretical prediction especially the longitudinal properties are found to agree well with experimental measurements. Therefore, the theoretical mechanical properties of laminates used in this investigation were evaluated using appropriate methods and are listed in Table 9.2.

Table 9.1. Summary of experimental tensile properties.

	Tensile strength σ (MPa)	Tensile modulus E (GPa)	Failure strain ε (%)
UD914L	1543±109	140±1.20	1.12±0.05
UD914T	54±5	8.96±0.06	0.62±0.06
UD920L	1580±110	136±0.97	1.14±0.04
UD920T	52±10	7.88±0.11	0.68±0.15
CP914	810±30	72±3.20	1.11±0.05

Table 9.2. Summary of theoretical tensile properties.

Sample Code	Tensile strength σ (MPa)	Tensile modulus E (GPa)
UD914L	2132.57	139.56
UD914T	48.25	9.51
UD920L	2137.00	139.56
UD920T	34.90	9.18
CP914	810.30	72.12

It can be seen that the experimental tensile modulus results agree well with the prediction. The longitudinal strength of unidirectional laminates is approximately 25% less than the prediction. The transverse tensile strength of unidirectional laminates is higher than the theoretical prediction.

It can be seen that there are no significant differences in longitudinal properties of UD914 and UD920 samples, although there are significant differences in transverse properties. The differences in longitudinal properties are less than 3% and the transverse properties are more than 4%. The longitudinal tensile strength and failure strain of UD920 samples are 2.4% and 1.8% higher than UD914 samples, respectively. The longitudinal tensile modulus is 2.3% lower. The transverse failure strain of UD920 is 9.7% higher and, the tensile strength and tensile modulus are 4.3% and 12% lower than UD914, respectively.

It is evident from Table C.4-8 that the scatter in the tensile strength properties is higher for almost all the laminates. However, the scatter in the tensile modulus and failure strain is relatively less. The overall scatter is higher for UD920 than other samples. The scatter in tensile strength of laminates is due to the strength properties of the fibres. In unidirectional laminates the longitudinal properties are controlled mainly by the fibre and hence the statistical distribution of fibre strength can be expected to affect the laminates. The strength properties of the fibres are statistically distributed and found to follow a Weibull type distribution (Weibull 1939, Zweben and Rosen 1970).

9.1.2 Stress-strain behaviour

The typical stress-strain behaviour of 0° and 90° unidirectional and cross-ply laminates is shown in Figure 9.1, including the failure points of other samples. It can be seen that the longitudinal stress-strain behaviour of most of the laminates is linear up to their fracture. There is no significant difference in the behaviour of UD914 and UD920 samples. Slight deviation from the linear behaviour was observed for transverse stress-strain behaviour of UD914 and UD920 samples. The non-linear behaviour of transverse laminates is not very significant, however, noticeable. Cross-ply samples show no sign of non-linear behaviour.

It can be seen that the larger strain to failure of epoxy 920 resin (refer Table 4.2) is not transferred to the laminates. This is true for both longitudinal and transverse strain of UD920 samples. The stress-strain behaviour shows that the longitudinal and transverse behaviour is dominated by the fibres. Similarly, cross-ply samples show that the stress-strain behaviour is dominated by the 0° plies.

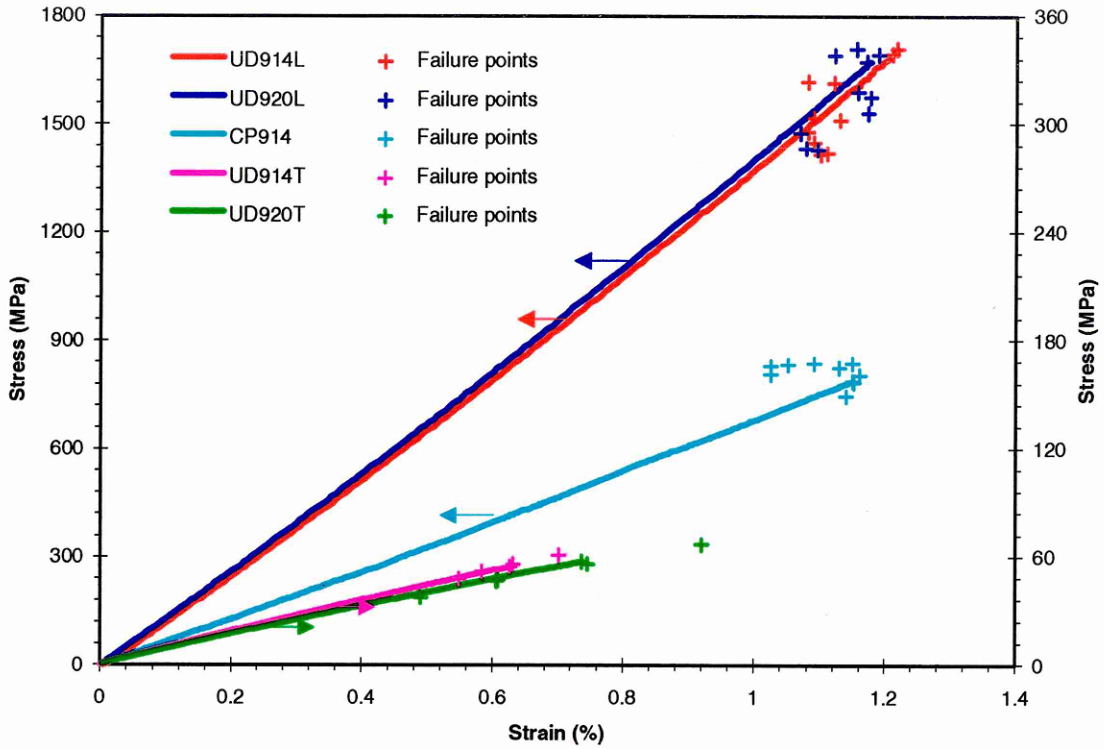

Figure 9.1. Typical longitudinal stress-strain behaviour of unidirectional and cross-ply samples.

9.1.3 Failure modes

The tensile failure modes of the 0° and 90° unidirectional and cross-ply samples are shown in Figure 9.2-10. The general failure pattern of UD914 and UD920 samples are distinctive, though the differences in the mechanical properties are not very significant.

The typical failure pattern of UD914L samples is shown in Figure 9.2. The UD914L samples exhibit 'brush type' brittle failure pattern with excessive longitudinal splitting as described in section 2.3.1. In general, these longitudinal splits run along the length of the sample up to the end of tags or grip jaws and through the thickness. The width of the longitudinal splits approximately ranges between 0.1 mm to 5 mm. However, debris and fibre strands of width less than 0.1 mm were also emitted at the time of failure that accounts approximately 5% of the volume. Some of the samples show evidence of fibre pullout away from the tags, i.e., more than one width distance away and towards the centre. In most of the samples significant amount of fibre pullout appears to be concentrated near the end of the tags or grip jaws. This brush type failure pattern is normally due to dispersed fracture sites of multiple fracture of single fibres, longitudinal splits and fibre pullout (Purslow 1981, Jamison 1985).

The failure pattern of UD920L samples is shown in Figure 9.3. These samples failed in a brittle manner with fibre pullout and longitudinal splitting (refer section 2.3.1). The longitudinal splitting is relatively less in UD920L samples. In this case also, the longitudinal splits run along the length and through the thickness. More than 90% of the samples exhibited fibre pullout away from the tags. These samples also show evidence of fibre fracture sites between the longitudinal splitting.

The failure pattern of 90° unidirectional UD914 and UD920 samples are shown in Figure 9.4 and Figure 9.5, respectively. These samples failed in a brittle manner by matrix or interfacial failure. Several UD914T samples (80%) failed simultaneously at two locations, one near the end of the tag and the other at the centre. Few samples failed at one location and at the centre. Almost all the UD920T samples failed at one location. Most of the samples failed just away from the one width distance from the tag. Only a very few samples failed within one width distance. And none of the UD920T samples failed at the tag line.

The typical failure pattern of CP914 samples is shown in Figure 9.6. In this case, most of the samples failed at one location and one width distance away from the tags. Few samples failed at two locations, one near the tag line and the other away from the one width distance. These samples show evidence of delamination, fibre fracture, longitudinal splitting and matrix damage.

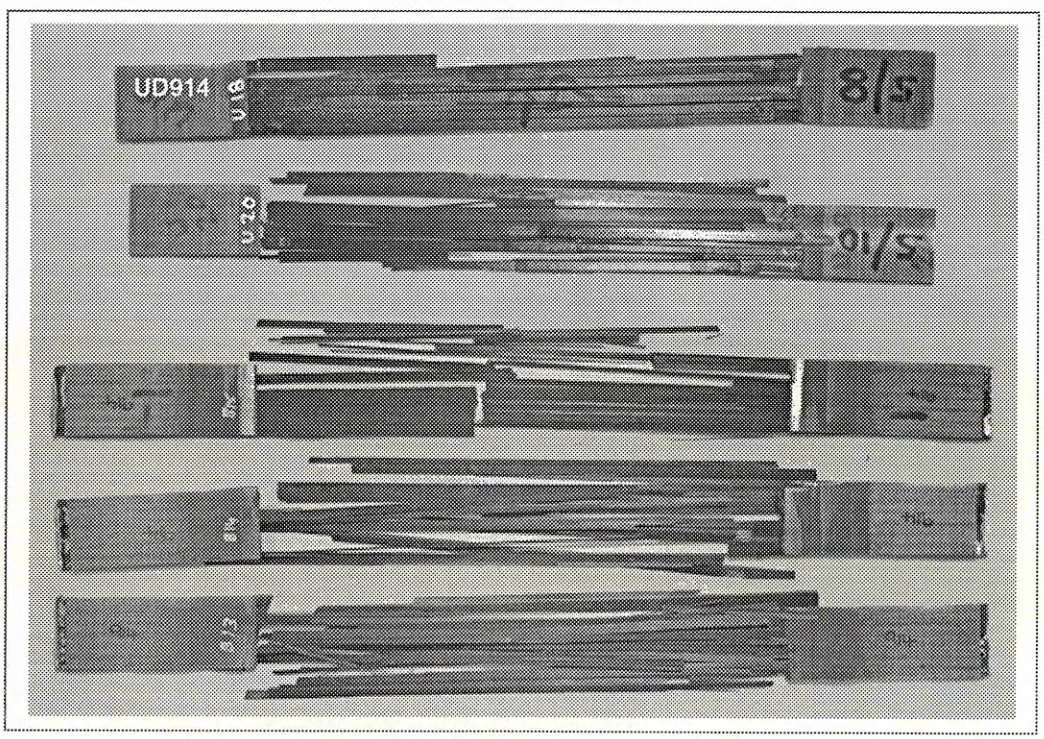

Figure 9.2. Tensile failure pattern of 0° unidirectional UD914L samples.

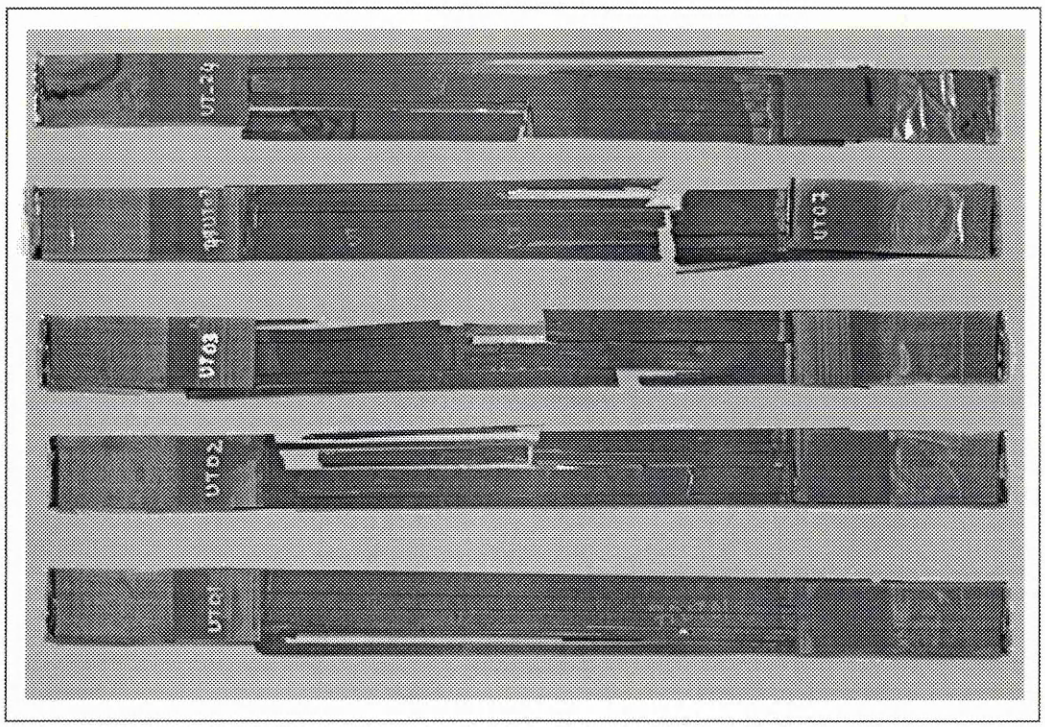

Figure 9.3. Tensile failure pattern of 0° unidirectional UD920L samples.

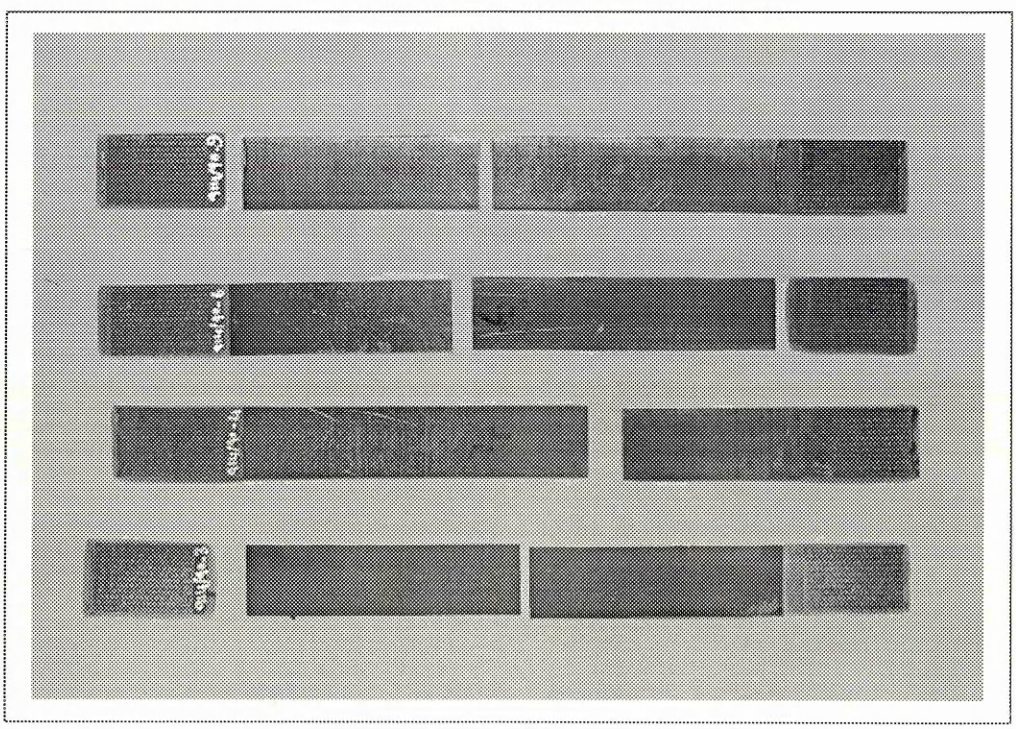

Figure 9.4. Tensile failure pattern of 90° unidirectional UD914T samples.

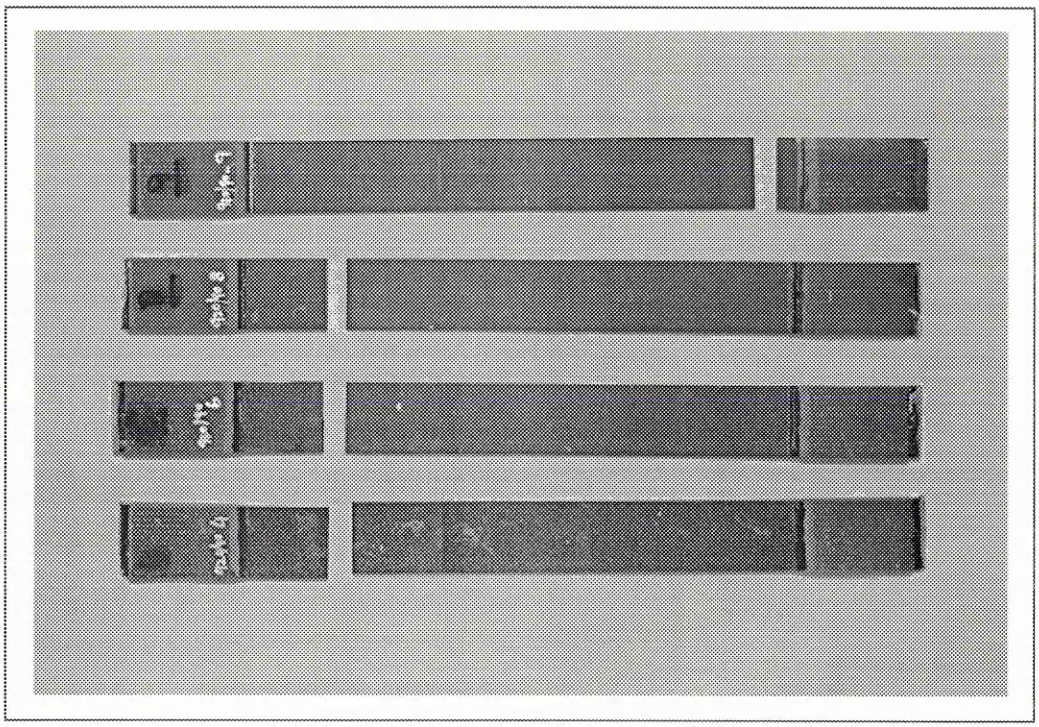

Figure 9.5. Tensile failure pattern of 90° unidirectional UD920T samples.

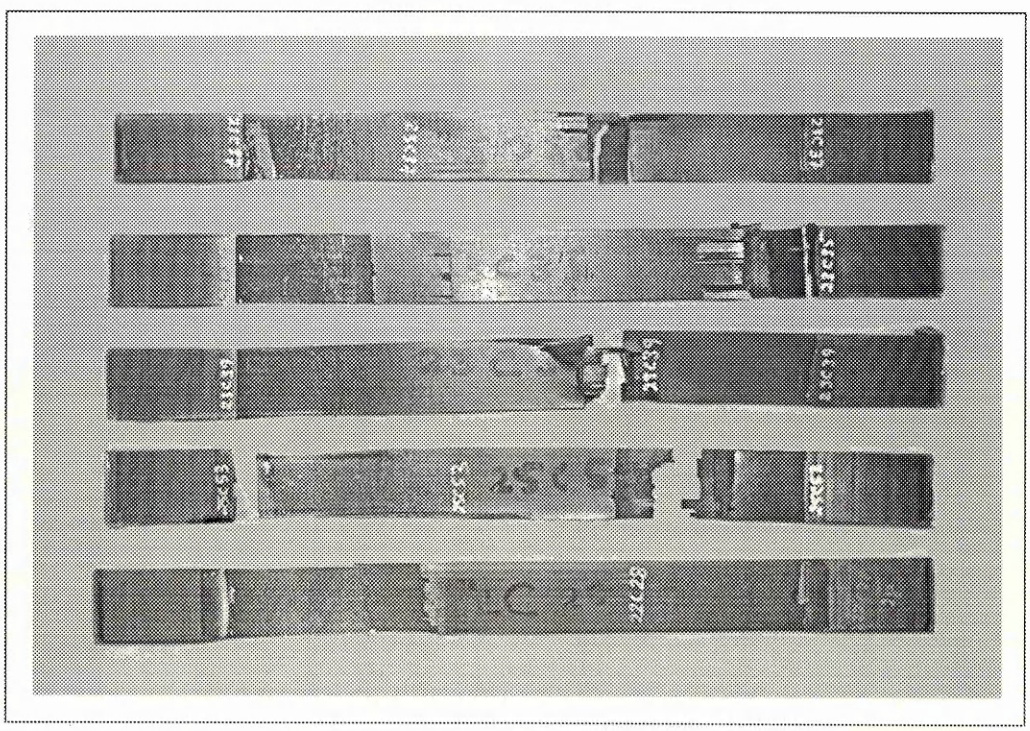

Figure 9.6. Tensile failure pattern of cross-ply CP914 samples.

9.2 ELECTRICAL RESPONSE

This section detail the results related to the electrical response of laminates to tensile loading. In this section importance is given mainly to electrical response. The strain and damage sensing capabilities are discussed in the subsequent sections. The resistance measurement method and the electrode configuration as described in section 4.5 were used. In order to compare the results the change in resistance, *dR*, is used in all the figures. This allows the comparison of results without the influence of the electrode resistance.

9.2.1 0° unidirectional samples

The electrical response of UD914L and UD920L samples to tensile loading is shown in Figure 9.7 and Figure 9.8, respectively. It is clear that in most of the samples the resistance increases with applied stress. The resistance increases linearly with applied stress up to 70% of the UTS. Above 70% of the stress level, the resistance increases non-linearly. Close to the UTS the resistance increases drastically. It can be seen that in UD914L samples the resistance increases in a stepwise or drastic manner above 70% of the UTS. Similar behaviour was exhibited by UD920L samples, also. However, in two of UD920L samples, the resistance was found to decrease with applied stress after 70% of the UTS. Some of the samples show step wise increase in resistance with applied stress below 70% of the UTS. Also, it can be seen that the deviation from linear behaviour for some of the samples starts as early as 40% of the UTS.

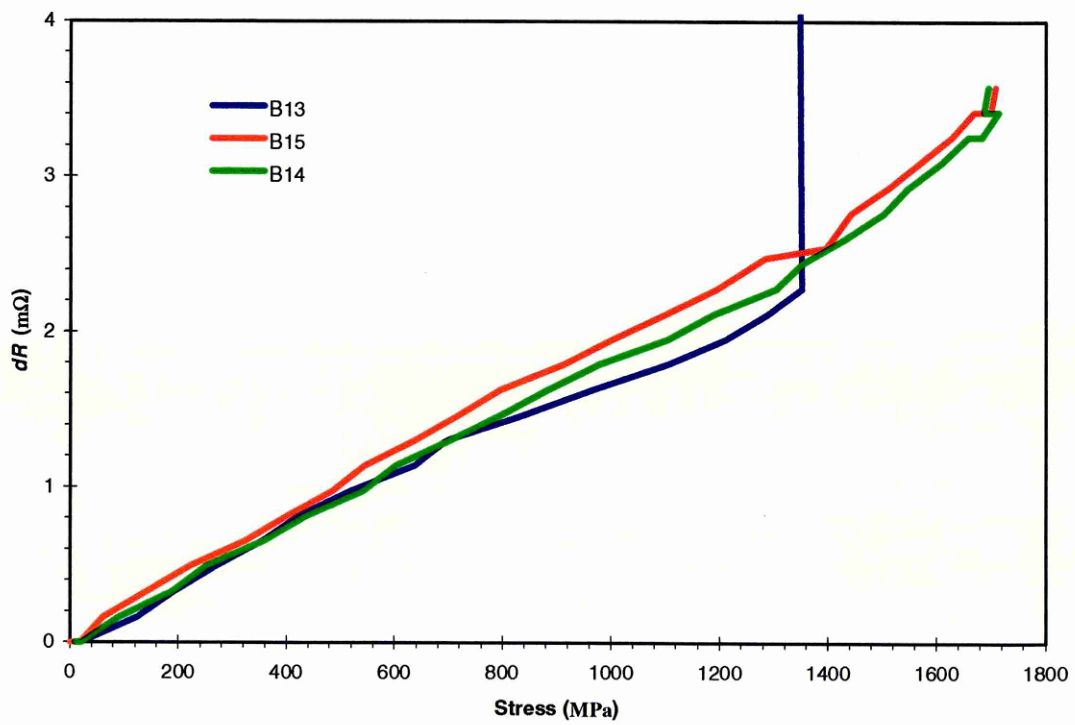

Figure 9.7. Electrical response of UD914L samples to longitudinal tensile loading.

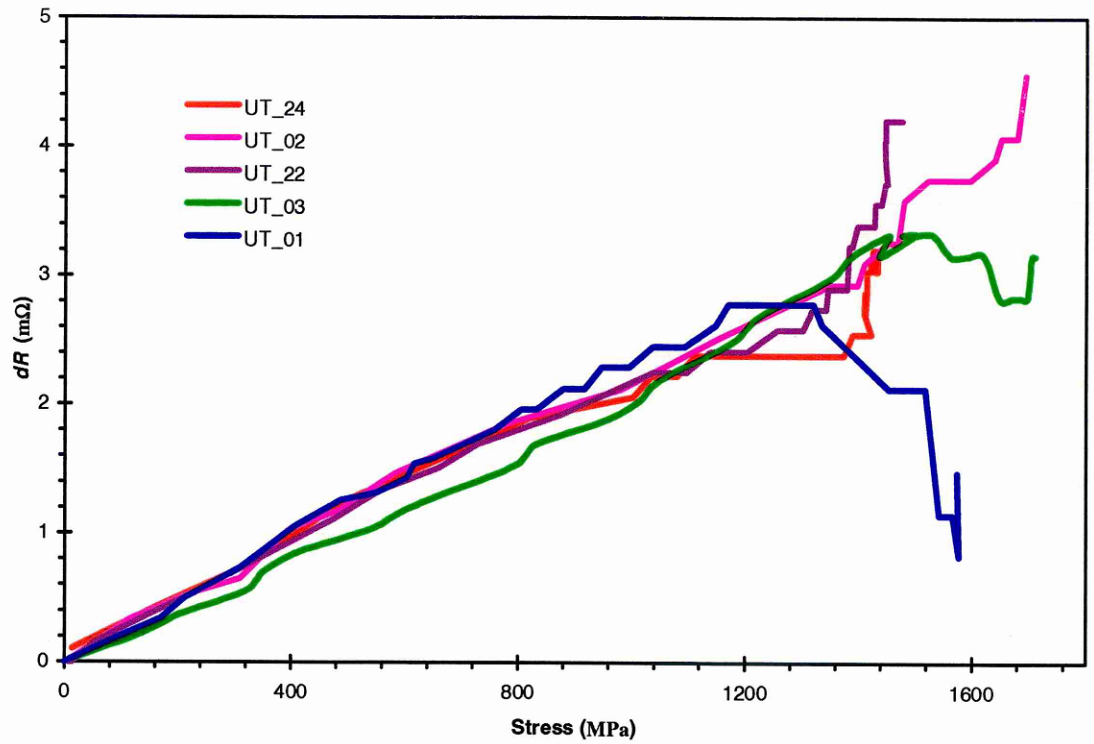

Figure 9.8. Electrical response of UD920L samples to longitudinal tensile loading.

The previous paragraph described the overall electrical behaviour of the laminates. In order to gain more insight, it is necessary to examine the electrical response of individual samples to applied stress. The electrical response depicted in figures may be indicating the strain and damage experienced by the samples. The individuality of electrical response may be indicating the damage initiation and the growth pattern of each of the samples.

In a tensile test the strain and the damage level of the samples are expected to increase with applied stress. Therefore, the resistance change with applied stress is an indication of the cumulative effect of both strain and damage of the samples. The strain in the samples can be predicted using the electrical resistance. (For derivation refer section 5.6 and strain prediction results refer section 9.3). By comparing the strain derived from the electrical resistance measurements and with the extensometer strain, the resistance changes due to damage alone can be obtained. This can be used to examine the resistance results for quantifying the damage. It can be shown that the increase in resistance up to approximately 70% of the stress level is mainly due to strain changes (section 9.3). The number of broken fibres derived from the damage component of electrical resistance by subtracting the strain component is presented in section 9.4.1.

The decrease in resistance with applied stress after 70% of UTS of some of the UD920L samples may be due to damage mechanisms other than fibre fracture. The electrode configuration used for the present measurement is mostly sensitive to fibre fracture, that is the resistance will increase with increase in number of fibre fracture. The other damage mechanism such as delamination or longitudinal splits can increase or decrease the resistance depending on the location of the damage and growth pattern. The electrode may not be sensitive at all, i.e., the electrical resistance may not change for damage mechanisms such delamination and longitudinal splits. This is possible because of the three dimensional conduction behaviour of UD laminates. The decrease in resistance of UD920L samples may be due to longitudinal splitting. The macroscopic examination of the failed samples was found to support the above. A relationship was found between the electrical behaviour and the number of longitudinal splits of the samples. It was measured that the number of longitudinal splits is higher for samples where the electrical resistance decreases with applied stress. These results are presented in section 9.4.1.

It can be seen that the final step or drastic increase in resistance leads to failure of the sample. The step wise increase in resistance was suggested to be due to fibre breaks (Schulte and Baron 1989). Therefore, the step wise increase in resistance of the samples below 70% of the UTS infers that single fibre or fibre strands breakage may not lead to the final catastrophic failure. This suggests that the failure of the samples is not dominated by the weakest link.

9.2.2 90° unidirectional samples

The electrical resistance measurement results related to 90° unidirectional laminates to tensile loading are shown in Figure 9.9 and Figure 9.10. It is clear from these figures that the resistance increases non-linearly with applied stress. The behaviour is similar for both UD914 and UD920 samples, though the magnitudes of resistance change at ultimate strength and the rate of change with applied stress are different. The magnitude of resistance change of UD920 samples is approximately 30% less than the UD914 samples. The electrical response of samples to tensile loading was found to follow a third order polynomial of the following form:

$$dR = a\,\sigma^3 + b\,\sigma^2 + c\,\sigma \qquad (9.1)$$

where, dR, is the change in resistance and, σ, is the tensile stress. The coefficients a, b and c in the above equation for all the UD914 and UD920 samples are shown in Table 9.3. These figures also illustrate that the results are consistent for all the samples within the category, although the failure points are different. Examination of failure points indicates that the change in resistance is higher for samples of larger strain to failure. A correlation was found between

the electrical resistance and tensile strength of 90° unidirectional samples. These results are presented in section 9.4.2.

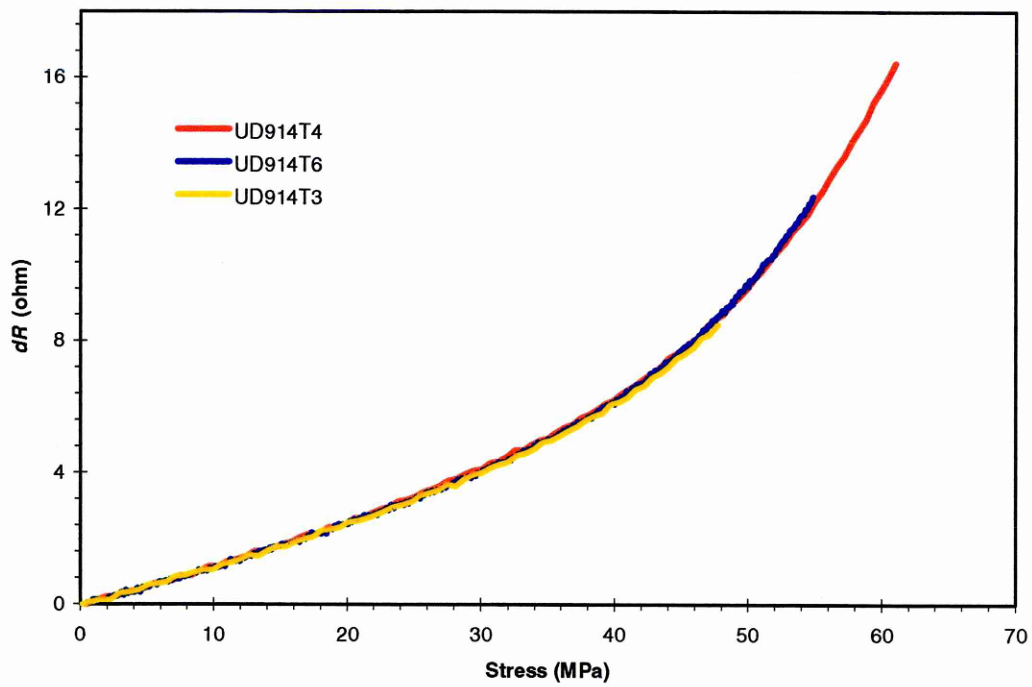

Figure 9.9. Electrical response of UD914T samples to transverse tensile loading.

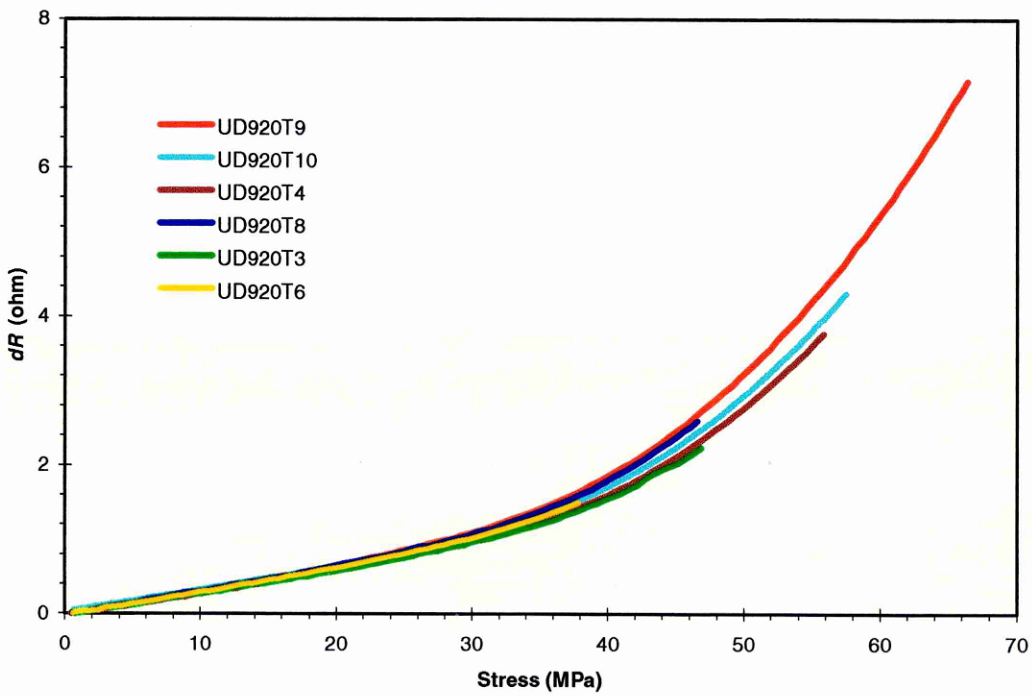

Figure 9.10. Electrical response of UD920T samples to transverse tensile loading.

Table 9.3. Polynomial coefficients of UD914T and UD920T samples

Sample code	Coefficients a	b	c
UD920_3	2.00E-05	-0.0006	0.0331
UD920_4	3.00E-05	-0.0011	0.0388
UD920_6	1.00E-05	-0.0001	0.0295
UD920_8	3.00E-05	-0.0009	0.0390
UD920_9	3.00E-05	-0.0012	0.0425
UD920_10	3.00E-05	-0.0014	0.0467
UD914_3	4.00E-05	-0.0008	0.1207
UD914_4	9.00E-05	-0.0037	0.1636
UD914_6	7.00E-05	-0.0026	0.1437
UD914_9	2.00E-05	-0.0005	0.0820

9.2.3 Cross-ply samples

The electrical resistance measurement results related to cross-ply samples are shown in Figure 9.11 and Figure 9.12. It can be seen that the CP914 samples exhibit two distinct types of behaviour. In general, the resistance increases non-linearly with applied stress. Fifty percent of the samples (Figure 9.11) are found to follow the non-linear behaviour of a third order polynomial of the following form:

$$dR = a\,\sigma^3 + b\,\sigma^2 + c\,\sigma \qquad (9.2)$$

where, dR, is the change in resistance and, σ, is the stress. The coefficients a, b and c in the above equation for all the samples are shown in Table 9.4. The cross-ply samples with this type of behaviour will be referred here as type I.

The rest, fifty percent of the samples were found to follow the behaviour as depicted in Figure 9.12. In these samples, three types of behaviour at three regions of stress level can be identified. The first region is from 0 to 40 % of the applied stress. In this region the resistance was found to increase gradually. Then, in the second region that covers 40 to 80% of the stress

range, no or only slight increases in resistance was observed. The third region is above 80% and up to the ultimate failure stress. In this region, the resistance was found to increase drastically with applied stress. The overall behaviour by is shown to follow a fourth order polynomial of the following form:

$$dR = a\,\sigma^4 + b\,\sigma^3 + c\,\sigma^2 + d\,\sigma. \qquad (9.3)$$

where, dR, is the change in resistance and, σ, is the stress. The coefficients a, b, c and d in the above equation for all the samples are shown in Table 9.4. The cross-ply samples with this type of behaviour will be referred here as type II.

Comparison of both the behaviours shows that the behaviour is almost the same up to 40% of the stress level. The difference in the behaviour starts only after this stress level.

The results shown in these figures are very interesting and they clearly highlight the damage sensing capabilities of ERM. Therefore, to understand further, cross-ply samples were subjected to various levels of tensile stress. The electrical response was measured for both loading and unloading of the sample. These samples were examined non-destructively using techniques such as C-scan and X-ray radiography. These results were then compared with the hysteresis of the electrical resistance. The details and the results are presented in section 9.4.3.

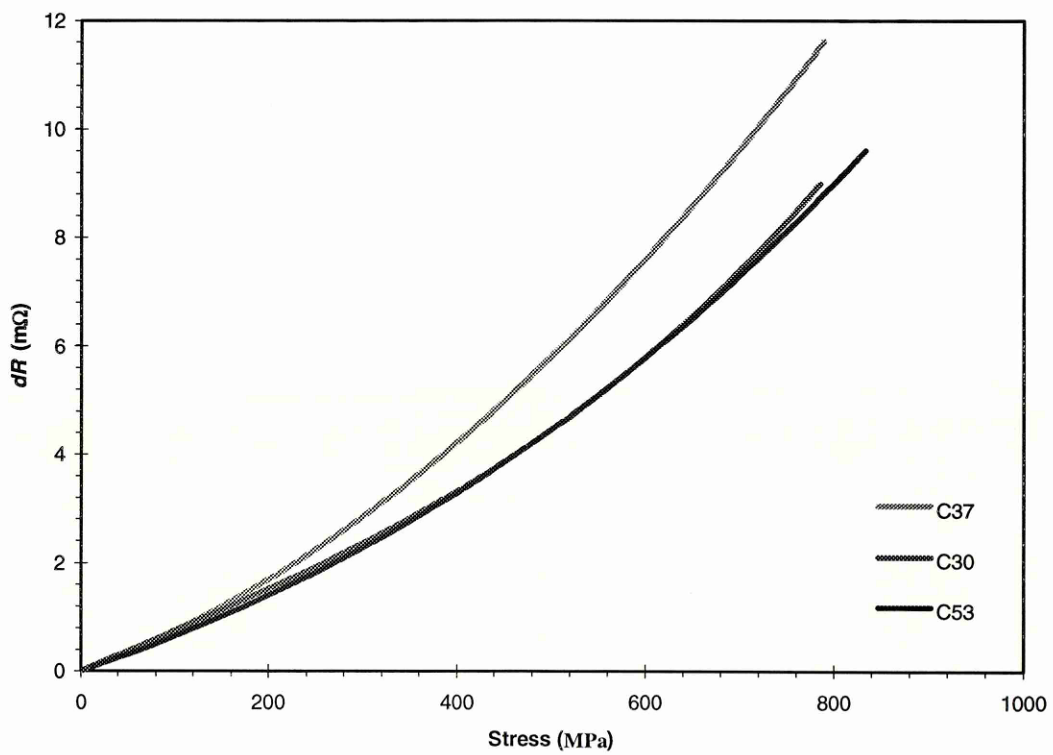

Figure 9.11. Electrical response of CP914 samples to tensile loading (Type I).

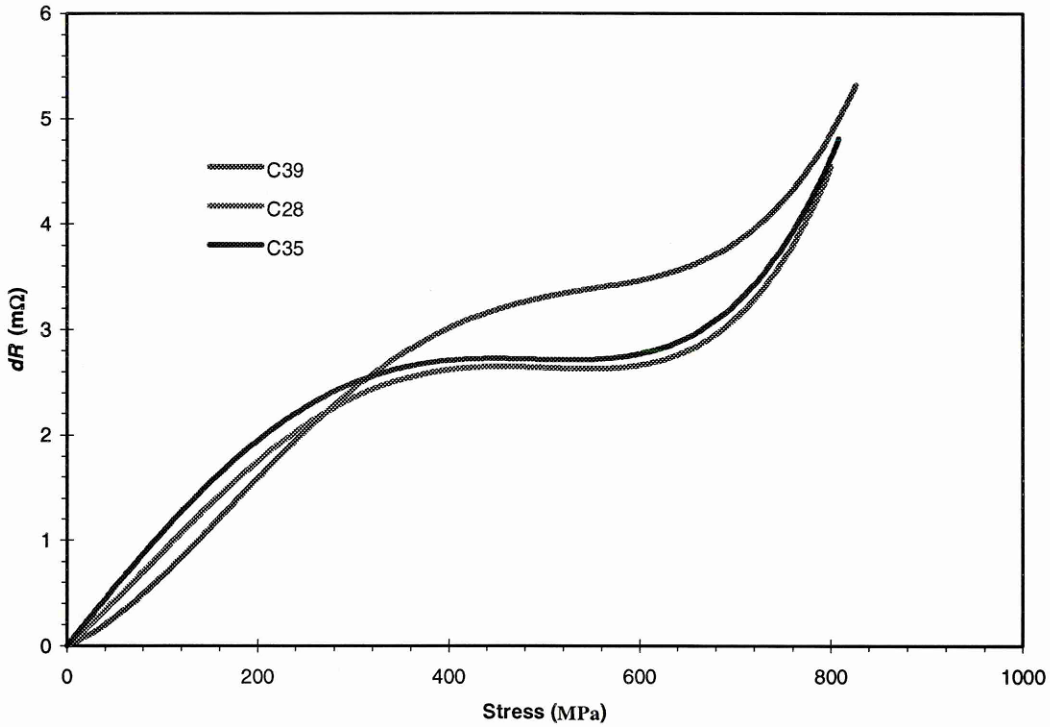

Figure 9.12. Electrical response of CP914 samples to tensile loading (Type II).

Table 9.4. Polynomial coefficient of CP914 samples.

Sample code	Coefficients			
	a	b	c	d
C37	6.00E-10	1.00E-05	0.0064	-
C30	8.00E-09	-1.00E-06	0.0075	-
C53	2.00E-09	5.00E-06	0.006	-
C39	7.00E-11	-1.00E-07	4.00E-05	0.0037
C28	7.00E-11	-8.00E-08	2.00E-05	0.0079
C53	5.00E-11	-5.00E-08	-1.00E-06	0.0111

9.3 STRAIN SENSING

This section describes results related to the strain sensing capabilities of the electrical resistivity measurement technique. The electrical resistance measurement results are compared with the strain measured using the extensometer. Where possible, new formulas and methods that are developed in the previous chapters were used to calculate the strain directly from the resistance

from the resistance measurements. In this section, representative samples from each type of laminates are used rather than all the samples. This helps to present the results in a concise and clear manner.

For 0° unidirectional samples the strain was calculated using the derivation as described in section 5.6. For all other samples the strain prediction from resistance measurement is not straight forward and hence the electrical resistance measurement results are compared figuratively with actual strain measured using the extensometer.

9.3.1 UD samples- longitudinal loading (0°)

The predicted strain and the actual strain results of UD914L and UD920L samples are shown in the Figure 9.13 and Figure 9.14, respectively. It can be seen that the ERM-predicts the strain very accurately up to 0.6% of actual strain. After this strain level, the ERM-strain deviates from the extensometer strain, indicating the onset of damage. This behaviour is similar for both UD914L and UD920L samples. The similarity highlights that both UD914L and UD920L samples indicate the strain up to the damage initiation point and then deviate depending on the type of damage propagation. As a strain sensor, it predicts the strain as long as there is no damage.

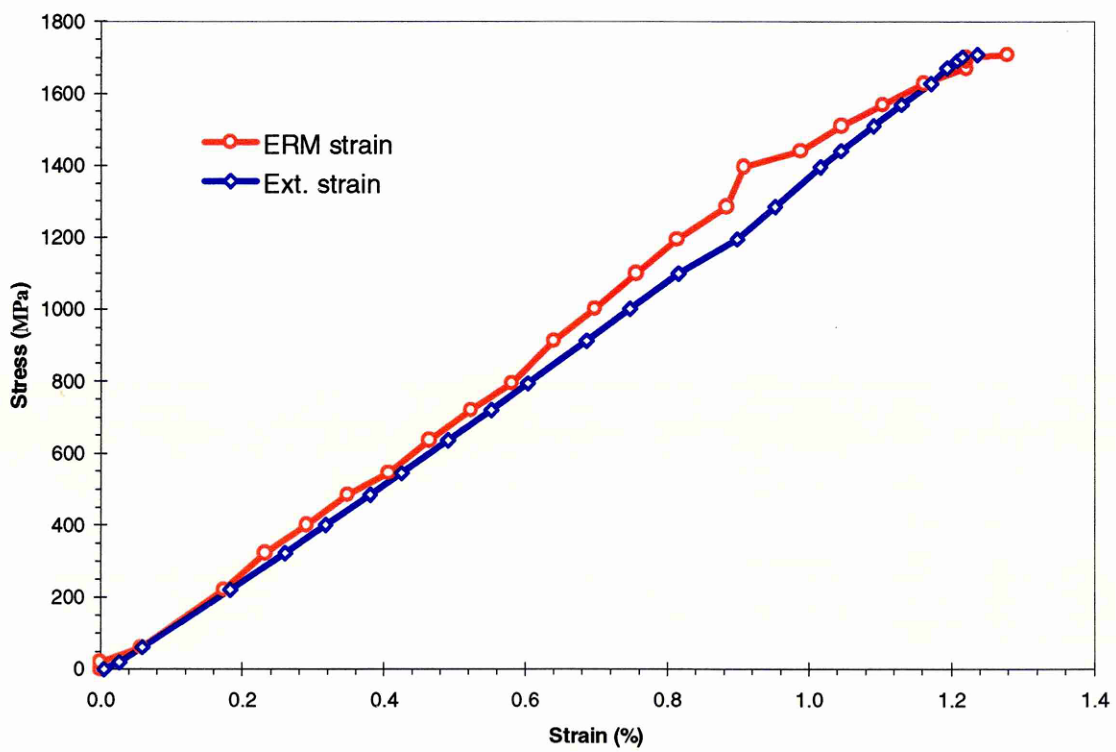

Figure 9.13. Comparison of strain measured using electrical resistance and extensometer of a typical UD914L sample.

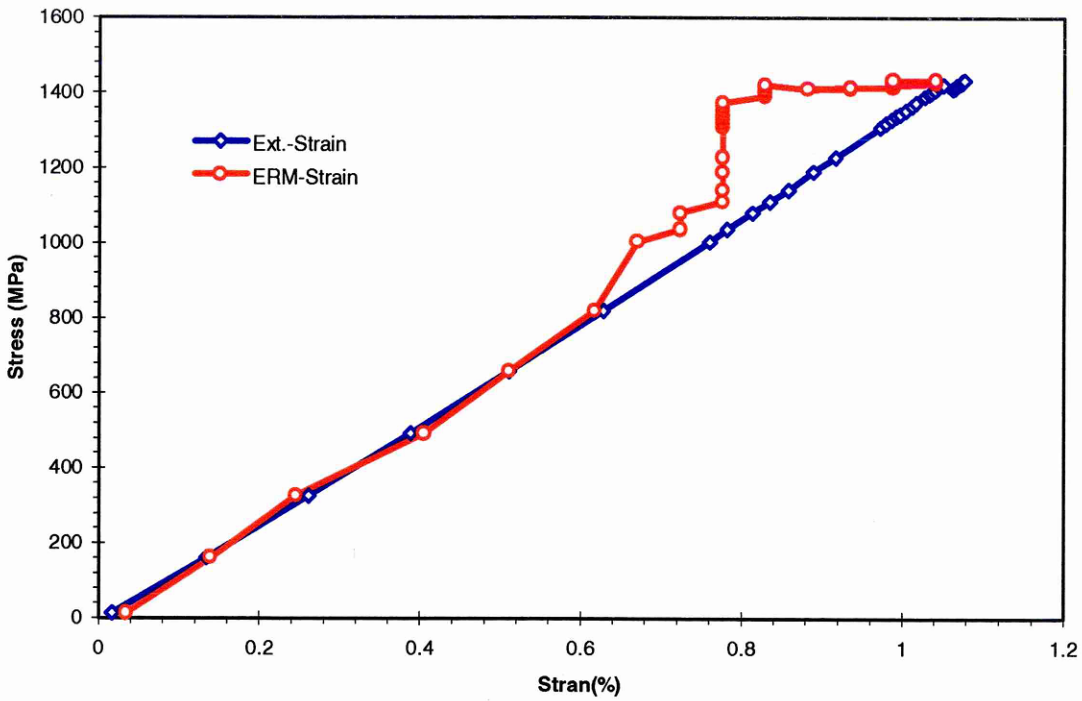

Figure 9.14. Comparison of strain measured using electrical resistance and extensometer of a typical UD920L sample.

9.3.2 UD samples-transverse loading (90°)

The comparison of electrical resistance and the strain of UD914T and UD920T samples to transverse loading are shown in Figure 9.15 and Figure 9.16, respectively. It can be seen that the increase in resistance with applied stress up to 40% of the stress level is almost linear, although the overall behaviour is non-linear. Comparison of this result with actual strain shows that the electrical resistance also possibly indicates the strain up to 40% of the stress level. After this the increase in the stress level may be due the damage. The transverse conduction is mainly due to fibre to fibre contacts. The increase in resistance represents the increase in fibre to fibre contact distance. In damage sensing, this fibre to fibre distance increase is equivalent fibre separation from the matrix. Thus, the increase in resistance with applied stress may be an indication of the initiation and growth of fibre and matrix debonding.

It may be noted that the strain was measured only in a 50 mm length at the centre of the sample. Almost all the samples failed out side of this gauge length area. The strain measured at the centre of the sample may not have influenced by the damage event that is happening away from this area. More over, the overall strain response is linear and does not show any deviation or non-linearity from the initial behaviour. Therefore, it can be suggested that the strain measured at the damage area may have good correlation with electrical resistance.

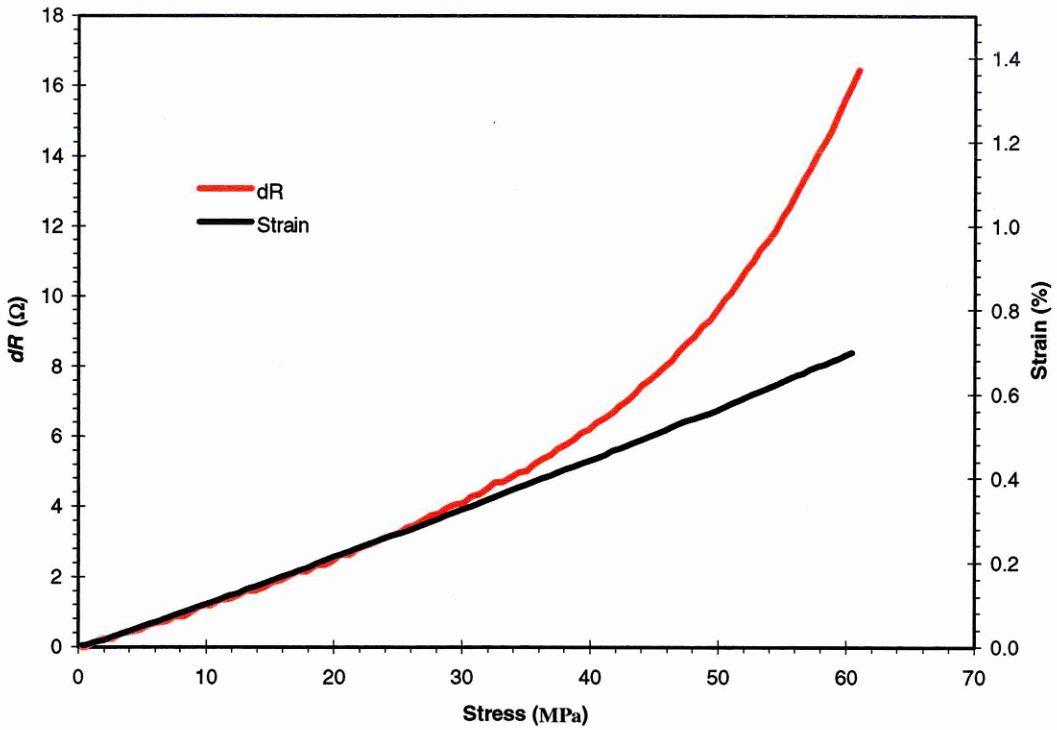

Figure 9.15. Comparison of electrical resistance and strain of a typical UD914T sample.

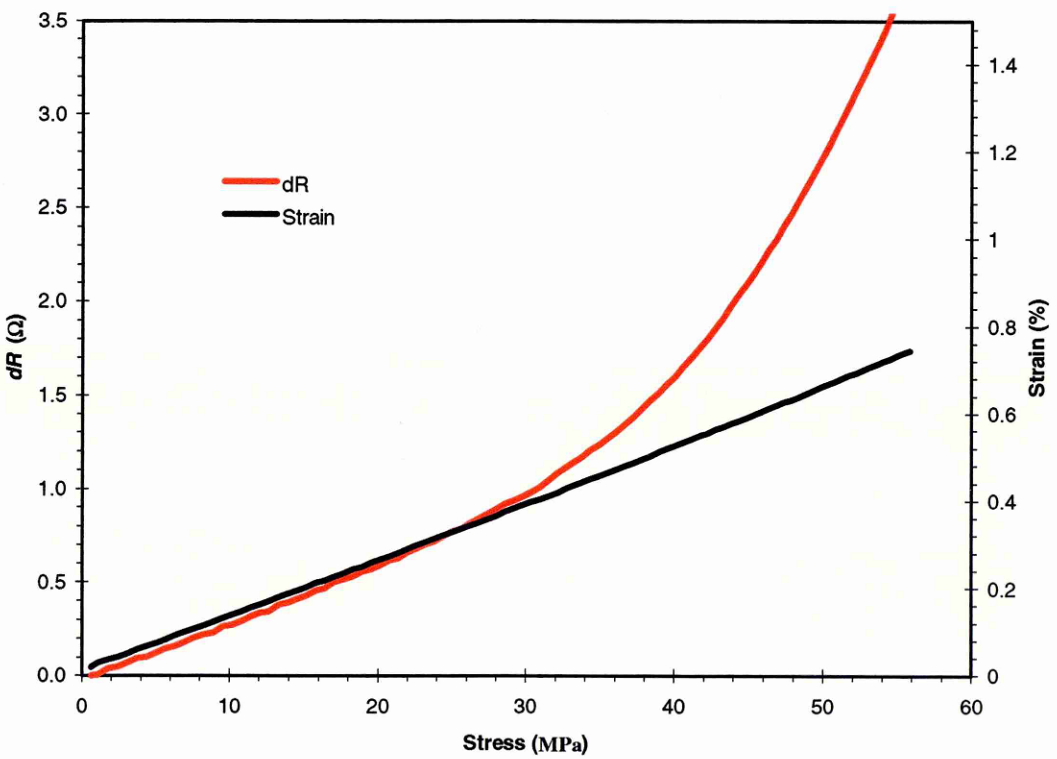

Figure 9.16. Comparison of electrical resistance and strain of a typical UD920T sample.

9.3.3 Cross-ply samples-tensile loading

The comparison of electrical resistance and strain of cross-ply samples is shown in Figure 9.17 and Figure 9.18. The results are compared for two typical samples from each category (type I and II, refer section 9.2.2). In CP914 samples also, the resistance was found to coincide with the strain up to 35% of the ultimate stress level for both types of samples.

It is clear from the figure that at this stress level (0 to 35% of UTS) the electrical resistance may be indicating the strain in the cross-ply laminates. After 70% of the UTS, the electrical resistance deviates from the strain with applied stress. However, it may be noted that the electrical resistance is almost constant or there is only a slight increase in resistance with in 40 to 70% of UTS range of type II samples. It appears that the strain component is not noticeable in this stress range. The resistance changes due to the damage may be responsible for this behaviour.

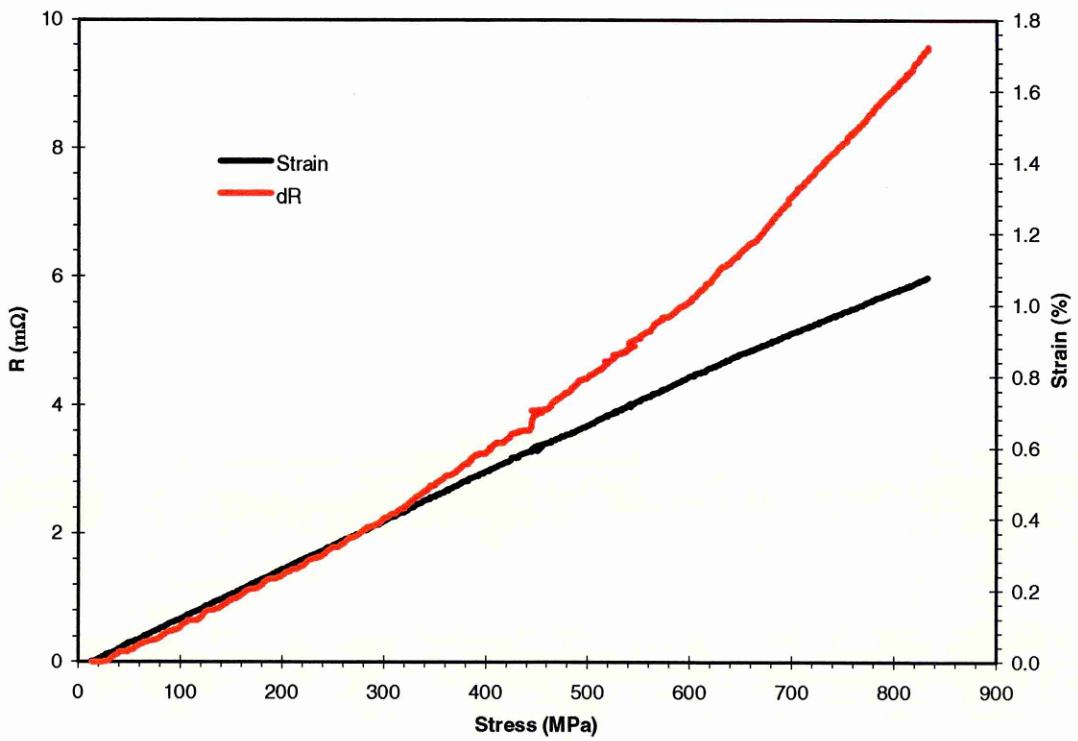

Figure 9.17. Comparison of electrical resistance with strain of a typical CP914 sample (Type I).

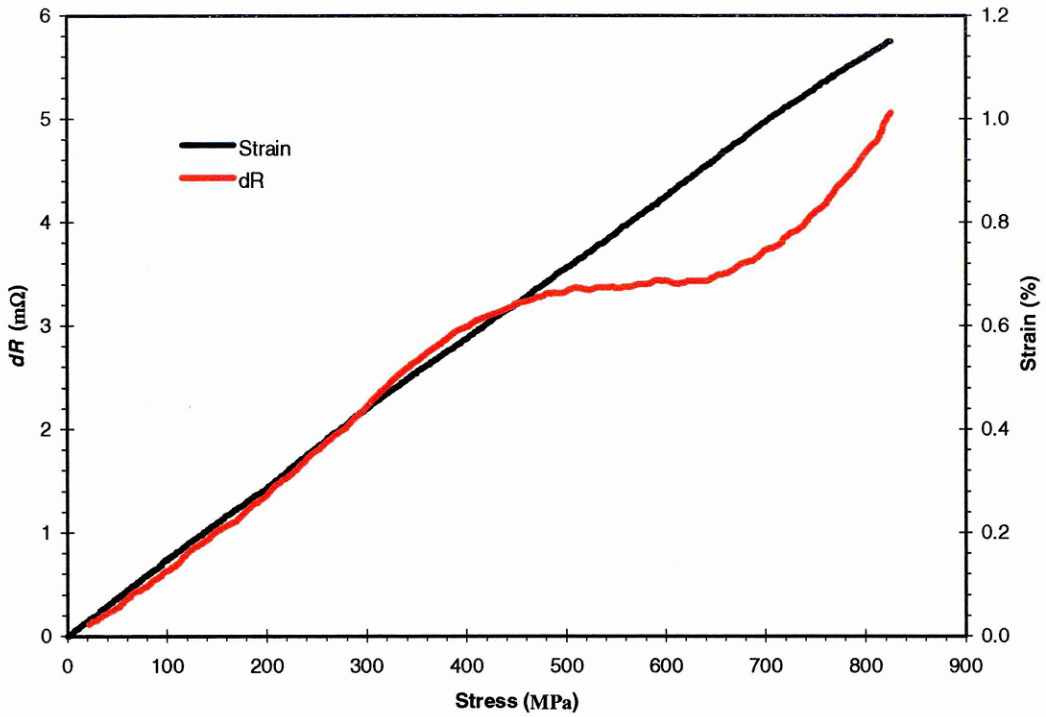

Figure 9.18. Comparison of electrical resistance and strain of a typical CP914 sample (Type II)

9.4 DAMAGE SENSING

This section examines the electrical resistivity measurement results related to the damage sensing capabilities of 0° and 90° unidirectional and cross-ply samples.

9.4.1 0° unidirectional samples

The results related to the damage sensing capabilities of unidirectional samples are shown in Figure 9.19-25. Figure 9.19 shows the normalised broken fibres Vs tensile stress of a typical UD914 and UD920 samples. As mentioned previously, the electrical resistance is mostly sensitive to fibre breaks. Therefore, two samples (B15 and UT02) that had more sites of fibre fracture (refer Figure 9.2 and Figure 9.3) were selected for this investigation. The damage component of the electrical resistance was calculated by subtracting the strain component of the resistance. The strain component was calculated using the relation derived in section 5.6. The parallel resistance model was used for quantifying the number of broken fibres from the damage component of the electrical resistance by assuming that the resistance change is only due to fibre breakage (refer section 5.1). The results are normalised as percentage of broken fibres and stress. The broken fibres were normalised with respect to the total number of fibres.

Similarly, the stress was normalised with respect to the ultimate tensile stress. It can be seen that the number of broken fibres increases drastically after 80% of the UTS. It can be seen in the figure that only 0.25 % of broken fibres is needed for the final catastrophic failure of unidirectional samples.

The results presented in Figure 9.19 are supported by the investigations by Jamison (1985). He observed similar behaviour, i.e., fibre fracture density with applied stress for unidirectional CFRP samples (refer section 2.3.1). It may be noted that the parallel resistance model does not account for the three-dimensional conduction process and multiple sites of fibre fracture (refer section 8.3.1). Therefore, the results presented in this figure should be taken as a demonstration of the quantitative damage sensing capabilities of the electrical resistance measurement technique.

Figure 9.20 shows the correlation between the longitudinal split and the electrical response of UD920 samples. The longitudinal splits of these samples were measured by adding up the length of the longitudinal splits (refer Figure 9.3). These results were then normalised by dividing the total longitudinal split length by sample gauge length. The figure clearly shows the correlation between the longitudinal split and the reduction in electrical resistance. It can be seen that the longitudinal split is higher for samples that have higher reduction in electrical resistance. It can also be seen that the longitudinal split is almost the same for samples that have positive increase in resistance at all stress levels. As outlined earlier, the reduction in electrical resistance of some of the samples due to the influence of longitudinal splits may be due to the complex three-dimensional electrical conduction mechanisms of unidirectional CFRP.

Figure 9.21 shows the comparison of electrical and acoustic emission response of a typical unidirectional longitudinal sample subjected to tensile loading. It is clear from the figure that the acoustic emission count increases drastically close to the failure stress. It appears that the AE response is not very sensitive to damage initiation. However, the increase in resistance was found to coincide with the rise in acoustic emission counts. It can be seen that the AE responds often after the electrical response to a damage event. It is found that the electrical resistance correlates better with the applied stress than the acoustic emission. The correlation coefficient between stress and electrical resistance is 0.94 and with acoustic emission count is 0.54. Acoustic emission monitors the stress wave generated by the damage process. This is often monitored using a transducer located at one end of the sample. Therefore, acoustic emission may not monitor all the damage because of the constraint in sensitivity to the damage process and propagation of sound waves in composite materials. It is evident from the results that the electrical resistance is more sensitive to applied stress and damage.

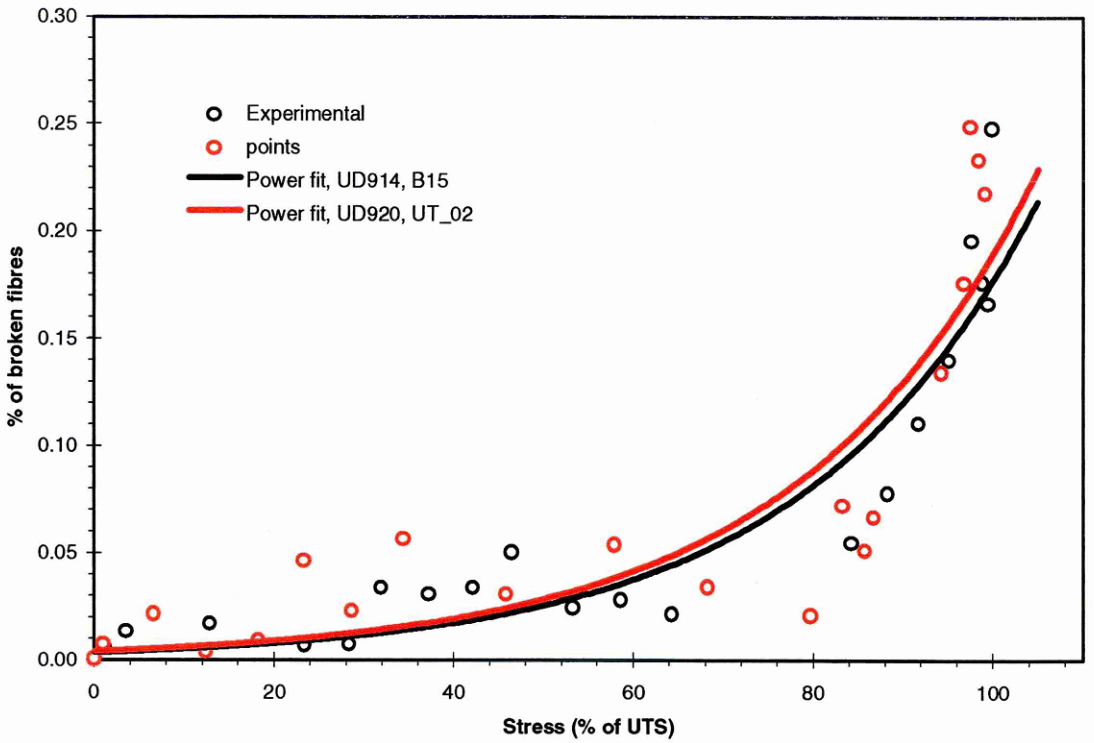

Figure 9.19. Fibre fracture Vs tensile stress of a typical UD914L and UD920L samples.

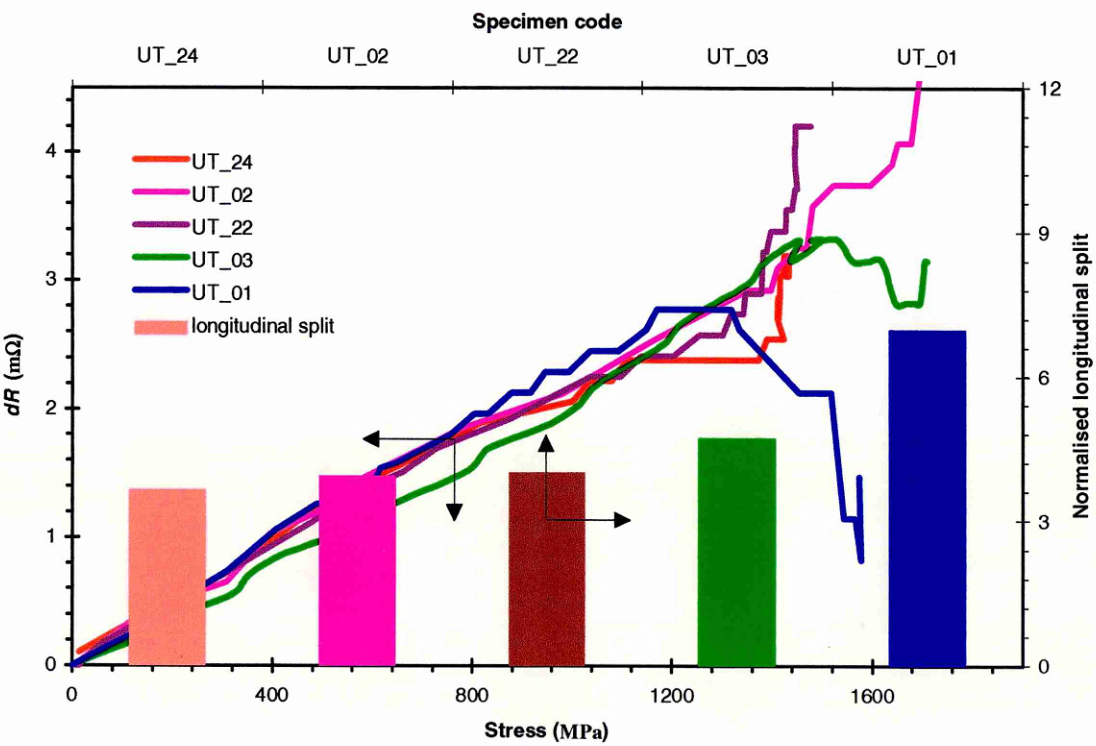

Figure 9.20. The correlation between longitudinal split and electrical resistance.

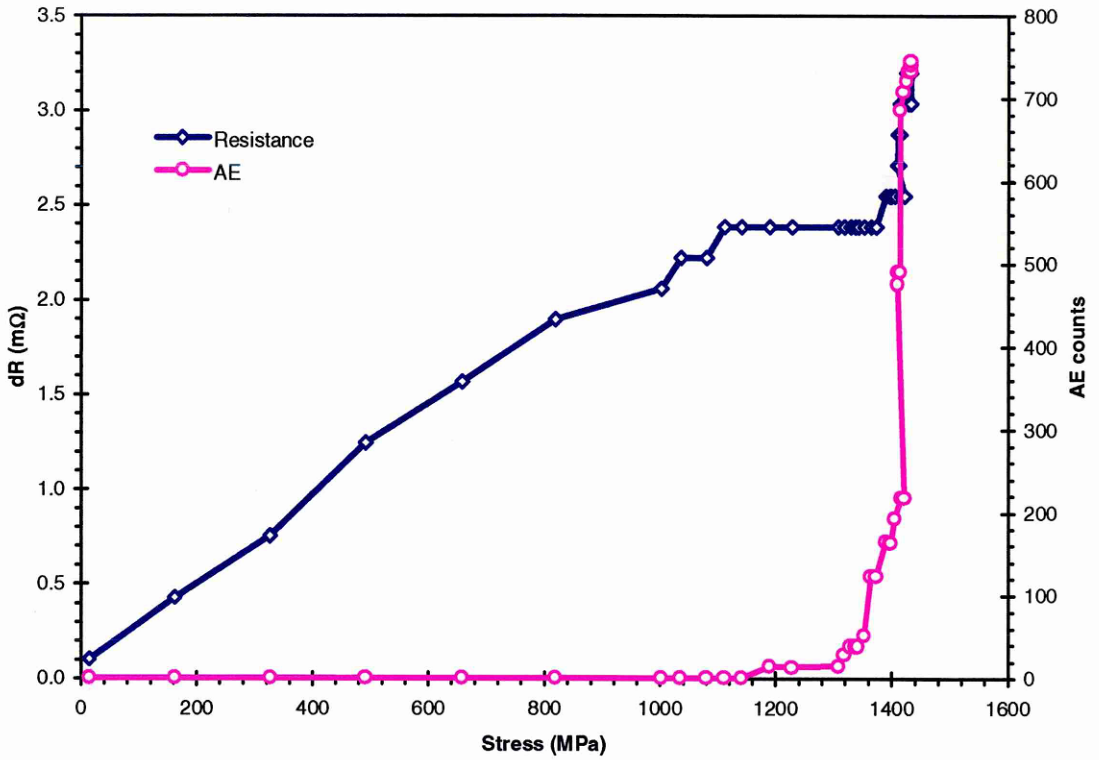

Figure 9.21. Comparison of electrical and acoustic emission response of a typical UD920 sample to tensile stress.

9.4.2 90° unidirectional samples

Figure 9.22 and Figure 9.23 shows the correlation between the tensile strength and the electrical resistance of UD914T and UD920T samples, respectively. The resistance shown in these figures represent the total change in resistance of the samples at the time of failure. It can be seen that the electrical resistance change is higher for samples with higher tensile strength. The change in electrical resistance increases with increasing tensile strength. This is true for both UD914 and UD920 samples. Almost all the samples follow this behaviour except one of the UD914 sample (UD914T9). The correlation coefficient of UD914 samples is 0.85, excluding UD914T9 is 0.99. Similarly, the correlation coefficient of UD920 samples is 0.96. It can be inferred from the strong correlation between tensile strength and electrical resistance that the electrical resistance indicates the extent of damage experienced by these samples prior to failure.

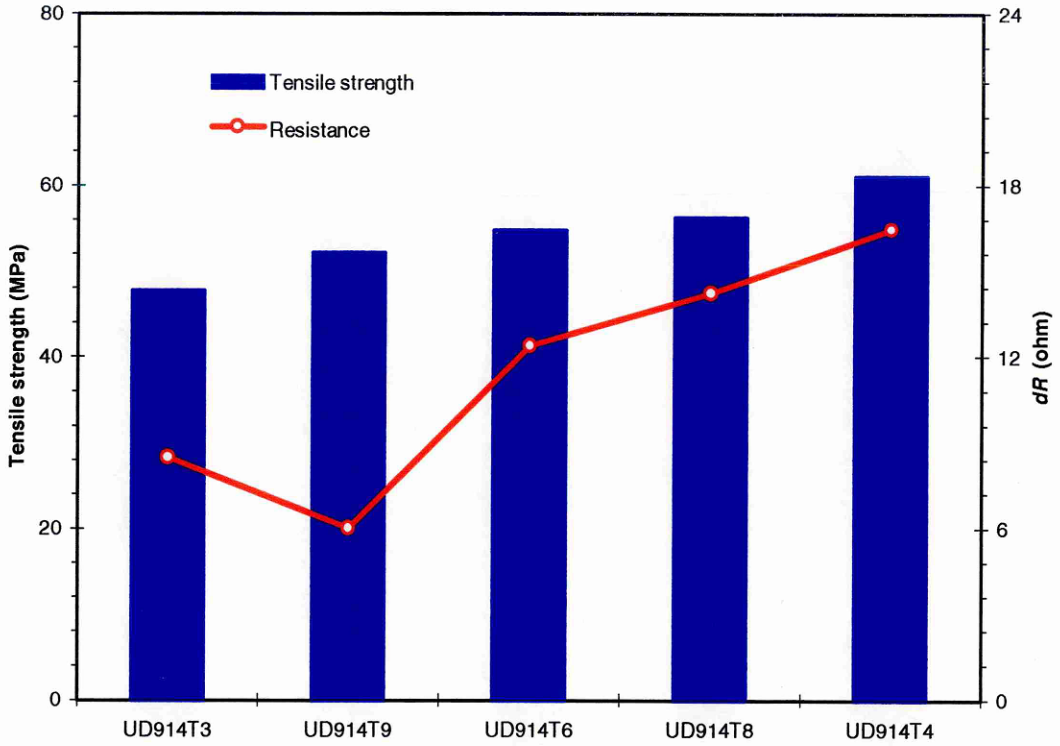

Figure 9.22. The correlation between tensile strength and electrical resistance of UD914T samples.

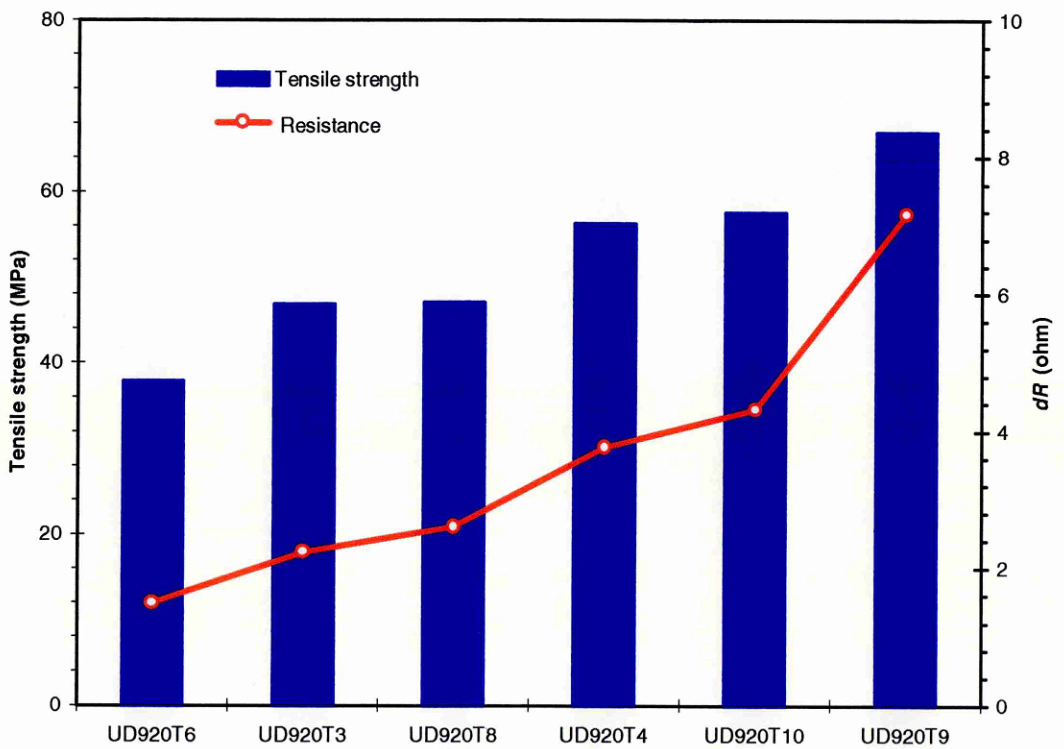

Figure 9.23. The correlation between tensile strength and electrical resistance of UD920T samples.

9.4.3 Cross-ply samples

The results related to the cross-ply samples subjected to various levels of tensile stress is shown in Figure 9.24 to 9.26. Figure 9.24 shows the hysteresis of electrical response. This figure shows one sample per stress level for better clarity of presentation. The strain hysteresis of a typical sample (C31) is also shown in this figure for comparison. The C-scan (Figure 9.25) and X-ray (Figure 9.26) results include two samples per stress level and a virgin sample. It can be seen that the electrical resistance does not return to the initial value after unloading. There is a permanent resistance change, and this resistance increases with increasing level of applied stress level. The permanent resistance change may be indicating the level of permanent damage to the samples. This is supported by the C-scan and X-ray results. The C-scan clearly shows that the damage level increases with the increase in stress level of the samples as indicated by the electrical resistance.

Hysteresis similar to the electrical response is exhibited by the strain response also. However, the magnitude of strain change is relatively lower than the resistance. It can also be seen that the samples subjected to 25% of UTS shows no sign of permanent resistance change. This indicates that stress levels below 25% of the UTS do not damage the sample permanently.

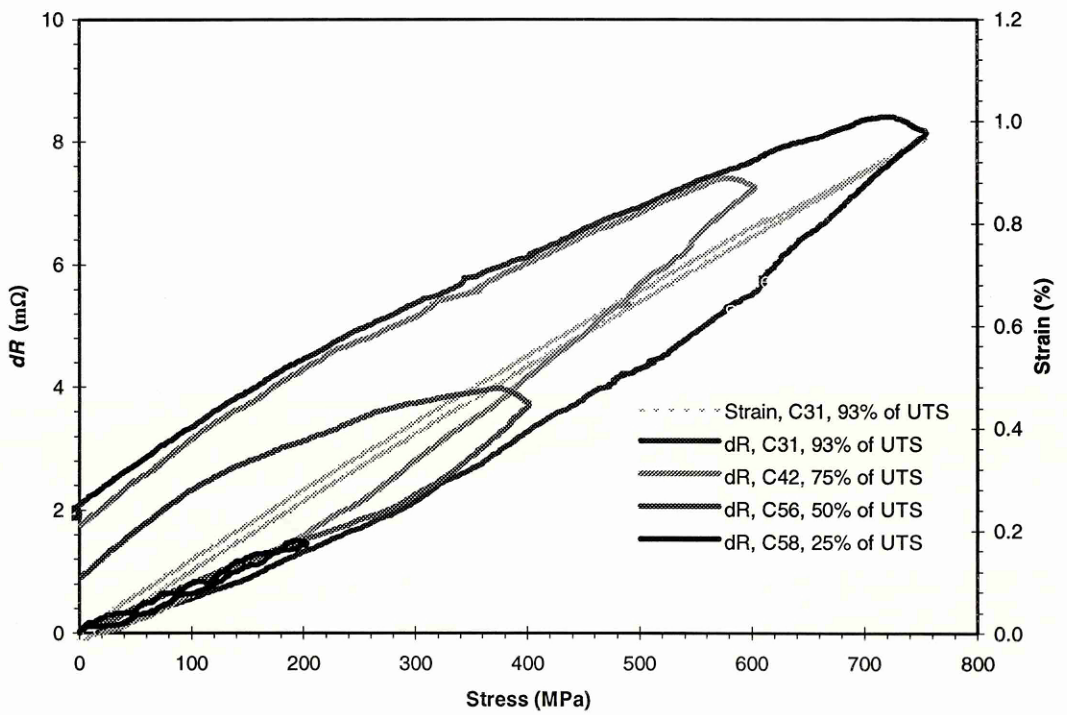

Figure 9.24. Electrical hysteresis of cross-ply samples subjected to various levels of tensile stress.

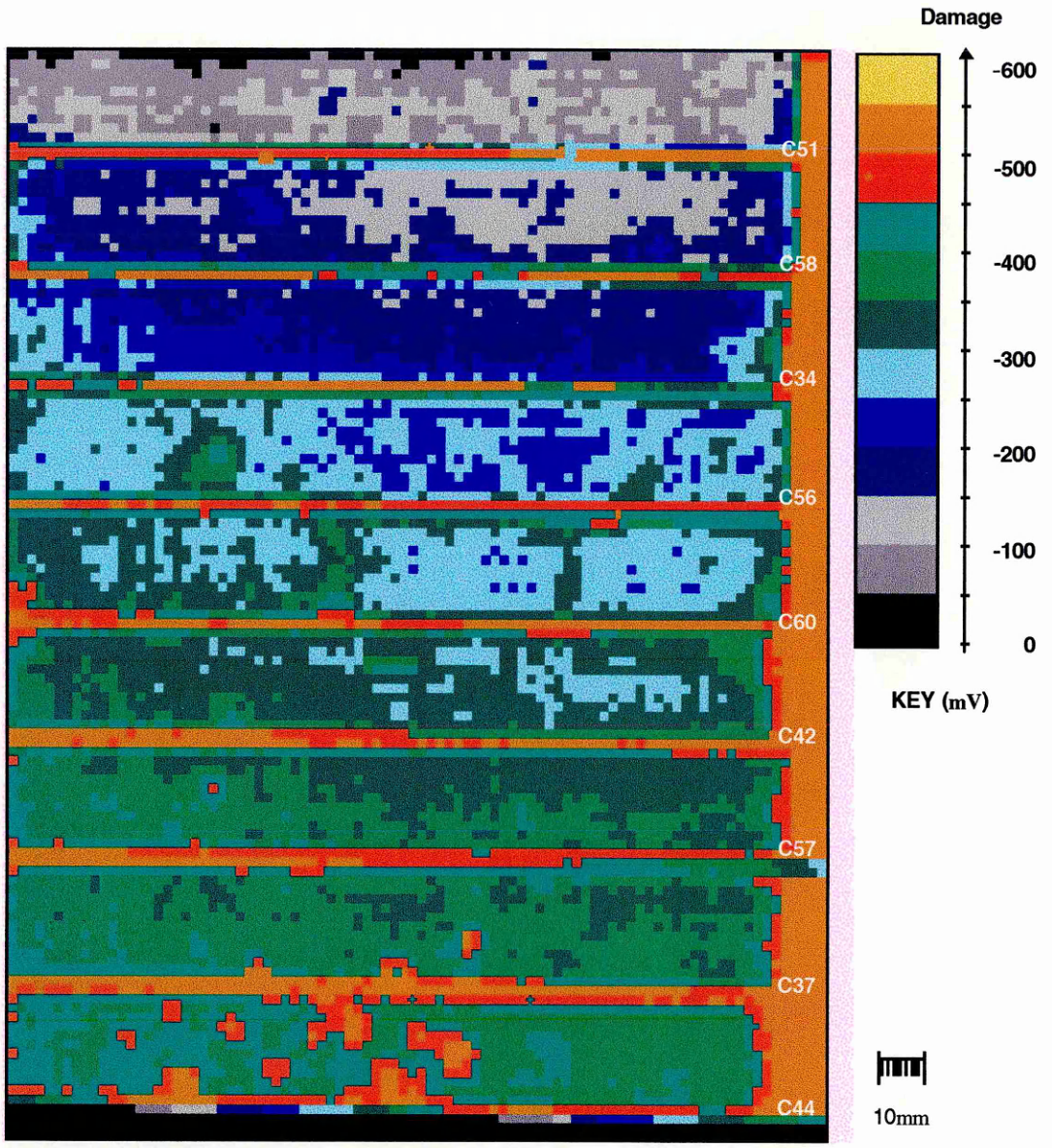

Sample code:

C51-Virgin	**C58** - 25% of UTS	**C56** -50% of UTS	**C42** - 75% of UTS	**C37** - 93% of UTS
	C34 - 25% of UTS	**C60** -50% of UTS	**C57** - 75% of UTS	**C44** - 93% of UTS

Freq. = 5 MHz **Gain = 50 dB** **Cross-ply** **Double Transmission**

Figure 9.25. C-scan results of cross-ply samples subjected to various levels of tensile stress illustrating the increase in damage level with applied stress.

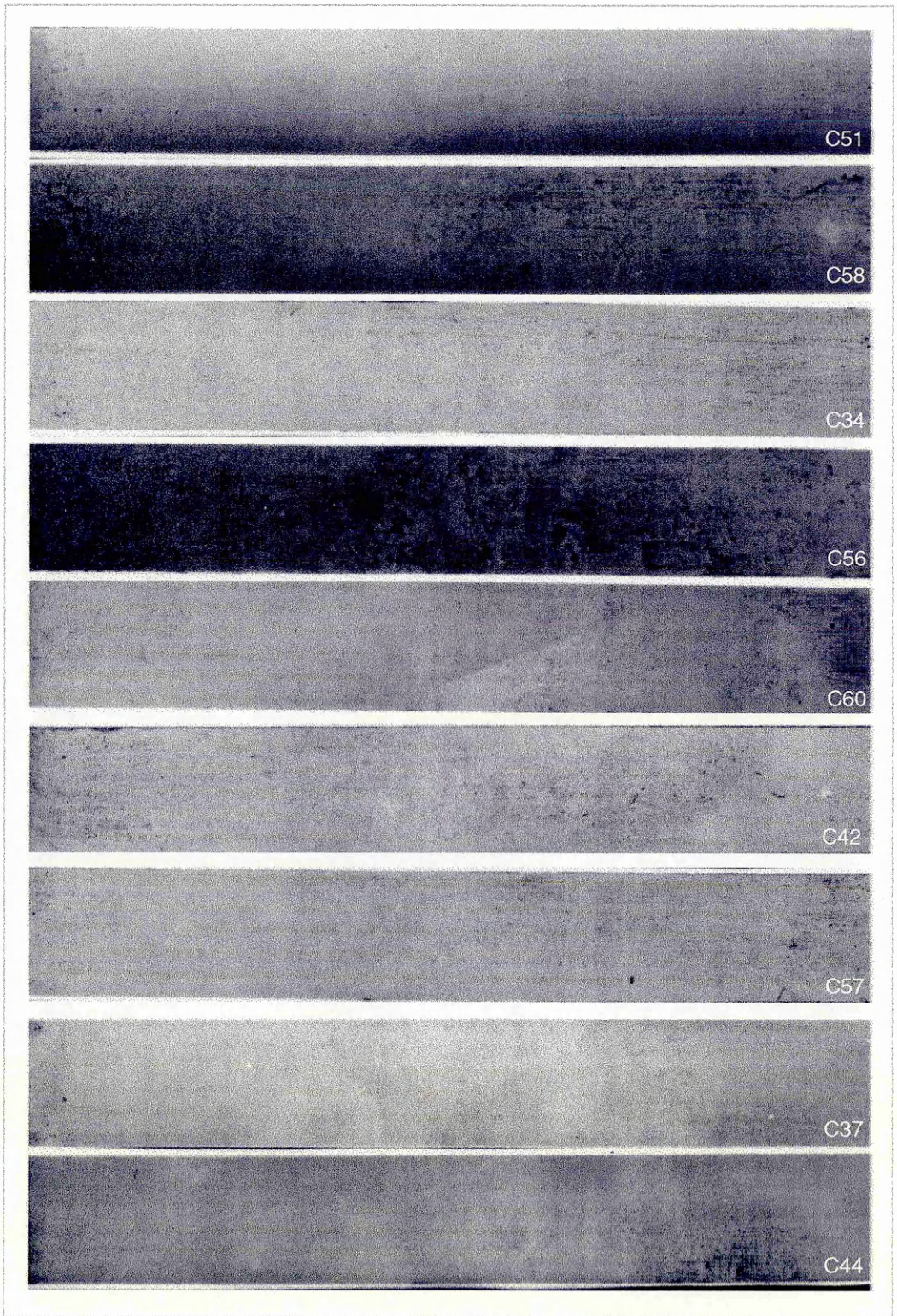

Figure 9.26. X-ray results of cross-ply samples subjected to various levels of tensile stress illustrating the increase in damage level with applied stress.
(For sample code refer Figure 9.25)

10

FATIGUE DAMAGE MECHANISMS

This chapter presents the results related to fatigue damage mechanisms of CFRP laminates. The electrical resistance measurement results related to fatigue damage are presented in three major sections demonstrating the overall behaviour, dependence of stress and dependence of life.

This chapter is organised as follows. The fatigue behaviour of UD914 and UD920 unidirectional and cross-ply samples are presented in section 10.1. The stress and strain based fatigue behaviour, comparison and the failure modes are also presented in this section. The electrical resistance measurement results related to fatigue damage is presented are section 10.2. Section 10.2.1 describes the over all electrical response of unidirectional samples subjected to fatigue loading. Section 10.2.2 presents results related to the dependence of electrical resistance on applied stress. This section also presents the comparison of electrical resistance measurements with C-scan and X-ray radiography results. The dependence of electrical resistance on fatigue life is examined in section 10.2.3. Section 10.2.4 compares the electrical resistance with elastic modulus. The correlation between longitudinal split growth rate and resistance is presented in section 10.2.5.

10.1 FATIGUE BEHAVIOUR

The fatigue behaviour of UD914 and UD920 samples is presented as S-N diagrams based on applied peak stress and peak strain verses number of cycles to failure in Figure 10.1 and Figure 10.2, respectively. The fatigue behaviour of CP914 samples is shown in Figure 10.3. It may be recalled that fatigue testing was carried out in load control (stress control).

The stress based S-N diagram is a conventional method of presenting fatigue results. The strain based S-N diagrams are suggested to be more informative (Talreja 1987) and have been used by many investigators (Curtis 1991a, Harris et al. 1990). This method allows easier comparison between materials and is suggested that it is easier to relate damage to the applied strain. The initial peak strain was determined by dividing the applied peak stress by the static tensile modulus. The strain based comparison of UD914 and UD920 is shown in Figure 10.4.

In this section the fatigue behaviour of UD914 is examined first followed by UD920. Then the comparison between the laminates is presented. This section also includes the fatigue behaviour of CP914 samples. The fatigue testing of CP914 samples was mainly aimed at demonstrating the damage sensing capabilities of ERM and hence the fatigue results are not supported by a large population of samples. So, the CP914 results are excluded from further discussion in this thesis. Moreover, the fatigue failure mechanisms of cross-ply samples are studied extensively and are relatively well understood. This section will concentrate mainly on unidirectional laminates.

The fatigue behaviour of UD914 samples agrees well with previously published results of similar brittle resin systems (Curtis 1991b, Konur and Mathews 1989). The behaviour of UD920 samples in principle agrees with the previously published results of epoxy based tough resin composites (Curtis 1991b, Cano and Dow 1992, Razvan and Reifsnider 1989). That is, superior low cycle and inferior high cycle fatigue behaviour. However, the overall fatigue performance of UD920 samples is relatively poor.

The S-N behaviour of UD samples can be mapped into two regions. The first region is a horizontal scatter band covering the stress level close to the UTS (i.e., above 80% of UTS). The second region is a sloping band below the horizontal band covering the stress level below 80% of UTS. The scatter in the horizontal band is higher, however, it appears that the scatter in the sloping band is less. This is similar for both UD914 and UD920 though the width and height of the bands are different.

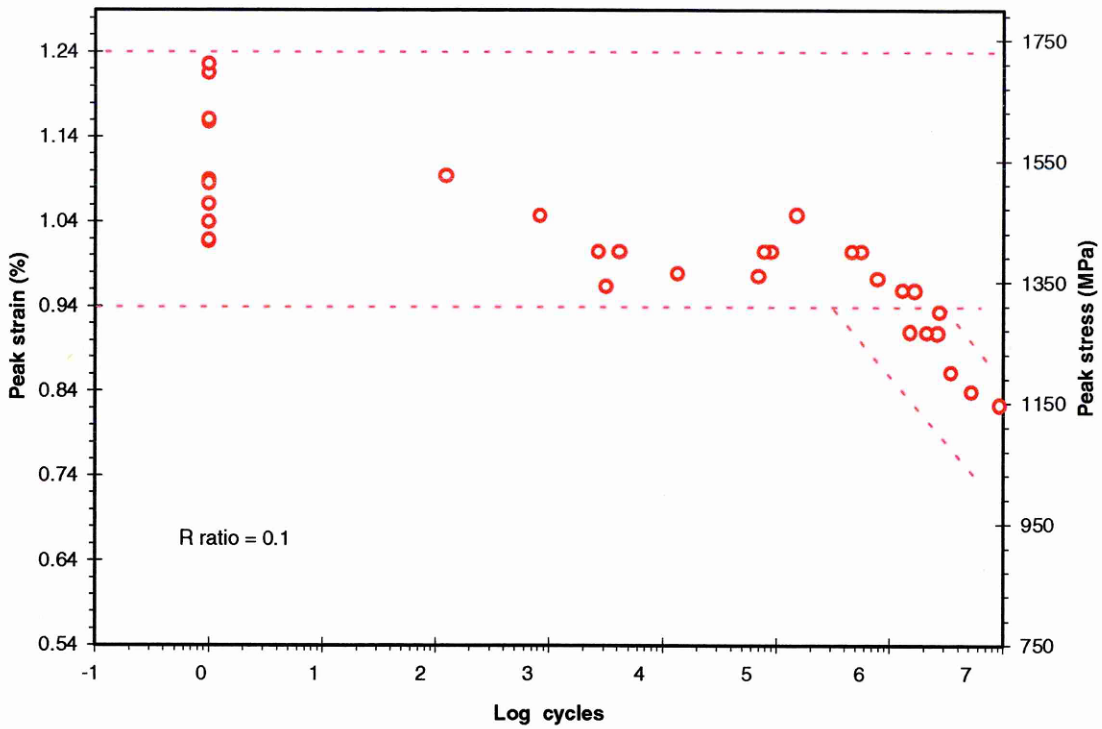

Figure 10.1. S-N diagram illustrating the fatigue behaviour of UD914 samples.

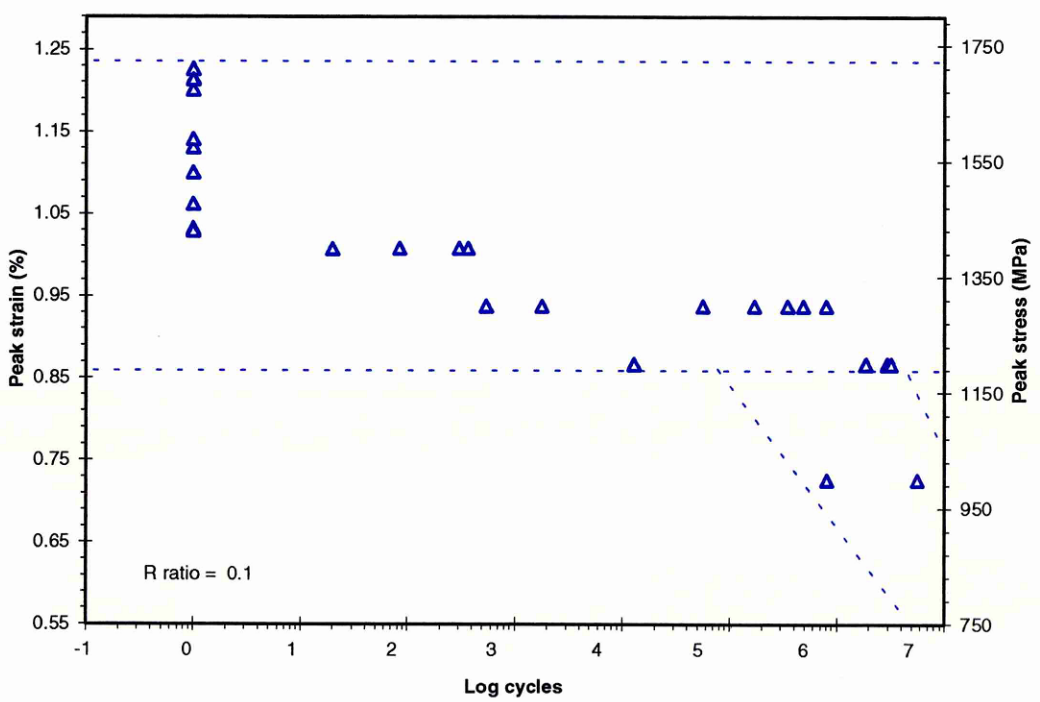

Figure 10.2. S-N diagram illustrating the fatigue behaviour of UD920 samples.

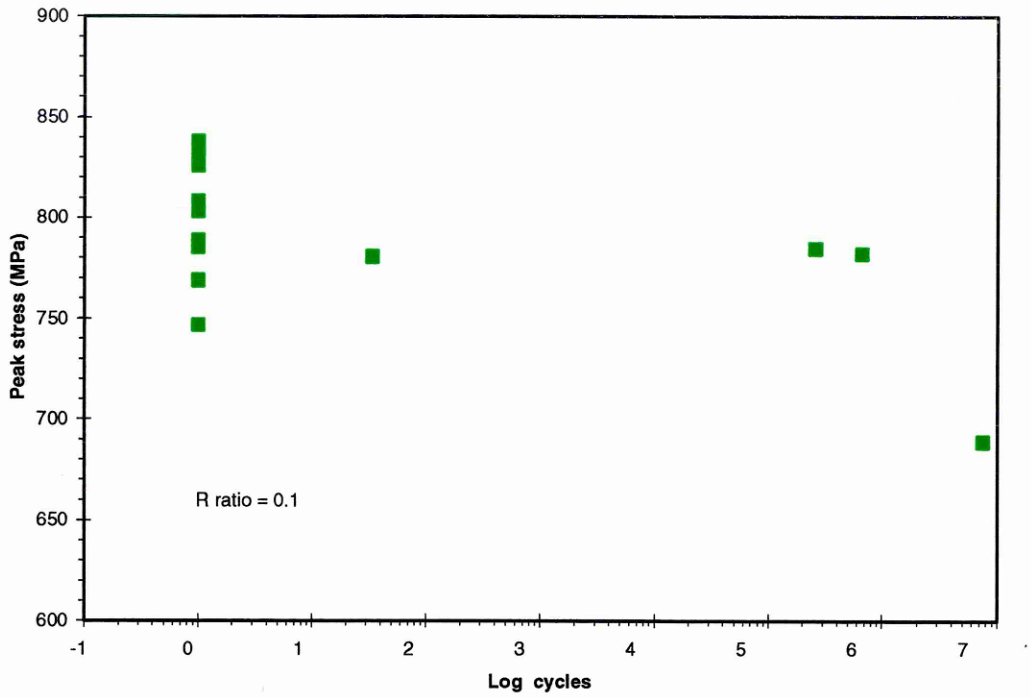

Figure 10.3. S-N diagram illustrating the fatigue behaviour of CP914 samples.

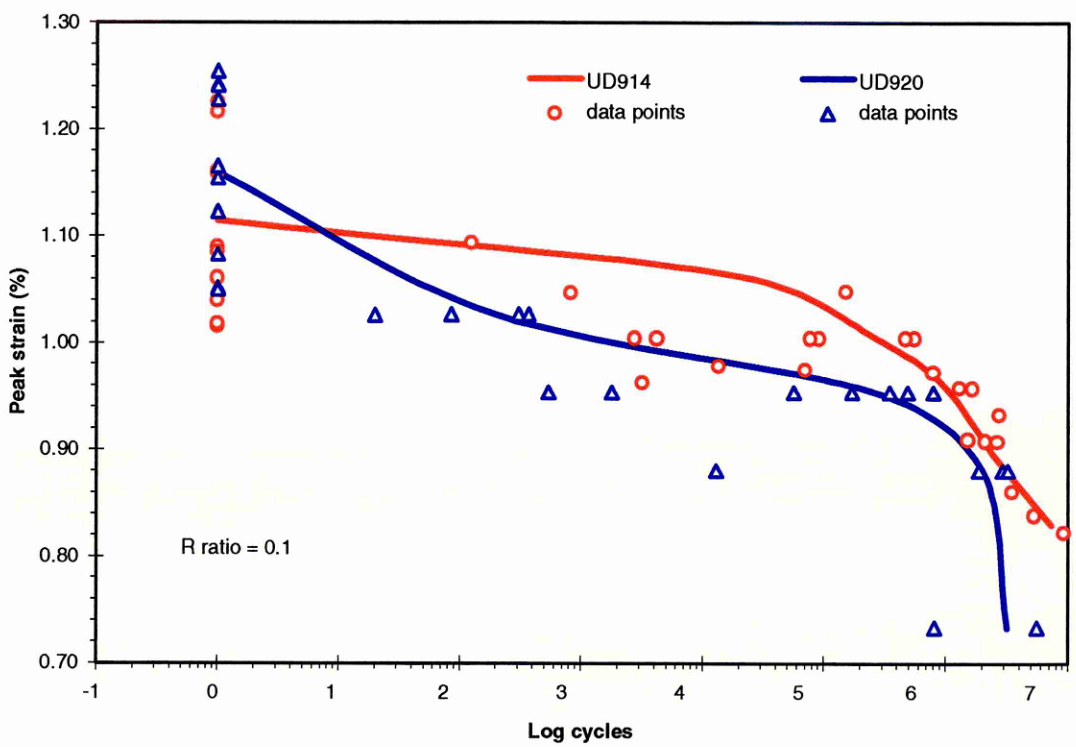

Figure 10.4. Strain based comparison of the fatigue behaviour of UD914 and UD920 samples.

If we compare Figure 10.1 and Figure 10.2, at stress levels close to the UTS (above 80% of UTS), both UD914 and UD920 exhibit similar behaviour in the horizontal scatter band. However, the horizontal scatter band is shifted to lower stress level for UD920 samples relative to UD914 samples. This band is dominated by fibre fracture failure modes (Talreja 1981) and hence the stress experienced by the fibres may influence the fatigue behaviour of samples in this region.

10.1.1 Failure modes

The fatigue failure modes of UD914 and UD920 samples are shown in Figure 10.5-10. These figures include a minimum of two samples to a maximum of nine samples per stress level. These samples are sorted in ascending order according to the number of cycles to failure at each stress level. The failure modes observed are in accordance with previously published results (Owen 1974, Awerbuch and Hahn 1977, Curtis 1991a, Curtis 1991b, Razvan and Reifsnider 1989, Razvan et.al 1992).

It is evident from these figures that the major damage modes are fibre fracture and longitudinal splitting. As with static failure, the fibre pullout of fatigue samples has also concentrated mainly at the end of the tag line or grip jaws. Fibre fracture sites away from the tag region were also been observed for some of the samples. The failure pattern of UD914 samples is much more brush-like with more longitudinal splitting. This type of failure pattern is mainly due to more fibre breakage (Awerbuch and Hahn 1977). The failure pattern of UD920 samples shows relatively less longitudinal splitting. This indicates, less fibre breakage and more matrix shear failure (Curtis 1991, Wang et.al. 1991).

It can be seen that the failure pattern changes from brittle brush type to brittle matrix shear failure with decrease in stress level. That is, the number of longitudinal splits decreases with decrease in stress level. Similarly, at each stress level the failure pattern changes with life. At higher stress levels (92% UTS of UD914 and 88% UTS of UD920 samples) the failure pattern is similar to the static failure pattern (refer section 9.1.3).

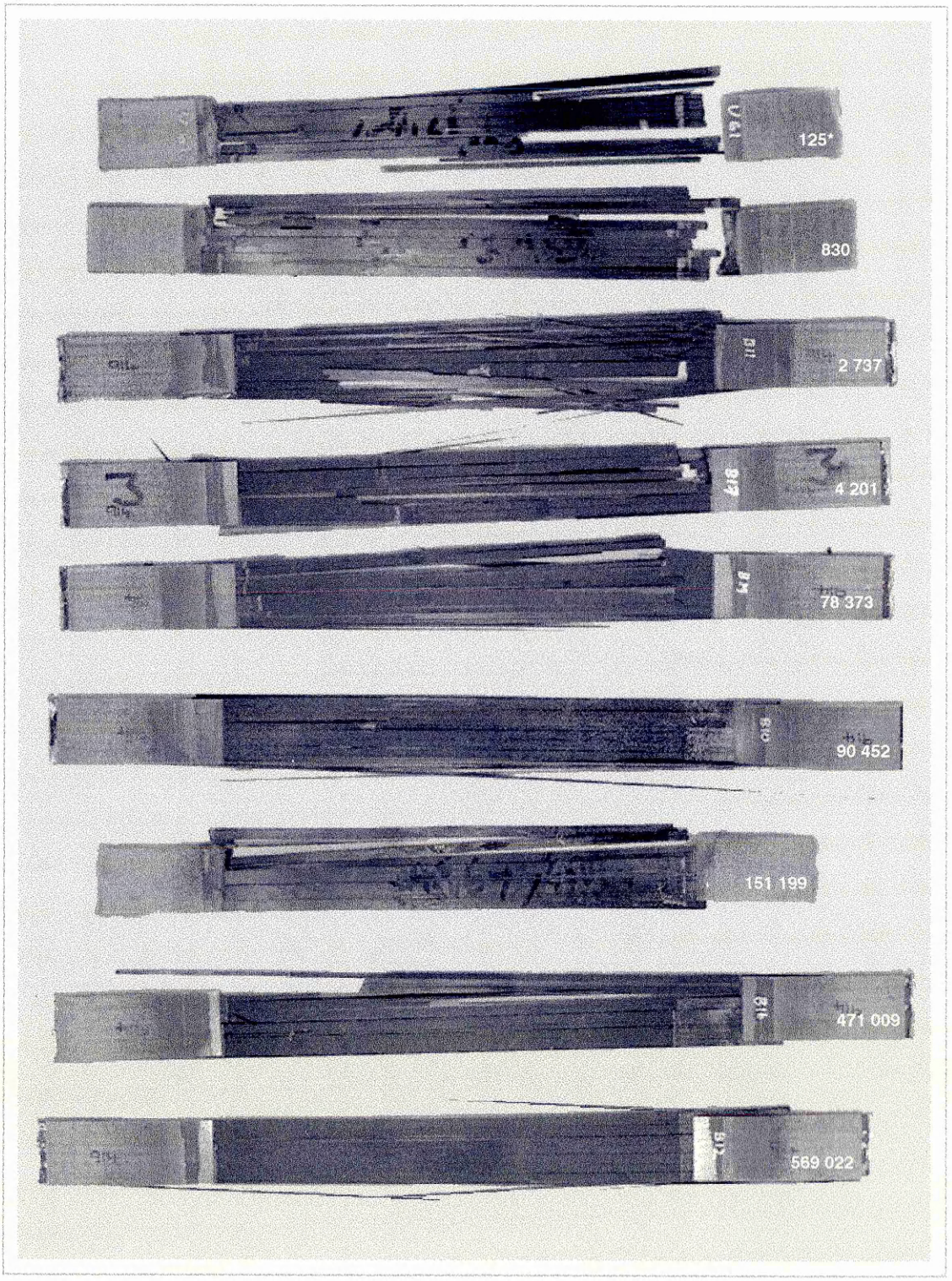

Figure 10.5. Fatigue failure modes of UD914 samples (92% of UTS).
*** Number of cycles to failure**

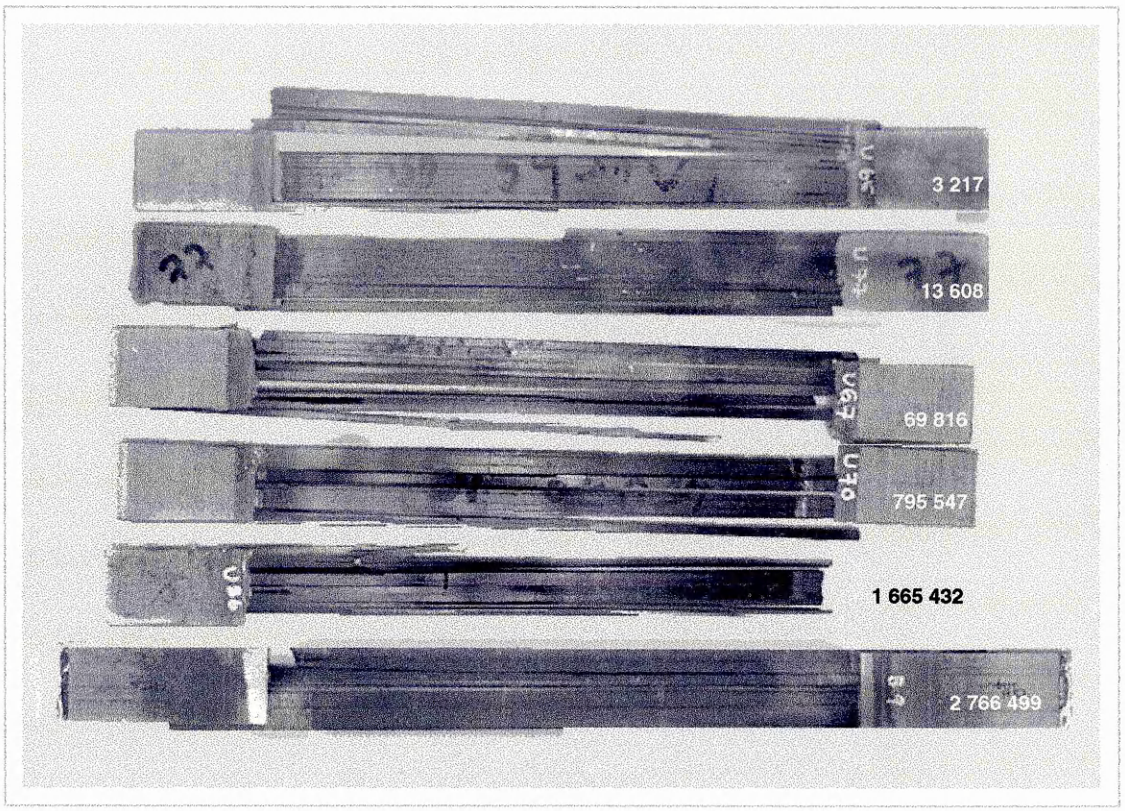

Figure 10.6. Fatigue failure modes of UD914 samples (88% of UTS).

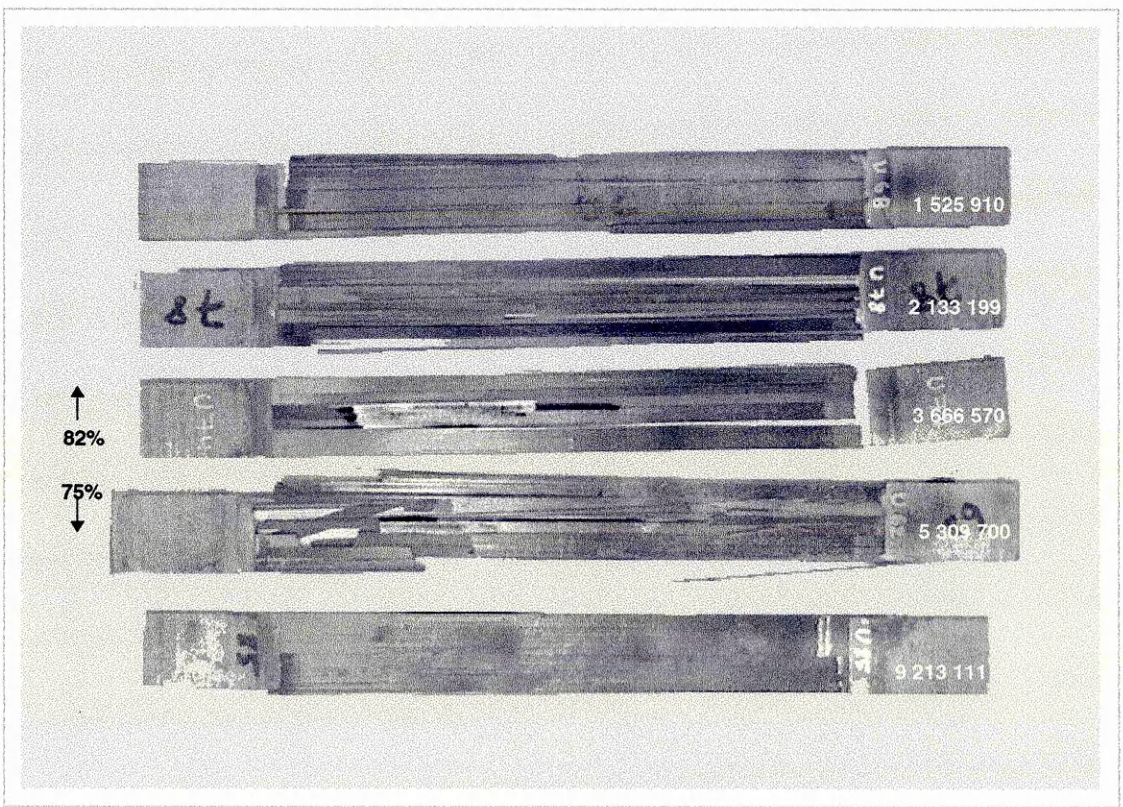

Figure 10.7. Fatigue failure mode of UD914 samples (82 and 75% of UTS).

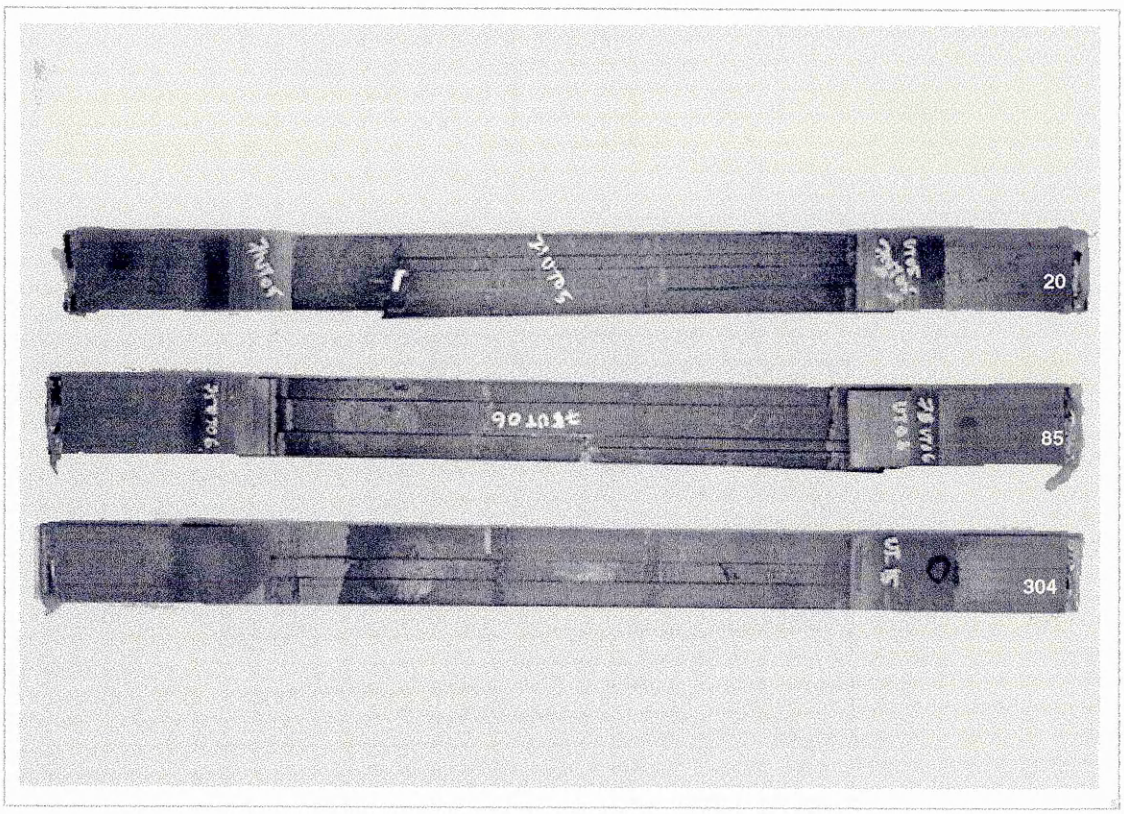

Figure 10.8. Fatigue failure mode of UD920 samples (88% of UTS).

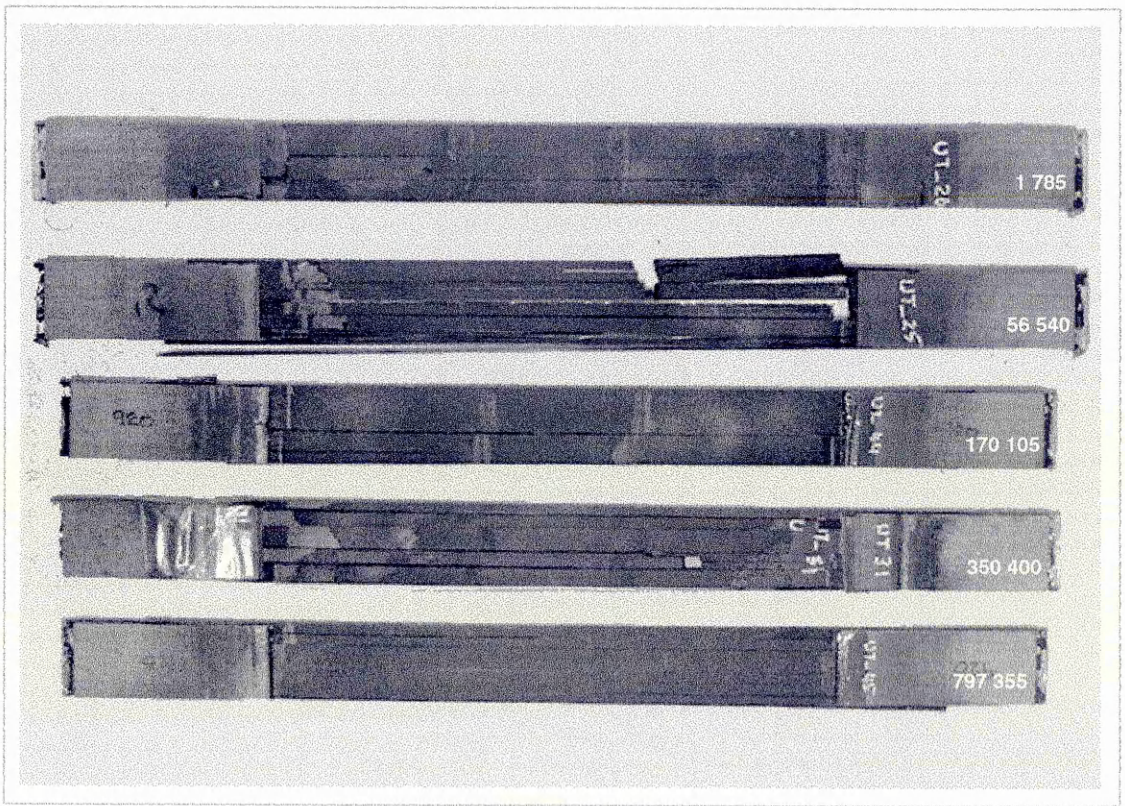

Figure 10.9. Fatigue failure mode of UD920 samples (82% of UTS).

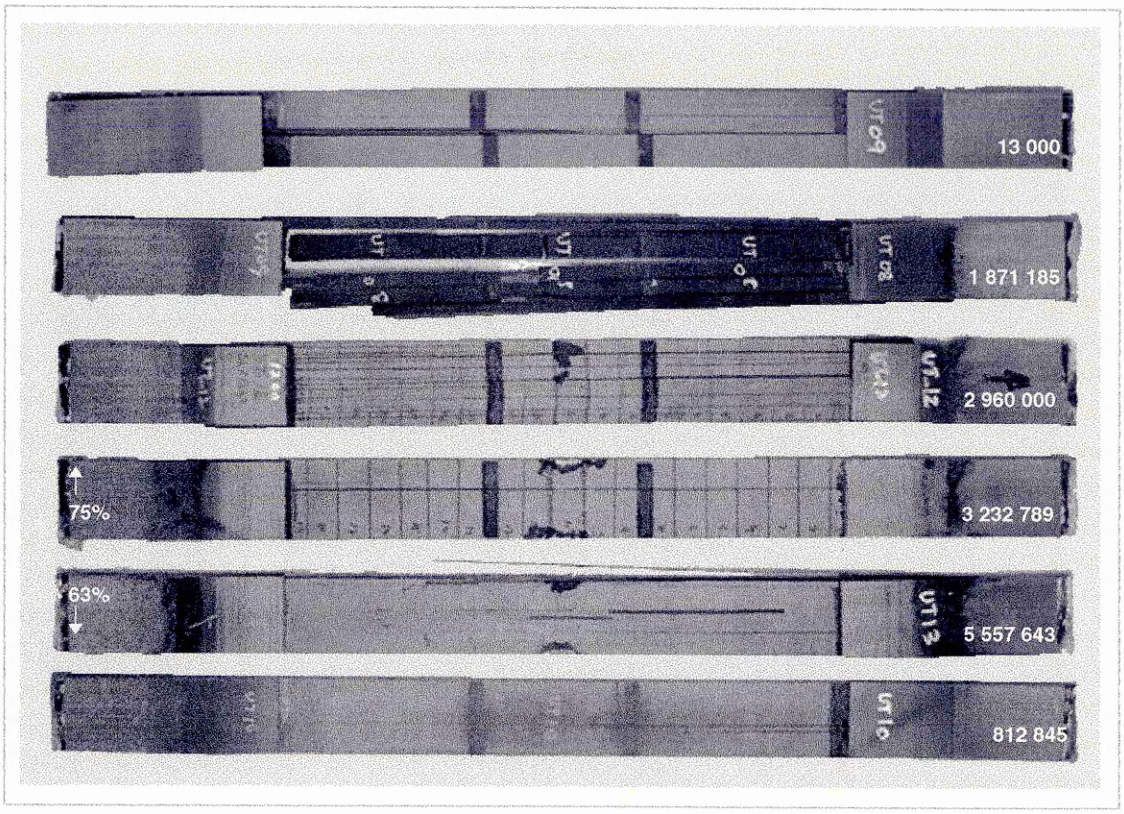

Figure 10.10. Fatigue failure mode of UD920 samples (75 and 63% of UTS).

10.2 ERM AND FATIGUE DAMAGE

The electrical resistivity measurements related to fatigue damage are shown in Figure 10.11-20. These figures include the results of both UD914 and UD920 samples subjected to fatigue testing at various stress levels. In order to highlight the multifunctional damage sensing capabilities of electrical resistivity measurement technique the results are divided into three major sections, examining

the overall behaviour,
dependence of stress and
fatigue life dependence.

Figure 10.11 and Figure 10.12 shows the results of all the samples including the runouts. These figures demonstrate the electrical response of UD914 and UD920 samples to fatigue damage. It can be seen that the electrical resistance increases with number of cycles to failure. The rate of change of resistance and the resistance change to failure are different for each sample. It can be seen that the electrical response of most of the samples correlates with applied stress and life. This will be examined in detail in the subsequent sections.

The electrode configuration of samples used in fatigue testing are mainly sensitive to fibre fracture. The experimental and computational simulation investigations of fibre fracture in chapter 8 indicate that the resistance will increase with number of fibre breaks. This is backed by the results of Schulte and Baron (1989). The tensile test results presented in chapter 9 also support the above. Therefore, the increase in resistance of fatigue samples may be mainly due fibre fractures. In unidirectional laminates fibre fracture is the major damage mechanism. The increase in electrical resistance of samples subjected to fatigue loading indicates the damage. Therefore, in the following discussions, the electrical resistance will be interpreted as damage.

The other major factor in fatigue testing that can influence the resistance is temperature. In fatigue testing of UD samples, the temperature was found to increase only up to a maximum of 4 ℃ from room temperature (22 ℃). A typical temperature profile of a fatigue sample with long life to failure is shown in Figure 10.13. The increase in resistance within this temperature range due to temperature, according to the temperature dependent resistivity investigation is 0.08 mΩ. This is approximately less than 1 % of the total resistance change observed in fatigue testing. Therefore, no correction was made for the results presented in this section for temperature from the temperature dependent investigations. However, necessary corrections were made for thermal emf as described in chapter 4. (For temperature dependent resistivity investigation, refer section 7.1.6.6).

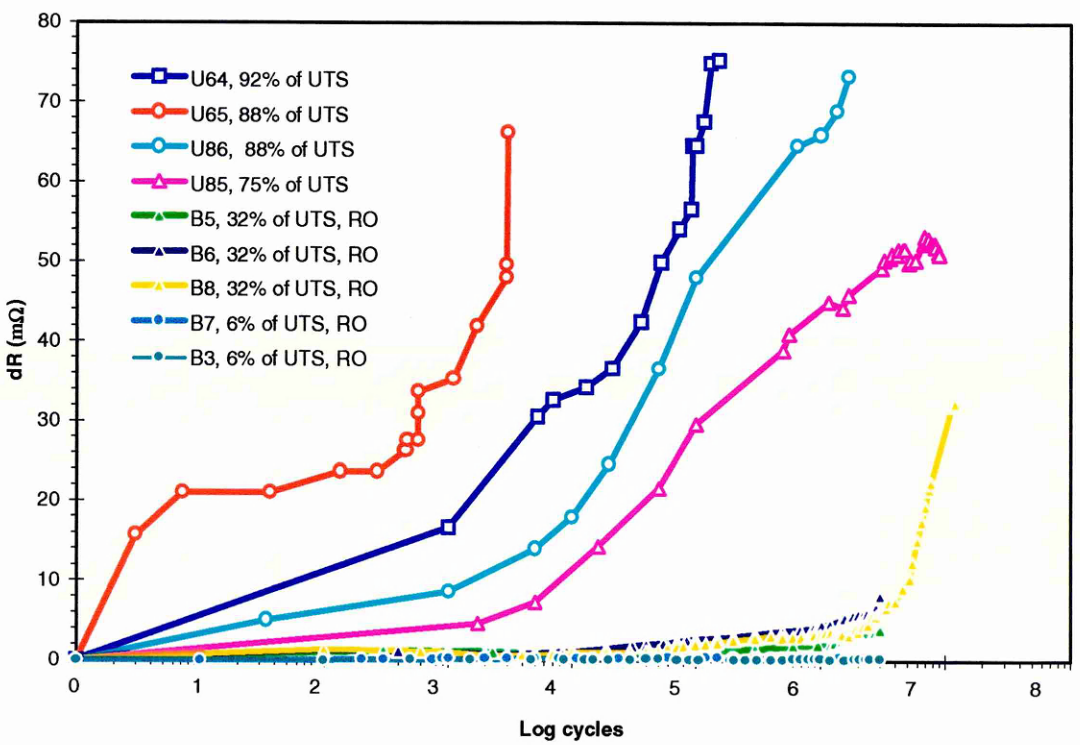

Figure 10.11. Electrical response of UD914 samples to fatigue loading.

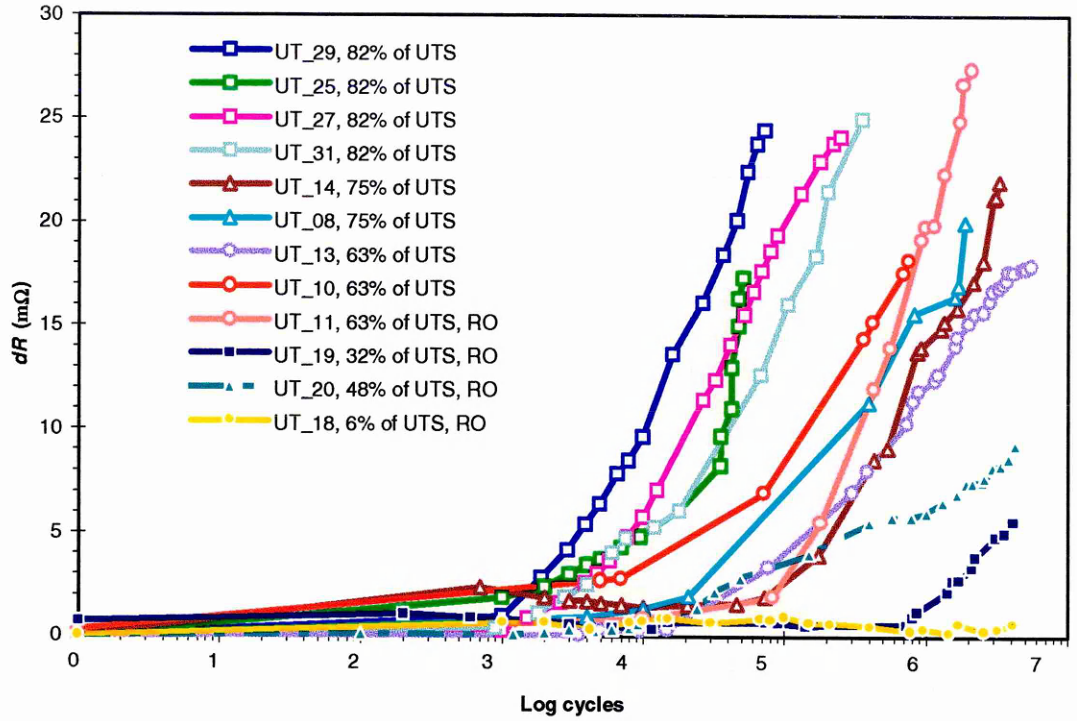

Figure 10.12. Electrical response of UD920 samples to fatigue loading.

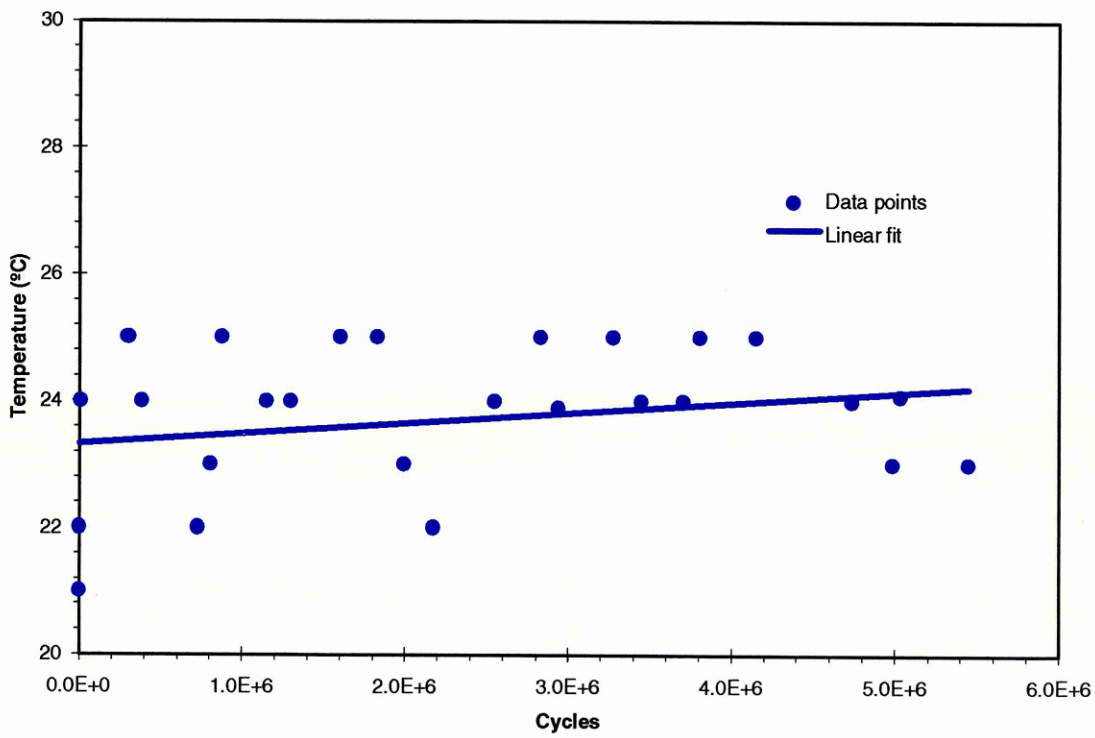

Figure 10.13. Temperature profile of a typical fatigue sample.

10.2.1 Overall behaviour

The overall electrical response of UD914 and UD920 samples to fatigue loading is shown in Figure 10.14-19. The aim of this section is to examine the relationship between fatigue life and electrical resistance or simply the fatigue damage. Most of the results are presented as normalised life and change in resistance or normalised resistance. This allows examination of the electrical response of UD samples to fatigue damage independent of other parameters that can influence the fatigue life.

Figure 10.14 and Figure 10.15 show the electrical resistance change of UD914 and UD920 samples to normalised life, i.e., percentage of life to failure, respectively. It can be seen that the electrical response of each sample is unique and is thought to be indicating the damage initiation and growth pattern. However, the overall behaviour of all the samples follows a generalised trend, i.e., the rate of change of resistance is higher in the initial part of the life and is lower in the rest of the life.

The difference in electrical behaviour from sample to sample is expected because of the inherent fatigue behaviour of CFRP samples. The fatigue damage mechanism is influenced by many parameters. The methods used to measure the damage generally show wide variation due to the inherent scatter associated with fatigue testing. Therefore, wide variation in electrical responses can be expected because, the electrical resistance changes according to the damage process. For example, for a given material configuration and applied stress level the sample life can vary approximately from 100 cycles to 500 000 cycles. Hence, the electrical resistance also is expected to vary depending on the damage level experienced by the sample.

The overall trend was determined using multiple curve fitting techniques. This is shown in Figure 10.14 and Figure 10.15 as thick dotted line. In UD920 samples, UT_25 was excluded from the curve fitting as the sample behaviour deviated much from the other samples. This sample had a much lower fatigue life. This is evident from the electrical resistance measurement results. This result is included in this section to show the wide variability of fatigue behaviour of CFRP samples.

The normalised change in resistance and life of UD914 and UD920 samples is shown in Figure 10.16 and Figure 10.17, respectively. In UD914 samples, 50% of the resistance change occurs within 5% of life and 75% of resistance change within 25% of life. The rest of the resistance change, i.e., 25% occurs in the remaining 75% of the life.

The overall normalised resistance of UD914 samples was found to follow a power type increase with normalised life of the following form:

$$dR = 39.2\ N^{0.1944} \qquad (10.1)$$

where, *dR*, is the change in resistance and, N, is the normalised life.

In UD920 samples, 50% of resistance change occurs within 10% of life and 75% of the resistance change with in 30% of life. There is only 25% of resistance change in the remaining 70% of life. The overall behaviour of UD920 samples was found to follow a polynomial type behaviour of the following form:

$$dR = 1e\text{-}07\ N^5 - 4e\text{-}05\ N^4 + 0.004\ N^3 - 0.2165\ N^2 + 6.0301\ N + 5.4093 \qquad (10.2)$$

where, *dR*, is the change in resistance and, N, is the normalised life.

The comparison of overall behaviour of UD914 and UD920 samples is shown in Figure 10.18. This figure clearly illustrates that the initial increase in resistance of UD914 samples is higher than for UD920. After 40% of life the resistance change is almost the same for both UD914 and UD920 samples. This behaviour indicates that the damage initiation and growth process of both UD914 and UD920 samples are different.

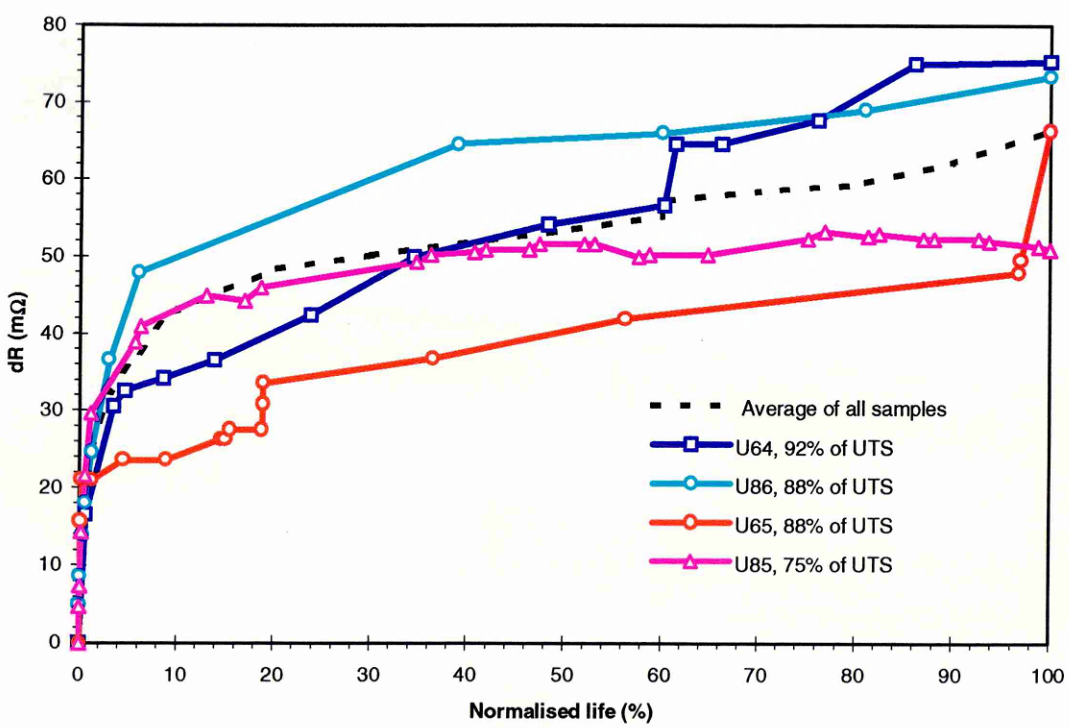

Figure 10.14. Overall electrical behaviour of UD914 samples.

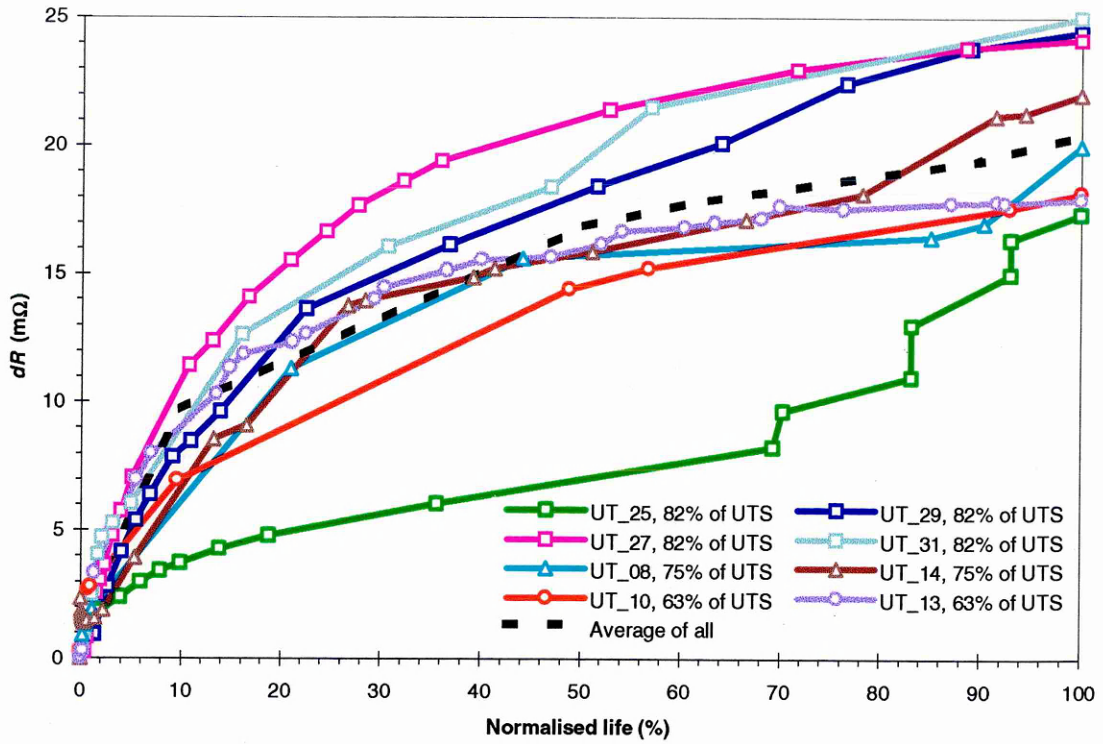

Figure 10.15. Overall electrical behaviour of UD920 samples.

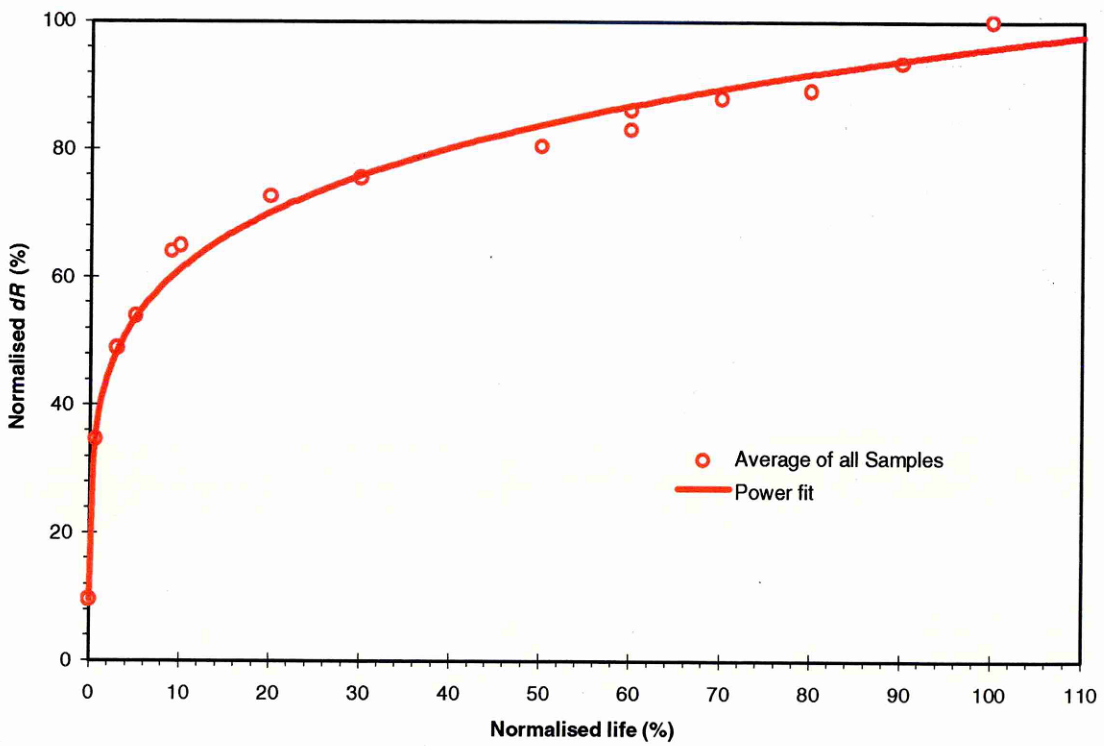

Figure 10.16. Normalised electrical response of UD914 samples .

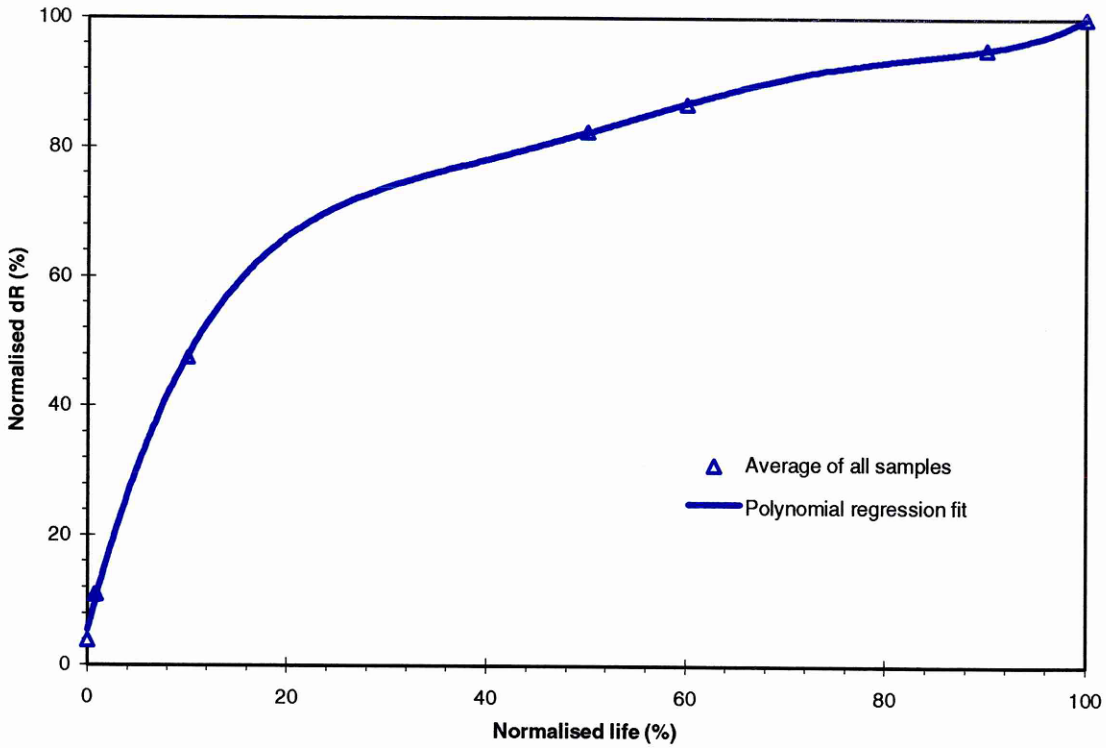

Figure 10.17. Normalised electrical response of UD920 samples.

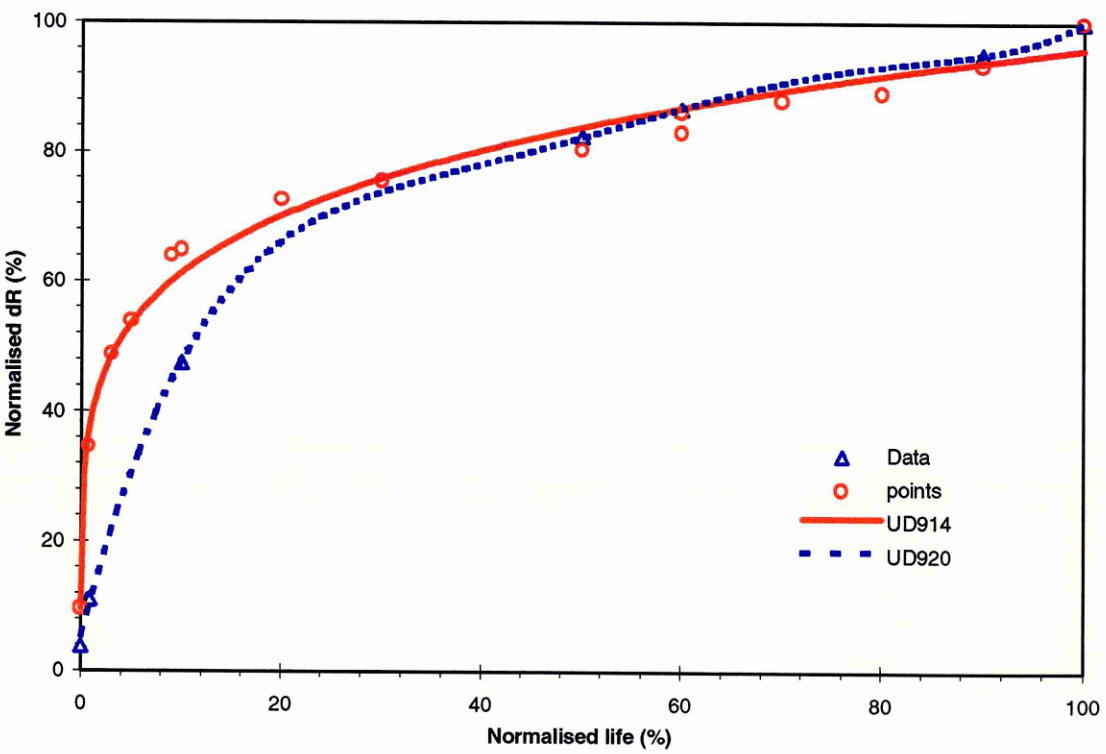

Figure 10.18. Comparison of normalised electrical behaviour of UD914 and UD920 samples.

10.2.2 Dependence on stress

Figure 10.19 and Figure 10.20 illustrates the electrical response of UD914 and UD920 samples to fatigue damage demonstrating its dependence on applied stress, respectively. This section also includes the results of samples subjected to stress levels below 50% of UTS and the related C-scan and X-ray radiography results. The expected life of these samples tested at stress levels below 50% of UTS are more than 4 million cycles and hence these samples were mostly terminated at around 4 million cycles for further investigations. One of the sample was cycled up to 12 million cycles without any sign of failure. In UD920, some of the samples tested above 50% of UTS were terminated at intermediate life in order to examine the samples using C-scan and X-ray radiography and compare the results with samples tested below 50% of UTS. The C-scan and X-ray radiography results are shown in Figure 10.21.

It is evident from Figure 10.19 and Figure 10.20 that the rate of change and the resistance change to failure are higher for samples subjected to higher stress levels. All the samples exhibit dependence on stress. However, some of the samples within 100 MPa difference in the stress level are found to over lap with the higher or lower stress level samples. For example, U65 did not show the dependence on stress in comparison with U64. However, it does show the stress dependence compared with samples tested below the stress level of U65.

These figures also illustrate that the electrical resistance of the samples subjected to stress levels below 50% of UTS increases with fatigue cycles. The 48% UTS stress level samples shows considerable increase in resistance. The samples tested at 32% of UTS also show slight increase in resistance but is relatively low. This indicates that the stress level below 50% of UTS can also damage the samples. The samples tested at 6% of UTS did not show any increase in resistance with fatigue cycles. The behaviour of 6% of UTS samples is almost flat. This indicates that there is no damage initiation at these stress levels within 4 million cycles. This (6% UTS stress level samples) also confirms that the electrical resistance is not influenced by magneto-mechanical effects.

The dependence on stress of the electrical resistance of fatigue samples indicates that the damage level increases with applied stress level. Even 30% of UTS stress level can damage the sample. This is supported by the C-scan and X-ray radiography results. The C-scan and X-ray radiography images show that the damage area increases with increase in applied stress.

Both C-scan and X-ray radiography are qualitative measures of damage. In order to make useful comparison with electrical resistance the damage area was calculated for both C-scan

and X-ray radiography results using an image analysis method. The image analysis equipment was set to measure the damage area by comparison with the virgin sample. Prior to image analysis, the C-scan attenuation results were calibrated with the virgin sample. The ultrasonic attenuation above the threshold of the virgin sample was considered as damage. Similarly, the X-ray results were also calibrated. The C-scan and X-ray radiography results are presented as percentage of damage area. These results were compared with the permanent resistance change of the samples, i.e., the difference in resistance before and after fatigue testing.

The comparison of electrical resistance with C-scan and X-ray radiography results is shown in Figure 10.23. It is clear from the figure that the permanent resistance change increases with applied stress level. The C-scan and X-ray results appear to compare well with electrical resistance. However, a better comparison can be made if we add the C-scan and X-ray radiography results together and compare them with electrical resistance (Permanent or total resistance change at runout). The combined results agrees well with the electrical resistance, because C-scan and X-ray radiography results are complementary to each other. For example, C-scan can detect delaminations and miss longitudinal splits, on the other hand X-ray radiography can detect longitudinal splits and miss delaminations. Therefore, in theory combination of C-scan and X-ray radiography results should give the overall measure of damage. The agreement of electrical resistance with combined C-scan and X-ray radiography results suggest that electrical resistance measures the overall damage.

Similar investigations were carried out on UD914 samples. The C-scan and X-ray radiography results of these samples have also shown that the damage level increases with applied stress as indicated by the electrical resistance.

It may be noted from the C-scan and X-ray radiography results that the damage mode also changes with applied stress. It can be seen that the over all damage level shown by C-scan is relatively lower for a 63% sample than for a 45% sample. However, the amplitude is higher, i.e., higher attenuation. At lower stress level the damage may be mainly due to matrix cracks scattered throughout sample. As the stress level increases, the damage modes appear to be dominated by a single mode of damage, in this case longitudinal splits.

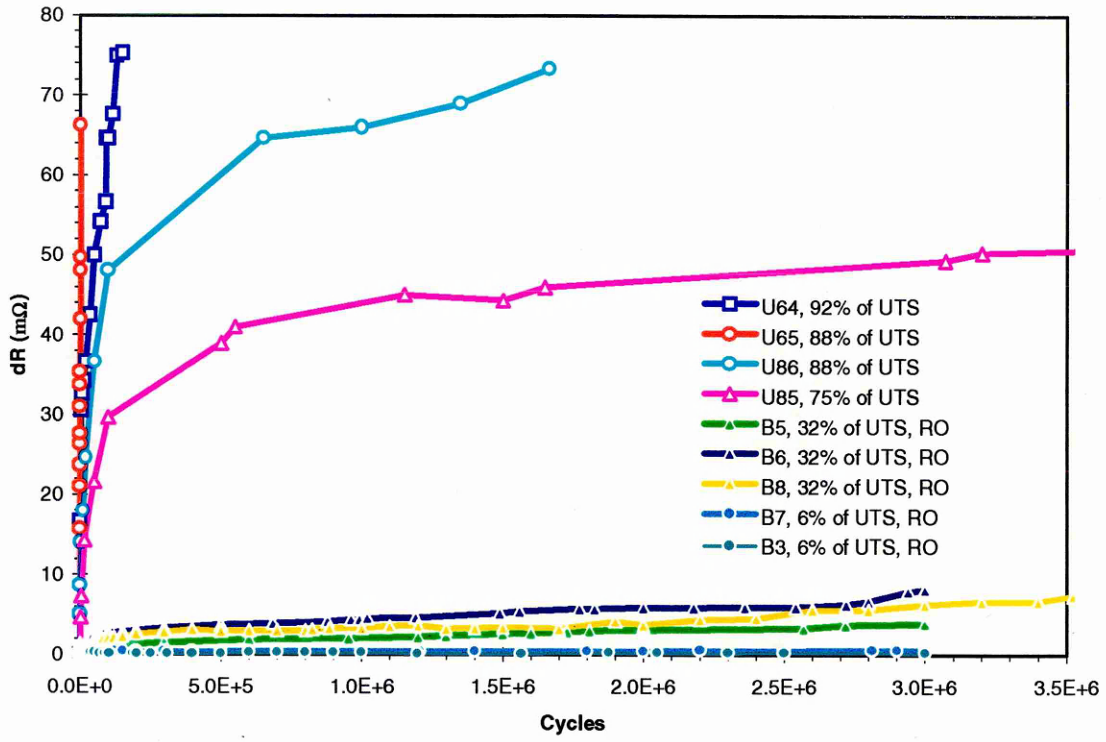

Figure 10.19. Electrical response of UD914 samples illustrating the dependence on stress.

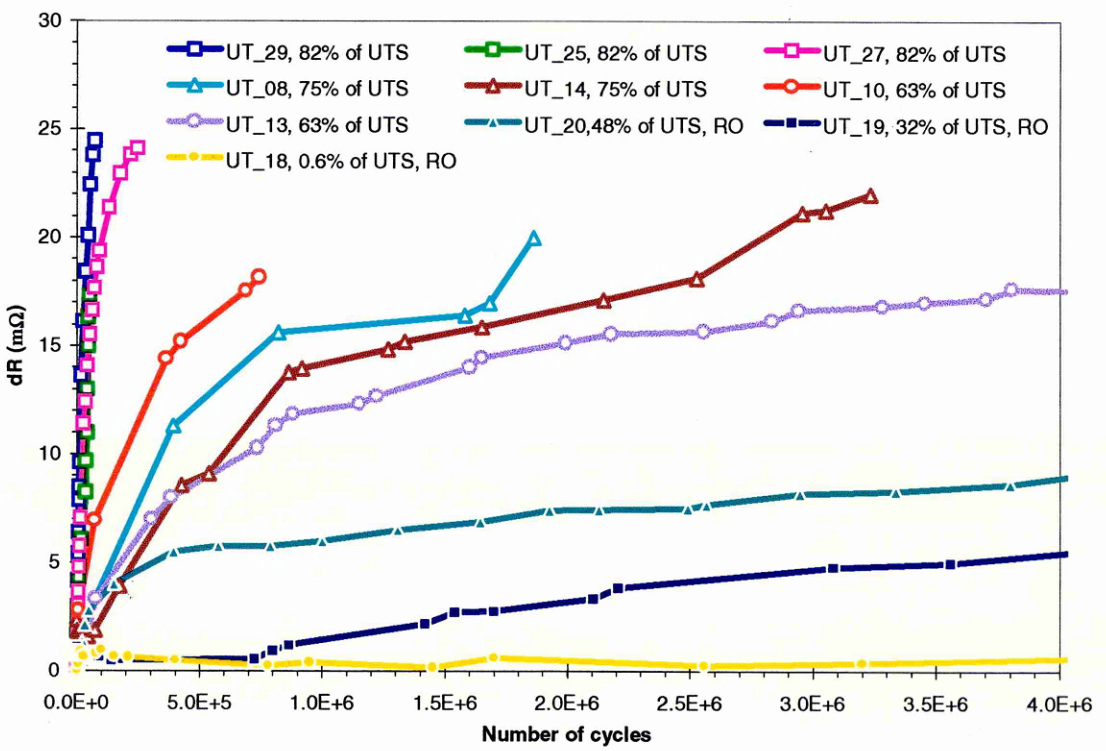

Figure 10.20. Electrical response of UD920 samples illustrating the dependence on stress.

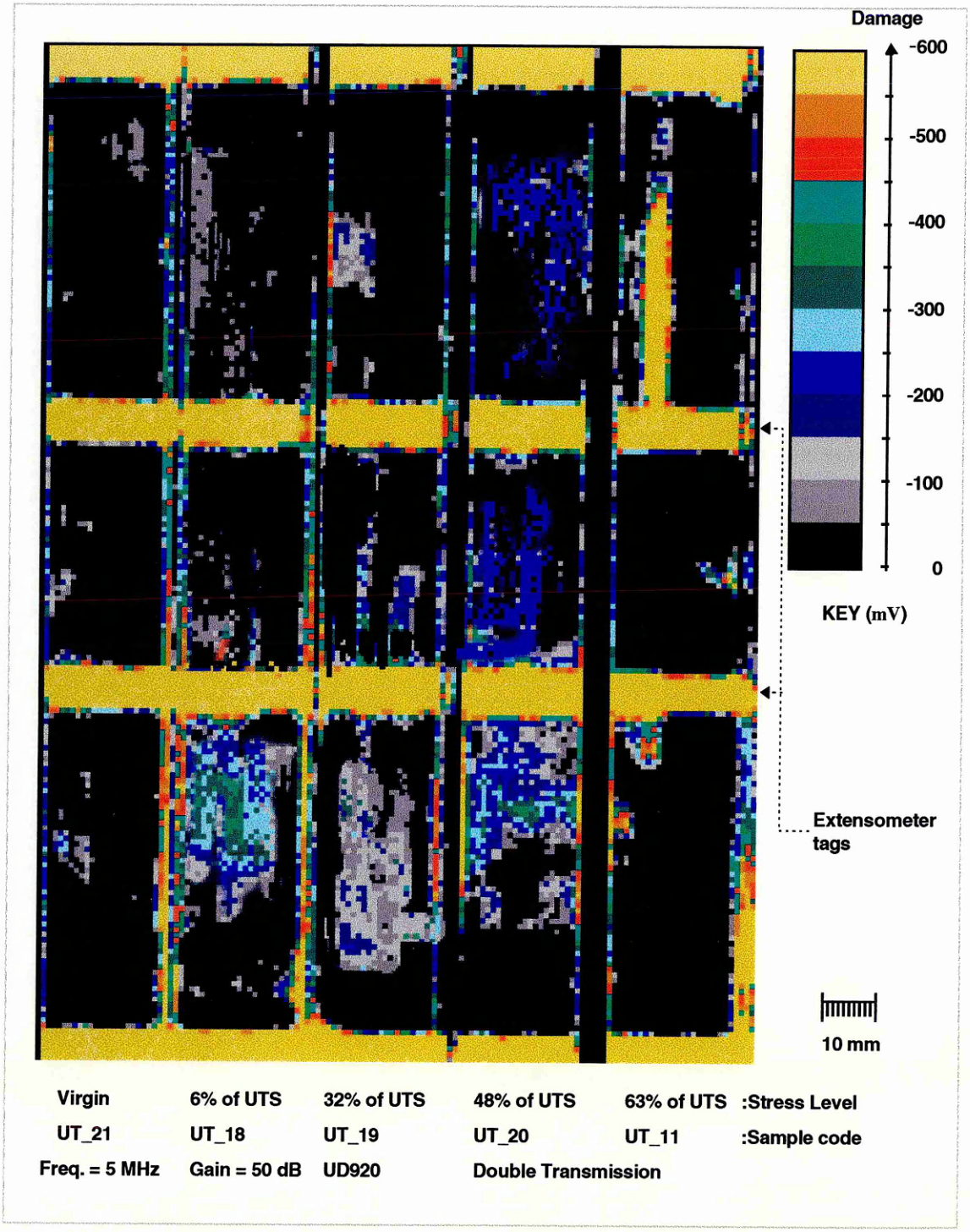

Figure 10.21. C-scan results of UD920 samples subjected to various levels of fatigue loading, illustrating the increase in damage level with applied stress.

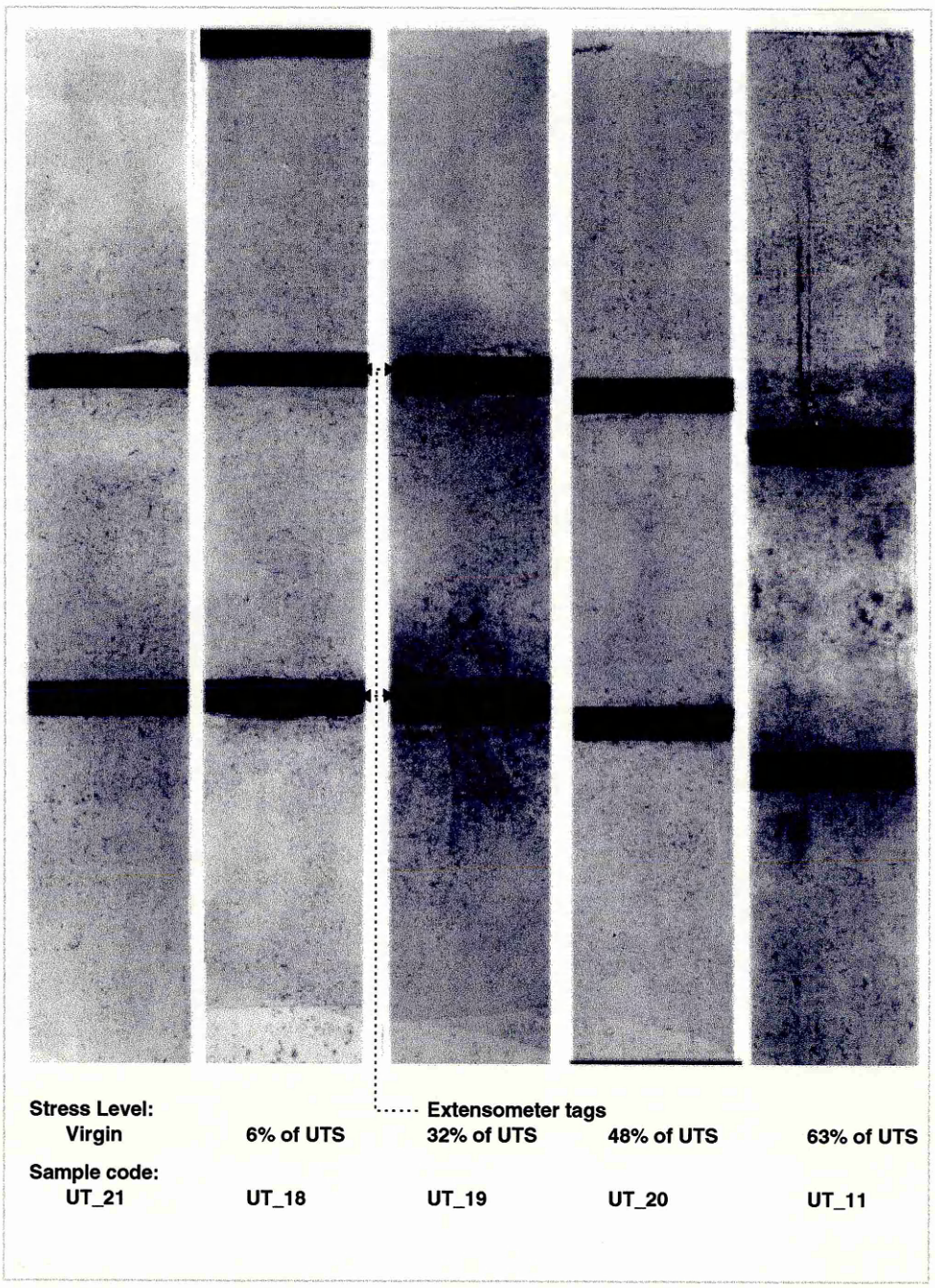

Figure 10.22. X-ray radiograph of UD920 samples subjected to various levels of fatigue loading, illustrating the increase in damage level with applied stress.

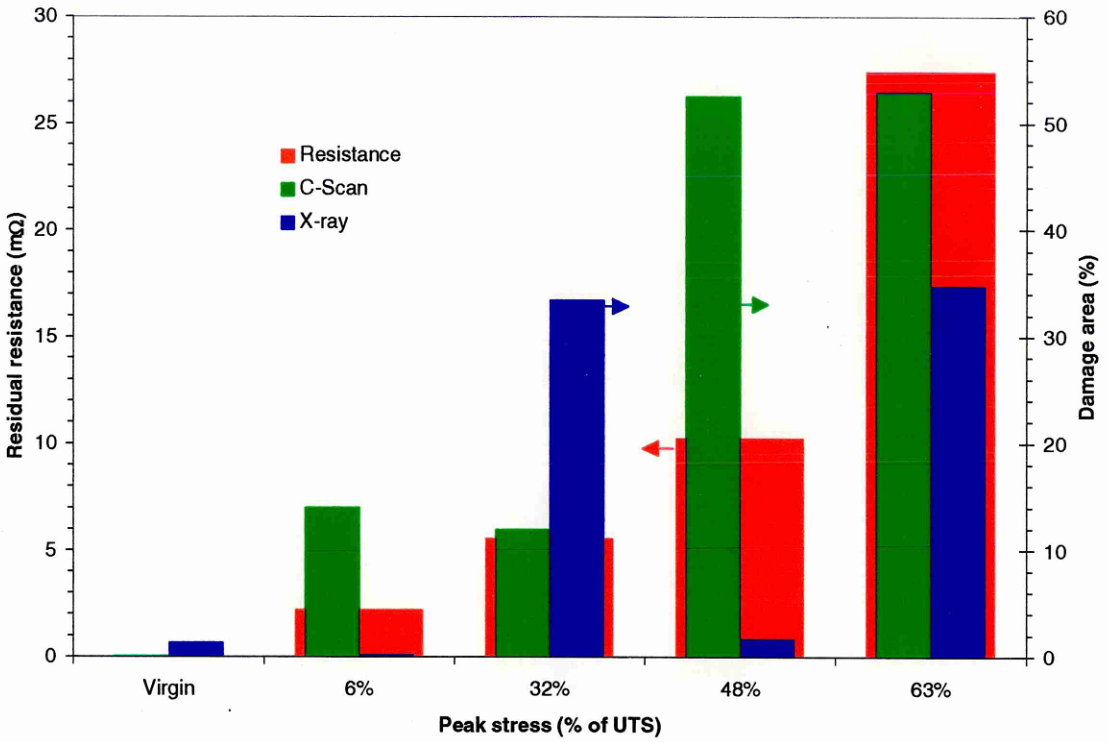

Figure 10.23. Comparison of C-scan and X-ray results with electrical resistance.

10.2.3 Dependence of life

Figure 10.24 and Figure 10.25 illustrates the correlation between the electrical resistance and the life of the samples. These figures only include the samples that are failed, run outs are not included. The electrical resistance measurement results are overlapped with the S-N diagram. These results clearly indicate the correlation between the life and the electrical resistance. It is previously mentioned that some of the samples did not show a stress dependence. However, it can be seen that almost all the samples show dependence of life. The correlation between electrical resistance and life for all the samples was found to be more than 0.90. This highlights that the electrical resistance measures the damage and is very useful in life prediction.

Fatigue testing usually results in wide scatter in life for similar configuration, material and applied stress level. For example, if we compare the fatigue life of U65 and U86 of UD914 samples, the life to failure of U65 is 3217 and U86 is 1 665 432 cycles. Both samples were subjected to 87% of UTS stress level and the difference in life is 1 662 215 cycles. This is because of the difference in the damage initiation and growth pattern of the above samples. To the author's knowledge, it appears that there are no techniques that can indicate this difference as a damage parameter. However, It is clear from the figure that the electrical resistance indicates the reason for such wide scatter in life. The rate of change of resistance is higher for U65 and is lower for U86. If we consider electrical resistance as a damage parameter, then the

rate of damage initiation and growth for U65 is higher than U86. A similar comparison can be made between samples tested at the same stress level of UD920 samples.

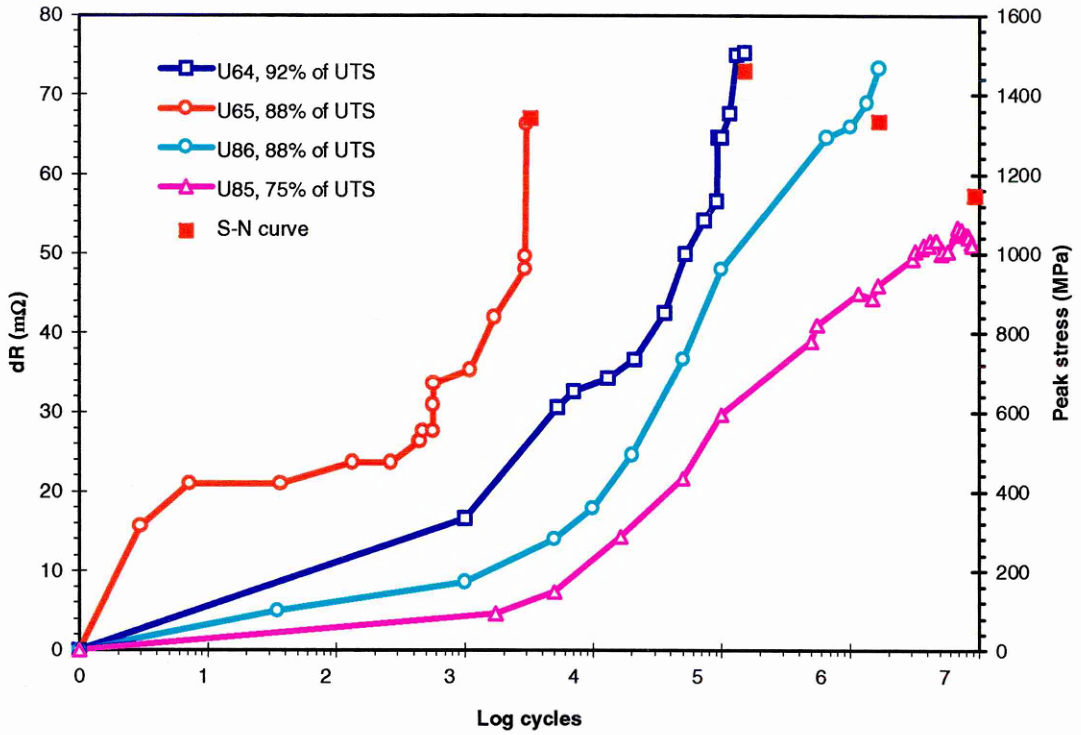

Figure 10.24. Electrical response of UD914 samples illustrating the dependence of life.

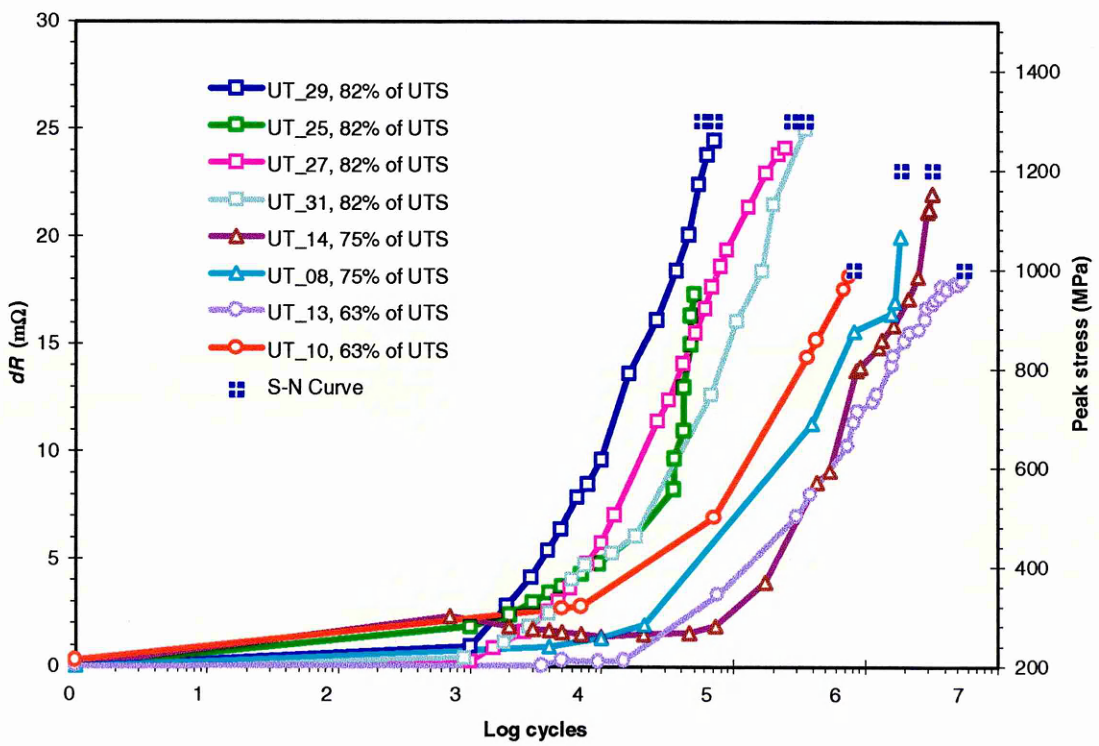

Figure 10.25. Electrical response of UD920 samples illustrating the dependence of life.

10.2.4 ERM and modulus

This section compares the electrical resistance and elastic modulus of a typical fatigue sample subjected to 63% of UTS fatigue loading. The elastic modulus has been used by many investigators as a good measure of fatigue damage. The elastic modulus was found to be influenced by fibre breaks and longitudinal splits (Steif 1984, Whitworth 1987). Figure 10.26 shows the normalised tangent modulus and the electrical resistance change of a typical UD914 sample subjected to fatigue loading. The elastic modulus was normalised with respect to the initial sample modulus.

It is evident from the figure that the change in electrical resistance is mirrored by the change in normalised tangent modulus. A strong correlation (correlation coefficient of -0.96) between electrical resistance and tangent modulus was found. The negative sign in the correlation coefficient represents the decrease in modulus with increase in resistance. However, the correlation between the compliance and electrical resistance is 0.96. This result is another proof that the electrical resistance change is a measure of damage.

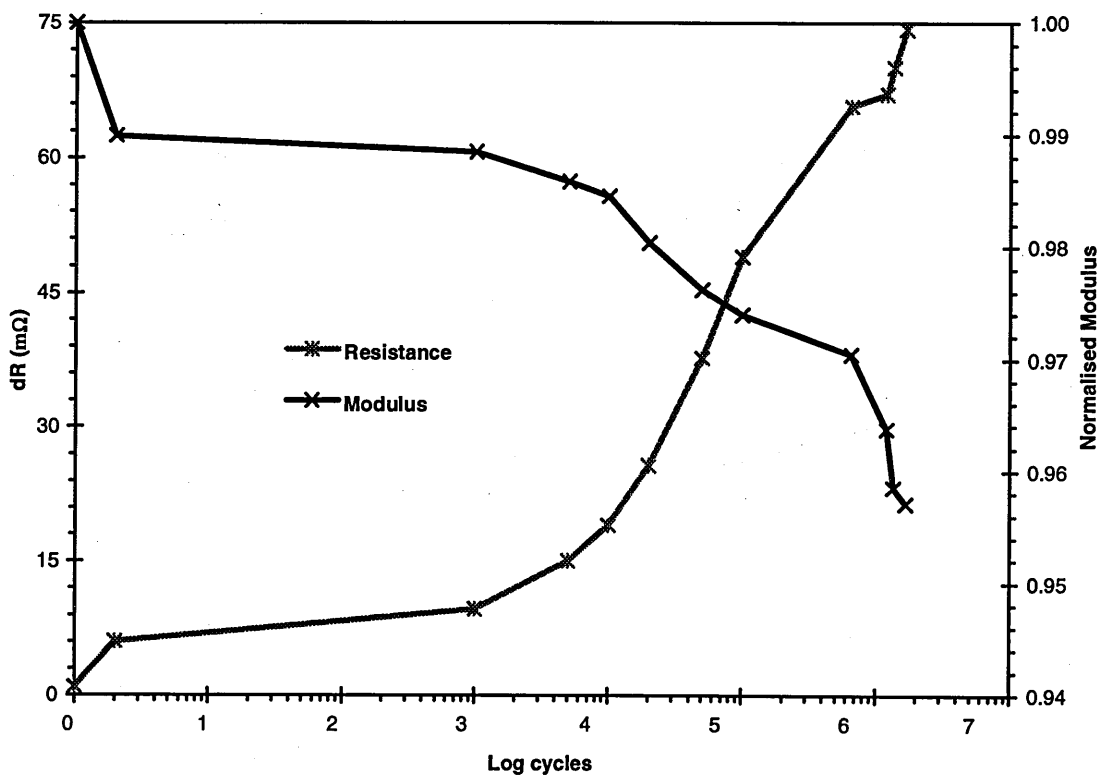

Figure 10.26. Comparison between changes in modulus and resistance with fatigue life.

10.2.5 Longitudinal split growth rate

Figure 10.27 illustrates the electrical response of a typical UD914 sample to longitudinal split growth subjected to 63% of UTS stress level fatigue loading. Electrode configuration as described in section 8.2.2 was used to measure the transverse resistance of the sample. The longitudinal split was grown from a circular hole of 1 mm diameter. The crack growth was measured using optical microscope also.

It was observed that the longitudinal splits developed very early in the of life of the sample. These splits initiated at the tangents to the holes and grew as four cracks up and down the specimen length and parallel to the fibre direction. It is evident from Figure 10.27 that the electrical resistance correlates well with longitudinal split length. This figure demonstrates the capabilities of the electrical resistance measurement technique to sense longitudinal split growth under fatigue loading conditions.

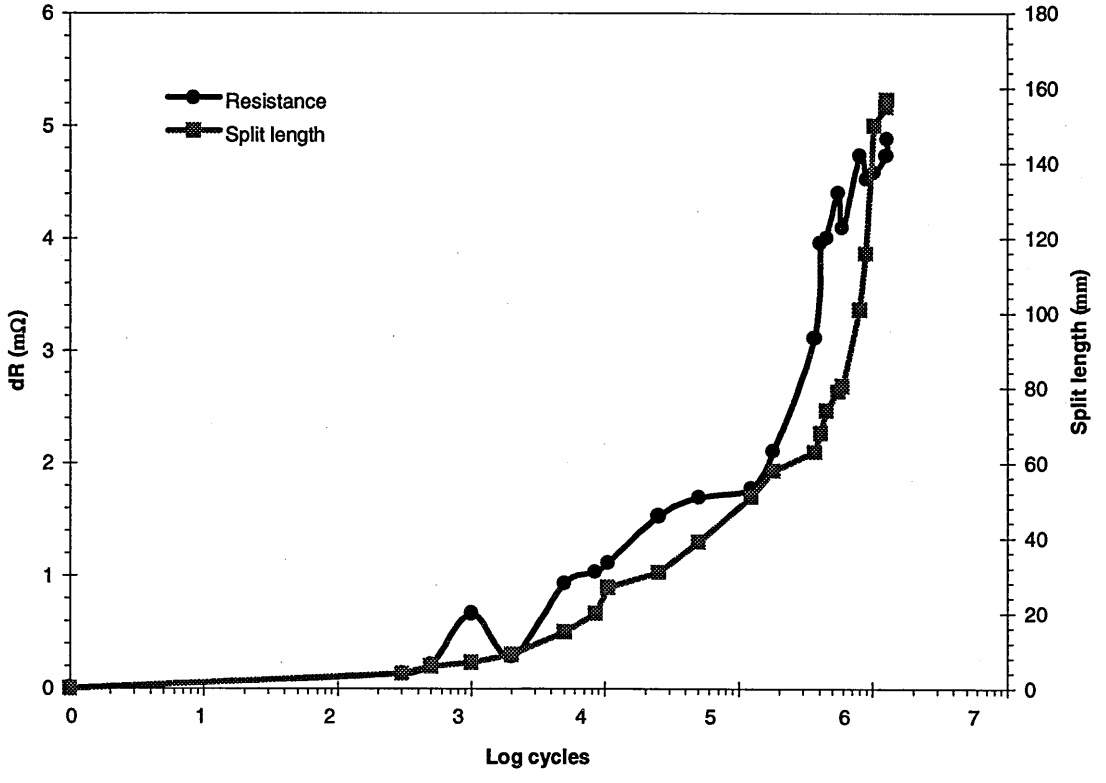

Figure 10.27. Electrical response of a typical UD914 sample to longitudinal split growth.

11

CONCLUSIONS AND FUTURE WORK

This chapter is concerned with the conclusions and future work. More than 80% of the results reported in this thesis are new and are not previously published. Therefore, each section may form or have formed a basis for a minimum of one publication. The basic concepts and preliminary results are published else where (Thiagarajan and Irving 1994, Thiagarajan et al. 1994).

The major conclusions drawn from the investigations reported in this thesis are divided as far as possible into separate sections based on the chapters. The sections 11.1 to 11.8 present the major conclusions. The conclusions related to the smart capabilities are presented in section 11.9. The future perspective of electrical resistivity measurement technique is described in section 11.10. Section 11.11 describes the future works.

11.1 LITERATURE REVIEW

- A comprehensive literature survey has been made of the damage modes, tensile failure mechanisms, fatigue damage mechanisms and damage models of unidirectional CFRP laminates. Cross-ply laminates were also considered. An extensive literature survey has been made of the electrical resistivity measurements of carbon fibres, epoxy resins and carbon fibre reinforced composites. The electrical models related to the conduction behaviour of CFRP laminates were reviewed.

11.2 TEST METHODS

- As outlined in section 4.5.1, tags different to those specified in ASTM D3039 were used in this thesis. A satisfactory tag configuration was developed that promoted failure away from the grip region. However, the results show that the expectation of failure away from the grip region is conservative. The bi-axial stress state at the grip line and the strong anisotropic properties of unidirectional CFRP may promote failure preferentially at the grip line.

- The specimen configuration was modified to introduce current injection and potential measuring points. A satisfactory specimen configuration was designed to isolate the electrode during mechanical loading.

- An experimental setup was developed based on a digital data acquisition system that can monitor and record up to sixteen channels including electrical potential, load, strain, position, temperature and acoustic emission counts simultaneously under static and fatigue loading conditions.

11.3 ELECTRODES

- The influence of electrodes on the resistance of the samples has been over looked by previous investigators. The influence of electrode on the electrical properties of CFRP laminates was investigated. It has been demonstrated in this thesis that the measured electrical resistance of CFRP samples is influenced by the type of electrode used for the resistance measurements.

- New electrode configuration and formation methods were developed. The results presented in this thesis show that these electrodes minimise the electrode effects and reduces the scatter in the measured electrical resistance of the samples due to the electrode.

11.4 ELECTRICAL PROPERTIES

- The electrical properties of CFRP samples were measured using more than three hundred samples. The electrical properties reported in this thesis are in agreement with the previously published results (refer table 3.4). However, direct comparison would be futile because the previously published results do not take in to account of the electrode resistance.

- The electrical properties of CFRP laminates were established without the influence of the electrode and specimen geometry.

- The experimental observation of the dependence of longitudinal resistivity on sample length was demonstrated to be due the effect of the electrode.

- The temperature dependent electrical behaviour of CFRP laminates was reported. The temperature coefficient of resistivity of samples used in mechanical testing were established. The temperature dependent resistivity investigations demonstrated the complex conduction mechanisms of CFRP laminates. The transverse temperature dependent resistivity of UD920 samples shows a transition from negative to positive temperature coefficient.

- It has been established from the specimen geometry dependent resistivity investigations and the experimental damage simulation investigations that the conduction mechanism of unidirectional CFRP is a three-dimensional process.

- The results presented in this thesis, show that the longitudinal electrical properties are dominated by the fibres. The transverse electrical properties are complex and dominated by the fibre, matrix and their interaction. The possible mechanisms of transverse conduction were proposed.

11.5 ELECTRICAL MODELS

- The parallel resistance model was modified to suit the present application. It was confirmed that the parallel resistance model predicts the longitudinal electrical properties of unidirectional CFRP laminates fairly accurately. The comparison of fibre breaks simulated by the experimental methods and parallel resistance model demonstrated that the parallel resistance model predicts the trend, however, it fails to predict the actual behaviour due to the inherent assumptions of the model and the three-dimensional conduction mechanism of unidirectional CFRP laminates.

- A new-random resistor network model (two-dimensional) was developed using new algorithms and approaches to predict the transverse electrical resistivity of CFRP laminates and to simulate the effects of damage. For comparison purpose, the existing lattice models were also modelled.

- The simulation investigations have shown that the proposed new random resistor network model simulates the fibre distribution better than the existing models and close to the real fibre distribution.

- It has been established as mentioned previously that the conduction mechanism of unidirectional CFRP is a three-dimensional process and complex. A new three-dimensional model based on the unit cell assemblage was developed to simulate the effects of damage and the effect of electrode on sensing different types of damage

- The validity of the proposed three-dimensional unit cell assemblage model was established by comparing the experimental damage simulation results with the computational simulation results. It was shown that the proposed new three-dimensional model predicts accurately the effects of damage on changes in electrical resistance.

11.6 DAMAGE SIMULATION

- Based on the experimental and computational simulation investigations, the schematic electrical analogy of damage modes such as fibre breaks, matrix cracks, delamination and longitudinal splits were established. The electrode configuration to detect the above damage modes were also established.

- Based on the parallel resistance model simulation results, it has been shown that the change in electrical resistance is a function of fibre resistivity. In other words, detection of fibre break is a function of fibre resistivity.

- The simulation results confirm that the fibre breaks can be detected using electrical resistance measurement technique when the current flows along the fibre direction. It was shown that the fibre breaks can be detected even if the current flows transverse to the fibre direction. These simulation results have demonstrated that longitudinal splits and delamination can also be detected.

- The simulation investigations of the effects of electrode location on sensing different modes of damage demonstrated that the fibre breaks can be detected using all three types of electrodes considered. These results have also shown that longitudinal splits and delaminations are sensitive only to a particular type of electrode configuration. That is longitudinal splits and delaminations are detected only when the current flows orthogonal to the direction of damage propagation. In summary, these results have shown that the damage detection is a function of electrode location.

- These simulation results have also demonstrated that the change in electrical resistance due to the effects of damage are different for different types of CFRP laminates. That is, the electrical properties of the constituents and hence their composites influence the changes in electrical resistance due to the damage.

- The computational simulation investigations have also shown that the changes in electrical resistance are influenced by the location of the damage, i.e., damage detection is a function of position of the damage. In reverse, these results imply that the damage can be located from the electrical resistance change. From the electrode and damage location investigations, it was inferred that the combination of two or more electrodes could be used to detect the type of damage as well as the location.

11.7 TENSILE FAILURE MECHANISMS

- The tensile properties, stress-strain behaviour and failure modes of CFRP samples reported in this thesis are in general agreement with the previously published results. The electrical response of 0° and 90° unidirectional and cross-ply samples were shown to be indicating the combined effect of the strain and damage.

- In 0° unidirectional samples, in general, it was demonstrated that the electrical response indicated the strain up to 70% of the UTS and damage above 70%. The strain predicted using the electrical resistance was shown to agree very well with the strain measured using the extensometer. These results demonstrated the strain sensing capabilities of the electrical resistivity measurement technique. The reduction in electrical resistance of some of the UD920 samples above 70% of UTS were attributed to the longitudinal splits. A correlation was established between the longitudinal splits and the reduction in electrical resistance.

- The fibre breaks due to tensile loading were predicted using the damage component of the electrical resistance by subtracting the strain component. The fibre breaks predicted from the electrical resistance measurement were shown to agree well with previously published results. From these results, it was shown that only 0.25% of fibre breaks are needed for a catastrophic failure of a unidirectional CFRP laminate.

- In 90° unidirectional samples, it was demonstrated that the electrical resistance measures the strain up 30% of the UTS. In these samples a correlation was established between tensile strength and the changes in electrical resistance. These results suggested that the strong correlation is an indication that the changes in electrical response may be demonstrating the damage initiation and propagation pattern of 90° laminates.

- In cross-ply samples also, it was demonstrated figuratively that the electrical resistance response and strain coincide up to 35% of UTS. The cross-ply samples subjected to various stress levels have shown that the permanent change in electrical resistance increases with increase in applied stress level. The permanent change in resistance may be indicating the damage level experienced by the samples. That is, change in electrical resistance indicates the damage level. These results were supported by C-scan and X-ray radiography results.

11.8 FATIGUE DAMAGE MECHANISMS

- The fatigue behaviour of carbon fibre reinforced brittle (UD914) and tough resin (UD920) based unidirectional laminates were investigated. In general, the fatigue behaviour and the failure modes were in agreement with the previously published results. These investigations have confirmed the poor high cycle fatigue behaviour of tough resin based composites. The fatigue behaviour of UD920 samples was poorer than the UD914 samples.

- These results have also confirmed that the tough resin based composites are more susceptible to longitudinal splitting than the brittle resin composites. The failure pattern of these samples has also shown that at lower stress level the longitudinal splits are the major damage modes. At higher stress level, the failure modes are dominated by fibre fracture and longitudinal splitting.

- The electrical response of unidirectional samples subjected to various stress levels were measured. The overall electrical response of UD914 samples was established to follow a power law increase with fatigue life. Similarly, the UD920 samples were found to follow a polynomial law increase with fatigue life.

- It was established that the electrical response of each sample is unique and believed to be indicating the damage initiation and propagation pattern. The evidence presented in this thesis has shown that the electrical response is indicating the damage level experienced by the samples subjected to fatigue loading. This was confirmed by comparing the electrical resistance response with elastic modulus, acoustic emission, C-scan and x-ray results.

- Simultaneous measurement of elastic modulus and change in electrical resistance with fatigue cycling has shown a strong correlation between the two sets of measurement, both are related to fatigue damage.

- The evidence presented in this thesis shows that the longitudinal split growth rate under fatigue loading can be monitored.

- The electrical response of samples subjected to various levels of fatigue loading have shown that the damage level increases with increase in applied stress level. These results indicated by the electrical resistance were supported by the C-scan and X-ray results. It was shown that even stress levels of 30% of UTS damage the sample.

- A correlation was established between rate of change in electrical resistance and fatigue life. The average correlation coefficient of resistance and life of all the samples is 0.96. It was demonstrated that the samples with higher rate of change in resistance have shorter life. The implication of these results is that the electrical resistivity measurement can be used to predict fatigue life.

11.9 SMART CAPABILITIES

The evidence presented in this thesis demonstrated the smart capabilities of electrical resistivity measurement technique.

- The results presented have shown that ERM can measure both strain and damage in CFRP laminates under static and fatigue loading conditions.
- The results also demonstrated that the damage can be quantified.
- Moreover, simulation results have shown that the electrical resistance is sensitive to the type of damage as well as the location.

11.10 FUTURE OF ERM

The future of the electrical resistivity measurement technique is very promising. The smart capabilities of electrical resistivity measurement technique indicate that this technique can change the way in which the future aircraft will be built and flown. The electrical resistivity measurement technique can be used from 'cradle to grave', i.e., from fabrication to the final failure of the structure. Some of the possible capabilities are listed below.

- The resistive heating capabilities of carbon fibres can be used to fabricate the carbon fibre reinforced thermoplastic composites.
- During the fabrication process, the resistivity measurements can be used to monitor the cure.
- After fabrication, this technique can provide in-service information about the load or strain.
- If the structure is damaged during service, ERM can indicate the type of damage and location.
- The structure can be discarded or repaired after certain levels of damage as indicated by the ERM.
- The resistive heating properties of carbon fibres can also be used for deicing.
- The conductive networks, if designed to carry higher current can then be used for lightning protection by providing conductive paths.
- A typical example of the use of condition monitoring capabilities of ERM is shown in Figure 11.1.

11.11 FUTURE WORK

In general, all the investigations reported in thesis need to be demonstrated for multi-directional laminates. The proposed new random resistor network model can be used to investigate percolation phenomena of the short fibre composites. This model allows to model the fibre distribution closer to the real laminate. Therefore, the capabilities of this model to model more accurately the behaviour and predict the properties of composite laminates that mainly depends on the fibre distribution can be explored.

The three-dimensional model developed in this thesis provides a powerful tool in that various experiments can be carried out computationally. For example, this model can be used to study the interaction of different damage modes on changes in electrical resistance. In future, this can be used to detect and locate damage by processing the electrical signals from different electrodes, and hence this potential can be explored.

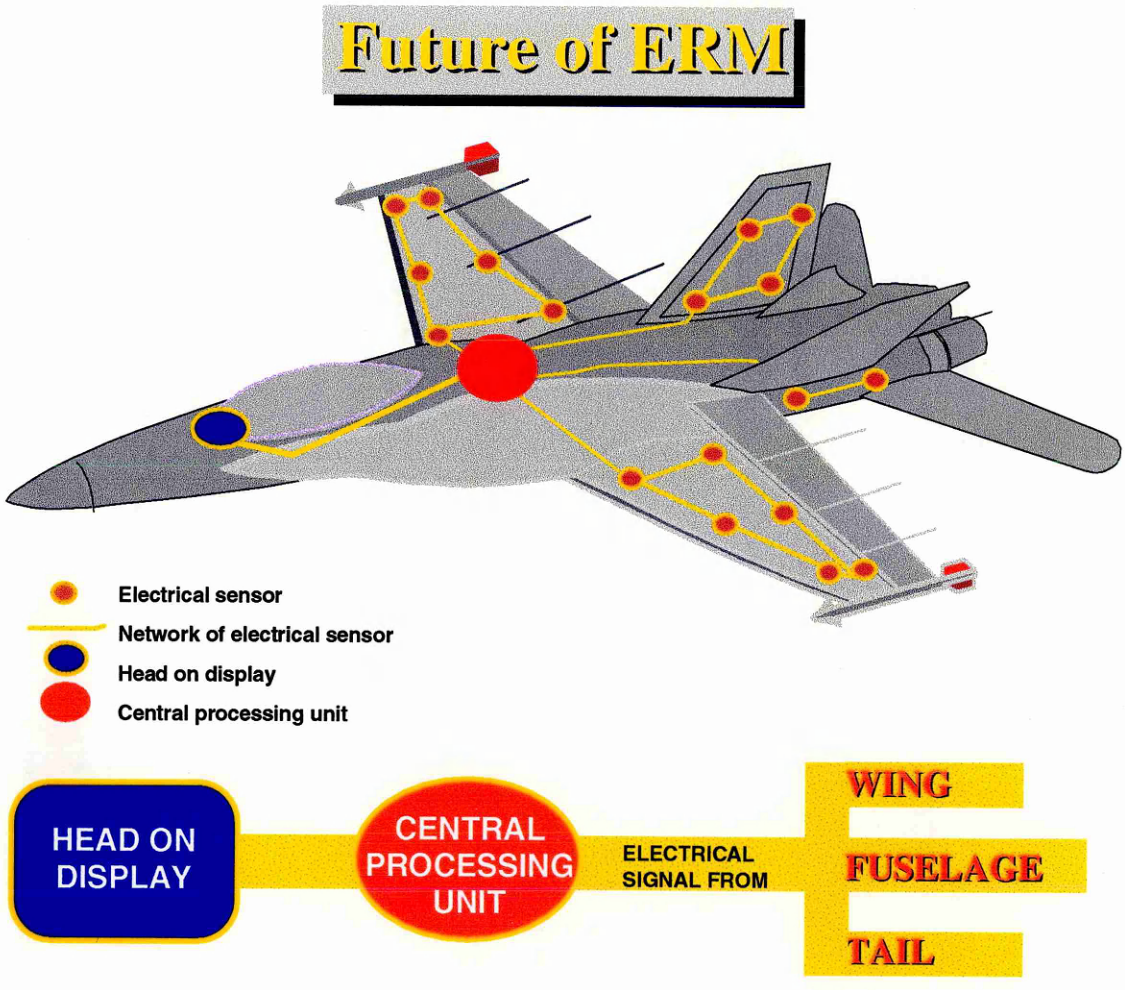

Figure 11.1. The future of condition monitoring in aircraft.

Regarding the future of ERM, the development any new technique needs to follow the following four stages:

(1) Demonstration using specimens in a laboratory level,

(2) Demonstration using panels in a laboratory level,

(3) Demonstration using scale down models in a laboratory level,

(4) Demonstration in a real structure.

In this thesis most of the smart damage sensing capabilities were demonstrated. Therefore, the next stage is to demonstrate the capabilities using panel level samples, and then stage third and fourth.

REFERENCES

Agarwal, B. D., and Broutman, L. J. 1990. Analysis and performance of fiber composites. John Wiley and sons, Inc., New York.

Allen, D. H., Lo, D. C., Georgiou, I. T., and Harris, C. E. 1990. A model for predicting damage induced fatigue life of laminated composite structural components. In: 17th ICAS Proceedings, Stockholm, Sweden, September. 9-14, 1990, 682-692.

Awerbuch, J., and Hahn, H. T. 1977. Fatigue and proof-testing of unidirectional graphite/epoxy composite. In: Reifsnider, K. L., and Lauraitis, K. N., (eds.), Fatigue of Filamentry Composite Materials, ASTM STP 636, ASTM, Philadelphia, 248-266.

Awerbuch, J., and Hahn, H. T. 1981. Off-Axis fatigue of graphite/epoxy composite. In: Fatigue of fibrous composite materials, ASTM STP 723, ASTM, Philadelphia, 1981, 243-273.

Bailey, J. E., Curtis, P. T., and Parvizi, A. 1979. On the transverse cracking and longitudinal splitting behaviour of glass and carbon fibre reinforced epoxy cross ply laminates and the effects of Poisson and thermally generated strain. Proceedings of the Royal Society of London, Series A, Vol. 366, 599-623.

Bardal, E., Berge, T., Grovlen, M., Haagensen, P. J., and Forre, B. M. 1982. A pulsed d.c. method for the measurement of low rates of fatigue crack growth. In: Beevers, C. J. (ed.), Advances in Crack Length Measurements, Engineering Materials Advisory Services, 139-158.

Batdorf, S. B., 1982. Tensile strength of unidirectionally reinforced composites -I. Journal of Reinforced Plastics and Composites, Vol. 12, 153-164.

Bathias, C. 1989a. The damaging of composite materials: mechanisms and detection. In: Branco, M. C., and Rosa, G. L. (eds.), Advances in Fatigue Science and Technology, Kluwer Academic Publishers, Boston, 659-676.

Bathias, C. 1989b. The fatigue of high performance composite materials. In: Branco, M. C., and Rosa, L G., (eds.), Advances in fatigue science and technology, Kluwer Academic Publishers, Boston, 659-676.

Bathias, C. 1991. Fracture and fatigue of high performance composite materials: mechanisms and prediction. Engineering Fracture Mechanics, Vol. 40, No. 4/5, 757-783.

Belani, J. G., and Broutman, L. J. 1978. Moisture induced resistivity changes in graphite-reinforced plastics. Composites, Vol. 9, No. 4, 273-277.

Bernel, J. D. 1924. The structure of graphite, Proceedings of the Royal Society of London, Series A, Vol. 106, 749-773.

Blackman, L. C. F. (ed.) 1970. Modern aspects of graphite technology, Academic Press, London and New York.

Blatt, F. J. 1968. Physics of electronic conduction in solids. McGraw-Hill Book Company, New York.

Boissonade, J., Barreau, F., and Carmona, F.1983. The percolation of fibres with random orientations: a Monte Carlo study. Journal of Physics. A: Math. Gen. Vol. 16, 2777-2787.

Boller , K. H. 1969. Fatigue fundamentals for composite materials. In: Composite Materials: Testing and Design, ASTM STP 460, 217-235.

Bonora, N., Marchetti, M., and Milella, P. P. 1992. Theoretical forecasting and experimental validation of damage tolerance and accumulation in glass/epoxy laminates. Journal of Reinforced Plastics and Composites, Vol. 11, No. 1, 56-81.

Bott, D. C. 1986. Structural basis for semiconductor and metallic polymers. In: Skotheim, T. A. (ed.), Handbook of conducting polymers, Vol. 2, Marcel Dekker Inc., New York. 1191-1232.

Bratley, P., and Fox, B. L.. 1988. ALGORITHM 659: Implementing Sobol's quasirandom sequence generator, ACM Transactions on Mathematical Software, Vol. 14, No. 1, 88-100

Bridge, B. 1989. Theoretical modelling of the critical volume fraction for percolation conductivity in fibre-loaded conductive polymer composites. Journal of Material Science Letters, Vol. 8, No. 1, 102-103.

Bridge, B., Folkes, M. J., and Jahankhani, H. 1988. Electrical conduction phenomena between adjacent stainless steel fibres in a thermoplastic matrix, Journal of Material Science, Vol. 23, No. 6, 1955-1960

Bright, A. A., and Singer, L. S. 1979. The electronic and structural characteristics of carbon fibers from mesophase pitch, Carbon, Vol. 17, No. 1, 59-69.

Bruggeman, D. A. G. 1935. Berechnung verschiedener physikalischer konstanten von heterogenen substanzeb. Annalen der Physik, Leipz, Vol. 5, No. 24, 636-664.

Bull, D. A., Jackson, G. A., and Smithers, B. W. 1981. Radio frequency characteristics of carbon fibre composite materials, The Radio and Electronic Engineer, Vol. 51, No. 10, 505-513.

Cano, R. J., and Dow, M. W. 1992. Properties of five toughened matrix composite materials, NASA TP 3254, 57 pages.

Carmona, F. and El Amarti, A . 1987. Anisotropic electrical conductivity in heterogeneous solids with cylindrical conducting inclusions, Physical Review B, Vol. 35, No. 7, 3284-3290.

Carmona, F. and El Amarti, A. 1992. Temperature and pressure dependence of the conductivity anisotropy of unidirectional short carbon fiber filled polymers, Journal of Material. Research, Vol. 7, No. 1, 1-7.

Carmona, F., Canet, R., and Delhaes, P. 1987. Piezoresistivity of heterogeneous solids. Journal of Applied Physics, Vol. 61, No. 7, 2550-2557.

Carmona. F., Valot, E., Servant, L., and Ricci, M. 1992. Random media with temperature controlled connectivity. Journal of Physics. I France, Short Communications, Vol. 2, 503-510.

Carmona. F., Barreau, F., Delhaes, P., and Canet, R. 1980. An experimental model for studying the effect of anisotropy on percolative conduction. Journal of Physique-Letter, Vol. 41, No. 15. L-531-534.

Carmona. F., Prudhon, P. and Barreau, F. 1984. Percolation in short fibres epoxy resin composites: conductivity behaviour and finite size effects near threshold. Solid State Communications, Vol. 51, No. 4, 255-257.

Chamis, C. C., and Ginty, C. A. 1989. Fiber composite structural durability and damage tolerance: simplified predictive methods. In: Lagace, P.A., (ed.), Composite Materials: Fatigue and Fracture, 2nd Vol., ASTM STP 1012, American Society for Testing of Materials, Philadelphia, 338-355.

Chatterjee, S. N., Wang, E. C. J., and Yen, C. F. 1993. Modelling ply crack growth in laminates under combined stress states composite materials. In: Stinchcomb, W. W. and Ashbaugh, N. E. (eds.), Fatigue and Fracture, Fourth Volume, ASTM STP 1156, ASTM, Philadelphia, 195-217.

Chen, A. S., and Harris, B. 1993. Fatigue -induced damage mechanisms in carbon fibre-reinforced plastic composites, Journal of Materials Science, Vol. 28, 2013-2027.

Chua, L. O., and Lin, P-M. 1975. Computer-aided analysis of electronic circuits, Prentice-Hall, Inc., New Jersey.

Ciriscioli, P. R. Wang, Q., and Springer, G .S. 1992. Autoclave curing-comparisons of model and test results. Journal of Reinforced Plastics and Composites, Vol. 26, No. 1, 90-102.

Coleman, B. D. 1958. On the strength of classical fibres and fibre bundles. Journal of Mechanics and Physics of Solids, Vol. 7, 60-70.

Conor, P. C., and Owston, C. N. 1969. Electrical resistance of single carbon fibres. Nature, Vol. 223, 1146 and 1147.

Cox, H. L. 1952. The elasticity and strength of paper and other fibrous materials, British journal of applied physics, Vol. 3, 72-79.

Coyle, R. A., and Wicks, B. J. 1974. The structure and mechanical properties of carbon fibres. Metallurgy Note 98, ARL, Melbourne, 26 pages.

Curtis, P. T. 1986. Investigation of the tensile fatigue behaviour of improved carbon fibre composite materials. In: Sixth International Conference on Composite Materials, Vol. 6, Elsevier Applied Science, London.

Curtis, P. T. 1991a. Tensile fatigue mechanisms in unidirectional polymer matrix composite materials. TR 91011, Royal Aircraft Establishment Farnborough, Hampshire, 21 pages.

Curtis, P. T. 1984. A computer model of the tensile failure process in unidirectional fibre composites. TR 84024, Royal Aircraft Establishment, Farnborough, UK. 25 pages.

Curtis, P. T., 1991b. Tensile fatigue mechanisms in unidirectional polymer matrix composite materials. International Journal of Fatigue, Vol. 13, No. 5, 377-382.

Daniel, H. E. 1948. The statistical theory of the strength of bundles of threads. I. Proceedings of the Royal Society, Series A, Vol. 183, 405-435.

Delmonte, J. 1981. Technology of carbon and graphite fiber composites. Van Nostrand Reinhold Company, New York.

Dharan, C. K. H. 1975. Fatigue failure mechanisms in a unidirectional reinforced composite materials. In: Fatigue of Composite Materials, ASTM STP 569, American Society for Testing and Materials, 171-188.

Dillon, R. O., Kirby, R. D. and Spain, I. L. 1989. The electrical noise of carbon fibres. Journal of Applied Physics, Vol. 66, No. 9, 4284-4287.

Dingle, R. B. 1950. The electrical conductivity of thin wires. Proceedings of the Royal Society of London, Series A ,Vol. 201, No. 1067, 545-560.

Dixon, L. A. 1960. Epoxy insulation in new form moulding compound and machine shock. In: National conference on the application of electrical insulation, Third annual , 1960 Chicago, Illuinosis, 27-29.

Ehrburger, P., and Donnet, J. B. 1985. Surface treatment of carbon fibres for resin matrices. In: Watt, W. and Perov, B. V. (eds.) 1985. Strong fibres. Elsevier Science Publishers B.V, Amsterdam, 577-603.

Essam, J. W. 1980. Percolation theory, Reports of Progress in Physics, Vol. 53, No. 7, 833-912.

Fischbach, D. B. 1980. Observations on the properties and structure of carbon fibres. In: Carbon'80, Preprints of 3rd International Carbon Conference, Baden-Baden, 590-597.

Fischbach, D. B., and Komaki, K. 1977. Electrical resistance of carbon fibres. In: Extended Abstracts of 14th Biennial Carbon Conference, Pennsylvania State University, 191-198.

Fisher, Chr., and Arendts, F. J. 1993. Electrical crack length measurement and the temperature dependence of the mode I fracture toughness of carbon fibre reinforced plastics. Composites Science and Technology, No. 46, 319-323.

Fujii, T., and Maekawa, Z. 1979. Study on the fatigue of fiber reinforced composites based on the fatigue damage process of unit model, Bulletin of the JSME, Vol. 22, No. 164, 125-130.

Fuoss, R. M. 1939. Electrical properties of solids. Journal of American Chemical Society, Vol. 61, 2329-2334.

Fuwa, M., Harris, B. and Bunsell, A. R. 1975. Acoustic emission during cyclic loading of carbon-fibre-reinforced plastics. Journal of Physics. D: Applied Physics, Vol. 8, 1460-1471.

Gaier, J. R., Hambourger, P. D., and Slabe, M. E. 1991. Resistivity of pristine and intercalated graphite fiber epoxy composites. Carbon, Vol. 29, No. 3, 313-320.

Gajda, W. J. 1978. Fundamental study of the electromagnetic properties of advanced composite materials. Rome Air Development Center (RBCT), Griffiss AFB NY 13441, RADC-TR 78-158, 44 pages.

Garcia, R., Evans, R. E., and Palmer, R. J. 1987. Structural property improvements through hybridised composites. In: Johnston, N. J. (ed.) Toughened Composites, ASTM STP 937, ASTM, Philadelphia, 1987, 397-412.

Gent, A. N., and Wang, C. 1993. What happens after a fibre breaks-pull-out or resin cracking? Journal of Material Science, Vol. 28, 2494-2500.

Goetchius, G. M. 1987. Fatigue of composite materials. In: Advanced Composites III, Expanding the Technology, Detroit, Proceedings of the 3rd Annual Conference on Advanced Composites, 15-17, September. 1987, ASM, 289-298.

Goodier, J. N. 1933. Concentration of stress around spherical and cylindrical inclusions and flaws, Journal of Applied Mechanics, Transactions of ASME, Vol. 55. APM-55-7, 39-44.

Gottesman, T., Hashin, Z., and Brull, M. A. 1980. Effective elastic moduli of cracked fiber composites. In: Bunsell, A. R. et al. (eds.), Advances in composite materials, Third International Conference on Composite Materials, Paris, France, Pergamon Press, Oxford, 749-758.

Guigon, M., Oberlin, A., Desarmot, G. 1984. Microtexture and structure of some high-modulus, PAN-base carbon fibers. Fiber Science and Technology, Vol. 20, 177-198.

Hahn, H. T. 1979. Fatigue behaviour and life prediction of composite laminates. In: Composite Materials: Testing and Design, Fifth Conference, ASTM STP 674, 383-417.

Harris, B. 1977. Fatigue and accumulation of damage in reinforced plastics. Composites, Vol. 8, No. 4, 214-226.

Harris, B., Reiter, H., Adam, T., Dickson, R. F., and Fernando, G. 1990. Fatigue behaviour of carbon fibre reinforced plastics. Composites, Vol. 21, No. 3, 232-242.

Hashin, Z. 1968. Assessment of the self consistent scheme approximation: conductivity of particulate composites, Journal of Composite materials, Vol. 2, 284-300.

Hashin, Z. 1986. Analysis of stiffness reduction of cracked cross-ply laminates. Engineering Fracture Mechanics, Vol. 25, Nos. 5/6, 771-778.

Henaff-Gardin, C. and Lafarie-Frenot, M. C. 1991. Fatigue crack propagation in transverse plies of long fibre reinforced composite laminates. In: Baptiste, D. (ed.), Mechanics and Mechanisms of Damage in Composites and Multi-Materials, ESIS11, Mechanical Engineering Publication, London, 55-66.

Highsmith, A. L., and Reifsnider, K. L. 1982. In: Reifsnider, K. L., (ed.) Damage in Composite materials: Basic Mechanisms, Accumulation, Tolerance and Characterization, ASTM-STP 775, 40-62.

Hwang, W., and Han, K. S. 1989. Fatigue of composite materials - damage model and life prediction. In: Lagace, P.A. (ed.), Composite Materials: Fatigue and Fracture , Second Volume, ASTM STP 1012, American Society for Testing and Materials, Philadelphia, 87-102.

Jamison, R. D. 1985. The role of microdamage in tensile failure of graphite/epoxy laminates. Composites Science and Technology, Vol. 24, 83-99.

Jaussaud, J. A. M. 1992. Toughness transfer between unreinforced matrix and fibre composites. PhD Thesis, Cranfield university, Bedford, UK.

Jaworske, D. A., Vannucci, D. R., and Zinolabedini, R. 1987. Mechanical and electrical properties of graphite fiber-epoxy composites made from pristine and bromine intercalated fibers. Journal of Composite Materials, Vol. 21, 580-592.

Johnson, J. B. 1928. Thermal agitation of electricity in conductors, Physical Review, Vol. 32, 97-109.

Johnson, W. 1985. The structure of PAN based carbon fibres and relationship to physical properties. In: Watt, W. and Perov, B. V. (eds.), Strong fibres. Elsevier Science Publishers B.V, Amsterdam, 389-443.

Jones, F. L. 1957. The physics of electrical contacts. The Clarendon Press, Oxford.

Jones, R. M. 1975. Mechanics of composite materials, McGraw-Hill, New York.

Joy, T., and Strieder, W. 1979. Percolation in a thin ply of unidirectional composite. Journal of Composite Materials, Vol. 13, 72-78.

Joy, T., Ajmera, P., and Strieder, W. 1980. Effect of thickness on single ply percolation and conductivity. Journal of Composite Materials. Vol. 14, 130-141.

Kachanov, L. M. 1958. On the creep rupture time, TVZ. A. N. SSR, Otd, Tekhn. Nauk 8, 26-31.

Kaddour, A. S., Al-Salehi, F. A. R., Al-Hassani, S. T. S., and Hinton, M. J. 1994. Electrical resistance measurement technique for detecting failure in cfrp materials at high strain rates. Composites Science and Technology, Vol. 51, 377-385.

Kam, C. Y. and Walker, J. V. 1987. Toughened composites selection criteria. In: Johnston, N. J. (ed.), Toughened composites, ASTM STP 937, ASTM, Philadelphia, 9-22.

Kamimura, K. 1985. Continuum damage approach to mechanical behaviour of damaged laminate and a modelling of damage parameter. In: Cardon, A. H. and Verchery, G. (eds.), Mechanical Characterisation of Load Bearing Fibre Composite Laminates, Elsevier, London, 115-126.

Kelly, A., and Parkhouse, G. 1993. Fibre packing in three dimensions. In: In: Sixth International Conference on Composite Materials, Vol. 6, Elsevier Applied Science, London, 231-236.

Kemp, M. 1994. Self-sensing composites for smart damage detection using electrical properties, In: Second European Conference on Smart structures and Materials, Glasgow, 12-14 October 1994. 136-139.

Kerner, E. H. 1956a. The elastic and thermo-elastic properties of composite media. Proceedings of the Physical Society of London, B69, No. 8, 808-813.

Kerner, E. H. 1956b. The electrical conductivity of composite media. Proceedings of the Physical Society of London, B69, No. 8, 802-812.

Kinchin, G. H. 1953. The electrical properties of graphite. Proceedings of the Royal Society of London, Series A, Vol. 217, 9-26.

Kirkpatrick, S. 1973. Percolation and conduction. Reviews of Modern Physics, Vol. 45, No. 4, 574-588.

Knibbs, R. H., and Morris, J. B. 1974. The effects of fibre orientation on the physical properties of composites. Composites, Vol. 5, 209-218.

Knibbs, R. H., Baker, D. J., and Rhodes, G. 1971. The thermal and electrical properties of carbon fibre uni-directional reinforced epoxy composites. In: 26th Annual Technical Conference, Reinforced Plastics/Composites Division, The Society of the Plastics Industry, Inc., Section 8-F, 1-10

Konkin, A. A., 1985. Properties of carbon fibres and fields of their application. In: Watt, W. and Perov, B. V. (eds.) 1985. Strong fibres. Elsevier Science Publishers B.V, Amsterdam, 241-273.

Konur, O., and Mathews, F. L. 1989. Effect of the properties of the constituents on the fatigue performance of composites: a review. Composites, Vol. 20, No. 4, 317-328.

Krajcinovic, D. 1984. Continuum Damage Mechanics. Applied Mechanics Reviews, Vol. 37, No. 1, 1-6.

Kroschwitz, J. I. 1988. Electrical and electronic properties of polymers: a state-of-the-art compendium. John Wiley and sons, New York.

Kung, J. T., and Amason, M. P. 1978. Electrical conductive characteristics of graphite composite structures. In: 19th International Symposium on Electromagnetic Compatibility, IEEE, Seattle, Washington, 2-4 August, 1977. IEEE 77CH1231-0EMC, 403-408.

Laws, N., Dvorak, G. J., and Hejazi, M. 1985. Stiffness changes in unidirectional composites caused by crack systems. Mechanics of Materials, Vol. 2, 123-137.

Lee. H., and Neville. K. 1967. Handbook of epoxy resin. McGraw-Hill book company, New York.
Li, P., Strieder, W., and Joy, T. 1982. Random lattice electrical conductivity calculations for a graphite/epoxy ply of finite thickness. Journal of Composite Materials, Vol. 16, 53-64.

Liebmann, W. K. and Miller, E. A. 1963. Preparation, phase-boundary energies, and thermoelectric properties of InSb-Sb eutectic alloys with ordered microstructures. Journal of Applied Physics, Vol. 34, No. 9, 2653-2659.

Littlewood, S., and Briggs, B. F. N. 1978. Investigation of current-interruption by metal-filled epoxy resin. Journal of Physics D, Vol. 11, 1457.

Lodge, K. J. 1982. Electrical properties of joints in carbon fibre composites, Composites, Vol. 13, 305.

Lovell, D. R. 1986. A comparison of available carbon fibers. In: Carbon fibres technology, uses and prospects, edited by The plastics and Rubber Institute, London, Noyes Publications, New Jersey, 39-47.

Lovell, D. R. 1991. Carbon and high-performance fibres directory. Chapman & Hall, London.

Lu, T. J., and Chow, C. L. 1992. A constitutive theory of matrix cracking and interply delaminations in orthotropic laminated composites. Journal of Reinforced Plastics and Composites, Vol. 11, No. 5, 494-536.

Martin, B. G. 1977. The electrical behaviour of thermosetting epoxy resins during the cure cycle. Materials Evaluation, Vol. 35, No. 6, 48-50 & 55.

Miller, M. 1969. Bounds for effective electrical, thermal and magnetic properties of heterogeneous materials. Journal of Mathematical Physics, Vol. 14, No. 11, 1988-2004.

Miwa, M., and Endo, I. 1994. Critical fibre length and tensile strength for carbon fibre-epoxy composites. Journal of Materials Science, Vol. 29, 1174-1178.

Moriya, K., and Endo, T. 1990. A study on flaw detection method for cfrp composite laminates (Ist report): the measurement of crack extension in CFRP composites by electrical potential method. Transactions of the Japan Society of Aero Space Science, Vol. 32, No. 98, 184-196.

Nairn, J. A. and Hu, S. 1994. Matrix microcracking, In: Talreja, R. (ed.), Damage mechanics of composite materials, Elsevier Science B.V., Amsterdam. 187-243.

Nedele, M. R., and Wisnom, M. R. 1994. Three-dimensional finite element analysis of the stress concentration at a single fibre break. Composites Science and Technology, Vol. 51, 517-524.

Nicodemo, L., Nicolais, G., Romeo, G., and Scafora, E. 1978. Temperature effect o the electrical resistivity of metal/polymer composites. Polymer Engineering and Science, Vol. 18, 293.

O'Brien, T. K. 1982. Characterization of delamination onset and growth in a composite laminate. In: Damage in Composite Materials, ASTM STP 775, ASTM, Philadelphia, 140-167.

OBrien, T. K., and Salpekar, S. A. 1993. Scale effects on the transverse tensile strength of graphite/epoxy composites. In: Camponeschi, E. T. (ed.), Composite materials: Testing and Design, Vol. 11, ASTM STP 1206, ASTM, Philadelphia, 23-52.

Ochiai, S., Schulte, K., and Peters, P. W. M. 1991 Strain concentration factors for fibres and matrix in unidirectional composites, Composites science and Technology, Vol. 41, 237-265.

Ott, H. W. 1988. Noise reduction techniques in electronic systems. John Wiley & Sons, New York.

Owen, M. J. 1974. Fatigue of carbon-fiber reinforced plastics. In: Broutman, L. J. (ed.), Fracture and Fatigue, Academic Press, New York and London, 341-369.

Owen, M. J., and Morris, S. 1970. Fatigue behaviour of orthogonally cross-plied carbon-fibre-reinforced plastics under axial loading. In: 25th S.P.I , Washington, D. C., Section 8E, Paper No. 51.

Owston, C. N. 1970. Electrical properties of single carbon fibres. British Journal of Applied Physics: 3. Physics.D, Vol. 3, 1615-1626.

Paluch, B. 1993. Analysis of geometric imperfections in unidirectionally reinforced composites. In: Sixth International Conference on Composite Materials, Vol. 6, Elsevier Applied Science, London, 305-310.

Pass, M. H. J. W., Schreurs, P. J. G., Oomens, C. W. J., and Janssen, J. D. 1991. A stochastic approach to fatigue damage modelling. In: Baptiste, D. (ed.), Mechanics and mechanisms of Damage in Composites and Multi-Materials, ESIS11, Mechanical Engineering Publications, London, 159-170.

Peirce, F. T. 1926. Tensile tests for cotton yarns - The weakest link, Theorems on the strength of long and of composite specimens, Journal of the Textile Institute, Vol. 17, T355-368.

Petitpas, E., Renault, M,. and Valentin, D. 1989. Fatigue damage mechanisms in $(0,90)_s$ composite laminate. Journal of Materials Science Letters, Vol. 8, 1029-1031.

Petitpas, E., Renault, M. and Valentin, D. 1990. Fatigue behaviour of cross-ply CFRP laminates made of T300 or T400 fibres. International Journal of Fatigue, Vol. 12, No. 4, 245-251.

Poursartip, A., and Ashby, M. F. 1983. The fatigue damage-mechanics of carbon-fibre reinforced laminates. CUED/MATS/TR.101, Cambridge University

Prabhakaran, R. 1990. Damage assessment through electrical resistance measurement in graphite fiber reinforced composites. Experimental Techniques, 16-20.

Przyluski, J. 1991. Conducting polymers - electrochemistry, Sci-Tech Publications, Brookfield, USA.

Purslow, D., and Childs, R. 1986. Autoclave moulding of carbon fibre-reinforced epoxies. composites, Vol. 17, No. 2, 127-136.

Rask, O. N., and Robinson, D. A. 1988. Graphite as an embedded strain gauge material-technical note. SAMPE Journal, 52-55.

Razvan, A., Simonds, R. A., Reifsnider, K. L., and Stinchcomb, W. W. 1992. Effects of load train alignment on the fatigue characteristics of unidirectional graphite/epoxy composite materials. Journal of Reinforced Plastics and Composites, Vol. 11, No. 3, 310-323.

Razwan, A., and Reifsnider, K. L. 1989. Influence of fibre fracture on the response of unidirectional composite laminates-I, In: Proceedings of the American Society for Composites, 4th Technical Conference on Composite Materials, Blacksburg, VA, October 3-6, Virginia Polytechnic Institute and State University, 791-801.

Reifsnider, K. L., Stinchcomb, W. W., and O'Brien, T. K. 1977. Frequency effects on a stiffness-based fatigue failure criterion in flawed composite specimens. In: Reifsnider, K. L. and Lauraitis, K. N., (eds.), Fatigue of Filamentary Composite Materials, ASTM STP 636, American Society for Testing and Materials, 152-170.

Reifsnider, K. L. 1977. Some fundamental aspects of fatigue and fracture response of composite materials. In: 14th Annual Meeting of Society of Engineering Science, Lehigh University, Bethlehem, PA. November 1977.

Reifsnider, K. L. (ed.). 1991. Fatigue of composite materials. Vol. 4, Composite Material series, Elsevier, Amsterdam.

Reifsnider, K. L., and Gao, Z. 1991. A micromechanics model for composites under fatigue loading. International Journal of Fatigue, Vol. 13, No. 2, 149-156.

Reifsnider, K. L. and Highsmith, A. L. 1982. The relationship of stiffness changes in composite laminates to fracture-related damage mechanisms. In: Proceedings of the Second USA-USSR symposium, Bethlehem, USA, March 1981, Martinuus Nijhoff Publishers, Hague, 279-290.

Reifsnider, K. L., Schulte, K., and Duke, J. C. 1983. Long-term fatigue behaviour of composite materials. In: O'Brien, T. K. (ed.), ASTM STP 813, American Society of Testing and Materials, Philadelphia, 136-159.

Renard, J., Favre, J. P., and Jeggy, Th. 1993. Influence of transverse cracking on ply behaviour: introduction of a characteristic damage variable. Composites Science and Technology. Vol. 46. 29-37.

Reynolds, W. N. 1973. Structure and physical properties of carbon fibers. In: Walker, P. L., and Thrower, P. A., (eds.), Chemistry and Physics of Carbon, Vol. 11, Marcel Dekker, Inc., New York. 1-67.

Robinson, D. A. 1987. Failure modes in composite materials. AD-A182 527, Trident scholar project report. United states Naval Academy, Annapolis, Maryland, 54 pages.

Robson, D., Assabghy, F. Y. I. and Ingram, D. J. E. 1972. Some electronic properties of Polyacrylonitrile-based carbon fibres. Journal of Physics D: Applied Physics, Vol. 5, 169-179.

Rosen, B. W. 1964. Tensile failure of fibrous composites, AIAA Journal, Vol. 2, No. 11, 1985-1991.

Ruschau, G. R., and Newnham, R. E. 1992. Critical volume fractions in conductive composites. Journal of Composite Materials, Vol. 26, No. 18, 2727-2735.

Saunders, G. A. 1970. Electron transport in graphites and carbons. In: Blackman, L. C. F. (ed.), Modern aspects of graphite technology, Academic Press, London.

Schulte, K., and Stinchcomb, W. W. 1989. Damage mechanisms-including edge effects- in carbon fibre-reinforced composite materials. In: Friedrich, K. (ed.), Applications of Fracture Mechanics to Composite Materials, Elsevier Science Publishers B.V., Amsterdam, 273-325.

Schulte, K., and Baron, Ch. 1989. Load and failure analysis of cfrp laminates by means of electrical resistivity measurements. Composites Science and Technology, Vol. 36, 63-76.

Seanor, D. A. 1982. Electrical properties of polymers, Academic press, London.

Sendeckyi, G. P. 1991. Life prediction for resin-matrix composite materials. In: Reifsnider, K. L. (ed.). Fatigue of composite materials. Vol. 4, Composite Material series, Elsevier, Amsterdam, 431-483.

Shackelford, J. F. 1992. Introduction to materials science for engineers, Macmillan Publishing Company, New York.

Sharbaugh, A. H. 1965. Introduction to electrical property tests. In: Schmitz, J. V. (ed.), Testing of polymers, Vol. 1, Interscience Publishers, New York.

Shindo, A. 1961. Studies on graphite fibre. Report 317, Governmnet Research Institute, Osaka, Japan.

Simmons, J. G. 1984. Electronic Conduction through thin insulating films. In: Maissel, L. I., and Glang, R. (eds.), Handbook of Thin Film Technology. McGraw-Hill book Company, New York,

Simonds, R. A., Bakis, C. E., and Stinchcomb, W. W. 1989. Effects of fatigue response of graphite fiber composite laminates. In: Lagace, P.A. (ed.), Composite Materials: Fatigue and Fracture, Second Volume, ASTM STP 1012, ASTM, Philadelphia, 5-18.

Singh, D. B., Kumar, A., Tayal, V. P., and Sanyal, B. 1988. Effect of moisture and electronic packaging exalates on the electrical conductivity of epoxy laminate. Journal of Material Science, Vol. 23, No. 8, 3015-3025.

Smith, R. L., Phoenix, S. L., Greenfield, M., Henstenburg, R. B., and Pitt, R. 1983. Lower tail approximations for the probability of failure of three-dimensional fibrous composites with hexagonal geometry. Proceedings of the Royal Society of London, Series A, Vol. 388, No. 1795, 353-391.

Sobol, I. M. 1967. On the distribution of points in a cube and the approximate evaluation of integrals. Computational Mathematics and Mathematical Physics, Vol. 7, No. 4, 86-112.

Sobol, I. M. 1976. Uniformly distributed sequences with and additional uniform property. Computational Mathematics and Mathematical Physics, Vol. 16, No. 5, 236-242.

Sobol, I. M. 1979. On the systematic search in a hypercube. SIAM Journal of Numerical Analysis, Vol. 16, No. 5, 790-793.

Springer, G. S., Mashtizadeh, S. A., and Keller, R. B. 1979. Electrical hazards posed by graphite fibers. Journal of Composite Materials, Vol. 13, 225-231.

Steif, P. S. 1984. Stiffness reduction due to fiber breakage. Journal of Composite Materials.

Stinchcomb, W. W., and Bakis, C. E. 1991. Fatigue behaviour of composite laminates. In: Reifsnider, K. L. (ed.). Fatigue of composite materials. Vol. 4, Composite Material series, Elsevier, Amsterdam, 105-180.

Stone, D. E. W. 1971. The use of radiography in the non-destructive testing of composite materials. Royal Aircraft Establishment Farnborough, RAE TR 71235.

Sturgeon, J. B. 1978. Fatigue mechanisms, characterisation of defects and their detection in reinforced plastics materials, British Journal of NDT, 303-310.

Summerscales, J. 1990. Electrical and magnetic testing. In: Summerscales, J. (ed.), Non-destructive testing of Fibre-Reinforced Plastics Composites, Vol. 2, Elsevier Applied Science, London, 253-297.

Talreja, R. 1981. Fatigue of composite materials and fatigue-life diagrams. Proceedings of the Royal Society of London, Series A, Vol. 378, 461-475.

Talreja, R. 1985a. A continuum mechanics characterization of damage in composite materials. Proceedings of the Royal Society of London, Series A, Vol. 399, 195-216.

Talreja, R. 1985b. A conceptual framework for interpretation of fatigue damage mechanisms in composites. Journal of Composites Technology and Research, Vol. 71, 25-29.

Talreja, R. 1986. Stiffness properties of composite laminates with matrix cracking and interior delamination. Engineering Fracture Mechanics, Vol. 25, Nos. 4/5, 751-762.

Talreja, R. 1987. Fatigue of composite materials. Technomic Publishing Company, Inc., Pennsylvania, USA.

Talreja, R. (ed.), 1994. Damage mechanics of composite materials, Composite materials series, Vol. 9, Elsevier, Amsterdam.

Tarnopol'skii, Y. M. and Kincis, T. 1985. Static test methods for composites. Van Nostrand Reinhold Company. New York.

Taya, M., and Ueda, N. 1987. Predication of the in-plane electrical conductivity of a misoriented short fiber composite: fiber percolation model versus effective medium theory. Transactions of the ASME, The Journal of Engineering. Materials and Technology, Vol. 109, No. 3, 252-256.

Thiagarajan, C. 1989. Flaw detection and characterization of fiber reinforced composites using ultrasonics, M. Tech Thesis, Indian Institute of Technology, Bombay, India, 106 pages.

Thiagarajan, C., and Irving, P. E. 1994. In service damage monitoring techniques in polymer composites. In: Aerotech Conference Proceedings, Seminar 37, Paper No. C470/37/159. 7 pages.

Thiagarajan, C., Sturland, I., Tunnicliffe, D., and Irving, P. E. 1994. Electrical potential techniques for damage sensing in composite structures. In: Second European Conference on Smart structures and Materials, Glasgow, 12-14 October 1994. 128-131.

Thomson, L. F., Willson, C. G., Bowden, M. J. (eds.) 1994. Introduction to microlithography, American Chemical Society.

Thorne, D. J. 1985. Manufacture of carbon fibre from PAN. In: Watt, W. and Perov, B. V. (eds.) 1985. Strong fibres. Elsevier Science Publishers B.V, Amsterdam, 475-494.

Till, S. J., Brown, A. G., and Deshmukh, V. G. I. 1985. Reactive ion etching of polymide for multi-level resist and contact hole applications. Microelectronic Engineering, Vol. 3, 491-498.

Tohgo, K., Wang, A. S. D., and Chou, T. W. 1993. A criterion for splitting crack initiation in unidirectional fiber-reinforced composites. Journal of Composite Materials, Vol. 27, No. 11, 1054-1076.

Tse, K. W., Moyer, C. A., and Arajs, S. 1981. Electrical conductivity of graphite fiber-epoxy resin composites. Materials Science and Engineering, Vol. 49, 41-46.

Ueda, N., and Taya, M. 1986. Prediction of the electrical conductivity of two-dimensionally misoriented short fiber composites by a percolation model. Journal of Applied Physics, Vol. 60, No. 1, 459-461.

Volpe, V. 1980. Estimation of electrical conductivity and electromagnetic shielding characteristics of graphite/epoxy laminates. Journal of Composite Materials, Vol. 14, 189-198.

Wang, S. J., Baptiste, D., Bompard, Ph., and Francois, D. 1991. Microscopic failure mechanisms of an unidirectional glass fiber composite. Fatigue and Fracture of Engineering Materials, Structures, Vol. 14, No. 4, 391-403.

Wang, S. J., Baptiste, D., Bompard, Ph., and Francois, D. 1991. Fatigue damage mechanisms of a uni-directional glass-fibre-reinforced composite. In: Baptiste, D. (ed.), Mechanics and Mechanisms of Damage in Composite Materials and Multi-Materials, ESIS11, Mechanical Engineering Publications, London, 3-15.

Warfield, R. W, 1965. Characterization of polymers by electrical resistivity techniques, In: Schmitz, J. V. (ed.), Testing of polymers, Vol. 1, Interscience Publishers, New York.

Watt, W., and Johnson, W. 1966. High strength high modulus carbon fibres. The Engineer, Vol. 221, 815-821.

Watt, W., and Perov, B. V. (eds.) 1985. Strong fibres. Elsevier Science Publishers B.V, Amsterdam.

Weibull, W.. 1939. A statistical theory of the strength of materials, Ingeniors Vetenskaps Akademien, Handlingar, No. 151.

Wierzbicki, T., and Jones, N. 1989. Structural failure, John Wiley & Sons, Inc., New york.

Wilkins, D. J., Eisenmann, J. R., Camin, R. A., Margolis, W. S. and Benson, R. A. 1982. Characterizing delamination growth in graphite-epoxy. In: Reifsnider, K. L., (ed.) Damage in Composite materials: Basic Mechanisms, Accumulation, Tolerance and Characterization, ASTM-STP 775, 168-173.

Williamson, N. J., Kemp, R. M. J., and Curtis, P. T. 1994. Development of self-sensing 'smart' composites using electrical resistance properties. In: Sixth International Conference on Fibre Reinforced Composites, FRC 94, Newcastle, 1994, paper 17, Published by The Institute of Materials, London, 1-10.

Wolla, J. M., and Goree, J. G. 1987. Experimental evaluation of longitudinal splitting in unidirectional composites. Journal of Composite Materials, Vol. 21, 49-67.

Xia, Y., Yuan, J., and Yang, B. 1994. A statistical model and experimental study of the strain-rate dependence of the strength of fibres, Composites Science and Technology, Vol. 52, 499-504.

Yang, J. N., and Jones, D. L.. 1981. Load sequence effects on the fatigue of unnotched composite materials. In: Fatigue of Fibrous Composite Materials, ASTM STP 723, ASTM, Philadelphia, 213-232.

Yang, J. N. and Jones, D. L.. 1983. Load sequence effects on graphite/epoxy $[\pm 35]_{2s}$ laminates. In: O'Brien, T. K. (ed.), Long-Term Behaviour of Composites, ASTM STP 813, ASTM, Philadelphia, 246-262.

Yasin, M. J., El-Rihail, I., Ahmad, M. S., and Zihlif, A.M. 1987. The temperature dependence of the electrical resistivity of Celion carbon fibres. Materials Science and Engineering, Vol. 86, No. 1, 205-210.

Yen, C.-F. and Buesking, K. W. 1993. Material modelling for unidirectional glass and glass-ceramic matrix composites with progressive matrix damage. In: Stinchcomb, W. W. and Ashbaugh, N. E. (eds.), Composite Materials: Fatigue and Fracture, Fourth Volume, ASTM STP 1156, ASTM, Philadelphia, 176-194.

Zienkiewicz. O. C., and Taylor, R. L. 1989. The finite element methods. Fourth edition, Vol. 1, McGraw-Hill Book Company, London.

Ziman, J. M. 1960. Electrons and phonons: The theory of transport phenomena in solids, The Clarendon Press, Oxford.

Zweben, C., and Rosen, B. W., 1970. A statistical theory of material strength with application to composite materials. Journal of mechanics and Physics of solids, Vol. 18, 189-206.

Zweben, C. 1968. Tensile failure of fiber composites. AIAA Journal, Vol. 6, No. 12, 2325-2321.

APPENDIX

A

DAMAGE MODELS

This appendix is concerned with literature review of damage models and the proposed damage model. The literature review of the damage mechanics and micro-mechanics based damage models are described. This appendix also presents the details of a proposed fibre fracture damage model and the relevant results.

A.1. LITERATURE REVIEW

A brief introduction about the damage models is given in section 2.5. Models based on damage mechanics approach are classified according to their formulation into two, as listed below,

1. Continuum damage mechanics based models
2. Micro mechanics based models.

A.1.1. Continuum damage model

These models are based on continuum damage mechanics. Continuum damage mechanics (CDM) is defined as a branch of continuum solid mechanics. The formulation is based on the introduction of special field variables representing the ideal distribution of damage (Krajcinovic 1984). For example, changes in stiffness can be considered as a representation of damage. There are two types of CDM model. The first one follows the three steps (Model I):

1. Definition of internal variables, indicators of the mechanisms under consideration.
2. Constitutive equations involving the influence of these mechanisms on the behaviour of the materials.

3. Evolution equations describing their kinetics as a function of the applied mechanical loading.

The second type of model (Model II) is introduced in conjunction with CDM approach in classical lamination theory (CLT). It follows essentially the same step as the first one with a modified CLT between steps' two and three. In the final steps fatigue failure theories are used for life prediction.

CDM models based on damage mechanics were first used by Kachanov in 1958 for creep fatigue of metals. After that many researchers have successfully applied this concept for various fatigue problems in metals. The development of this approach in fatigue of metals is given by Krajcinovic (1984) in his recent review.

Talreja (1987) extended the concept of damage mechanics to composite materials. This type of model follows the steps as described in method I. In his work the damage was defined by a set of damage entities with various orientations and growth characteristics and to each damage mode, a vectorial quantity was assigned. Stiffness degradation of composite laminates of different stacking sequences due to the presence of damage was then obtained using the principles of continuum thermodynamics of irreversible processes. Many authors (Allen et al. 1990; Bonora et al. 1992) approached this problem in a similar way to Talreja with some modifications. More recently, Lu and Chou (1991) proposed a constitutive theory similar to the above approach.

Allen et al. (1990) in their series of papers incorporated classical lamination theory in conjunction with the damage mechanics approach. They developed a damage dependent constitutive equation at ply level. Kamimura (1985) used the effective stress concept to describe the damage behaviour. This model follows the steps as described in the model II.

The above are the two main types of CDM models. There are some other models that follow same general procedure with little modification. For example, Pass et al. (1991) proposed a model with damage variables based on a stochastic approach.

A.1.2. Micromechanics models

In the micromechanics approach a representative volume element (RVE) or a unit cell is constructed, in which the material configuration details such as fibre diameter and spacing, fibre orientation, ply thickness and orientation as well as the damage configuration details such as size, shape, orientation of cracks, voids, debonds etc. are incorporated.

After the formulation of RVE or unit cell a boundary value problem is formulated. The solution of this boundary value problem yields the damage response functions. The micromechanics approach characterises the damage directly and unambiguously. Its accuracy in determining the damage response is limited by the accuracy of solving the associated boundary value problem. Micromechanics models generally use fatigue failure theories to predict the fatigue life, when the fatigue characteristics of the individual laminas are known.

The literature on this type of model is very limited. The reason may be because of the additional complexities induced by material anisotropy and non-linearity. It may require elaborate numerical analyses, which inturn leads to large-scale super computing requirements. The important models are discussed below.

Reifsnider and Gao (1991) proposed two fatigue failure equations for fibre and matrix damage by considering the stresses in the fibre and matrix and with failure functions. They have proposed a model at micromechanics level. In this model fibres are considered as ellipsoidal inhomogenities in a matrix. They have developed a fatigue failure criterion for fibre failure and matrix cracking involving the stress in the fibres, the matrix and with an experimental fatigue failure function. They have applied the proposed model to unidirectional E-glass/Epoxy laminae under off-axis loading. They suggest that the formulation can be generalised.

Chamis et al. (1989) have proposed a simplified predictive method based on micromechanics and ply-influence coefficients. They have developed simplified equations to determine the ply-fatigue uniaxial stress at initial defect growth by knowing the other variables such as the service environment temperature and number of cycles. They suggest that such simplified theories are suitable for preliminary design. This model claims to be based on a micromechanics approach, but the derivation and the basic details are nor provided.

Fujii and Maekawa (1979) investigated the characteristic fatigue behaviour by studying the number of cycles to failure, the reduction in rigidity and residual strength in three type of composites (UD, CMRP, and WFRP). They have proposed a `unit damage model' using a fracture mechanics approach. This can be considered as a micromechanics model because it involves the ply thickness and volume fraction. The unit model has been considered as equivalent to a model consisting four springs with pin joint in centre. The stress strain relation and modulus of elasticity equation are given. They have described the fracture strength by Weibull distribution. Finally they derived failure mechanism equations for the three different

composites. Also they show that the experimental results agrees fairly well with experimental data.

A.2. PROPOSED FIBRE FRACTURE DAMAGE MODEL

The damage mechanisms of unidirectional composites are fibre fracture, matrix and interfacial damage. Fibre fracture is a major damage mechanism controlling the life of a laminate (Talreja 1987). However, it is the least studied and therefore least understood of all the fatigue damage mechanisms (Bathias 1989). Moreover, fibre composites are designed in such a way that most of the load is carried by the fibre. The load direction in many practical engineering applications is fibre dominated. Hence the fibre fracture may result in significant disturbances in the stress field. It is reported that at high stress level fatigue, fibre fractures are the dominant failure mechanism (Reifsnider 1991). In this work a damage model is proposed that is based on fibre fracture as the major damage mechanism.

A.2.1. Formulation

The formulation is based on Kachanov's damage mechanics approach. It is assumed that the applied stress is taken by the major load carrying member the fibre. The effective stress or the internal stress, $\sigma_{INT,}$ due to the applied stress, $\sigma_{APP,}$ can be written as follows.

$$\sigma_{INT} = \frac{\sigma_{APP}}{(1-D)}$$

Where, D is the damage parameter. In our case, D is the damage parameter indicating number of fibre breaks. When there are no fibre breaks, say at the start of the test the applied stress σ_{APP} equals to the internal stress σ_{INT} and D is equals to 0. The value of D becomes 1 when all the fibres are broken. During fatigue cycling the peak applied stress remains constant and fibre breaks are expected. It is assumed that after the fibre breaks the applied stress is redistributed to the remaining fibres. The stress is equally shared by the remaining fibres.

The effect of fibre breaks can be introduced in the above equation as the reduction in the cross sectional area. The total number of fibres in the laminates can be calculated using 'rule of mixtures'. The cross sectional area of the specimen can be modified as shown below to include the effects of fibre breaks.

$$A_{DAM} = a_f . V_f . N$$

Where, a_f, is the cross sectional area of single fibre, V_f, is Volume fraction and, N, is the total number of fibres.

A.2.2. Damage evolution

The damage evolution equation describes the damage process due the applied cyclic stress. In this case this equation (dD/dN) has to model the evolution of fibre breaks.

$$dD/dN = f(\sigma_{APP}, \text{Fibre breaks})$$

The damage evolution law in our case is that at least one fibre breaks per cycle. This assumption may not be realistic. However, this provides minimum possible fibre breaks and hence to calculate the minimum fatigue life. This sets the lower bounds for fatigue life prediction.

The time dependent phenomenon of fibre breaks can be used to support the above assumption (Reifsnider 1991). Fibre breaks are expected during fatigue. The stress wave created by the fibre breaks travels away from the fracture position at the speed of sound in the direction of wave propagation in that material. Information on the stress distribution caused by the fracture can travel to the neighbouring material at a rate limited by that propagation speed. So, there is an inherent limitation in the rate at which the fibre breaks in one position can cause break in another position by stress redistribution. Also, if we consider the fact that the distribution of fibre strength is statistical and, therefore the distance to the next statistically stronger fibre may be several hundred fibre diameters or more. And more over the load may by diminishing because of its cyclic nature. So during the time of travel it is possible that the next fibre to break as a result of stress redistribution may not fracture until the next loading cycle. So, It is reasonable to assume that the number of fibre breaks will be at least one per cycle.

A.2.3. Failure criterion

On the first application of the maximum stress the fibre having lower strength than the applied stress fails. Repeated application of the stress results in fibre breaks adjacent to the previously broken fibres. The load shed by the broken fibre is shared equally by the remaining fibres. This process continues till the stress in the remaining cross sectional area reaches its maximum load carrying capacity. At this point the remaining fibres in the specimen are no longer able to carry the applied load and hence the specimen will fail.

This model can be further improved by taking into account of the strength contribution of the broken fibre and the contribution of the matrix. Also if the fibre breaks are at different location it does not affect the other location. The fibre break continues in different region and the final failure occurs when all the fibres in one region breaks. This phenomenon can also be included in the above model. This model can also be generalised by considering the other damage mechanisms.

A.2.4. Results and discussion

The predicted life by the this proposed model and the experimental results at different stress level are shown in Figure. A.1. This model was developed based on fibre fracture. Fibre breaks are expected at higher stress level. Therefore, this model compares very well with the experimental results at high stress level fatigue.

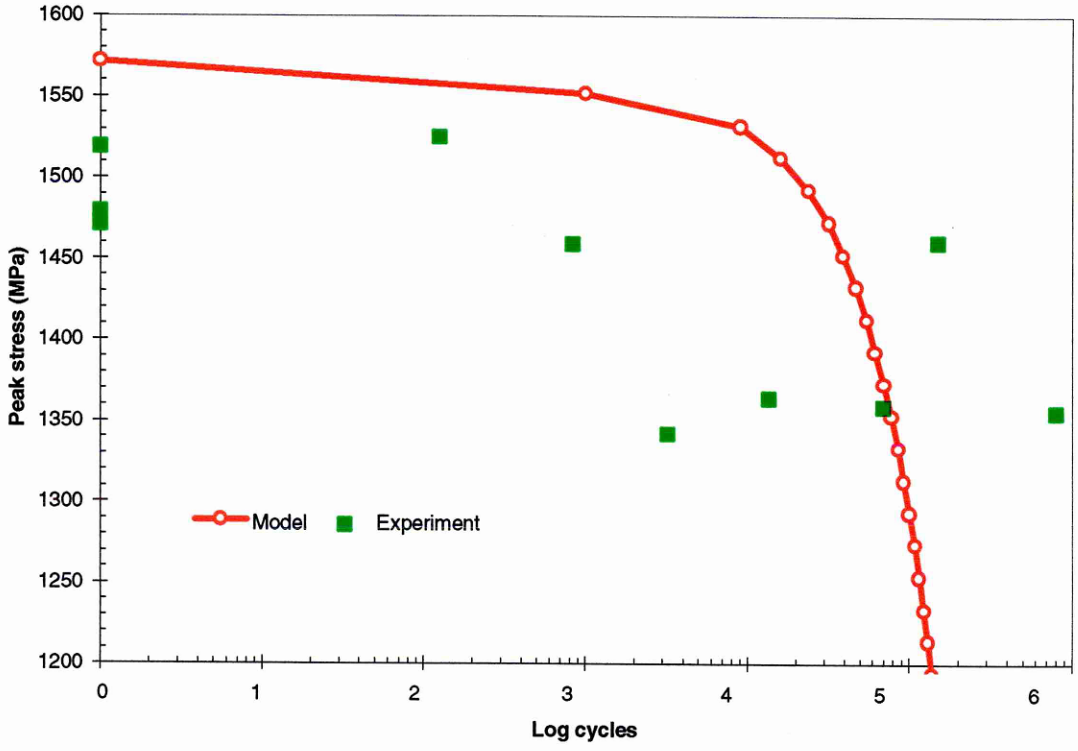

Figure A.1. Comparison of experimental results and the life predicted using the proposed model.

B

SPECIMEN DESIGN-
FINITE ELEMENT ANALYSIS

A two-dimensional plane stress finite element analysis was conducted using IDEAS finite element analysis software to assess the severity of transition from a constrained biaxial stress state at the grip line to a uniaxial stress state in the test section for unidirectional laminates. The main objective of this investigation was to determine if the influence of the grip region on the stress state in tension specimens could explain the observed tendency for the distribution of failures skewed toward the grip line of 0° unidirectional tensile tests.

The effects of the grip was simulated by constraining the axial and transverse displacements at one end of the sample. A uniform stress was applied at the opposite end to simulated the central region of the samples. The laminate design module available with IDEAS was used to model the unidirectional laminate. The properties predicted by this module were corrected and or verified using the experimental values reported in chapter 9. This model was simulated for UD914L samples for a applied uniaxial stress of 1000 MPa. The sample dimensions and boundary conditions are shown in Figure B.1. The FEM model was meshed using four-noded shell element with a uniform size of 5 x 5 mm.

The finite element analysis results are shown in Figure B.2. These results clearly shows the stress concentrations near the grip due to the biaxial stress state. Figure B.2 shows the axial stress distribution of unidirectional laminate. It can be seen from this figure that the axial stress distribution is different along the edges and the centre of the sample. Figure B.3 shows that the transverse stress distribution. It can be seen that transverse stress is higher along the grip line

and vanishes at a distance approximately one half of the specimen width. Figure B.4 shows the shear stress distribution. This figure shows that the shear stress distribution is asymmetric across the specimen width, with highest magnitudes occurring along the grip line at the specimen edges.

From these results, it can be suggested that the complex stress state at the grip line may be the predominant factor for the final failure location of unidirectional samples skewed towards the grip line.

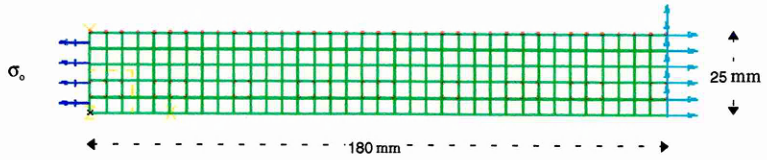

Figure B.1. The details of boundary conditions and FEM mesh of a unidirectional sample.

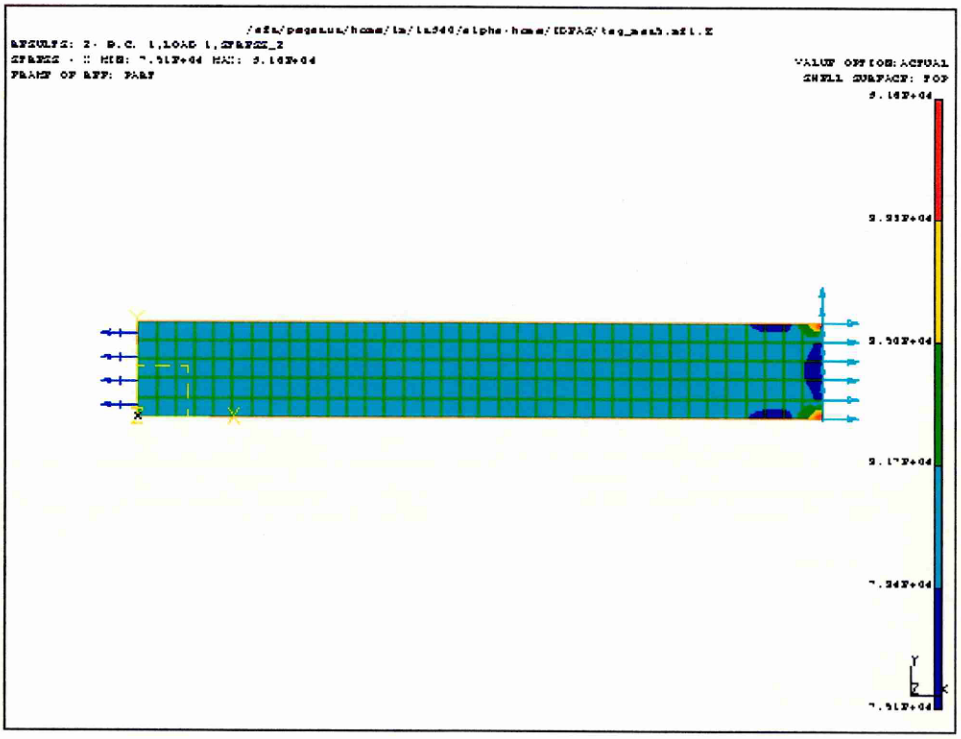

Figure B.2. Results showing the axial stress (σ_y) distribution in a unidirectional laminate.

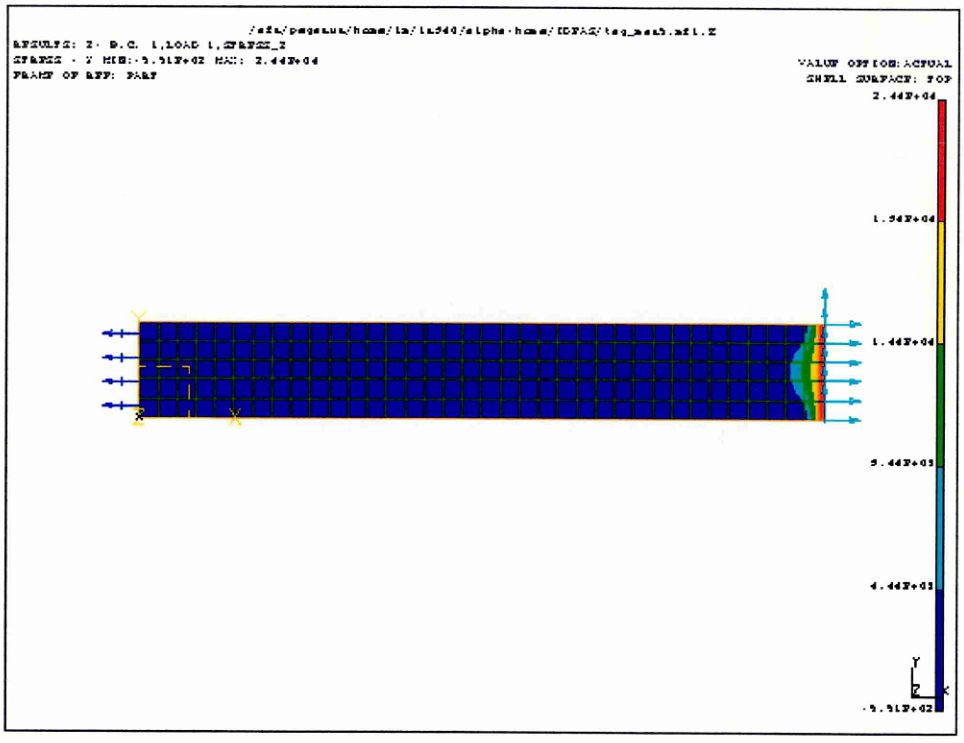

Figure B.3. Results showing the transverse stress (σ_y) distribution in a unidirectional laminate.

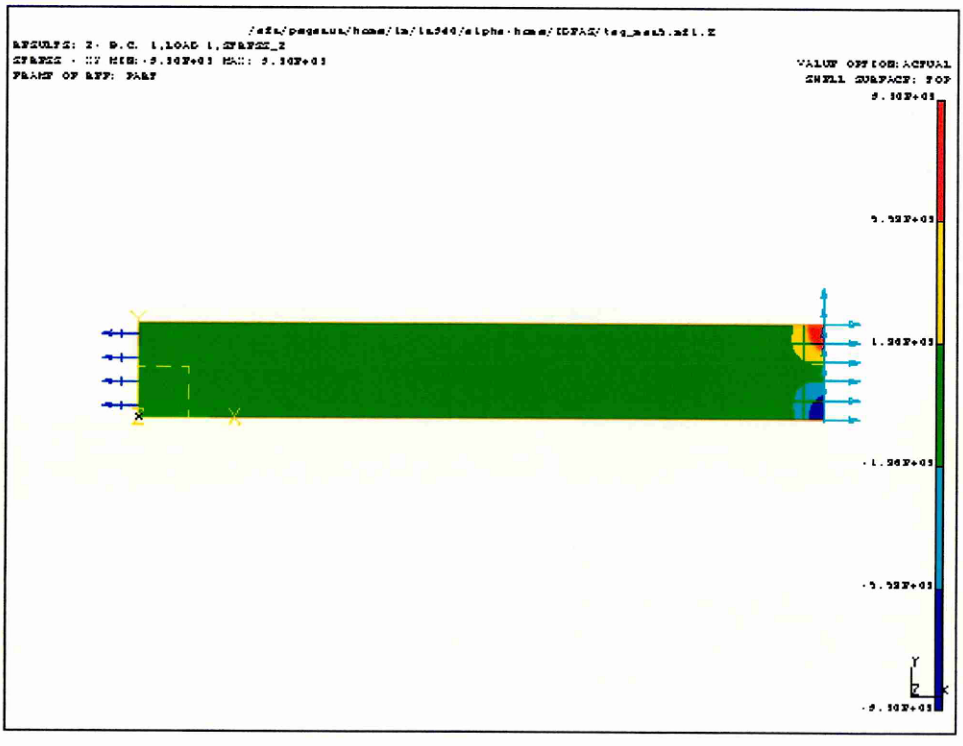

Figure B.4. Results showing the shear stress (τ_{xy}) distribution in a unidirectional laminate.

C

STATISTICAL SUMMARY OF ELECTRICAL AND MECHANICAL PROPERTIES

This appendix presents the statistical summary of the electrical and mechanical properties.

Table C.1. Statistical summary of longitudinal electrical properties.

Resistivity (mΩm)	UD914	UD914	UD920
	MT	DL	MT
Mean	0.039615	0.188013	0.048602
Standard Error	0.000506	0.049134	0.001013
Median	0.039184	0.1175	0.048501
Standard Deviation	0.002262	0.155374	0.006639
Sample Variance	5.12E-06	0.024141	4.41E-05
Kurtosis	-1.35435	-0.54031	-1.15188
Skewness	0.010031	0.954883	-0.03862
Range	0.007164	0.403917	0.024034
Minimum	0.035774	0.048583	0.037684
Maximum	0.042938	0.4525	0.061717
No. of samples	40	10	43
Confidence Level(95.0%)	0.001059	0.111148	0.002043

Table C.2. Statistical summary of transverse resistivity.

Resistivity (mΩm)	UD914 MT	UD920 MT	UD920 DL
Mean	182.2006	37.06262	35.08623
Standard Error	2.919638	1.360219	1.918476
Median	184.1616	36.19253	35.851
Standard Deviation	6.52851	4.301391	8.139403
Sample Variance	42.62144	18.50196	66.24988
Kurtosis	0.66898	-0.55909	-0.64265
Skewness	-0.79094	0.248378	-0.32655
Range	17.28722	13.64794	26.84412
Minimum	172.348	30.00531	21.80588
Maximum	189.6353	43.65325	48.65
No. of samples	10	10	18
Confidence Level(95.0%)	8.106232	3.077032	4.047636

Table C.3. Statistical summary of transverse resistivity of laminas.

Resistivity (mΩm)	UD914	UD920
Mean	285.94	129.37
Standard Error	15.11	9.13
Median	288.49	125.00
Standard Deviation	75.56	45.66
Sample Variance	5709.23	2084.43
Kurtosis	-0.95749	-0.04753
Skewness	0.049435	0.572181
Range	263.38	175.96
Minimum	160.75	66.94
Maximum	424.13	242.90
Confidence Level(95.0%)	31.19	18.85

Table C.4. Statistical summary of longitudinal tensile properties of UD914.

UD914L	Tensile strength σ (MPa)	Tensile modulus E (GPa)	Failure strain ε (%)
Mean	1543.347	139.456	1.123
Standard Error	34.607	0.395	0.016
Median	1516.000	139.165	1.105
Standard Deviation	109.436	1.248	0.051
Sample Variance	11976.230	1.557	0.002
Kurtosis	-1.361	-0.207	0.553
Skewness	0.399	0.086	1.361
Range	293.520	4.106	0.138
Minimum	1416.000	137.314	1.080
Maximum	1709.520	141.420	1.218
Count	10.000	10.000	10.000
Confidence Level(95.0%)	78.286	0.893	0.036

Table C.5. Statistical summary of transverse tensile properties of UD914.

UD914T	Tensile strength σ (MPa)	Tensile modulus E (GPa)	Failure strain ε (%)
Mean	54.402	8.958	0.619
Standard Error	2.204	0.028	0.013
Median	54.830	8.960	0.627
Standard Deviation	4.927	0.064	0.057
Sample Variance	24.279	0.004	0.003
Kurtosis	0.374	1.642	0.303
Skewness	-0.027	0.696	0.410
Range	13.300	0.175	0.152
Minimum	47.740	8.88	0.549
Maximum	61.040	9.055	0.701
Count	5.000	5.000	5.000
Confidence Level(95.0%)	6.118	0.079	0.071

Table C.6. Statistical summary of longitudinal tensile properties of UD920.

UD920L	Tensile strength σ (MPa)	Tensile modulus E (GPa)	Failure strain ε (%)
Mean	1580.409	136.318	1.138
Standard Error	34.678	0.306	0.014
Median	1581.640	136.158	1.156
Standard Deviation	109.661	0.968	0.044
Sample Variance	12025.560	0.938	0.002
Kurtosis	-1.667	-0.827	-1.348
Skewness	-0.205	0.699	-0.607
Range	279.308	2.784	0.120
Minimum	1430.760	135.238	1.069
Maximum	1710.068	138.022	1.189
Count	10.000	10.000	10.000
Confidence Level(95.0%)	78.447	0.693	0.032

Table C.7. Statistical summary of transverse tensile properties of UD920.

UD920T	Tensile strength σ (MPa)	Tensile modulus E (GPa)	Failure strain ε (%)
Mean	52.071	7.877	0.685
Standard Error	4.171	0.046	0.061
Median	51.665	7.922	0.673
Standard Deviation	10.218	0.113	0.149
Sample Variance	104.404	0.013	0.022
Kurtosis	-0.369	-0.576	0.204
Skewness	0.089	-0.946	0.474
Range	29.030	0.292	0.429
Minimum	37.830	7.697	0.491
Maximum	66.860	7.989	0.920
Count	6.000	6.000	6.000
Confidence Level(95.0%)	10.723	0.119	0.157

Table C.8. Statistical summary of tensile properties of CP914.

CP914	Tensile strength σ (MPa)	Tensile modulus E (GPa)	Failure strain ε (%)
Mean	809.702	72.065	1.108
Standard Error	9.333	1.018	0.017
Median	817.005	71.226	1.135
Standard Deviation	29.512	3.218	0.055
Sample Variance	870.967	10.358	0.003
Kurtosis	0.849	3.294	-1.347
Skewness	-1.104	1.709	-0.745
Range	91.170	11.396	0.135
Minimum	746.730	68.315	1.025
Maximum	837.900	79.711	1.160
Count	10.000	10.000	10.000
Confidence Level(95.0%)	21.112	2.302	0.039

Table C.8. Statistical summary of tensile properties of CP914.

CP914	Tensile strength σ (MPa)	Tensile modulus E (GPa)	Failure strain ε (%)
Mean	809.702	72.065	1.108
Standard Error	9.333	1.018	0.017
Median	817.005	71.226	1.135
Standard Deviation	29.512	3.218	0.055
Sample Variance	870.967	10.358	0.003
Kurtosis	0.849	3.294	-1.347
Skewness	-1.104	1.709	-0.745
Range	91.170	11.396	0.135
Minimum	746.730	68.315	1.025
Maximum	837.900	79.711	1.160
Count	10.000	10.000	10.000
Confidence Level(95.0%)	21.112	2.302	0.039